

**A Computational Study of the Fourth Painlevé Equation
and a Discussion of Adams Predictor-Corrector Methods**

by

Jonah A. Reeger

B.S., United States Air Force Academy, 2007

M.A., Rice University, 2009

A thesis submitted to the
Faculty of the Graduate School of the
University of Colorado in partial fulfillment
of the requirements for the degree of
Doctor of Philosophy
Department of Applied Mathematics

2013

This thesis entitled:
A Computational Study of the Fourth Painlevé Equation and a Discussion of Adams
Predictor-Corrector Methods
written by Jonah A. Reeger
has been approved for the Department of Applied Mathematics

Prof. Bengt Fornberg

Prof. Mark Ablowitz

Prof. Thomas Manteuffel

Prof. Barbara Prinari

Prof. Harvey Segur

Date _____

The final copy of this thesis has been examined by the signatories, and we find that both the content and the form meet acceptable presentation standards of scholarly work in the above mentioned discipline.

The views expressed in this thesis are those of the author and do not reflect the official policy or position of the United States Air Force, Department of Defense, or the U.S. Government.

Reeger, Jonah A. (Ph.D., Applied Mathematics)

A Computational Study of the Fourth Painlevé Equation and a Discussion of Adams Predictor-Corrector Methods

Thesis directed by Prof. Bengt Fornberg

This thesis explores two unrelated research topics. The first is a numerical study of the fourth Painlevé equation, while the second is a characterization of the stability domains of Adams predictor-corrector methods.

First, the six Painlevé equations were introduced over a century ago, motivated by theoretical considerations. Over the last several decades these equations and their solutions have been found to play an increasingly central role in numerous areas of mathematical physics. Due to extensive dense pole fields in the complex plane, their numerical evaluation remained challenging until the recent introduction of a fast ‘pole field solver’ (Fornberg and Weideman, *J. Comp. Phys.* 230 (2011), 5957-5973). This study adapts this numerical method to allow for either extended precision or faster numerical solutions to explore the solution space of the fourth Painlevé (P_{IV}) equation. This equation has two free parameters in its coefficients, as well as two free initial conditions. After summarizing key analytical results for P_{IV} , the present study applies this new computational tool to the the fundamental domain and a surrounding region of the parameter space. We confirm existing analytic and asymptotic knowledge about the equation, and also explore solution regimes which have not been described in the previous literature. In particular, solutions with the special characteristic of having adjacent pole-free sectors, but with no closed form, are identified.

Second, the extent that the stability domain of a numerical method reaches along the imaginary axis indicates the utility of the method for approximating solutions to certain differential equations. This maximum value is called the imaginary stability boundary (ISB). It has previously been shown that exactly half of Adams-Bashforth (AB), Adams-Moulton (AM), and staggered Adams-Bashforth methods have nonzero stability ordinates. In the last chapter of this thesis,

two categories of Adams predictor-corrector methods are considered, and it is shown that they have a nonzero ISB when (for a method of order p) $p = 1, 2, 5, 6, 9, 10, \dots$ for ABp - AMp and $p = 3, 4, 7, 8, 11, 12, \dots$ in the case of and $AB(p-1)$ - AMp .

Dedication

To my wife. Your love, support, and dedication have been my inspiration.

Acknowledgements

First, I owe a great many thanks to Bengt Fornberg. Bengt has been an outstanding mentor and advisor. He never failed to answer my questions thoroughly, no matter how trivial I thought he might find them, and he taught me that the frantic feeling throughout this journey was only natural. Likewise, Michelle Ghrist has been a great colleague, mentor, and friend, inspiring me to take on graduate education. Next, to the rest of my committee, Professors Ablowitz, Manteuffel, Prinari, and Segur, I am grateful for your time and advice. I sincerely hope that you find the results contained here as interesting as I did. Also, I am indebted to André Weideman and Peter Clarkson for their insights and comments along the way. Thank you to the faculty, staff, and students in APPM for helping me remain on track through it all. Finally, thank you to the United States Air Force and Air Force Institute of Technology for providing the opportunity of graduate education to a young officer.

Contents

Chapter		
1	Introduction	1
	1.1 History of the Painlevé Equations	1
	1.2 Organization of the thesis	4
2	Analytic Theory of P_{IV}	6
	2.1 Series Expansion	6
	2.2 Symmetry in the PIV Equation	7
	2.3 Solution Transformations	8
3	Closed Form Solutions	10
	3.1 Rational Solutions	10
	3.2 Special Function Solutions	13
	3.3 The Weyl Chambers	28
4	Asymptotic Approximations	30
	4.1 Asymptotically Decaying Solutions	30
	4.2 General Asymptotic Approximations	31
5	Computing solutions to IVPs and BVPs of the Painlevé Equations	33
	5.1 The Pole Field Solver	33
	5.1.1 A Description of the Pole Field Solver	33

5.1.2	A Brief Discussion on Implementing the Pole Field Solver	38
5.1.3	An Arbitrary Precision Pole Field Solver	38
5.1.4	Increasing the Speed of the Solver	43
5.2	Solving the BVPs	47
5.3	Visualization of pole locations and residues	49
5.3.1	Correcting Pole Locations Via Newton's Method	52
5.3.2	Correcting Pole Locations Via Roots of the Padé Denominator	53
5.4	Pole and Oscillation Counting	53
5.5	Exploring Solutions with a Pole at the Origin	58
6	Exploring Solutions of P_{IV} With No Closed Form	63
6.1	Confirming the Solution Transformations	63
6.2	Initial Explorations: Zero α and β	67
6.2.1	Sequences of Solutions Along $u'(0) = 0$, Varying $u(0)$	68
6.2.2	Sequences of Solutions Satisfying the Decaying Asymptotic Condition	72
6.3	Further Explorations: α and β Not Both Zero	74
6.3.1	An Exploration of the Fundamental Domain	74
6.3.2	Parameters Exterior to the Fundamental Domain	77
6.3.3	A Note on Connection Formulae	80
6.3.4	Solutions with a Pole-Free Half-Plane	82
6.3.5	Solutions With Adjacent Pole-Free Sectors	88
7	Conclusions about the Numerical Explorations of P_{IV}	93
8	Stability Ordinates of the Adams Predictor-Corrector Methods	95
8.1	Introduction and Assertions	95
8.2	Proof Methodology	102
8.3	Proof of the Assertions	106

8.3.1	AB_p - AM_p methods	106
8.3.2	$AB(p - 1)$ - AM_p methods	110
8.4	Conclusions	114
Bibliography		115
Appendix		
A	Paper 1-“Painlevé IV with Both Parameters Zero: A Numerical Study”	118
B	Paper 2-“Painlevé IV: A Numerical Study of the Fundamental Domain and Beyond”	145
C	Paper 3-“Stability Ordinates of Adams Predictor-Corrector Methods”	182

Tables

Table

1.1	Dimensions of the solution spaces of P_I , P_{II} and P_{IV}	3
3.1	Parameter choices and resulting simplest rational solutions to P_{IV}	10
3.2	Summary of the rational solution expressions that have been verified	13
3.3	Summary of the special function solution expressions that have been verified	28
5.1	Pole locations of $u_{1,2}^{[GH;1]}$ via computing the roots of $8z^6 + 4z^4 + 6z^2 + 3 = 0$	50
5.2	Pole locations of $u_{1,2}^{[GH;1]}$ determined by solving the undetermined system	52
5.3	Pole locations of $u_{1,2}^{[GH;1]}$ corrected via Newton's method	53
5.4	Pole locations of $u_{1,2}^{[GH;1]}$ corrected via roots of the Padé approximation denominator	53

Figures

Figure

1.1	Two views of the Weyl chambers and fundamental domain	3
3.1	Examples of the generalized Hermite polynomial solutions	11
3.2	Examples of the generalized Okamoto polynomial solutions	13
3.3	Examples of the solutions expressible in terms of the parabolic cylinder function for $k = 1, \nu = 0.5, \epsilon = -1$, and various D	15
3.4	Examples of the solutions expressible in terms of the parabolic cylinder function for various $k = 1, \nu = 0.5, \epsilon = 1$, and various D	16
3.5	Examples of the solutions expressible in terms of the parabolic cylinder function for $k = 1, \epsilon = 1, D = 1$ and various ν	17
3.6	Examples of the solutions expressible in terms of the parabolic cylinder function for $k = 2, \epsilon = 1, D = 1$, and various ν	18
3.7	Examples of the solutions expressible in terms of standard Hermite polynomials . . .	19
3.8	Examples of the solutions expressible in terms of the complementary error function .	20
3.9	Examples of the numerical solutions $u_{-\frac{1}{2},\epsilon,1}^{[WD;1]}$ with $(\alpha = \frac{5}{2}, \beta = -\frac{1}{2})$ and $(\alpha = -\frac{5}{2}, \beta = -\frac{1}{2})$	21
3.10	Examples of the numerical solutions $u_{-\frac{1}{2},\epsilon,1}^{[WD;2]}$ with $(\alpha = -2, \beta = -8)$ and $(\alpha = 2, \beta = -8)$	22
3.11	Examples of the numerical solutions $u_{-\frac{1}{2},\epsilon,1}^{[WD;3]}$ with $(\alpha = -\frac{1}{2}, \beta = -\frac{1}{2})$ and $(\alpha = \frac{1}{2}, \beta = -\frac{1}{2})$	23

3.12	Examples of the solutions expressible in terms of confluent hypergeometric functions for $n = 1$, $c_1 = 0$, $c_2 = 0$, and various ν	24
3.13	Examples of the solutions (pole locations can residues are shown) expressible in terms of confluent hypergeometric functions for $\nu = 0.5$, $c_1 = 0$, $c_2 = 0$, and various n . . .	25
3.14	Examples of the solutions expressible in terms of confluent hypergeometric and gamma functions with $\nu = 0.5$, $n = 1$, $c_2 = 0$ and various c_1	26
3.15	Examples of the solutions expressible in terms of confluent hypergeometric and gamma functions with $\nu = 0.5$, $n = 1$, $c_1 = 0$ and various c_2	27
5.1	Solution along the real axis to the test problem and order of the error using the Taylor series method and an adaptive Runge-Kutta method	34
5.2	Solution along the real axis to the test problem and order of the error using the Taylor series method and a Padé method	35
5.3	Example of the evaluation paths in the complex plane for the test problem using the pole avoidance strategy	36
5.4	Solution along the real axis to the test problem and order of the error using the Taylor series method, a Padé method, and the pole avoidance strategy	37
5.5	Example of the evaluation paths in the complex plane (shown with pole locations can residues) for a P_{IV} solution ($u_{4.5,2,0,0}^{[CH;1]}$ (3.6)) using the pole field solver	37
5.6	Log base 10 of the Relative error in computing $u_{4.5,2,0,0}^{[CH;1]}$ in extended precision and machine precision for a fixed order and step size using the pole field solver from a single initial condition	40
5.7	Log base 10 of the relative error and computation time when computing $u_{4.5,2,0,0}^{[CH;1]}$ in high precision for various orders and step sizes using the pole field solver starting from a single initial condition	41
5.8	Solution to P_{IV} beginning with the initial condition $k(D_{\frac{1}{2}\alpha-\frac{1}{2}}(\sqrt{2}z))^2$ where $z = z_0 = 4\sqrt{2}$	42

5.9	Solution to PIV beginning with the initial condition $k(D_{\frac{1}{2}\alpha-\frac{1}{2}}(\sqrt{2}z))^2$ where $z = z_0 = 6, 10,$ and 14	42
5.10	Profiler output for the m-file version of the “PIV_pole_field_solver” function	43
5.11	Profiler output for the C mex-file version of the “PIV_pole_field_solver” function	44
5.12	Profiler output for the m-file version of the “paths_eval” function	44
5.13	Profiler output for the C mex-file version of the “paths_eval” function	45
5.14	Solutions and log base 10 of the relative errors between the exact solution and numerical solutions using the C mex-file version and original m-file versions of the pole-field-solver when computing $u_{4.5,2,0,0}^{[CH;1]}$ from a single initial condition using the pole field solver	45
5.15	Relative error and solution times to compute the solution $u_{4.5,2,0,0}^{[CH;1]}$ over a region of the complex plane using only the m-file version of the pole field solver with various orders and step sizes and beginning with a single initial condition	46
5.16	Relative error and solution times to compute the solution $u_{4.5,2,0,0}^{[CH;1]}$ over a region of the complex plane using only the C mex-file version of the pole field solver with various orders and step sizes and beginning with a single initial condition	47
5.17	Pole locations and residues of $u_{1,2}^{[GH;1]}$	50
5.18	Contour plot of $ u_{1,2}^{[GH;1]} $ around the pole at $0.707106781186547i$	51
5.19	Number of poles on the positive and negative real axes for $\alpha = 0$ and $\beta = 0$	54
5.20	Sum of the number of oscillations and poles over a finite segment of the positive real axis and $\alpha = \beta = 0$	55
5.21	Number of oscillations and poles over a finite segment of the positive real axis and $\alpha = \beta = 0$	56
5.22	Initial conditions for solutions asymptotic to the roots w_{μ}^{\pm} , $\mu = \pm 1$, as $z \rightarrow +\infty$, $z \in \mathbb{R}$, for $\alpha = \beta = 0$	57
5.23	Legend and color bar for pole counting diagrams	58

5.24	A view of solutions (pole locations can residues are shown) with a pole at the origin in the case of $\alpha = 2$, $\beta = -2$, and $c = 0$	59
5.25	A caricature of the transition of a pole from the negative real axis to the positive real axis	60
5.26	A view of solutions (pole locations can residues are shown) with a pole at the origin in the case of $\alpha = 0$, $\beta = 0$, and $c = 0$	61
5.27	Location and number of poles on the real axis for $\alpha = \beta = 0$ when a pole is located at the origin	62
6.1	Solution to P_{IV} with $\alpha = 0.25$, $\beta = -0.125$, $u(0) = -1.5$ and $u'(0) = -1.5$	64
6.2	Zero and pole locations of solutions to P_{IV} resulting from the applications of the transformations to the solution with $\alpha = 0.25$, $\beta = -0.125$, $u(0) = -1.5$ and $u'(0) =$ -1.5	65
6.3	Solutions along the real axis resulting from the applications of the transformations to the solution with $\alpha = 0.25$, $\beta = -0.125$, $u(0) = -1.5$ and $u'(0) = -1.5$	66
6.4	Relative errors between the analytically transformed and numerically compute solu- tions of P_{IV} resulting from the applications of the transformations to the solution with $\alpha = 0.25$, $\beta = -0.125$, $u(0) = -1.5$ and $u'(0) = -1.5$	67
6.5	The eight sectors in the solutions of P_{IV}	68
6.6	Sequence of solutions for $\alpha = \beta = 0$ near $u_0 = 1.987405112326211 \dots$ along the line $u'(0) = 0$	69
6.7	Sequence of solutions for $\alpha = \beta = 0$ near $u_0 = 3.235356086736551 \dots$ along the line $u'(0) = 0$	69
6.8	Sequence of solutions for $\alpha = \beta = 0$ near $u_0 = 2.660688155172691 \dots$ along the line $u'(0) = 0$	71
6.9	Sequence of solutions for $\alpha = \beta = 0$ near $u_0 = 3.726596884689709 \dots$ along the line $u'(0) = 0$	71

6.10	Sequence of solutions for $\alpha = \beta = 0$ near $k = \frac{1}{\pi}$ in $k(D_{\frac{1}{2}\alpha - \frac{1}{2}}(\sqrt{2}z))^2$	72
6.11	Sequence of solutions for $\alpha = \beta = 0$ near $k = \frac{1}{2\pi}$ in $k(D_{\frac{1}{2}\alpha - \frac{1}{2}}(\sqrt{2}z))^2$	73
6.12	Number of poles on the positive real axis for $(\alpha = 0, \beta = -\frac{2}{9}), (\alpha = 0, \beta = -2),$ and $(\alpha = 1, \beta = 0)$	75
6.13	Solutions with adjacent pole free sectors for $\alpha = 0, \beta = -2, u'(0) = 0.$ and $u_0 =$ 3.170110354518507	75
6.14	Solutions with adjacent pole free sectors for $\alpha = 1, \beta = 0. u'(0) = 0,$ and $u_0 =$ 2.989670219313871	76
6.15	Number of poles on the positive real axis for $(\alpha = 0.5, \beta = -0.5), (\alpha = 0, \beta = -0.5),$ and $(\alpha = 0.5, \beta = 0)$	76
6.16	Number of poles on the positive real axis for parameter choices interior to the fun- damental domain	77
6.17	Number of poles on the positive real axis for parameter choices where $\alpha = 0$ and $\beta > 0$	78
6.18	Number of poles on the positive real axis for some parameters exterior to the funda- mental domain with $ \alpha $ and/or $ \beta $ equal to three	79
6.19	Number of poles on the positive real axis for some parameters exterior to the funda- mental domain with $ \alpha $ and/or $ \beta $ equal to four	80
6.20	Number of poles on the negative real axis, entire real axis, and positive real axis for $\alpha = 0.25$ and $\beta = -0.125$	81
6.21	Number of poles on the negative real axis, entire real axis, and positive real axis for $\alpha = 3$ and $\beta = -3$	82
6.22	Number of poles on the positive (right) and negative (left) real axis for solutions asymptotic to $w_{+1}^- \sim -\frac{2}{3}z$ as $z \rightarrow +\infty$ and $z \in \mathbb{R}$ and each α and β	83
6.23	Roots of the Okamoto I polynomials for orders $m = \pm 1, \pm 2, \pm 3, \pm 4$	84
6.24	Zero and pole locations of solutions to P_{IV} matching $w_{+1}^- \sim -\frac{2}{3}z$ as $z \rightarrow +\infty$ and $z \in \mathbb{R}$ with $\alpha = 2m$ and $\beta = 0$ for various values of m	85

6.25	Solutions to P_{IV} matching $w_{+1}^- \sim -\frac{2}{3}z$ as $z \rightarrow +\infty$ and $z \in \mathbb{R}$ normal to the parabola $\beta = -2(\alpha - 2)^2$	86
6.26	Solutions to P_{IV} matching $w_{+1}^- \sim -\frac{2}{3}z$ as $z \rightarrow +\infty$ and $z \in \mathbb{R}$ normal to the parabola $\beta = -2(\alpha + 2)^2$	87
6.27	Examples of $u_{\nu, \epsilon, d_1, d_2}^{[PC;k]}$, $k = 1, 2$, for $d_1 = 0$ or $d_2 = 0$	88
6.28	Solution types with adjacent pole free sectors for $\alpha = 1$ and $\beta = 0$	90
6.29	Solution types with adjacent pole free sectors for $\alpha = 0$ and $\beta = -2$	90
6.30	Solution types with adjacent pole free sectors for $\alpha = 0.5$ and $\beta = -0.5$	91
6.31	Solution types with adjacent pole free sectors for $\alpha = 0$ and $\beta = -0.5$	92
8.1	The stability domains for the AB and AM methods of orders 1, 2, and 3	98
8.2	The stability domains for the predictor corrector methods of various orders	100
8.3	Magnified views of the stability domains for the predictor corrector methods of various orders near the origin	101

Chapter 1

Introduction

This thesis contains two very different research topics. First, a fairly new numerical method is applied to the fourth Painlevé equation to explore the vast regions of the solution space that have not been considered in the literature. Second, the utility of Adams Bashforth predictor-Adams Moulton corrector methods for first order ordinary differential equations with imaginary spectra is considered. We begin with the study of the fourth Painlevé equation.

1.1 History of the Painlevé Equations

At the turn of the twentieth century Paul Painlevé sought all second order ordinary differential equations (ODEs) of the form

$$\frac{d^2}{dz^2}w(z) = F\left(z, w(z), \frac{d}{dz}w(z)\right)$$

with F a rational function of $w(z)$ and $\frac{d}{dz}w(z)$, and $w(z)$ locally analytic in z satisfying a special property. This property, now known as the Painlevé property, is characterized by solutions of the ODEs free from movable branch points, but with the possibility of movable poles or movable isolated essential singularities.

Roughly fifty equations featuring the Painlevé property have been found since the initial investigation, forty-four of which can be reduced to linear equations or P_I to P_{VI} or solved in

terms of elliptic functions. The remaining six equations dubbed P_I through P_{VI} are

$$\frac{d^2}{dz^2}u(z) = 6u(z)^2 + z \quad (\text{P}_I)$$

$$\frac{d^2}{dz^2}u(z) = 2u(z)^3 + zu(z) + \alpha \quad (\text{P}_{II})$$

$$\frac{d^2}{dz^2}u(z) = \frac{1}{u(z)} \left(\frac{d}{dz}u(z) \right)^2 - \frac{1}{z} \frac{d}{dz}u(z) + \frac{\alpha u(z)^2 + \beta}{z} + \gamma u(z)^3 + \frac{\delta}{u(z)} \quad (\text{P}_{III})$$

$$\frac{d^2}{dz^2}u(z) = \frac{1}{2u(z)} \left(\frac{d}{dz}u(z) \right)^2 + \frac{3}{2}u(z)^3 + 4zu(z)^2 + 2(z^2 - \alpha)u(z) + \frac{\beta}{u(z)} \quad (\text{P}_{IV})$$

$$\begin{aligned} \frac{d^2}{dz^2}u(z) = & \left(\frac{1}{2u(z)} + \frac{1}{u(z)-1} \right) \left(\frac{d}{dz}u(z) \right)^2 - \frac{1}{z} \frac{d}{dz}u(z) + \frac{(u(z)-1)^2}{z^2} \left(\alpha u(z) + \frac{\beta}{u(z)} \right) + \\ & \frac{\gamma u(z)}{z} + \frac{\delta u(z)(u(z)+1)}{u(z)-1} \end{aligned} \quad (\text{P}_V)$$

$$\begin{aligned} \frac{d^2}{dz^2}u(z) = & \frac{1}{2} \left(\frac{1}{u(z)} + \frac{1}{u(z)-1} + \frac{1}{u(z)-z} \right) \left(\frac{d}{dz}u(z) \right)^2 - \left(\frac{1}{z} + \frac{1}{z-1} + \frac{1}{u(z)-z} \right) \frac{d}{dz}u(z) + \\ & \frac{u(z)(u(z)-1)(u(z)-z)}{z^2(z-1)^2} \left(\alpha + \frac{\beta z}{u(z)^2} + \frac{\gamma(z-1)}{(u(z)-1)^2} + \frac{\delta z(z-1)}{(u(z)-z)^2} \right) \end{aligned} \quad (\text{P}_{VI})$$

where α , β , γ , and δ are arbitrary parameters in \mathbb{C} .

When these equations are considered as boundary value problems (BVPs), their solution space is as large as the number of arbitrary parameters in the equation, and the two boundary conditions (BCs). Similarly, when cast as an initial value problem (IVP), the solution space is defined, again, by the number of arbitrary parameters, but also by two initial conditions (ICs).

For P_{II} through P_{VI} , very special parameter choices lead to solutions in terms of either rational or special functions. Table 1.1 and figure 1.1 highlight some of these special choices for P_I , P_{II} and P_{IV} . Note that in figure 1.1 the black lines indicate solutions expressible in terms of special functions while the dark (blue) and light (yellow) hexagrams indicate rational solutions. The shaded grey region is the fundamental domain, which will be further explained in section 3.3. The triangular regions in the left frame of figure 1.1 are known as the Weyl chambers [26].

	Parameters	Number of IC/BCs	Dimension of Solution Space	Space of Closed Form Solutions
P_I		2	2	None
P_{II}	α	2	3	$\alpha = 1, 2, 3, 4, \dots$ Single Rational $\alpha = \frac{1}{2}, \frac{3}{2}, \frac{5}{2}, \dots$ 1-Parameter Airy
P_{IV}	α, β	2	4	See Figure 1.1

Table 1.1: A description of the solution spaces of P_I , P_{II} and P_{IV} .

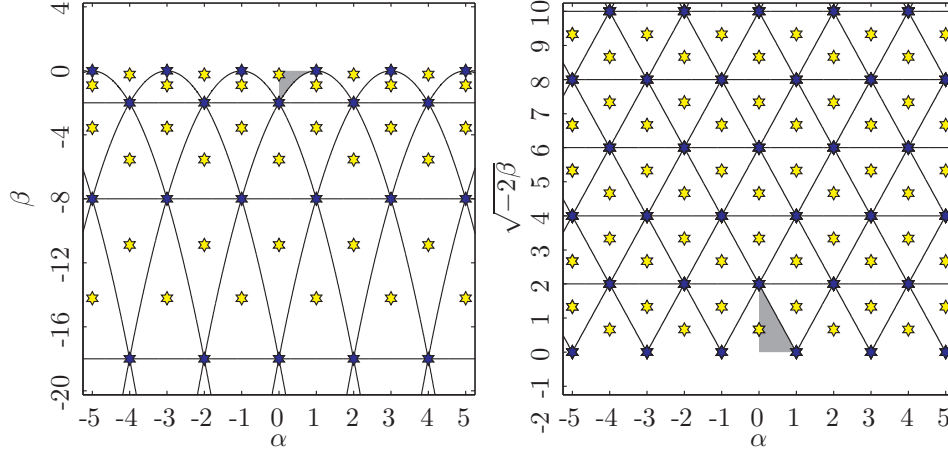


Figure 1.1: A view of the Weyl Chambers. The shaded region indicates the fundamental domain given in (3.7).

Aside from these special parameter choices, solutions of the Painlevé equations generally have an infinity of poles and cannot be written explicitly in terms of rational or special functions. Therefore, these solutions are typically dubbed Painlevé transcendents. To avoid confusion with those elementary functions that are typically dubbed transcendental, we will drop the phrase transcendent and instead refer to these solutions as having no closed form.

Some solutions with no closed form have been found that are pole free across the entire real axis or even an entire half-plane. For instance, P_I has the tritronqué solution [12] that is smooth for an entire half-plane and P_{II} has the Hastings-McLeod [27] and Ablowitz-Segur [1] solutions, which are both at least bounded over the entire real axis. Later in this thesis, evidence will show that P_{IV} also has classes of solutions that have vast smooth regions in the complex plane.

Alternative forms of P_I through P_{VI} are considered elsewhere. For instance, each of the equations can be represented as a Hamiltonian system or as the compatibility condition of a linear

system [14]. Likewise, P_{IV} has a representation known as the symmetric P_{IV} or sP_{IV} system [14]. Further, P_{IV} can be cast as a Riemann-Hilbert problem for limited choices of α and β and numerically solved using a software package discussed in [39]. The method discussed later in this thesis is several orders of magnitude faster, is not limited to specific choices of α and β , and makes it unnecessary to consider any of these other forms when exploring the solution space. We present theory and perform computation only on the second order ODE form of P_{IV} presented earlier in this section.

1.2 Organization of the thesis

As stated previously, this thesis covers two very different topics. First, existing theory of P_{IV} applicable to any α and β is covered in chapter 2.

This is followed by a discussion of the rational and elementary special function solutions described in the literature. Those that are discussed were confirmed numerically, and a sampling of them is given in chapter 3.

Third, in chapter 4 the known asymptotic approximations are presented with computational solutions that explore beyond those that have been previously presented. The asymptotic approximations available in the literature are provided along with a discussion of dominant asymptotic behavior for solutions that are asymptotically smooth.

Chapter 5 supplies a description of the fairly new numerical method that made this research possible. Various adaptations of the numerical method are presented to overcome difficulties involving computational precision and time. Further, the methodology used to visualize individual solutions of P_{IV} in the complex plane and the approach for examining possible solution types for a fixed choice of α and β are presented (including solutions with a pole at the origin).

The methods of chapter 5 provide for the many numerical explorations in chapter 6. These numerical explorations have led to the identification of two types of solutions that are common to all α and β with the notable property of having at least two pole-free sectors in the complex plane.

Conclusions about this study of the fourth Painlevé equation are finally presented in chapter

7.

With discussions of the first topic complete, we continue with the second topic. Chapter 8 discusses the stability theory of general and predictor-corrector multistep methods. Two assertions are made and proved that allow for the selection of a predictor-corrector method of any order to solve a first order ODE with an imaginary spectrum.

Chapter 2

Analytic Theory of P_{IV}

This chapter provides some of the general analytical information available pertaining to all solutions of P_{IV} (i.e. regardless of α and β). This information includes the series expansion about a pole, symmetries in the ODE, and solution transformations.

2.1 Series Expansion

In a neighborhood of a pole z_0 we can determine the coefficients of the Laurent expansion of P_{IV} by substituting a truncated expansion into P_{IV} (as was done for P_{II} in [20]). For instance, substituting

$$u(z) = \frac{a_{-1}}{z - z_0} + a_0 + a_1(z - z_0) + a_2(z - z_0)^2 + a_3(z - z_0)^3 + a_4(z - z_0)^4 + O((z - z_0)^5), \quad (2.1)$$

we are left with the nontrivial choices

$$\begin{aligned} a_{-1} &= \pm 1 \\ a_0 &= -z_0 \\ a_1 &= \frac{1}{3}(-4 \pm z_0^2 \pm 2\alpha) \\ a_2 &= c \\ a_3 &= \frac{1}{45}(\pm 26 \mp 36cz_0 + 20z_0^2 \mp z_0^4 - 32\alpha \mp 4z_0^2\alpha \pm 14\alpha^2 \pm 9\beta) \\ a_4 &= \frac{1}{9}(\mp 9c + 5z_0 + 3cz_0^2 \mp 2z_0^3 + 6c\alpha \mp 4z_0\alpha). \end{aligned}$$

This leaves the choice of $+1$ or -1 for a_{-1} and only one further free parameter c (first appearing in a_2). In agreement with this, all poles in the solutions to P_{IV} are simple and have residue of either $+1$ or -1 .

2.2 Symmetry in the PIV Equation

The notation $P_{IV}(\alpha, \beta)$ is used in, for instance, [26] to indicate the set of all solutions of P_{IV} for the particular α and β . Direct inspection of P_{IV} shows that if $u(z) \in P_{IV}(\alpha, \beta)$, then [26]

$$-u(-z) \in P_{IV}(\alpha, \beta), \quad (2.2)$$

$$-iu(-iz) \in P_{IV}(-\alpha, \beta), \text{ and} \quad (2.3)$$

$$iu(iz) \in P_{IV}(-\alpha, \beta). \quad (2.4)$$

These symmetries provide at least one counterpart to any solution presented in this thesis for the same choice of α and β . Similar inspection of the other Painlevé equations shows that the first of these symmetries holds for any parameter choice in the equation P_{III} , but it does not hold for P_I , P_{II} , P_V , or P_{VI} [43].

2.3 Solution Transformations

The equations P_{II} through P_{VI} have collections of transformations relating solutions for given parameters to those of different choices. For instance, the equations ([14], [32])

$$u_{1,\mu}^{\pm}(u(z), z) = \pm \frac{1}{2\mu u(z)} \left(\frac{d}{dz} u(z) \mp \mu(u(z)^2 + 2zu(z)) - \mu\sqrt{-2\beta} \right) \quad (2.5)$$

$$u_{2,\mu}^{\pm}(u(z), z) = \frac{\left(\frac{d}{dz} u(z) \pm \mu\sqrt{-2\beta}\right)^2 + (4\alpha + 4\mu \mp 2\sqrt{-2\beta})u(z)^2}{2u(z) \left(u(z)^2 + 2zu(z) - \mu\frac{d}{dz} u(z) \mp \sqrt{-2\beta}\right)} - \frac{u(z)^2(u(z) + 2z)^2}{2u(z) \left(u(z)^2 + 2zu(z) - \mu\frac{d}{dz} u(z) \mp \sqrt{-2\beta}\right)} \quad (2.6)$$

$$u_{3,\mu}^{\pm}(u(z), z) = u(z) + \frac{2 \left(1 - \mu\alpha \mp \frac{1}{2}\mu\sqrt{-2\beta}\right) u(z)}{\frac{d}{dz} u(z) \pm \mu\sqrt{-2\beta} + \mu(2zu(z) + u(z)^2)} \quad (2.7)$$

$$u_4^{\pm}(u(z), z) = \pm \frac{\left(\frac{d}{dz} u(z) \mp (u(z)^2 + 2zu(z))\right)^2 + 2\beta}{2u(z) \left(\frac{d}{dz} u(z) \mp (u(z)^2 + 2zu(z)) \pm 2\alpha + 2\right)} \quad (2.8)$$

$$u_5^{\pm}(u(z), z) = u(z) + \frac{(2 + 2\alpha \pm \sqrt{-2\beta})u(z)}{\frac{d}{dz} u(z) - 2zu(z) - u(z)^2 \mp \sqrt{-2\beta}} + \frac{2 \pm \sqrt{-2\beta}}{M^{\pm}(u(z), z)} + \frac{(2\alpha - 2 \mp \sqrt{-2\beta})u(z)M^{\pm}(u(z), z)}{u(z)(4 \pm 2\sqrt{-2\beta}) - \left(\frac{d}{dz} u(z) - 2zu(z) - u(z)^2 \mp \sqrt{-2\beta}\right) M^{\pm}(u(z), z)} \quad (2.9)$$

relate $u(z) \in P_{IV}(\alpha, \beta)$ to $u_{k,\mu}^{\pm}(z) \in P_{IV}(\alpha_{k,\mu}^{\pm}, \beta_{k,\mu}^{\pm})$, $k = 1, 2, \dots, 5$. In these equations $\mu = \pm 1$ and

$$M^{\pm}(u(z), z) = \frac{1}{2}u(z) + z + \frac{(2 + 2\alpha \pm \sqrt{-2\beta})u(z)}{\frac{d}{dz} u(z) - 2zu(z) - u(z)^2 \mp \sqrt{-2\beta}} + \frac{\frac{d}{dz} u(z) \mp \sqrt{-2\beta}}{2u(z)}.$$

Confining this study to solutions that are real on the real axis limits these transformations to $\beta \leq 0$.

The transformed solutions $u_{k,\mu}^{\pm}$, $k = 1, 2, 3$, and u_k^{\pm} , $k = 4, 5$ occur for the parameter choices

$$\alpha_{1,\mu}^{\pm} = \frac{1}{4}(\pm 2\mu - 2\alpha \pm 3\sqrt{-2\beta}) \text{ and } \beta_{1,\mu}^{\pm} = -\frac{1}{2} \left(1 \pm \alpha\mu + \frac{1}{2}\mu\sqrt{-2\beta}\right)^2 \quad (2.10)$$

$$\alpha_{2,\mu}^{\pm} = \alpha + \mu \text{ and } \beta_{2,\mu}^{\pm} = -\frac{1}{2}(2 \mp \mu\sqrt{-2\beta})^2 \quad (2.11)$$

$$\alpha_{3,\mu}^{\pm} = \frac{3}{2}\mu - \frac{1}{2}\alpha \mp \frac{3}{4}\sqrt{-2\beta} \text{ and } \beta_{3,\mu}^{\pm} = -\frac{1}{2} \left(\mu - \alpha \pm \frac{1}{2}\sqrt{-2\beta}\right)^2 \quad (2.12)$$

$$\alpha_4^{\pm} = \alpha \pm 2 \text{ and } \beta_4^{\pm} = \beta \quad (2.13)$$

$$\alpha_5^{\pm} = \alpha \text{ and } \beta_5^{\pm} = -\frac{1}{2}(4 \pm \sqrt{-2\beta})^2. \quad (2.14)$$

The composite transformations $u_4^{\pm} = u_{2,\pm}^+(u_{2,\pm}^-(u(z), z), z)$ and $u_5^{\pm} = u_{2,\mp}^+(u_{2,\pm}^-(u(z), z), z)$ are discussed in [14], [18], [34]. Equations (2.5) through (2.7) are given explicitly here because $u_{2,+1}^-$

has the incorrect sign following the first term in the numerator and u_4^- is missing a minus sign at the beginning of the entire expression when presented in [14].

These transformations generate hierarchies of solutions beginning with a simple rational or special function solution as a seed. Such hierarchies are discussed in further detail in, for instance, [13], [14], [26], and [35]. The rational and special function solutions that are included in these hierarchies are discussed in chapter 3.

Chapter 3

Closed Form Solutions

This chapter presents the various known closed form solutions to the P_{IV} equation. Unless otherwise specified, these are here presented in the way of Clarkson [14]. Notice in figure 1.1 that the parameter choices that lead to such solutions are a very small subset, leaving vast unexplored expanses in the α versus β space. Interestingly, these closed form solutions only exist for $\beta \leq 0$.

3.1 Rational Solutions

We begin with the simplest rational solutions to the P_{IV} equation. Two of these are nontrivial entire solutions to the equation, as shown in table 3.1.

α	β	$u(z)$
± 2	-2	$\pm \frac{1}{z}$
0	-2	$-2z$
0	$-\frac{2}{9}$	$-\frac{2}{3}z$

Table 3.1: Parameter choices and resulting simplest rational solutions to P_{IV} .

These three solutions further describe the simplest members of classes of solutions described as the " $-\frac{1}{z}$ ", " $-2z$ ", and " $-\frac{2}{3}z$ " hierarchies. More complicated members of the " $-\frac{1}{z}$ " and " $-2z$ " hierarchies of solutions are described by generalized Hermite polynomials. The generalized Hermite polynomials (see, e.g., [35]) begin with $H_{0,0} = H_{0,1} = H_{1,0} = 1$ and $H_{1,1} = 2z$ and continue by

$$2mH_{m+1,n}H_{m-1,n} = H_{m,n}H''_{m,n} - (H'_{m,n})^2 + 2mH_{m,n}^2$$

$$2nH_{m,n+1}H_{m,n-1} = -H_{m,n}H''_{m,n} + (H'_{m,n})^2 + 2nH_{m,n}^2$$

for $m, n \in \mathbb{Z}^+$. With these polynomials defined, P_{IV} has rational solutions, $u(z; \alpha, \beta)$, defined by [14]

$$\begin{aligned} u_{m,n}^{[GH;1]} &= u(z; 2m + n + 1, -2n^2) = \frac{d}{dz} \ln \left(\frac{H_{m+1,n}}{H_{m,n}} \right) \\ u_{m,n}^{[GH;2]} &= u(z; -(m + 2n + 1), -2m^2) = \frac{d}{dz} \ln \left(\frac{H_{m,n}}{H_{m,n+1}} \right) \\ u_{m,n}^{[GH;3]} &= u(z; n - m, -2(m + n + 1)^2) = -2z + \frac{d}{dz} \ln \left(\frac{H_{m,n+1}}{H_{m+1,n}} \right). \end{aligned}$$

Notice that for the choices of $(m, n) = (0, 1)$, $(m, n) = (1, 0)$ and $(m, n) = (0, 0)$ we have $u_{0,1}^{[GH;1]} = u(z; 2, -2) = \frac{1}{z}$, $u_{1,0}^{[GH;2]} = u(z; -2, -2) = -\frac{1}{z}$ and $u_{0,0}^{[GH;3]} = u(z; 0, -2) = -2z$, respectively.

Figure 3.1 contains various examples of the solutions expressible in terms of Generalized Hermite Polynomials. The images display the pole locations and their corresponding residue with dark circles for +1 and light circles for -1 (blue and yellow, respectively, where color is available).

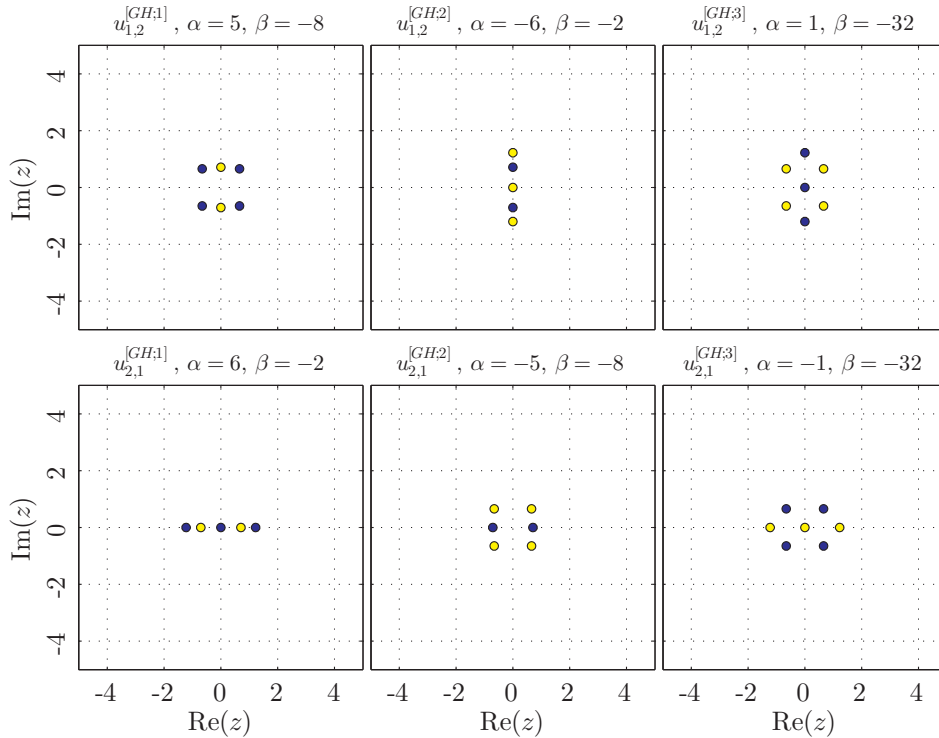


Figure 3.1: Examples of the solutions (pole locations can residues are shown) expressible in terms of Generalized Hermite Polynomials: $u_{1,2}^{[GH;1]}$ (top left), $u_{1,2}^{[GH;2]}$ (top center), $u_{1,2}^{[GH;3]}$ (top right), $u_{2,1}^{[GH;1]}$ (bottom left), $u_{2,1}^{[GH;2]}$ (bottom center), and $u_{2,1}^{[GH;3]}$ (bottom right).

The " $-\frac{2}{3}z$ " hierarchy of solutions is described by an entirely different set of polynomials. The Okamoto polynomials (see, e.g., [35]) begin with $Q_{0,0} = Q_{0,1} = Q_{1,0} = 1$ and $Q_{1,1} = \sqrt{2}z$ and continue by

$$\begin{aligned} Q_{m+1,n}Q_{m-1,n} &= \frac{9}{2} [Q_{m,n}Q''_{m,n} - (Q'_{m,n})^2] + [2z^2 + 3(2m+n-1)] Q_{m,n}^2 \\ Q_{m,n+1}Q_{m,n-1} &= \frac{9}{2} [Q_{m,n}Q''_{m,n} - (Q'_{m,n})^2] + [2z^2 + 3(1-m-2n)] Q_{m,n}^2. \end{aligned}$$

Again, with these polynomials defined, P_{IV} has rational solutions, $u(z; \alpha, \beta)$, defined by [14]

$$\begin{aligned} u_{m,n}^{[OK;1]} &= u\left(z; 2m+n, -2\left(n - \frac{1}{3}\right)^2\right) = -\frac{2}{3}z + \frac{d}{dz} \ln\left(\frac{Q_{m+1,n}}{Q_{m,n}}\right) \\ u_{m,n}^{[OK;2]} &= u\left(z; -m-2n, -2\left(m - \frac{1}{3}\right)^2\right) = -\frac{2}{3}z + \frac{d}{dz} \ln\left(\frac{Q_{m,n}}{Q_{m,n+1}}\right) \\ u_{m,n}^{[OK;3]} &= u\left(z; n-m, -2\left(m+n + \frac{1}{3}\right)^2\right) = -\frac{2}{3}z + \frac{d}{dz} \ln\left(\frac{Q_{m,n+1}}{Q_{m+1,n}}\right). \end{aligned}$$

Similar to the discussion above if we choose $(m, n) = (0, 0)$ we have $u_{0,0}^{[OK;1]} = u_{0,0}^{[OK;2]} = u_{0,0}^{[OK;3]} = u\left(z; 0, -\frac{2}{9}\right) = -\frac{2}{3}z$. Interestingly, we can achieve the $-\frac{2}{3}z$ result with any of the three possible Okamoto type solutions. Figure 3.2 displays examples of the solutions expressible in terms of the Okamoto Polynomials.

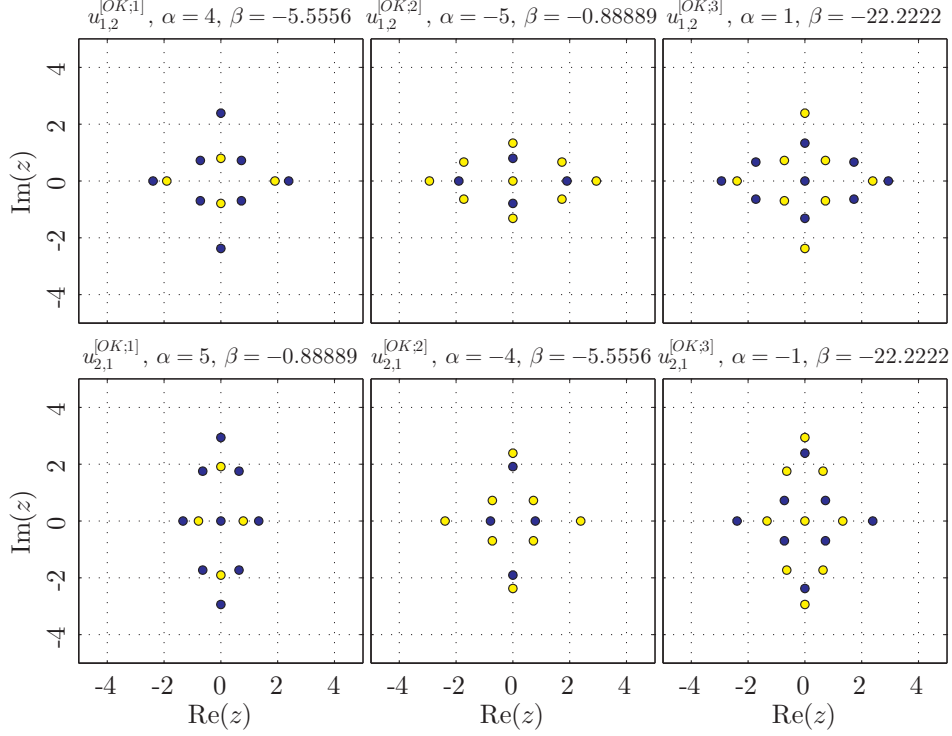


Figure 3.2: Examples of the solutions (pole locations can residues are shown) expressible in terms of Generalized Okamoto Polynomials: $u_{1,2}^{[OK;1]}$ (top left), $u_{1,2}^{[OK;2]}$ (top center), $u_{1,2}^{[OK;3]}$ (top right), $u_{2,1}^{[OK;1]}$ (bottom left), $u_{2,1}^{[OK;2]}$ (bottom center), and $u_{2,1}^{[OK;3]}$ (bottom right).

The table 3.2 summarizes which of these rational solution expressions have been verified numerically.

Solution Type	Verified?
$u_{m,n}^{[GH;k]}$, $k = 1, 2, 3$	Yes
$u_{m,n}^{[OK;k]}$, $k = 1, 2, 3$	Yes

Table 3.2: Summary of the rational solution expressions that have been verified.

3.2 Special Function Solutions

In addition to the rational solutions P_{IV} has solutions expressible in terms of parabolic cylinder functions or, equivalently, Whittaker functions (see, e.g., [38] for descriptions of these functions and their properties). Let $\epsilon = \pm 1$ and $\nu \notin \mathbb{Z}$ and let $D_\nu(\zeta)$ be the parabolic cylinder

function satisfying

$$\frac{d^2}{d\zeta^2} D_\nu(\zeta) = \left(\frac{1}{4}\zeta^2 - \nu - \frac{1}{2} \right) D_\nu(\zeta) \quad (3.1)$$

with boundary conditions

$$D_\nu(\zeta) \sim \zeta^\nu \exp\left(-\frac{1}{4}\zeta^2\right), \quad \zeta \rightarrow +\infty. \quad (3.2)$$

Also, let $W_{\kappa,\mu}(\zeta)$ and $M_{\kappa,\mu}(\zeta)$ be the Whittaker functions, which both satisfy

$$\frac{d^2}{d\zeta^2} w(\zeta) + \left(-\frac{1}{4} + \frac{\kappa}{\zeta} + \frac{\frac{1}{4} - \mu^2}{\zeta^2} \right) w(\zeta) = 0.$$

P_{IV} has solutions, $u(z; \alpha, \beta)$, given by [14]

$$u_{\nu,\epsilon,d_1,d_2}^{[PC;1]} = u(z; -\epsilon(\nu+1), -2\nu^2) = -\epsilon \frac{d}{dz} \ln(\psi_\nu(z; \epsilon)) \quad (3.3)$$

$$u_{\nu,\epsilon,d_1,d_2}^{[PC;2]} = u(z; -\epsilon\nu, -2(\nu+1)^2) = -2z + \epsilon \frac{d}{dz} \ln(\psi_\nu(z; \epsilon)) \quad (3.4)$$

with

$$\begin{aligned} \psi_\nu(z; \epsilon) &= \left[d_1 D_\nu(\sqrt{2\epsilon z}) + d_2 D_\nu(-\sqrt{2\epsilon z}) \right] \exp\left(\frac{1}{2}\epsilon z^2\right) \\ &= \left[\tilde{d}_1 M_{\frac{1}{2}\nu+\frac{1}{4}, \frac{1}{4}}(\epsilon z^2) + \tilde{d}_2 W_{\frac{1}{2}\nu+\frac{1}{4}, \frac{1}{4}}(\epsilon z^2) \right] \frac{\exp(\frac{1}{2}\epsilon z^2)}{z^{\frac{1}{2}}} \end{aligned}$$

and d_1 , d_2 , \tilde{d}_1 and \tilde{d}_2 arbitrary constants related by

$$\begin{aligned} \tilde{d}_1 &= \frac{\sqrt{\pi} 2^{\frac{1}{2}\nu+2}}{\epsilon^{\frac{1}{4}} \Gamma(-\frac{1}{2}\nu)} d_2 \\ \tilde{d}_2 &= \frac{2^{\frac{1}{2}\nu}}{\epsilon^{\frac{1}{4}}} (d_1 + d_2). \end{aligned}$$

Substituting $\psi_\nu(z; \epsilon)$ into $u_{\nu,\epsilon,d_1,d_2}^{[PC;k]}$, $k = 1, 2$, it is easy to see that d_1 and d_2 (likewise, \tilde{d}_1 and \tilde{d}_2) can be combined into a single parameter $D = \frac{d_2}{d_1}$ ($\tilde{D} = \frac{\tilde{d}_2}{\tilde{d}_1}$). This is helpful in viewing the various behaviors of these solutions when varying the parameters, therefore such solutions will now be renamed $u_{\nu,\epsilon,D}^{PC,k}$, $k = 1, 2$. Figures 3.3 through 3.6 exhibit the different types of solutions $u_{\nu,\epsilon,D}^{[PC;k]}$ that can be obtained by changing D , ϵ , ν , and k .

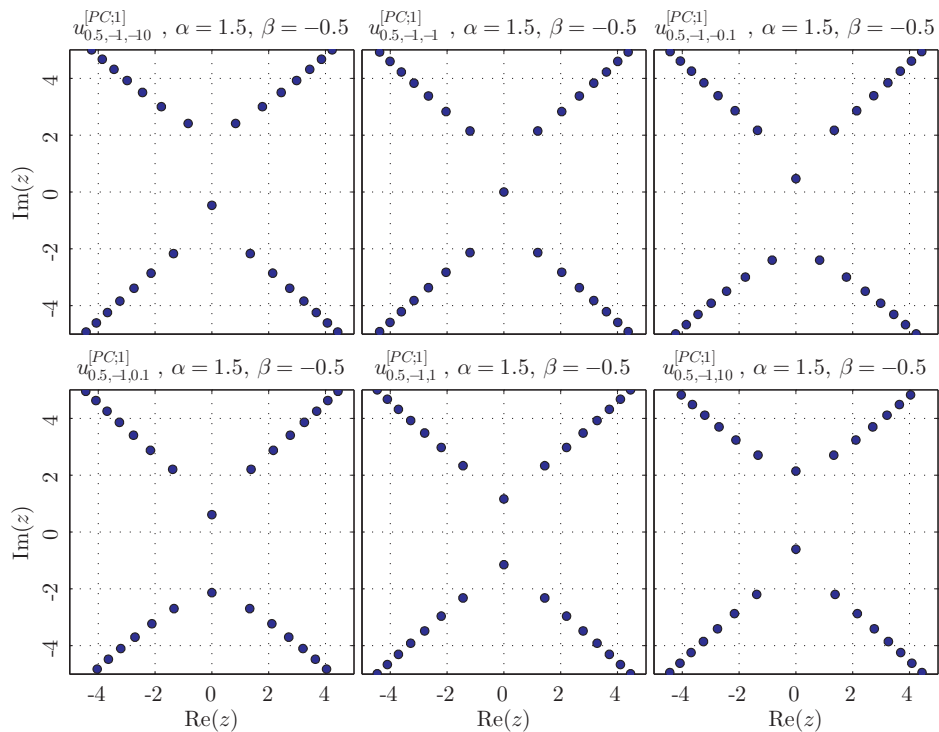


Figure 3.3: Examples of the solutions (pole locations can residues are shown) expressible in terms of the parabolic cylinder function. Here $k = 1$, $\nu = 0.5$ and $\epsilon = -1$ for all figures as D is varied.

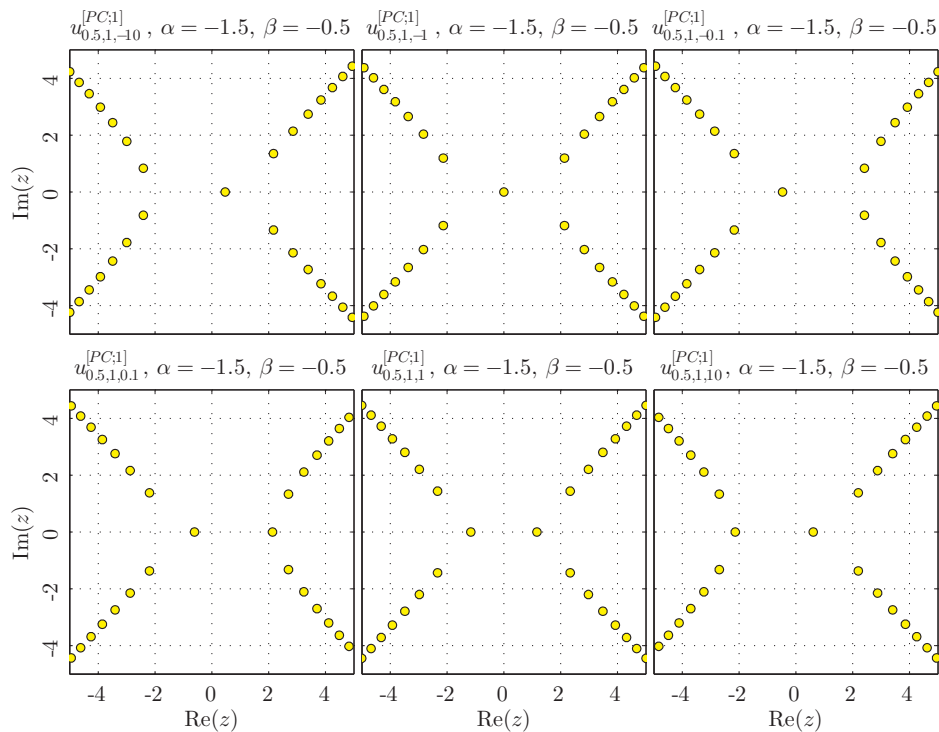


Figure 3.4: Examples of the solutions (pole locations can residues are shown) expressible in terms of the parabolic cylinder function. Here $k = 1$, $\nu = 0.5$ and $\epsilon = 1$ for all figures as D is varied.

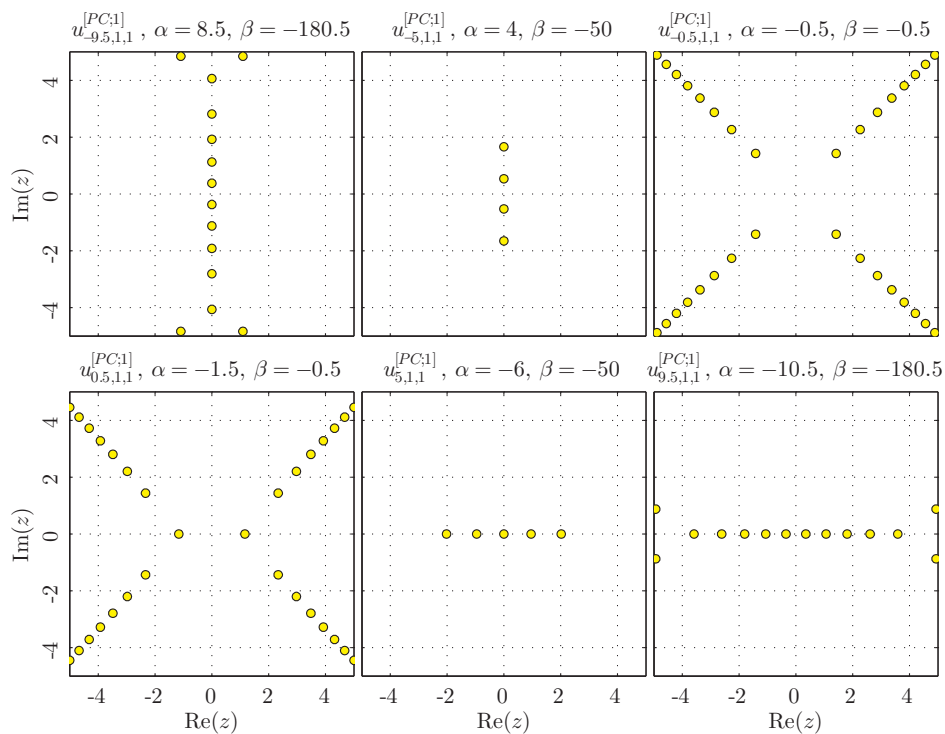


Figure 3.5: Examples of the solutions (pole locations can residues are shown) expressible in terms of the parabolic cylinder function. Here $k = 1$, $\epsilon = 1$, and $D = 1$ and ν is varied.

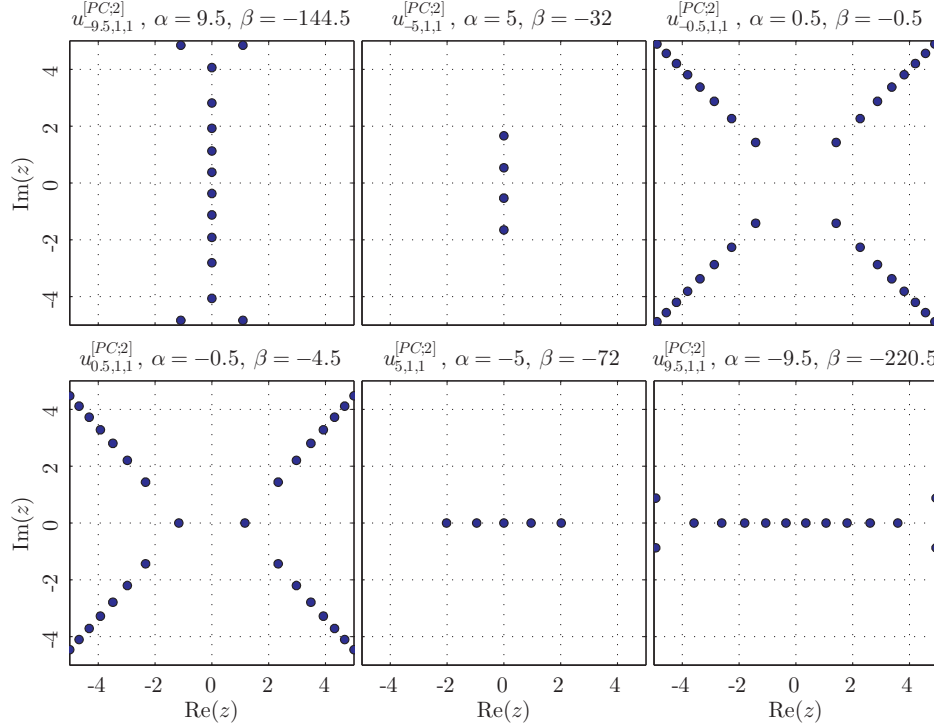


Figure 3.6: Examples of the solutions (pole locations can residues are shown) expressible in terms of the parabolic cylinder function. Here $k = 2$, $\epsilon = 1$ and $D = 1$ and ν is varied. Notice that when $k = 2$, the residue of the poles corresponding to the choice of ϵ is opposite that resulting from the choice of ϵ for $k = 1$.

Particular choices of $\nu \in \mathbb{R}$ allow the solutions $u_{\nu,\epsilon,D}^{[PC;1]}$ and $u_{\nu,\epsilon,D}^{[PC;2]}$ to be expressed in simpler forms. For instance, if $\nu \in \mathbb{Z}^+$ it is shown that the special function solutions reduce to [14]

$$u_{\nu,\epsilon}^{[SH;1]} = u(z; \epsilon(\nu + 1), -2\nu^2) = -\epsilon \frac{d}{dz} \ln (H_\nu(\sqrt{\epsilon}z)) \quad (3.5a)$$

$$u_{\nu,\epsilon}^{[SH;2]} = u(z; -\epsilon\nu, -2(\nu + 1)^2) = -2z + \epsilon \frac{d}{dz} \ln (H_\nu(\sqrt{\epsilon}z)), \quad (3.5b)$$

where

$$H_n(z) = (-1)^n \exp(z^2) \frac{d^n}{dz^n} (\exp(-z^2)),$$

$n \in \mathbb{Z}^+$, is the standard Hermite polynomial (see, e.g., [38]). For examples of the standard Hermite polynomial solutions see figure 3.7.

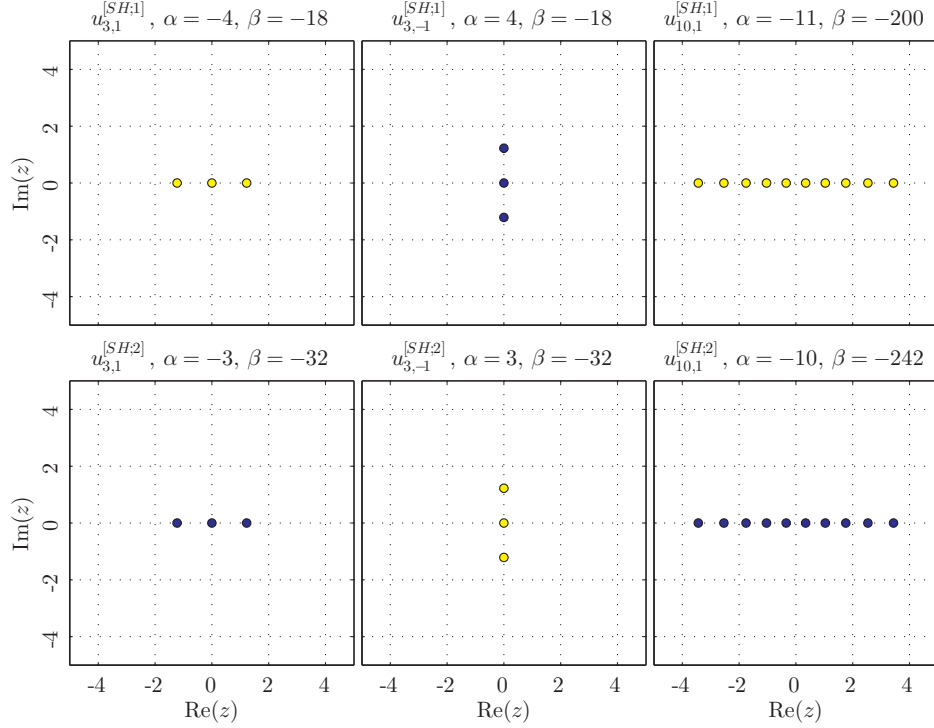


Figure 3.7: Examples of the solutions expressible in terms of standard Hermite polynomials: $u_{3,1}^{[SH;1]}$ (top left), $u_{3,-1}^{[SH;1]}$ (top middle), $u_{10,1}^{[SH;1]}$ (top right), $u_{3,1}^{[SH;2]}$ (bottom left), $u_{3,-1}^{[SH;2]}$ (bottom middle), and $u_{10,1}^{[SH;2]}$ (bottom right) (pole locations can residues are shown).

Also, if $\nu = 0$ then the solutions of P_{IV} can be expressed as [14]

$$u_D^{[CE;1]} = u(z; 1, 0) = -\frac{2 \exp(-z^2)}{\sqrt{\pi} (D + \operatorname{erfc}(z))}$$

$$u_D^{[CE;2]} = u(z; -1, 0) = \frac{2i \exp(z^2)}{\sqrt{\pi} (D + \operatorname{erfc}(iz))},$$

where

$$\operatorname{erfc}(z) = 1 - \operatorname{erf}(z) = \frac{2}{\sqrt{\pi}} \int_z^\infty \exp(-t^2) dt$$

is the complementary error function (see, e.g., [38]). For examples of the complementary error function solutions see figure 3.8.

There is also a so-called “half-integer hierarchy” [14] that is expressed in terms of parabolic cylinder functions and can be found simply by considering $u_{-\frac{1}{2},1}^{[PC;k]}$, $k = 1, 2$, as the simplest members.

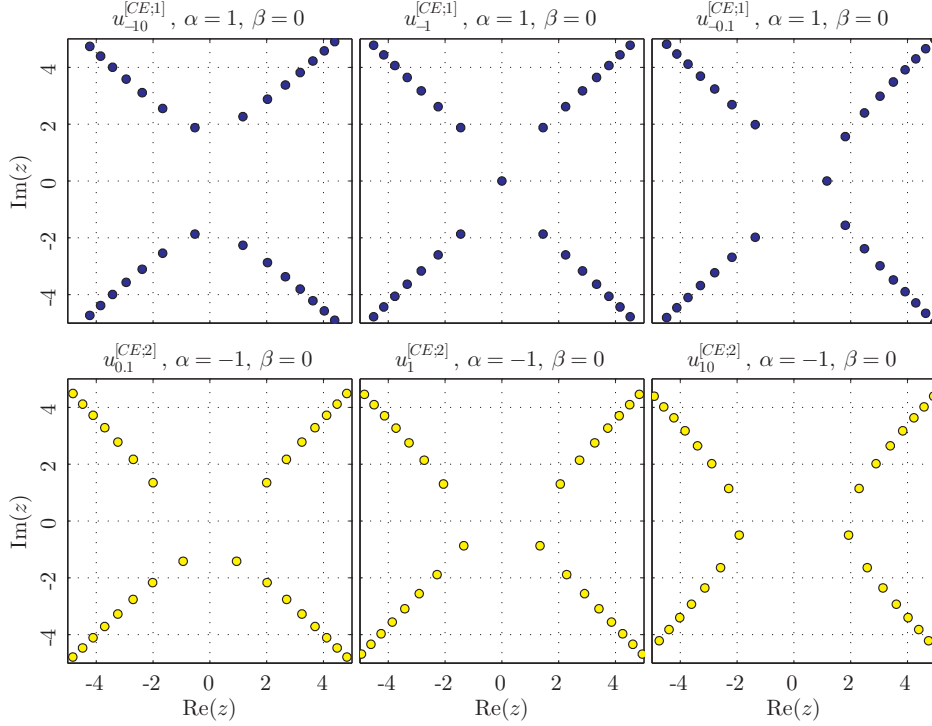


Figure 3.8: Examples of the solutions expressible in terms of the complementary error function: $u_{-10}^{[CE;1]}$ (top left), $u_{-1}^{[CE;1]}$ (top middle), $u_{-0.1}^{[CE;1]}$ (top right), $u_{0.1}^{[CE;2]}$ (bottom left), $u_1^{[CE;2]}$ (bottom middle), and $u_{10}^{[CE;2]}$ (bottom right) (pole locations can residues are shown).

Now, in [14], [15], [21], and [37] further classes of solutions in terms of the parabolic cylinder function are presented. Define

$$\tau_{n,\nu}(z; \epsilon) = \mathcal{W} \left(\psi_\nu(z; \epsilon), \frac{d}{dz} \psi_\nu(z; \epsilon), \dots, \frac{d^{n-1}}{dz^{n-1}} \psi_\nu(z; \epsilon) \right),$$

with $n \in \mathbb{Z}$, $\psi_\nu(z; \epsilon)$ defined as above, and \mathcal{W} the Wronskian determinant, then it is stated in [15] that solutions of P_{IV} can also be written as

$$\begin{aligned} u_{\nu,\epsilon,n}^{[WD;1]} &= u(z; \epsilon(2n - \nu), -2(\nu + 1)^2) = -2z + \epsilon \frac{d}{dz} \ln \left(\frac{\tau_{n+1,\nu}(z; \epsilon)}{\tau_{n,\nu}(z; \epsilon)} \right) \\ u_{\nu,\epsilon,n}^{[WD;2]} &= u(z; \epsilon(2\nu - n), -2(n + 1)^2) = \epsilon \frac{d}{dz} \ln \left(\frac{\tau_{n,\nu}(z; \epsilon)}{\tau_{n,\nu+1}(z; \epsilon)} \right) \\ u_{\nu,\epsilon,n}^{[WD;3]} &= u(z; -\epsilon(n + \nu), -2(\nu - n + 1)^2) = \epsilon \frac{d}{dz} \ln \left(\frac{\tau_{n,\nu+1}(z; \epsilon)}{\tau_{n+1,\nu}(z; \epsilon)} \right). \end{aligned}$$

However, consider even $n = 1$. Then $u_{\nu,\epsilon,1}^{[WD;k]}$, $k = 1, 2, 3$ can be evaluated easily for an initial condition at some point $z_0 \in \mathbb{C}$ to start the pole field solver. If these are indeed solutions to P_{IV} ,

then the solution should not change (for fixed ν , ϵ , n , d_1 and d_2) if z_0 is changed. However, we do not find this to be the case when $k = 2, 3$. For each $k = 1, 2, 3$ the solutions $u_{-\frac{1}{2},1,1}^{[WD;k]}$ are given in figures 3.9, 3.10, and 3.11, respectively, for various z_0 . Notice that no two frames are the same in figures 3.10 and 3.11 suggesting that the expressions $u_{\nu,\epsilon,n}^{[WD;k]}$, $k = 2, 3$, may be incorrect. On the other hand, all frames in each row of figure 3.9 are identical, indicating that the expression $u_{\nu,\epsilon,n}^{[WD;1]}$ is correct.

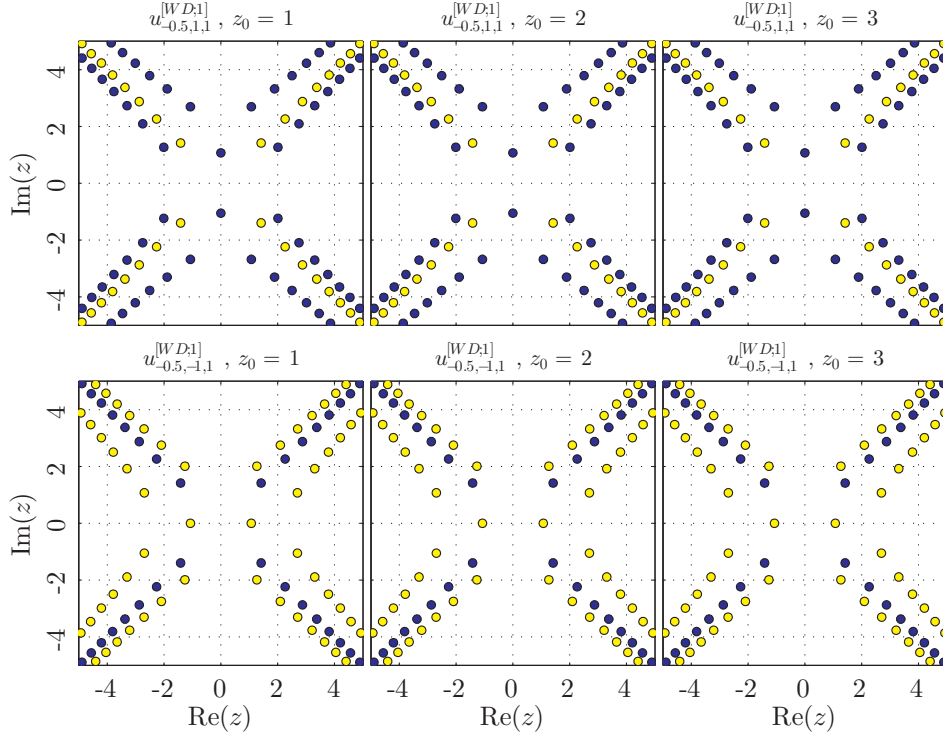


Figure 3.9: Examples of the numerical solutions $u_{-\frac{1}{2},\epsilon,1}^{[WD;1]}$ (pole locations can residues are shown) starting with high precision initial conditions from $u_{-\frac{1}{2},\epsilon,1}^{[WD;1]}$ computed at $z = z_0$. In this case $(\alpha = \frac{5}{2}, \beta = -\frac{1}{2})$ (top) and $(\alpha = -\frac{5}{2}, \beta = -\frac{1}{2})$ (bottom). In each row the frames are identical indicating that the expression $u_{\nu,\epsilon,n}^{[WD;1]}$ is correct.

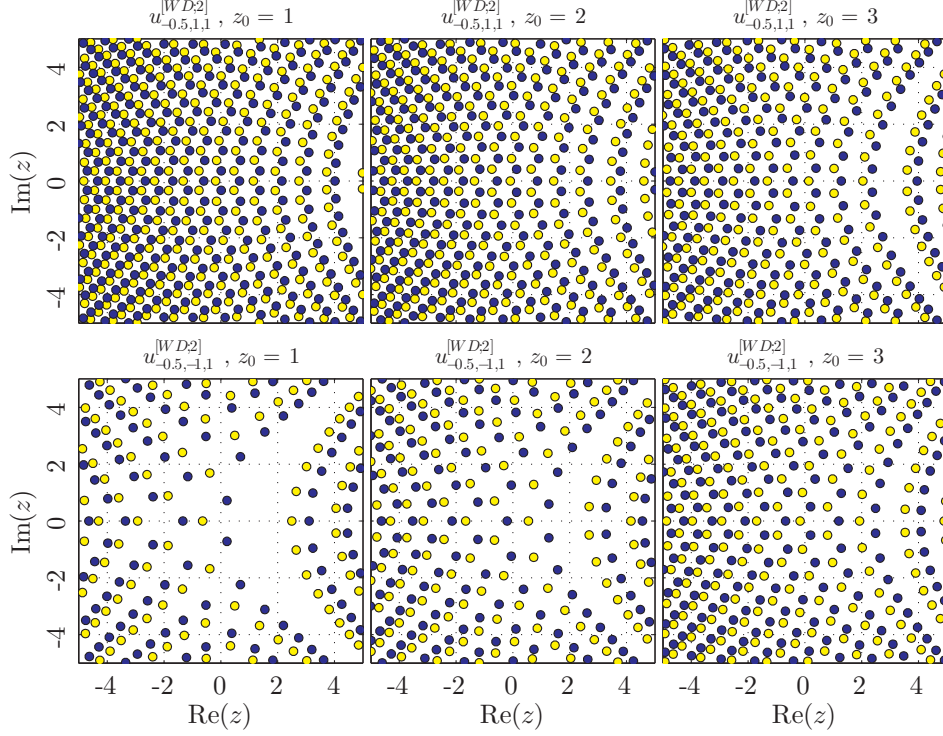


Figure 3.10: Examples of the numerical solutions $u_{-\frac{1}{2},\epsilon,1}^{[WD;2]}$ (pole locations can residues are shown) starting with high precision initial conditions from $u_{-\frac{1}{2},\epsilon,1}^{[WD;2]}$ computed at $z = z_0$. In this case ($\alpha = -2, \beta = -8$) (top) and ($\alpha = 2, \beta = -8$) (bottom). In each row no two frames are the same indicating that we cannot verify the expression $u_{\nu,\epsilon,n}^{[WD;2]}$.

Solutions described by confluent hypergeometric functions were recently found [9], [10], and [11] and the parameter choices leading to these solutions are a subset of those generating $u_{\nu,\epsilon,n}^{[WD;1]}$.

Let

$$v_0(z) = e^{-\frac{1}{2}z^2} \left({}_1F_1 \left(-\frac{1}{2}\nu, \frac{1}{2}; z^2 \right) + 2z \frac{\Gamma(-\frac{1}{2}\nu + \frac{1}{2})}{\Gamma(-\frac{1}{2}\nu)} (c_1 + ic_2) {}_1F_1 \left(-\frac{1}{2}\nu + \frac{1}{2}, \frac{3}{2}; z^2 \right) \right),$$

where $n \in \mathbb{Z}^+$, $\nu, c_1, c_2 \in \mathbb{R}$ and ${}_1F_1$ is the confluent hypergeometric function [38, Chapter 13]. To make the notation of [11] explicit, we define for $j = 1, 2, \dots$,

$$v_j(z) = \frac{1}{\sqrt{2}} \left(\frac{d}{dz} v_{j-1}(z) + z v_{j-1}(z) \right).$$

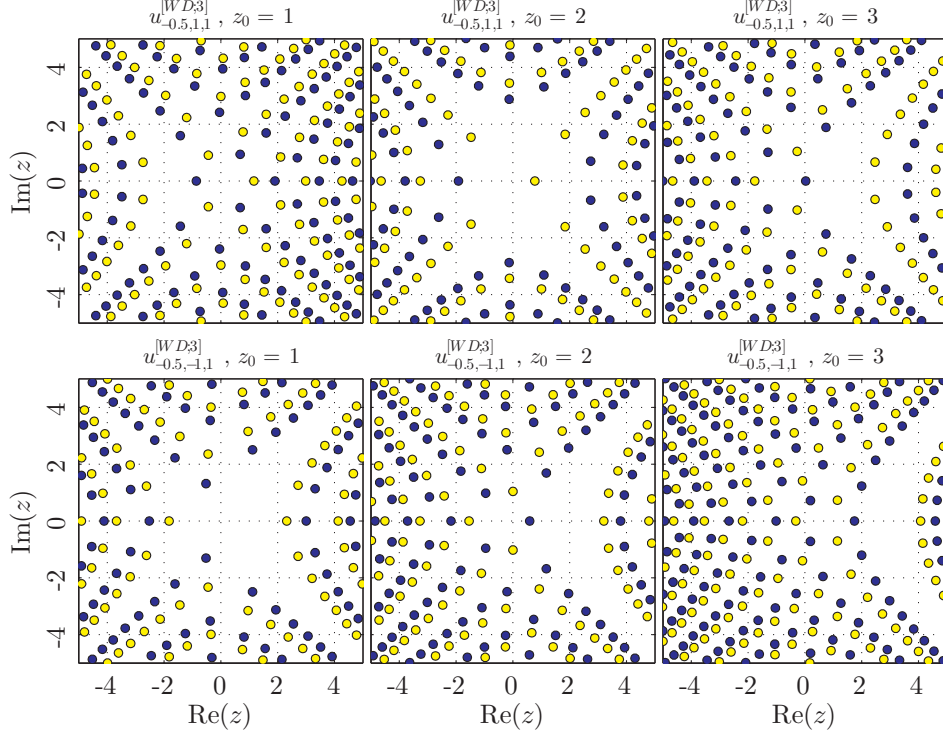


Figure 3.11: Examples of the numerical solutions $u_{-\frac{1}{2},\epsilon,1}^{[WD;3]}$ (pole locations can residues are shown) starting with high precision initial conditions from $u_{-\frac{1}{2},\epsilon,1}^{[WD;3]}$ computed at $z = z_0$. In this case ($\alpha = -\frac{1}{2}, \beta = -\frac{1}{2}$) (top) and ($\alpha = \frac{1}{2}, \beta = -\frac{1}{2}$) (bottom). In each row no two frames are the same indicating that we cannot verify the expression $u_{\nu,\epsilon,n}^{[WD;2]}$.

Then P_{IV} has solutions [11]

$$u_{\nu,n,c_1,c_2}^{[CH;1]} = u(z; 2n - \nu, -2(\nu + 1)^2) = -z - \frac{d}{dz} \ln \left(\frac{\mathcal{W}(v_0(z), v_1(z), \dots, v_{n-1}(z))}{\mathcal{W}(v_0(z), v_1(z), \dots, v_n(z))} \right), \quad (3.6)$$

$n > 0$ with \mathcal{W} the Wronskian determinant, which can be reduced to [11]

$$u_{\nu,0,c_1,c_2}^{[CH;1]} = u(z; -\nu, -2(\nu + 1)^2) = -z + \frac{d}{dz} \ln(v_0(z)),$$

in the case of $n = 0$. Further, if $c_2 = 0$ (chosen to arrive at solutions that are real along the real axis) a one parameter family of solutions $P_{IV}(2n - \nu, -2(\nu + 1)^2)$ exists for each fixed value of ν and n . For examples of the confluent hypergeometric function solutions see figures 3.12 through 3.15.

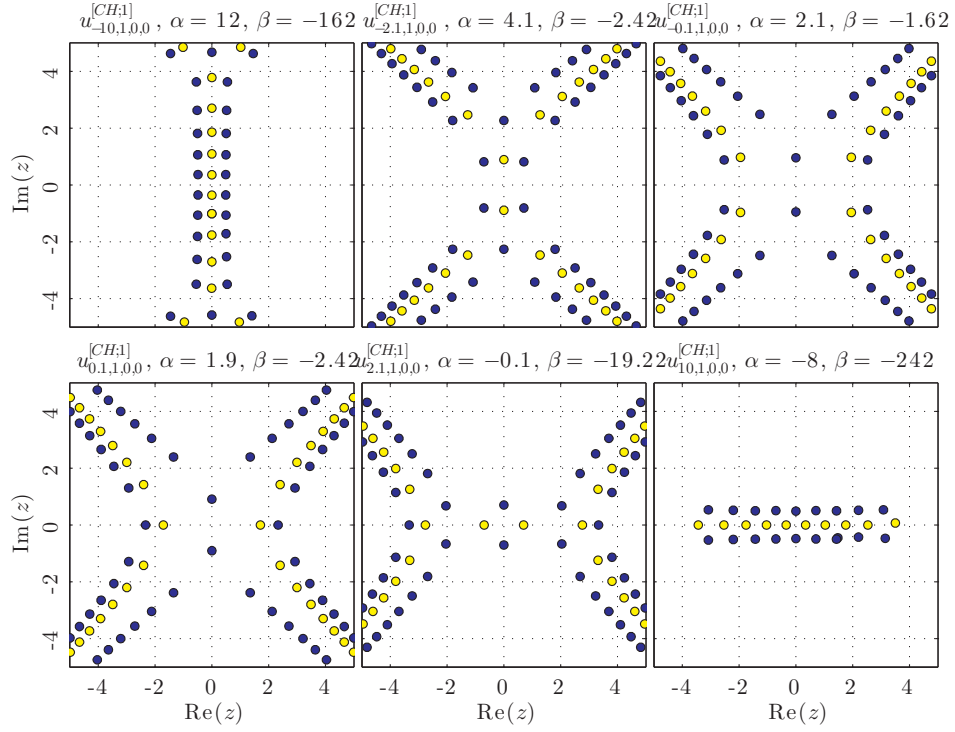


Figure 3.12: Examples of the solutions (pole locations can residues are shown) expressible in terms of confluent hypergeometric function. This figure shows what happens to the solutions as ν is varied with $n = 1$, $c_1 = 0$, and $c_2 = 0$. Only pole locations and residues are shown with dark (blue) circles indicating residue of +1 and light (yellow) circles residue of -1.

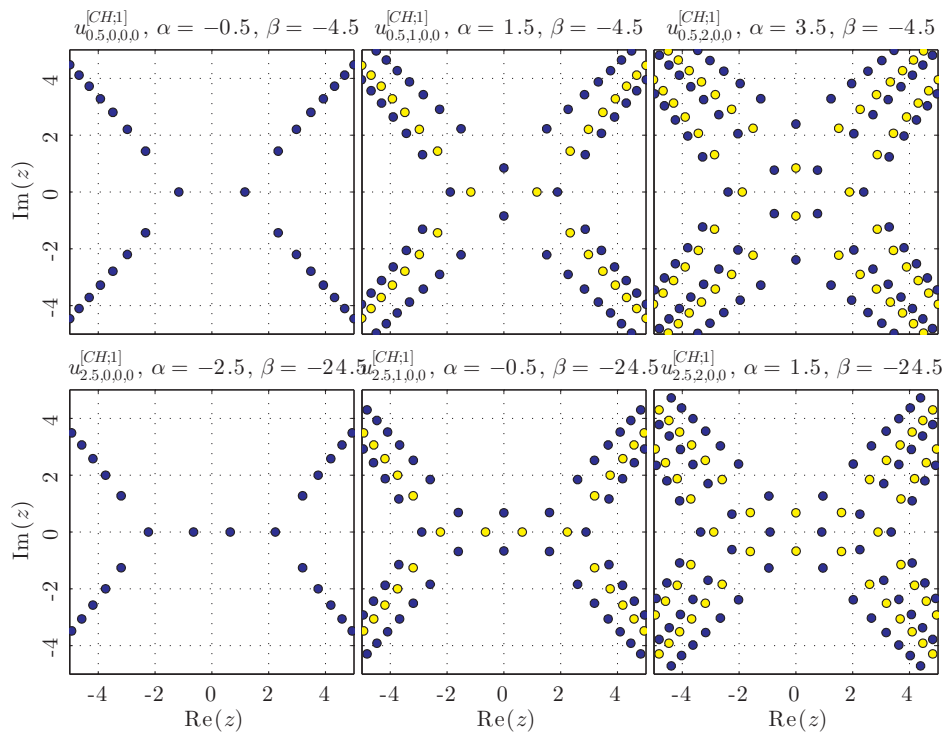


Figure 3.13: Examples of the solutions expressible in terms of confluent hypergeometric function. This figure shows what happens to the solutions as n is varied with $\nu = 0.5$, $c_1 = 0$, and $c_2 = 0$. Only pole locations and residues are shown with dark (blue) circles indicating residue of $+1$ and light (yellow) circles residue of -1 .

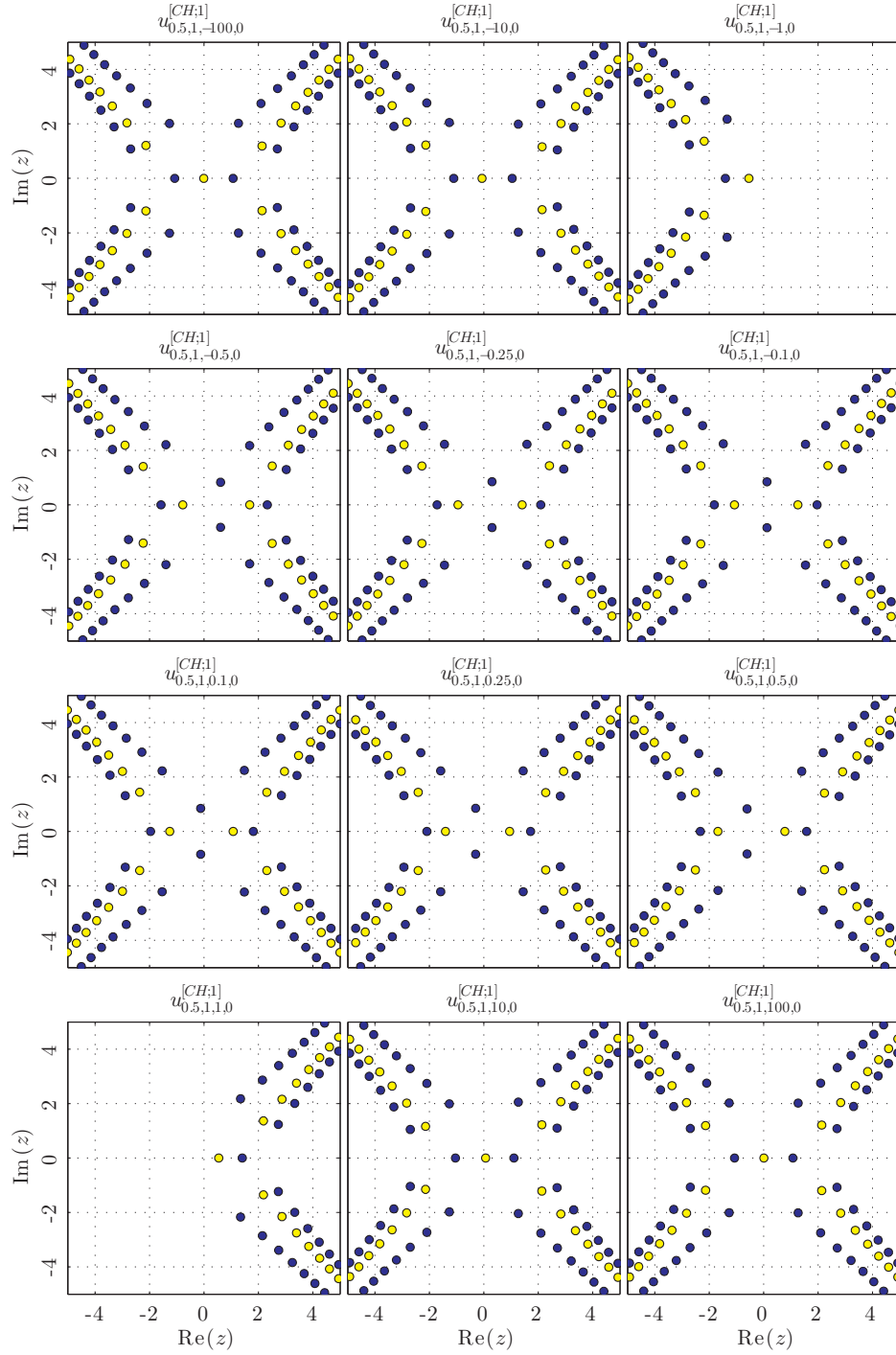


Figure 3.14: Examples of the solutions (pole locations can residues are shown) expressible in terms of confluent hypergeometric and gamma functions. All solutions occur for $\alpha = 0.5$ and $\beta = -12.5$. This figure shows what happens to the solutions as c_1 is varied with $\nu = 0.5$, $n = 1$, and $c_2 = 0$. Only pole locations and residues are shown with dark (blue) circles indicating residue of +1 and light (yellow) circles residue of -1.

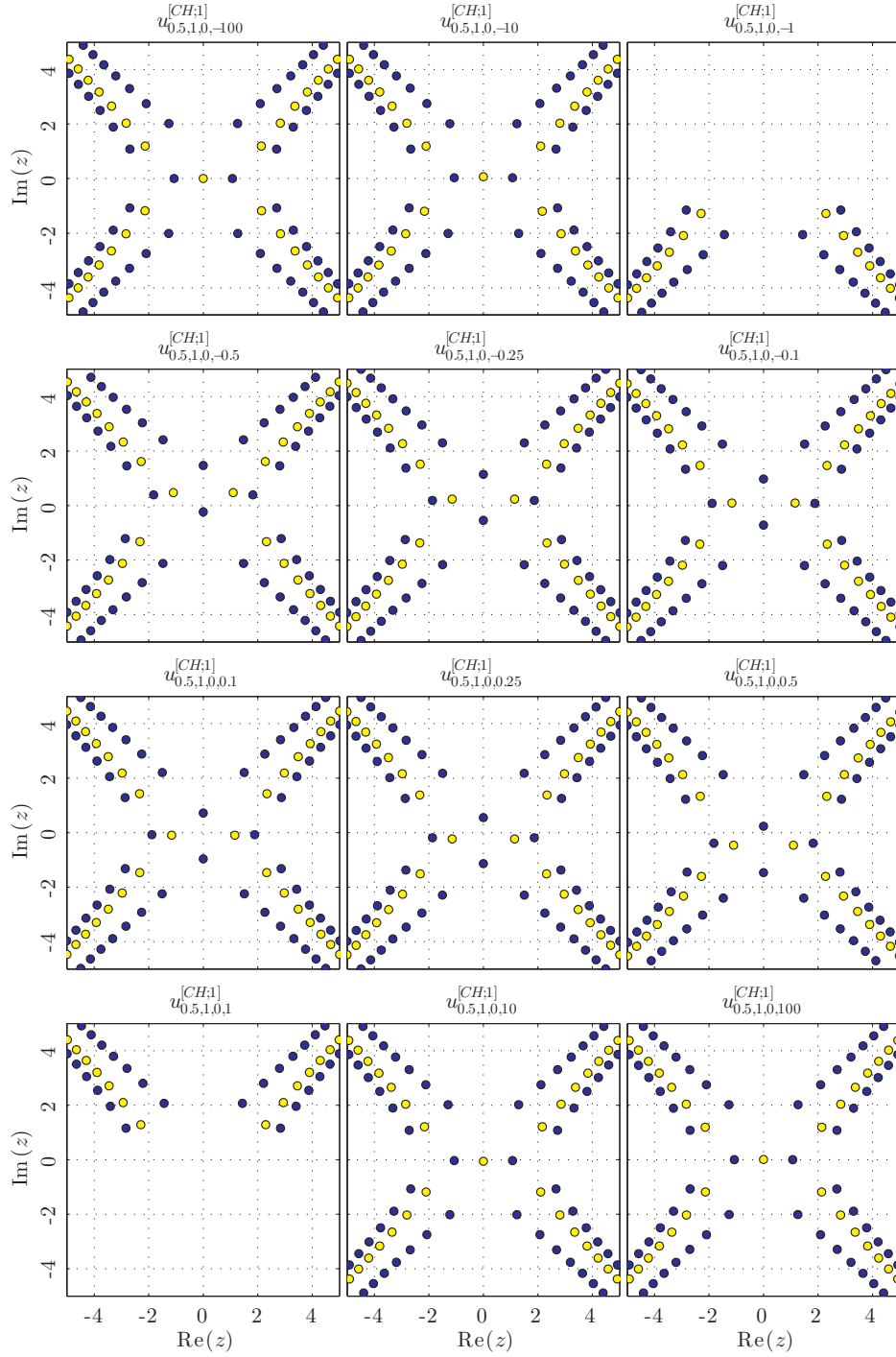


Figure 3.15: Examples of the solutions (pole locations can residues are shown) expressible in terms of confluent hypergeometric and gamma functions. All solutions occur for $\alpha = 0.5$ and $\beta = -12.5$. This figure shows what happens to the solutions as c_2 is varied with $\nu = 0.5$, $n = 1$, and $c_1 = 0$. Only pole locations and residues are shown with dark (blue) circles indicating residue of +1 and light (yellow) circles residue of -1.

We stated earlier that the solutions $u_{\nu,n,c_1,c_2}^{[CH;1]}$ are a subset of $u_{\nu,\epsilon,n}^{[WD;1]}$. In fact, when $n = 0$ and

$\epsilon = 1$ we can choose [42]

$$d_1 = 2\sqrt{2} - 2\sqrt{2}(c_1 + ic_2)$$

$$d_2 = 2\sqrt{2} + 2\sqrt{2}(c_1 + ic_2)$$

to arrive at identical solutions.

The table 3.3 summarizes whether each of the expressions in terms of special functions have been verified.

Solution Type	Verified?
$u_{\nu,\epsilon,d_1,d_2}^{[PC;k]}$, $k = 1, 2$	Yes
$u_{\nu,\epsilon}^{[SH;k]}$, $k = 1, 2$	Yes
$u_D^{[CE;k]}$, $k = 1, 2$	Yes
$u_{\nu,n,c_1,c_2}^{[CH;1]}$	Yes
$u_{\nu,\epsilon,n}^{[WD;1]}$	Yes
$u_{\nu,\epsilon,n}^{[WD;k]}$, $k = 2, 3$	No

Table 3.3: Summary of the special function solution expressions that have been verified.

3.3 The Weyl Chambers

The known symmetries, solution transformations, and closed form solutions provide a key for describing the parameter space of P_{IV} with $\beta \leq 0$. They allow the (α, β) space to be described by the so-called Weyl chambers (see e.g., [11], [13, Section II-A], [26, Section 26]), which feature a complete regularity in the $(\alpha, \sqrt{-2\beta})$ -plane. The right frame of figure 1.1 shows this regularity (i.e. the Weyl chambers are the regular triangular regions), while both frames show the locations of all of the (α, β) pairs described in the literature, and repeated in chapter 3, leading to rational and special function solutions. For instance, the dark (blue)/light (yellow) hexagrams indicate the parameter values that admit instances of solutions described by Generalized Hermite/Okamoto polynomials. Similarly, the parameter choices along the black lines admit special function solutions that are described by combinations of either parabolic cylinder functions or confluent hypergeometric functions. Finally, along the line $\sqrt{-2\beta} = 0$ (i.e. $\beta = 0$), which is not drawn explicitly, the decaying asymptotic conditions discussed later in section 4.1 occur.

When extended to complex α and β a single chamber in theory provides all of the necessary information to construct solutions for every arbitrary (α, β) pair. Gromak, et al, state in [26, Section 25], “To construct the solutions of P_{IV} for arbitrary values of parameters (α, β) it is sufficient to construct solutions for every (α, β) in the domain

$$\mathcal{F} := \left\{ (\alpha, \beta) \mid 0 \leq \operatorname{Re}(\alpha) \leq 1, \operatorname{Re}(\sqrt{-2\beta}) \geq 0, \operatorname{Re}(\sqrt{-2\beta} + 2\alpha) \leq 2 \right\}.” \quad (3.7)$$

Then it is only a matter of applying the transformations of section 2.3 to the solutions in the fundamental domain.

The region \mathcal{F} (for $\alpha, \beta \in \mathbb{R}$) is indicated by the shaded region in either frame of figure 1.1. Every parameter choice either marking a closed form solution or satisfying the asymptotic approximation (4.2) occurs for $\beta \leq 0$. Therefore, part of this study will be devoted to the unexplored region of $\beta > 0$.

Chapter 4

Asymptotic Approximations

Much of the early computational work on PIV has been completed to verify its asymptotic approximations that had no poles on the real axis. This was likely done because of the difficulty experienced by typical ODE solvers when encountering a pole. For instance, Bassom, et al, [6] explore solutions with very particular parameter choices using a classical fourth order Runge-Kutta scheme, a sixth-order scheme, and an Adams Moulton predictor-corrector method, each of which are rendered useless after encountering a pole. The particular parameter choices will be discussed in the following subsections.

4.1 Asymptotically Decaying Solutions

We now consider the special case of P_{IV} with only the parameters $\alpha \in \mathbb{R}$ and $\beta = 0$. This particular form of P_{IV} is presented in [38, Section 32.11] and is in contrast to those presented in [6] and [14], where the change of variables

$$u(z) = 2\sqrt{2}w(x)^2 \text{ and } z = \frac{1}{2}\sqrt{2}x$$

is applied. We also impose the boundary conditions

$$u(z) \rightarrow 0, \text{ as } z \rightarrow +\infty. \tag{4.1}$$

The NIST handbook [38] suggests that any nontrivial solution of P_{IV} with $\beta = 0$ satisfying (4.1) is asymptotic to

$$k \left[D_{\frac{1}{2}\alpha - \frac{1}{2}}(\sqrt{2}z) \right]^2 \text{ as } z \rightarrow +\infty \text{ and } k \neq 0. \tag{4.2}$$

$D_\nu(\zeta)$ is as described previously in (3.1) and (3.2).

There is a critical value of k given by [38]

$$k^* = \frac{1}{\sqrt{\pi}\Gamma(\frac{1}{2}\alpha + \frac{1}{2})}$$

such that when $0 \leq k < k^*$ there are no poles on the real axis. We can further distinguish between two cases for α for this choice of k . First, if $\alpha \in \mathbb{Z}^+$ and odd, then $u(z)$ is asymptotic to $k2^{\frac{1}{2}\alpha - \frac{1}{2}}z^{\alpha-1}\exp(-z^2)$ as $z \rightarrow -\infty$. Otherwise, $u(z)$ is asymptotic to $-\frac{2}{3}z + \frac{4}{3}d\sqrt{3}\sin(\phi(z) - \theta_0) + O(z^{-1})$ for $z \rightarrow -\infty$, where $\phi(z) = \frac{1}{3}\sqrt{3}z^2 - \frac{4}{3}d^2\sqrt{3}\ln(\sqrt{2}|z|)$. Here we define d and θ_0 by the connection formulas given by $d^2 = -\frac{1}{4}\sqrt{3}\pi^{-1}\ln(1 - |\mu|^2)$ and $\theta_0 = \frac{1}{3}d^2\sqrt{3}\ln(3) + \frac{1}{3}\pi\alpha + \frac{1}{4}\pi + \arg(\mu) + \arg(\Gamma(-\frac{2}{3}i\sqrt{3}d^2))$, where $\mu = 1 - \frac{2k\pi^{3/2}\exp(-i\frac{\pi}{2}\alpha)}{\Gamma(-\frac{1}{2}\alpha + \frac{1}{2})}$. Next, for $k = k_*$, $u(z)$ again has no poles on the real axis and is asymptotic to $-2z$ for $z \rightarrow -\infty$. Finally, if $k > k^*$, then $u(z)$ has poles on the real axis whose locations are dependent on k .

4.2 General Asymptotic Approximations

Applying the method of dominant balance (see, e.g., [8, Section 3.4]) to P_{IV} , assuming that $\frac{d^2}{dz^2}u(z)$ and $\frac{1}{2u(z)}\left(\frac{d}{dz}u(z)\right)^2$ are small relative to the remaining terms as $z \rightarrow +\infty$ (likewise, $z \rightarrow -\infty$) leads to the quartic equation

$$\frac{3}{2}w(z)^4 + 4zw(z)^3 + 2(z^2 - \alpha)w(z)^2 + \beta = 0. \quad (4.3)$$

with solutions

$$w_\mu^\pm(z; \alpha, \beta) = -\frac{2}{3}z \pm \frac{1}{2}f(z) + \mu\frac{1}{2}\sqrt{g(z) \mp \frac{32(3\alpha z + z^3)}{27f(z)}}, \quad (4.4)$$

where

$$\begin{aligned} f(z) &= \sqrt{\frac{8}{9}(\alpha + z^2) + \frac{2^{\frac{1}{3}}(72\beta + 16(\alpha - z^2)^2)}{9a(z)} + \frac{1}{9 \times 2^{\frac{1}{3}}}a(z)}, \\ g(z) &= \frac{16}{9}(\alpha + z^2) - \frac{2^{\frac{1}{3}}(72\beta + 16(\alpha - z^2)^2)}{9a(z)} - \frac{1}{9 \times 2^{\frac{1}{3}}}a(z), \\ a(z) &= \left(64b(z) + \sqrt{-4(72\beta + 16(\alpha - z^2)^2)^3 + 4096b(z)^2}\right)^{\frac{1}{3}}, \\ b(z) &= 54\beta z^2 + 27\beta(\alpha - z^2) - 2(\alpha - z^2)^3, \end{aligned}$$

and $\mu = \pm 1$. The roots of (4.3) supply asymptotic approximations as $z \rightarrow \pm\infty$, $z \in \mathbb{R}$, and any choice of α and β . Asymptotic expansion as $z \rightarrow +\infty$ reveals that for all α and β

$$w_{+1}^+(z; \alpha, \beta) = \frac{\sqrt{-2\beta}}{2z} + \frac{\alpha\sqrt{-2\beta} + 2\beta}{4z^3} + O\left(\frac{1}{z^5}\right) \quad (4.5)$$

$$w_{-1}^+(z; \alpha, \beta) = -\frac{\sqrt{-2\beta}}{2z} + \frac{-\alpha\sqrt{-2\beta} + 2\beta}{4z^3} + O\left(\frac{1}{z^5}\right) \quad (4.6)$$

$$w_{+1}^-(z; \alpha, \beta) = -\frac{2}{3}z + \frac{\alpha}{z} - \frac{2(2\alpha^2 + 3\beta)}{8z^3} + O\left(\frac{1}{z^5}\right) \quad (4.7)$$

$$w_{-1}^-(z; \alpha, \beta) = -2z - \frac{\alpha}{z} + \frac{6\alpha^2 + \beta}{8z^3} + O\left(\frac{1}{z^5}\right). \quad (4.8)$$

Only the latter two roots are available as asymptotic approximations when $\beta > 0$ if we wish to consider only solutions that are real along the real axis. Later in this thesis, ICs leading to solutions asymptotic to (4.5)-(4.8) will be marked in several figures, described as pole counting diagrams, as follows: w_{+1}^+ with dark (blue) diamonds, w_{-1}^+ light (yellow) diamonds, w_{+1}^- light (yellow) circles, and w_{-1}^- dark (blue) circles. For simplicity, these asymptotic behaviors will be presented only as $z \rightarrow +\infty$, $z \in \mathbb{R}$, although the symmetry (2.2) indicates that there are solutions satisfying analogous asymptotic behaviors as $z \rightarrow -\infty$. The expansions (4.5)-(4.8) can be shown to be consistent with the assumptions made in their derivations. No other smooth behaviors than these were observed for alpha and beta non-zero. However, in the case of $\beta = 0$, parabolic cylinder functions arise from a dominant balance that keeps the second derivative term.

Chapter 5

Computing solutions to IVPs and BVPs of the Painlevé Equations

5.1 The Pole Field Solver

The extensive pole fields appearing in the solutions of the Painlevé equations have motivated the development of various solution techniques over the years since their discovery. Many of the previous methods were limited in the choice of α and β by considering special forms of the equation (e.g. Riemann Hilbert problems [39]), constrained to the real axis (e.g. [16] or [6]), or restricted to a small domain around the origin (e.g. [36]). Some of these methods sought to avoid poles by first employing various techniques to detect the singularities, and then computing the solution along a path taking an excursion around the singularity (e.g [16]). A survey of many of these existing numerical methods appears in [40]. The numerical scheme developed by Fornberg and Weideman [19] is particularly well suited to computing these solutions in the vicinity of poles over vast regions of the complex plane, while allowing the consideration of arbitrary α and β . This section presents a description of, implementation considerations for, and improvements in speed and accuracy for this new method.

5.1.1 A Description of the Pole Field Solver

Consider the test problem $\frac{d}{dz}u(z) = z^2 + u(z)^2$, $u(0) = 0$, featured in [19], with the solution

$$u(z) = z \frac{J_{\frac{3}{4}}\left(\frac{z^2}{2}\right)}{J_{-\frac{1}{4}}\left(\frac{z^2}{2}\right)}.$$

Suppose a Taylor series

$$u(z) \approx \sum_{n=0}^{N+M} a_n (z - z_k)^n$$

for $u(z)$ about a point z_k is available, with N and M nonnegative integers. The solution of the ODE at another point z_{k+1} could then be found approximately by evaluating the series, provided z_{k+1} is inside the radius of convergence of the series. A variety of other ODE solvers could also be applied in an attempt to find the solution at z_{k+1} . Figure 5.1 applies the previously discussed Taylor series method and MATLAB[®]'s [33] built-in function “ode45,” an adaptive Runge-Kutta method, to the test problem. A pole necessarily lies outside the radius of convergence of the Taylor series and continuity conditions are not met for the Runge-Kutta method so both methods break down.

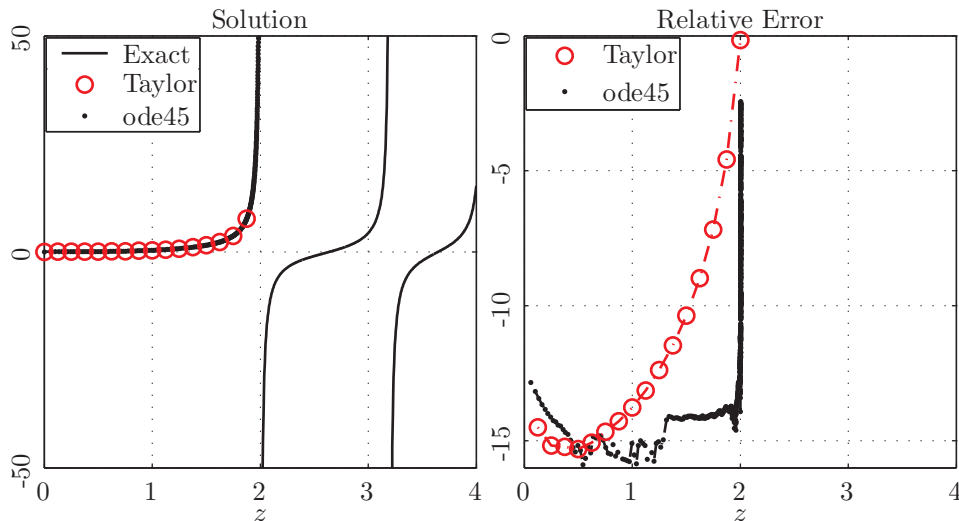


Figure 5.1: Solution along the real axis (left) to the test problem and order of the error (right) using the Taylor series method and an adaptive Runge-Kutta method.

Alternatively, the power series can be replaced by a rational approximation (Padé approximation)

$$u(z) \approx \frac{\sum_{n=0}^N A_n (z - z_k)^n}{\sum_{n=0}^M B_n (z - z_k)^n},$$

where $B_0 \doteq 1$ and A_0, A_1, \dots, A_N and B_1, B_2, \dots, B_M are chosen so that

$$\sum_{n=0}^{N+M} a_n z^n \approx \frac{\sum_{n=0}^N A_n z^n}{\sum_{n=0}^M B_n z^n}.$$

It was shown by Willers [44] that this conversion allows the Taylor method to step through a pole. Figure 5.2 shows that the Padé method applied to the test problem successfully integrates through the pole; however, some accuracy is lost.

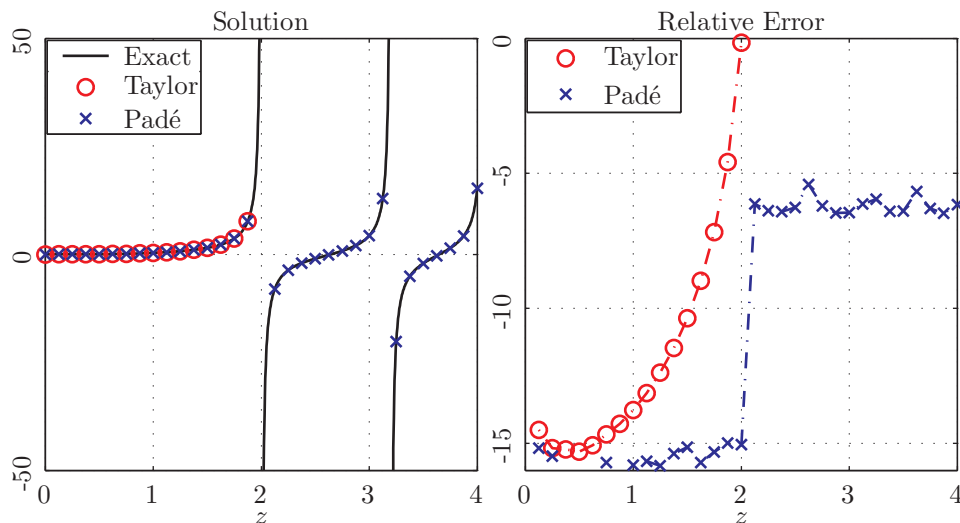


Figure 5.2: Solution along the real axis (left) to the test problem and order of the error (right) using the Taylor series method and a Padé method.

The need to overcome the loss in accuracy led to the numerical scheme introduced in [19], which features very high orders of accuracy (typically 30 to 50), minimal loss of accuracy in the vicinity of poles, and a flexible path selection strategy that can efficiently cover large areas of the complex plane. The computation of the numerical solution of the IVP at a single point used the following strategy, which will be called pole avoidance:

- (1) Choose the location of the initial condition as the first expansion point.
- (2) Compute the Padé approximation about the expansion point.
- (3) Evaluate the Padé approximation a distance h away in each of five directions in a swath directed toward the target point and choose as the next expansion point the one with the smallest solution magnitude.
- (4) Unless the target point has been reached, return to step 2.

The extension of this method that allows for the visualization of the solution over a region of the complex plane is called the pole field solver.

- (1) Set up a coarse grid of target points in the complex plane.
- (2) Select the target points in random order.
- (3) Apply the pole avoidance strategy to reach a predetermined neighborhood of the current target point, starting from the closest point that has already been evaluated. In the first step this is the location of the IC.
- (4) Repeat step 3 until all of the coarse grid target points have been accounted for, then set up a fine grid at the desired evaluation points.
- (5) Compute a single last step from each of the coarse grid points to several nearby fine grid evaluation points.

This approach is most advantageous in regions where poles are present and allows for the rapid visualization of solutions in the complex plane. Applying the pole field solver to the test problem in a neighborhood of the real axis results in the paths visualized in figure 5.3. Note that due to the random ordering in step 2 of the pole field solver, these paths are not unique.

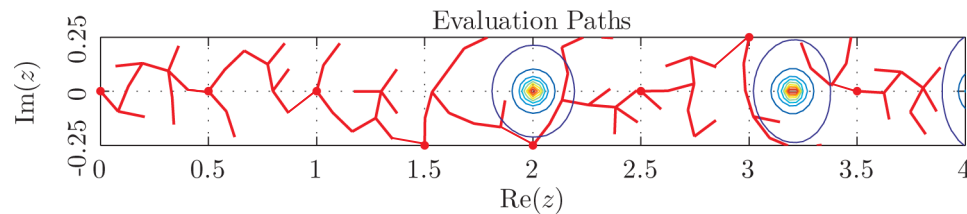


Figure 5.3: Example of the evaluation paths in the complex plane for the test problem using the pole avoidance strategy.

Taking these evaluation paths to the target point results in the accuracy being maintained across the entire solution interval.

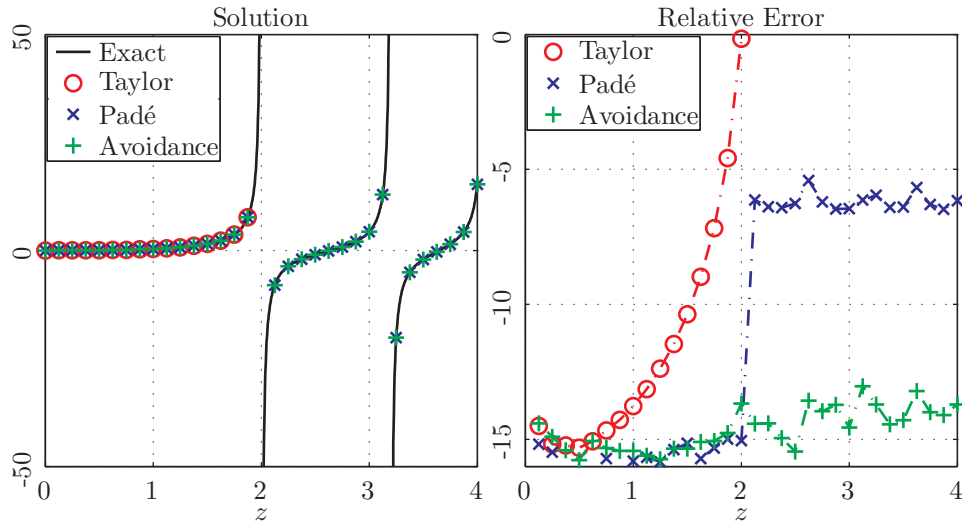


Figure 5.4: Solution along the real axis (left) to the test problem and order of the error (right) using the Taylor series method, a Padé method, and the pole avoidance strategy.

Figure 5.5 provides an example of the paths selected to avoid the poles when computing the solution $u_{4.5,2,0,0}^{[CH;1]}$ (3.6) over a region of the complex plane starting from a single initial condition. Evaluation of this solution at $161 \times 161 = 25921$ points with a step size of 0.25 takes only approximately 0.35 seconds on a Pentium i7-2600 at 3.40 GHz and 16.0 GB RAM.

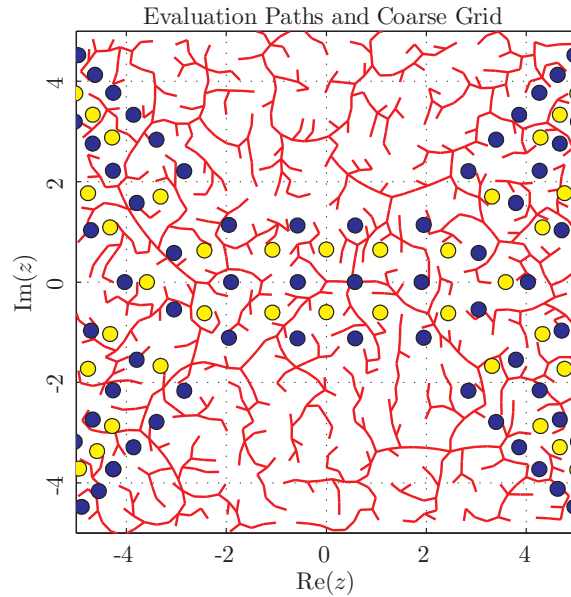


Figure 5.5: Example of the evaluation paths in the complex plane for a P_{IV} solution ($u_{4.5,2,0,0}^{[CH;1]}$ (3.6)) using the pole field solver.

5.1.2 A Brief Discussion on Implementing the Pole Field Solver

Implementation of the steps listed in section 5.1.1 could be done in many different ways. However, the implementation used in this thesis relies on MATLAB[®]'s [33] and LAPACK's [3] various robust linear algebra solvers. First, consider the power series

$$u(z) = \sum_{j=0}^N c_j z^j + O(z_{N+1}). \quad (5.1)$$

This is computed as in section 2.1.2 of [19] by integrating a truncated Taylor series with known coefficients c_0, c_1, \dots, c_K to find the next coefficient c_{K+1} . This is done in a subfunction we call “create_taylor_P4”.

The rational approximation (or, here, Padé approximation) can be computed for $M < N$ by equating (5.1) and

$$u(z) \approx \frac{\sum_{j=0}^M a_j z^j}{1 + \sum_{j=1}^{N-M} b_j z^j} \quad (5.2)$$

and solving for a_j and b_j . This requires the solution of a linear system which is performed easily in MATLAB[®] [33] and LAPACK [3] using “fast” Toeplitz solvers as discussed in section 5.2 of [19]. We choose N even and require that $M = \frac{N}{2}$ for simplicity in our implementation. This is completed in the subfunction “convert_to_pade”.

Simple evaluation of (5.2) is completed in a subfunction called “evaluate_pade”. Beginning with the initial conditions, a higher level function called “paths_eval” loops through the randomly ordered coarse grid target points computing a path using the pole avoidance strategy from the nearest point with a value for $u(z)$ and $u'(z)$ available. An even higher level “PIV_pole_field_solver” computes the last step from the coarse grid target points to the fine grid evaluation points. The computation of the Taylor coefficients in this last step takes advantage of MATLAB[®]'s [33] vectorization operations and is done in a function called “create_taylor_P4v”

5.1.3 An Arbitrary Precision Pole Field Solver

An important aspect of the explorations performed in this thesis is the verification of some solutions never discussed previously in the literature. For instance, a class of solutions is discussed

that are characterized by an entire half-plane with only a finite number of poles. These verifications often require extended precision computations using the pole field solver. Extended precision computations are also necessitated by the decaying asymptotic conditions discussed frequently in the literature, and by the verification of the many Bäcklund and Schlesinger transformations that were already discussed in section 2.3.

These extended precision computations are handled by adapting the pole field solver to work within the ADVANPIX: Multiprecision Computing Toolbox [2] within MATLAB[®] [33]. This environment allowed the straightforward translation of the pole avoidance strategy and pole-field solver by simply recasting all inputs and parameters to the multiprecision (“mp”) type. Further calculations automatically dealt with such “mp” variables in high precision.

As a prototype I considered the solution $u_{\nu,n,c_1,c_2}^{[CH;1]}$ in terms of confluent hypergeometric functions (3.6) with the parameter choices $\nu = 4.5$, $n = 2$, $c_1 = 0$, and $c_2 = 0$, which was shown previously in figure 5.5. As a reminder, the parameters ν , n , c_1 , and c_2 are used in the definition of (3.6), while α and β are parameters in the P_{IV} equation. Figure 5.6 highlights the difference between solutions computed using the machine precision and extended precision pole field solvers. In both frames the appropriate pole field solver is started with a extended precision initial condition at 0.5. Notice that the error patterns in the solutions are similar, but the extended precision solver maintains greater precision through pole fields and even smooth regions.

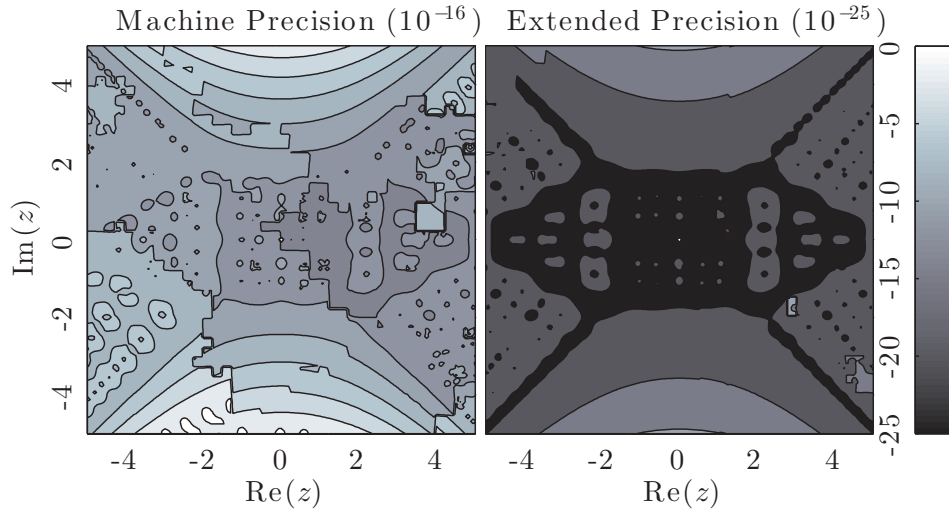


Figure 5.6: Left: Log base 10 of the relative error in the numerical solution of $u_{4.5,2,0,0}^{[CH;1]}$ computed at machine precision using order 30 Padé approximations and step size of 0.0625. Right: Log base 10 of the relative error in the numerical solution of $u_{4.5,2,0,0}^{[CH;1]}$ computed at 25 digits of accuracy using order 40 Padé approximations and step size of 0.25. In both cases the pole field solver is started with a high precision initial condition at 0.5. Notice that the error patterns in the solutions are the same.

Now, considering various continuation step sizes ranging from 0.005 to 0.5 along with the selection of orders 10, 16, 20, 26, \dots , 76, 80 (these are the orders of the Taylor series used to generate the coefficients of the Padé approximations) I computed the numerical solution of the prototype at $z = 5$ (again starting at $z = -5$). The solution was computed using only the pole avoidance strategy along a single path from $z = -5$ to $z = 5$.

Figure 5.7 shows that as the step size is decreased and/or the order is increased the accuracy improves as expected. However, the right frame of figure 5.7 also shows how impractical the use of extended precision arithmetic can be, considering how long a solution takes to compute.

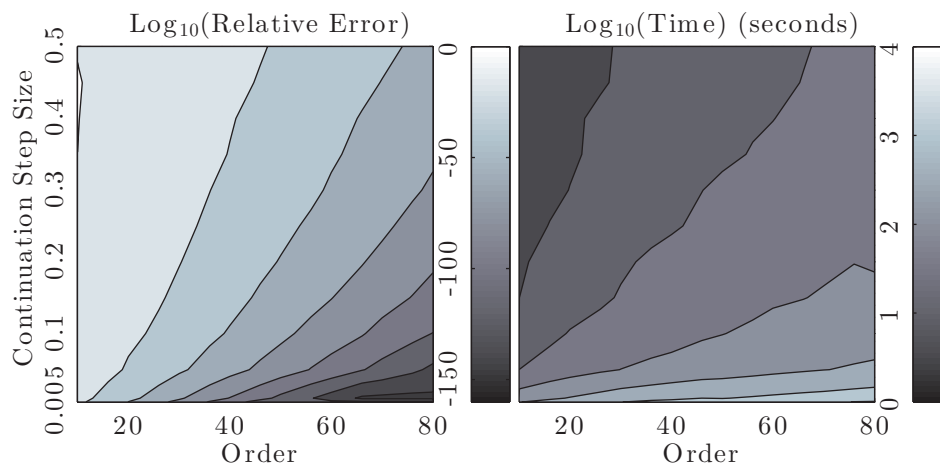


Figure 5.7: Left: Log base 10 of the relative error for various choices of step size and order. Right: Time to compute the single path from $z = 5$ to $z = -5$.

Still, the utility of such an approach is undeniable when confirming certain aspects in the literature. For instance, figure 1 in [43] shows that when confirming the decaying asymptotic conditions (4.2) $|z|$ must be chosen large enough to make the asymptotic approximation valid and small enough to be accurately represented in machine precision (here, 10^{-16}). Likewise, if we consider the solution in figure 5.8 where (4.2) was used as an initial condition with $z = z_0 = 4\sqrt{2}$ (discussions of this choice of z_0 can be found in [43]) there are poles in the left half-plane that should not be there based on the numerical evidence given in [43]. We then assumed that if z_0 were increased, these poles should move further out of the frame since the approximation becomes more accurate as $z \rightarrow +\infty$.

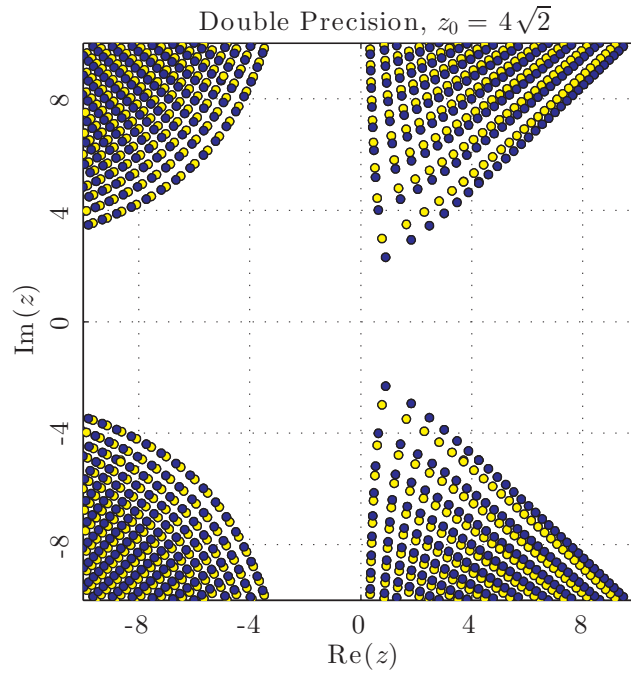


Figure 5.8: Solution to P_{IV} beginning with the initial condition (4.2) where $z = z_0 = 4\sqrt{2}$. Notice the extraneous poles in the left half-plane.

Increasing z_0 , of course, required computations in extended precision. Employing the high precision version of the pole field solver, I was easily able to move the poles further to the left as can be seen in figure 5.9.

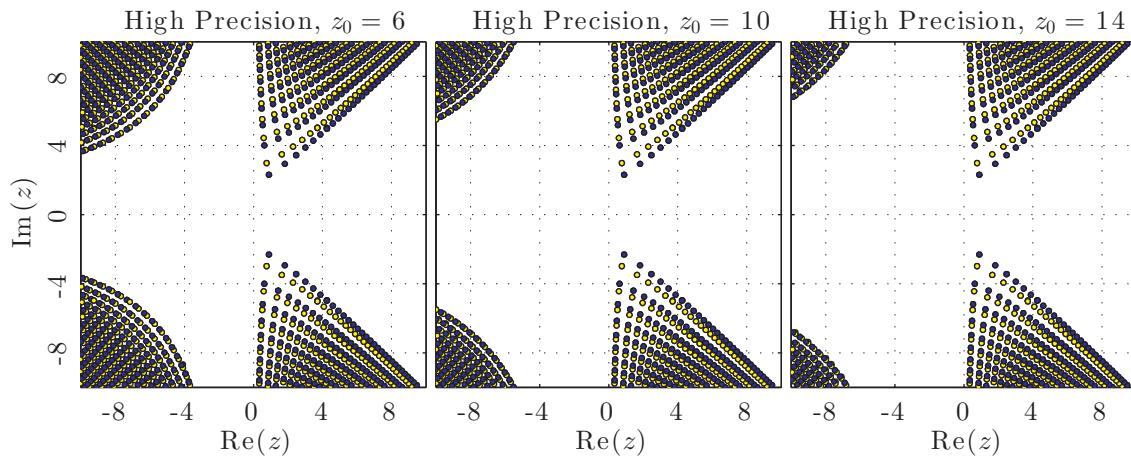


Figure 5.9: Solution to P_{IV} beginning with the initial condition (4.2) where $z = z_0 = 6, 10, \text{ and } 14$. Notice the extraneous poles in the left half-plane move further to the left as z_0 increases.

5.1.4 Increasing the Speed of the Solver

Along with the need for an extended precision solver, there were also situations that required greater speed when a solution could be computed at machine precision. This situation arose the most when generating what we will refer to as pole (oscillation) counting diagrams.

This need led to the conversion of portions of the code to C mex-files in MATLAB® [33], which are compiled C functions that can interface directly with MATLAB®. Based on the names of the subfunctions given in section 5.1.2 the image from MATLAB®'s [33] profiler in figure 5.10 timing shows that the subfunctions “create_taylor_P4”, “evaluate_pade”, “create_taylor_P4v”, and “convert_to_pade” each use a significant amount of computation time.

Profile Summary

Generated 05-Dec-2012 10:45:38 using cpu time.

Function Name	Calls	Total Time	Self Time*	Total Time Plot (dark band = self time)
PIV_pole_field_solver_wo_mex	1	34.070 s	3.978 s	
paths_eval_wo_mex	1	26.348 s	7.652 s	
create_taylor_P4	10555	15.887 s	15.887 s	
evaluate_pade	41100	3.014 s	3.014 s	
create_taylor_P4v	1	1.841 s	1.841 s	
convert_to_pade	10555	1.698 s	1.698 s	

Figure 5.10: Profiler output for the m-file version of the “PIV_pole_field_solver” function.

Conversion of each of these functions to their C mex-file counterparts “create_taylor_P4_mex”, “evaluate_pade_mex”, “create_taylor_P4v_mex”, and “convert_to_pade_mex_zgesv” results in significant improvements in computation time. This is shown in figure 5.11.

Profile Summary

Generated 05-Dec-2012 10:48:55 using cpu time.

Function Name	Calls	Total Time	Self Time*	Total Time Plot (dark band = self time)
PIV_pole_field_solver	1	10.676 s	4.668 s	
paths_eval	1	5.650 s	4.577 s	
nearest_neighbor_mex (MEX-file)	25600	0.603 s	0.603 s	
convert_to_pade_mex_zgesv (MEX-file)	10524	0.236 s	0.236 s	
evaluate_pade_mex (MEX-file)	41096	0.219 s	0.219 s	
create_taylor_P4v_mex (MEX-file)	1	0.219 s	0.219 s	
create_taylor_P4_mex (MEX-file)	10524	0.139 s	0.139 s	

Figure 5.11: Profiler output for the C mex-file version of the “PIV_pole_field_solver” function.

Now figure 5.11 also shows a subfunction “nearest_neighbor_mex” which replaces line number 49 in figure 5.12. The improvement is shown in figure 5.13.

paths_eval_wo_mex (1 call, 26.348 sec)

Generated 05-Dec-2012 10:46:32 using cpu time.

Lines where the most time was spent

Line Number	Code	Calls	Total Time	% Time	Time Plot
63	<code>c=create_taylor_P4([z,zuup(ki,...</code>	10555	15.948 s	60.5%	
49	<code>[~,ki] = min(abs(zuup(1:kz,1)-...</code>	25600	6.085 s	23.1%	
64	<code>[a,b] = convert_to_pade(c); ...</code>	10555	1.821 s	6.9%	
75	<code>zud(:,2:3) = evaluate_pade(a,b...</code>	15500	1.330 s	5.0%	
73	<code>zs = h*(zg-z)/abs(zg-z)*zc; ...</code>	15500	0.169 s	0.6%	
All other lines			0.995 s	3.8%	
Totals			26.348 s	100%	

Figure 5.12: Profiler output for the m-file version of the “paths_eval” function.

paths_eval (1 call, 5.650 sec)

Generated 05-Dec-2012 10:49:59 using cpu time.

Lines where the most time was spent







Line Number	Code	Calls	Total Time	% Time	Time Plot
45	<code>ki=nearest_neighbor_mex(real(z...</code>	25600	3.350 s	59.3%	
60	<code>[ar,ai,br,bi]=convert_to_pade_...</code>	10524	0.315 s	5.6%	
76	<code>[ur,ui,upr,upi]=evaluate_pade_...</code>	15496	0.252 s	4.5%	
59	<code>[cr,ci] = create_taylor_P4_mex...</code>	10524	0.231 s	4.1%	
63	<code>zuup(ki,4:order+5) = [a;b].'; ...</code>	10524	0.221 s	3.9%	
All other lines			1.281 s	22.7%	
Totals			5.650 s	100%	

Figure 5.13: Profiler output for the C mex-file version of the “paths_eval” function.

Recall the solution in figure 5.5. If we compare the analytical solution (3.6) with the numerical solutions (computed using the m-file and C mex-file versions of the pole field solver) along the real axis we find that the relative error from the analytical solution is almost identical for the pole field solver using the C mex-file versions and the one using only m-files. This can be seen in figure 5.14.

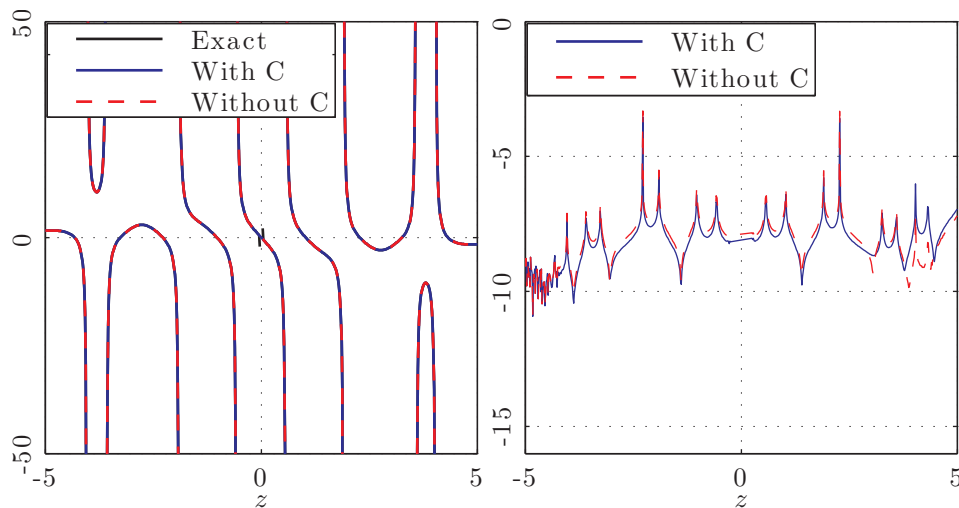


Figure 5.14: Solutions along the real axis (left) and log base 10 of the relative errors (right) between the analytical solution (3.6) and numerical solutions using the C mex-file version and original m-file versions of the pole-field-solver when computing $u_{4.5,2,0,0}^{[CH;1]}$ from a single initial condition using the pole field solver.

A comparison of solution times and relative errors when employing the pole field solver with various orders and step sizes can also be made for both the m-file and C mex-file versions. This comparison was made again on the closed form solution $u_{4.5,2,0,0}^{[CH;1]}$ shown in figure 5.5, but now the comparisons are made when computing a solution over a region of the complex plane. The relative errors and solution times are shown in figures 5.15 and 5.16. As expected, the C mex-file version performs better than the m-file version in solution time; however, both versions perform similarly when considering relative error.

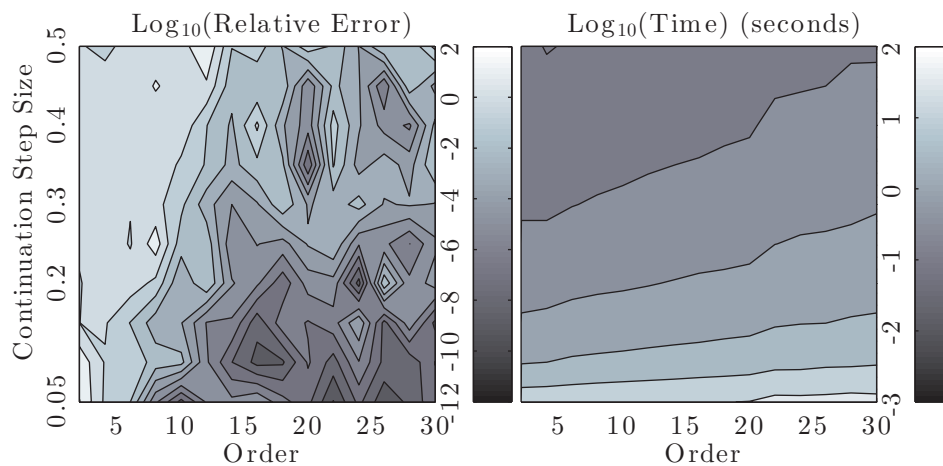


Figure 5.15: Statistics for computing the solution in figure 5.5 for $\text{Re}(z) \in [-5, 5]$ and $\text{Im}(z) \in [-5, 5]$ using only the m-file version of the pole field solver and beginning with initial conditions at $z = -5$. Left: Relative error at $z = 5$ for various choices of step size and order. Right: Time to compute the solution for various choices of step size and order.

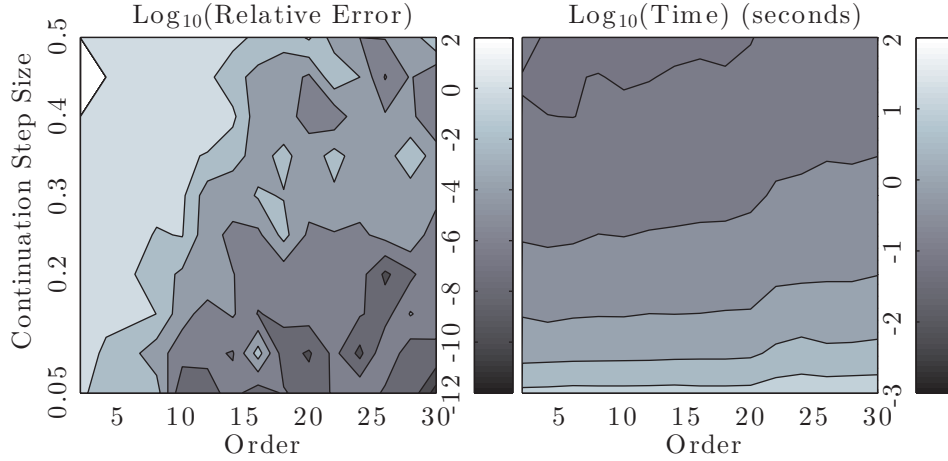


Figure 5.16: Statistics for computing the solution in figure 5.5 for $\text{Re}(z) \in [-5, 5]$ and $\text{Im}(z) \in [-5, 5]$ using only the C mex-file version of the pole field solver and beginning with initial conditions at $z = -5$. Left: Relative error at $z = 5$ for various choices of step size and order. Right: Time to compute the solution for various choices of step size and order.

5.2 Solving the BVPs

Consider the inequality constrained BVP

$$\frac{d}{dx}w(x) = f(x, w(x)) \quad (5.3)$$

$$|w(x_0) - w_0| \leq \epsilon \quad (5.4)$$

$$|w(x_f) - w_f| \leq \epsilon \quad (5.5)$$

with $x \in \mathbb{R}$ and $w \in \mathbb{R}^n$, $n \in \mathbb{Z}$. A BVP of this form is used to enforce the asymptotic conditions (4.5) through (4.8) when finding solutions of P_{IV} matching these conditions. We define $w \in \mathbb{R}^n$ since we consider P_{IV} as a first order system when solving the BVPs.

Collocation methods for the solution of such BVPs approximate the functions $w(x)$ by (piecewise) polynomials and require that the differential equations and initial conditions hold at specified points, called collocation points, in the interval $[x_0, x_f]$.

Legendre-Gauss-Lobatto (LGL) Pseudospectral (PS) methods are employed in this thesis. Here $w(x)$ is approximated by a polynomial of degree N and the collocation points are the roots

of the derivatives of the N^{th} order Legendre Polynomial

$$P_N(x) = \frac{1}{2^N N!} \frac{d^N}{dx^N} (x^2 - 1)^N$$

with the extra conditions that $x_0 = -1$ and $x_N = 1$ [41, Section 3.1]. For more information on Legendre polynomials see, e.g., [29]. The description of the Pseudospectral Collocation method appearing in this thesis will proceed in the same way as [41, Chapter 3]. The piecewise polynomials approximating $w(x)$ are defined by a given global basis function $\psi_i(x)$. That is, $w(x) \approx \sum_{i=0}^N a_i \psi_i(x)$. The Lagrange basis is chosen

$$\psi_i(x) = \prod_{\substack{j=0 \\ j \neq i}}^N \frac{(x - x_j)}{(x_i - x_j)}.$$

to take advantage of the useful property

$$\psi_i(x_j) = \begin{cases} 1, & \text{if } i = j, \\ 0, & \text{if } i \neq j, \end{cases}$$

so that $w(x_i) \approx a_i$. Further, the derivative of w can be approximated by $\frac{d}{dx} w(x) \approx \sum_{i=0}^N a_i \frac{d}{dx} \psi_i(x)$.

It is important to note that the roots of the derivatives of the Legendre polynomial of order N lie in the interval $(-1, 1)$, so that, along with the nodes x_0 and x_N , the collocation nodes lie generically in the interval $[-1, 1]$. To apply LGL PS collocation on an interval $[x_0, x_f]$, a change of variable $x(\chi) = \frac{(x_f - x_0)}{2}(\chi - 1) + x_f$ must be applied to scale the interval appropriately. This leads to a scaling of the differential equations by

$$\frac{d}{d\chi} w(x(\chi)) = \frac{d}{dx} w(x(\chi)) \frac{d}{d\chi} x(\chi) = \frac{d}{dx} w(x(\chi)) \frac{x_f - x_0}{2}.$$

The differentiation matrix (that is, $\mathbf{D}_{ij} = \frac{d}{dz} \psi_j(x_i)$) for Legendre-Gauss-Lobatto collocation is defined by

$$\mathbf{D}_{ij} = \begin{cases} \frac{P_N(x_i)}{P_N(x_j)} \frac{1}{x_i - x_j}, & i \neq j; \\ \frac{-N(N+1)}{4}, & i = j = 0; \\ \frac{N(N+1)}{4}, & i = j = N; \\ 0, & \text{otherwise,} \end{cases}$$

[17, Section III]. Applying LGL PS collocation the BVP is transformed into a nonlinear program in the variables $a_0, a_1, \dots, a_N \in \mathbb{R}^n$ that can be written in the form

$$\sum_{j=0}^N \mathbf{D}_{ij} a_j = \frac{x_f - x_0}{2} f(x_i, a_i), \quad i = 0, 1, \dots, N$$

$$|a_0 - w_0| \leq \epsilon,$$

$$|a_N - w_f| \leq \epsilon.$$

This nonlinear program is easily solved using MATLAB[®]'s [33] optimization toolbox by applying the “fmincon” function with a trivial objective, where choosing the “active-set” algorithm has performed the best.

5.3 Visualization of pole locations and residues

Recall the rational solutions of P_{IV} where, for example,

$$u_{1,2}^{[GH;1]} = u(z; 5, -8) = \frac{16z^5 + 16z^3 - 12z}{8z^6 + 4z^4 + 6z^2 + 3}, \quad (5.6)$$

with the pole locations and residues shown in figure 5.17.

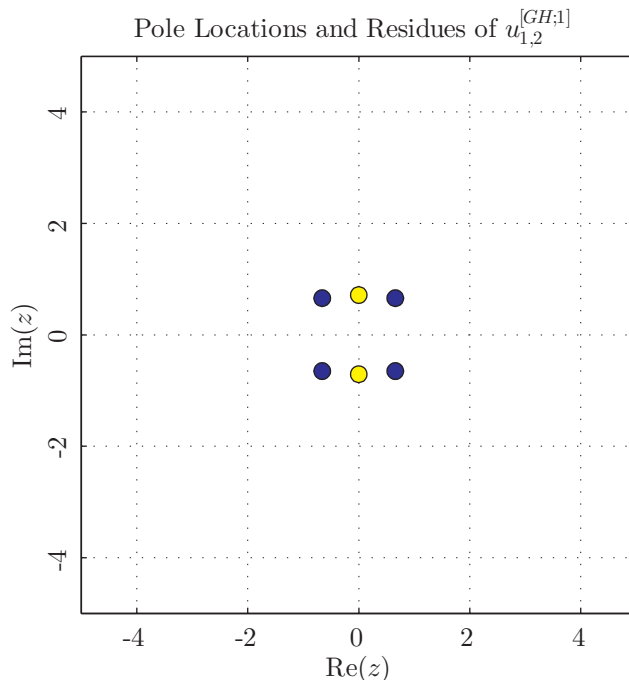


Figure 5.17: Pole locations and residues of (5.6).

Of course, the poles in this solution occur at the roots of the denominator and can be easily computed to arbitrary precision using any number of solvers. These pole locations are shown to machine precision in table 5.1.

Roots of $8z^6 + 4z^4 + 6z^2 + 3$
$-0.658037006476246 + 0.658037006476246i$
$-0.658037006476246 - 0.658037006476246i$
$0.658037006476246 + 0.658037006476246i$
$0.658037006476246 - 0.658037006476246i$
$0.707106781186547i$
$-0.707106781186547i$

Table 5.1: Pole Locations of $u_{1,2}^{[GH;1]}$ via computing the roots of the denominator of (5.6).

Such a concise visualization of rational solutions is simple; however, moving to even the closed form special function solutions in terms of parabolic cylinder or confluent hypergeometric functions eliminates our ability to simply compute roots of the denominator. Instead, consider as an example a contour plot like the one in figure 5.18 about the pole located at $0.707106781186547i$.

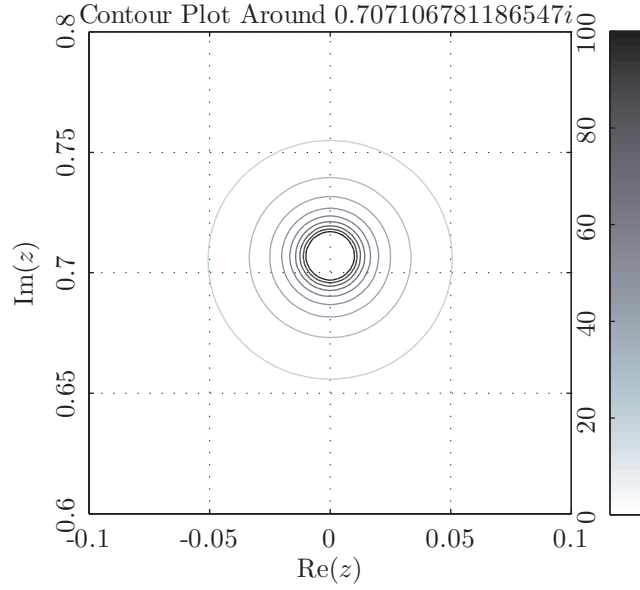


Figure 5.18: Contour plot of $|u_{1,2}^{[GH;1]}|$ around the pole at $0.707106781186547i$ of (5.6).

In the vicinity of a pole z_0 a solution of P_{IV} behaves as

$$u(z) \approx \frac{a_{-1}}{z - z_0}, \quad (5.7)$$

where $a_{-1} = \pm 1$. A contour plot like in figure 5.18 can easily provide several points, z_1, \dots, z_k , at which (5.7) can be evaluated simultaneously to determine z_0 and a_{-1} by solving the over-determined system of equations

$$\begin{bmatrix} 1 & u(z_1) \\ 1 & u(z_2) \\ \vdots & \vdots \\ 1 & u(z_k) \end{bmatrix} \begin{bmatrix} a_{-1} \\ z_0 \end{bmatrix} = \begin{bmatrix} z_1 u(z_1) \\ z_2 u(z_2) \\ \vdots \\ z_k u(z_k) \end{bmatrix}. \quad (5.8)$$

For example, by picking the points, z_1, \dots, z_k along the contours at $|u_{1,2}^{[GH;1]}| = 30$ and solving the systems (5.8) along each of these contours we are able to find the values in table 5.2.

Roots of $8z^6 + 4z^4 + 6z^2 + 3$	Over-determined Systems
$-0.658037006476246 + 0.658037006476246i$	$-0.657990889167198 + 0.657992354272110i$
$-0.658037006476246 - 0.658037006476246i$	$-0.657990889167378 - 0.657992354275692i$
$0.658037006476246 + 0.658037006476246i$	$0.657990889159593 + 0.657992354271594i$
$0.658037006476246 - 0.658037006476246i$	$0.657990889158462 - 0.657992354276616i$
$0.707106781186547i$	$-0.000000000003439 + 0.707153836604552i$
$-0.707106781186547i$	$-0.000000000006202 - 0.707153836608534i$

Table 5.2: Pole locations via computing the roots of the denominator of (5.6) (left) and via solving (5.8) with z_k along the contours $|u_{1,2}^{[GH;1]}| = 30$ (right). The incorrect digits on the right are underlined.

These pole locations are certainly not very accurate, and for the sake of comparing these locations with reasonable accuracy a correction must be made. Two separate methodologies were considered to make these corrections.

Both methodologies begin by letting $u(z)$ be a solution of P_{IV} and, with $j > 0$, \tilde{u}_j and \tilde{u}'_j be the function and derivative values computed by the pole field solver at the points \tilde{z}_j . Also, let z_0 be the pole location computed by solving (5.8) with z_k the points generated by the contour software along a contour $|u(z)| = U$.

5.3.1 Correcting Pole Locations Via Newton's Method

The first methodology entails applying Newton's method to $1/u(z)$. First, we find the value \tilde{z}_j nearest z_0 , call it \tilde{z}_0^0 . From \tilde{z}_0^0 we iterate using Newton's method on the function $1/u(z)$ until we find an approximate root, that is. a pole of $u(z)$. The Newton iteration is given simply by

$$\tilde{z}_0^{j+1} = \tilde{z}_0^j + \frac{u(\tilde{z}_0^j)}{u'(\tilde{z}_0^j)}, j = 1, 2, \dots,$$

where $u(\tilde{z}_0^j)$ and $u'(\tilde{z}_0^j)$ can be computed easily from the Padé approximation about z_0^{j-1} . The iteration is continued until $|1/u(\tilde{z}_0^j)| < \epsilon \ll 1$.

The second column of table 5.3 gives the resulting pole locations using this approach. We see that in this case the approximations of the pole location are many orders of magnitude more accurate.

Roots of $8z^6 + 4z^4 + 6z^2 + 3$	Corrected via Newton's Method
$-0.658037006476246 + 0.658037006476246i$	$-0.658037006502404 + 0.658037006452043i$
$-0.658037006476246 - 0.658037006476246i$	$-0.658037006502410 - 0.658037006453049i$
$0.658037006476246 + 0.658037006476246i$	$0.658037006497747 + 0.658037006452093i$
$0.658037006476246 - 0.658037006476246i$	$0.658037006497756 - 0.658037006453084i$
$0.707106781186547i$	$-0.000000000002518 + 0.707106781269720i$
$-0.707106781186547i$	$-0.000000000002512 - 0.707106781270804i$

Table 5.3: Pole locations via computing the roots of the denominator of (5.6) (left) and via solving (5.8) with z_k along the contours $|u_{1,2}^{[GH;1]}| = 30$ and correcting using Newton's method (right). The incorrect digits on the right are underlined.

5.3.2 Correcting Pole Locations Via Roots of the Padé Denominator

The second approach computes the roots of the denominator of the Padé approximation about z_0 using the built in “roots” function of MATLAB[®] [33]. Let Δz_0 be the root with the smallest modulus, and where the numerator of the approximation is not near zero. We update $z_1 = z_0 + \Delta z_0$ and define z_1 to be the pole location.

The second column of table 5.4 gives the resulting pole locations applying this approach. This time the values are even more accurate than those when generated by corrections via the Newton's method.

Roots of $8z^6 + 4z^4 + 6z^2 + 3$	Corrected via Roots of Padé Denominator
$-0.658037006476246 + 0.658037006476246i$	$-0.658037006476339 + 0.658037006476700i$
$-0.658037006476246 - 0.658037006476246i$	$-0.658037006476272 - 0.658037006475570i$
$0.658037006476246 + 0.658037006476246i$	$0.658037006475839 + 0.658037006476741i$
$0.658037006476246 - 0.658037006476246i$	$0.658037006476189 - 0.658037006475811i$
$0.707106781186547i$	$0.000000000000366 + 0.707106781187221i$
$-0.707106781186547i$	$0.000000000000298 - 0.707106781186046i$

Table 5.4: Pole locations via computing the roots of the denominator of (5.6) (left) and via solving (5.8) with z_k along the contours $|u_{1,2}^{[GH;1]}| = 30$ and correcting using the method of computing the roots of the Padé denominator (right). The incorrect digits on the right are underlined.

5.4 Pole and Oscillation Counting

We take advantage of the speed and accuracy of the pole field solver to explore the differences in solution characteristics for each fixed choice of α and β . This is done by varying $(u(0), u'(0)) \in \mathbb{R}^2$ and examining the number of poles and/or oscillations (i.e., a change in the sign of the derivative)

on either the positive or negative real axis. For instance, the color bar of figure 5.23 (adapted from [43]) indicates the number of poles on the negative and positive real axes in the left and right frames of figure 5.19, respectively, for the parameters $\alpha = \beta = 0$. This figure also indicates the ICs matching the asymptotic behaviors discussed in sections 4.1 and 4.2 by the markers that appear in the legend in figure 5.23.

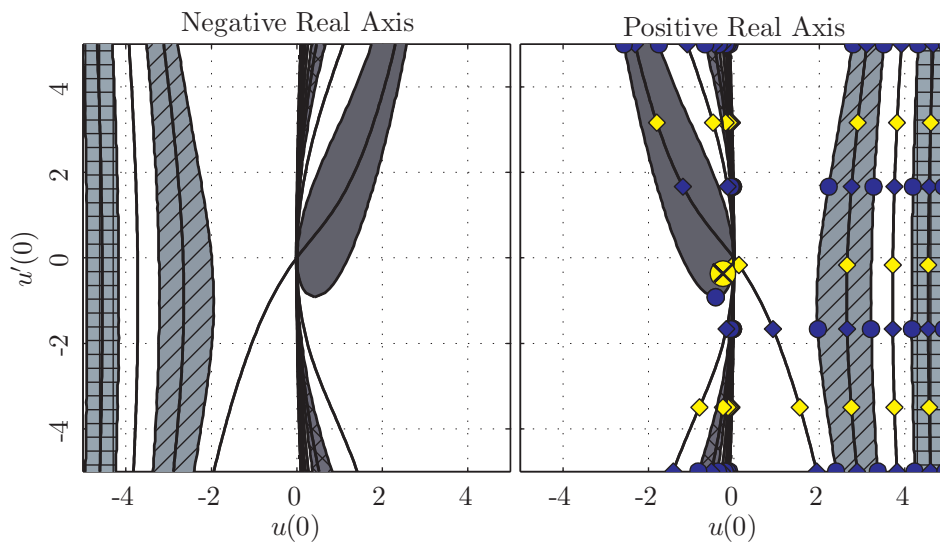


Figure 5.19: Number of poles on the positive and negative real axes for $\alpha = 0$ and $\beta = 0$ are indicated by the color bar in 5.23. Solutions satisfying the asymptotic behaviors of the roots of 4.3 as $z \rightarrow +\infty$ or $z \rightarrow -\infty$, $z \in \mathbb{R}$, are shown by the black lines. The markers in the right frame indicate which root the solution is asymptotic to as $z \rightarrow +\infty$, $z \in \mathbb{R}$, and these are described in the legend in figure 5.23.

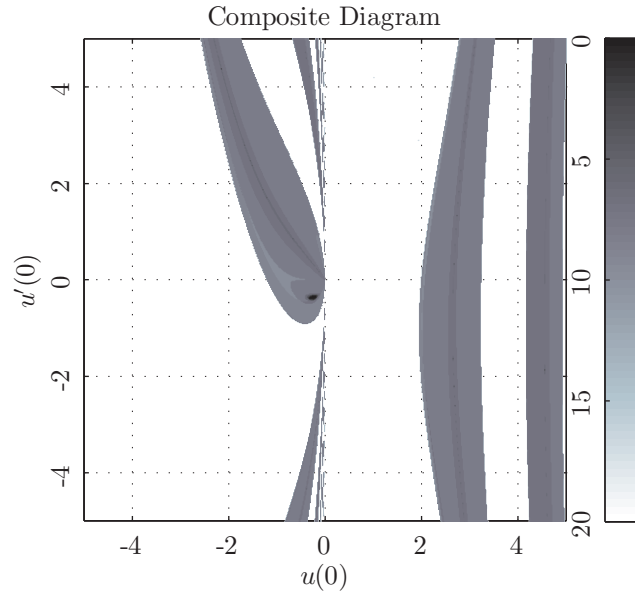


Figure 5.20: Sum of the number of oscillations for $z \in [0, 7]$ and the number of poles for $z \in [0, 15]$ and $\alpha = \beta = 0$. These are shown separately in the left and right frames of figure 5.21.

Arriving at figure 5.19 requires the refinement of an image like 5.20, which is a composition of the frames in figure 5.21. Figure 5.21 shows raw counts of the oscillations and poles that occur over a finite interval $([0, 15])$ on the positive real axis. These raw counts provide a map for locating solutions with special characteristics. For instance, regions that are shaded have a finite number of poles on the positive real axis where darker bands within such a region indicate solutions with few or no oscillations or poles on the positive real axis. Unshaded regions, then, indicate those ICs that generate solutions with an infinity of poles on the positive real axis. Investigations performed by zooming in on these darker bands and edges of the shaded regions indicate that solutions with these ICs admit the asymptotic behavior given by the roots of (4.3) as $z \rightarrow +\infty$, $z \in \mathbb{R}$.

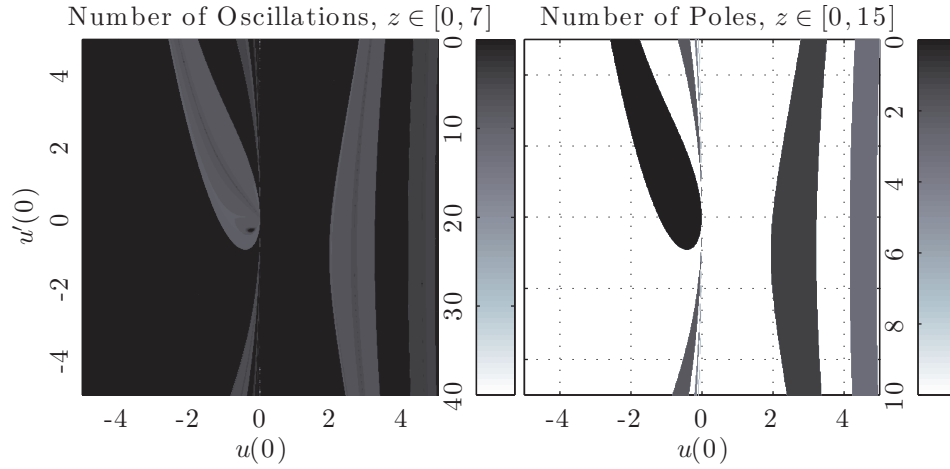


Figure 5.21: Left: Number of oscillations on the positive real axis for $z \in [0, 7]$ and $\alpha = \beta = 0$. Right: Number of poles on the positive real axis for $z \in [0, 15]$ and $\alpha = \beta = 0$.

Finding a large number of these initial conditions by manually zooming in on the edges and darker bands proved very time consuming and the figures 5.20 and 5.21 alone did not locate all of the ICs with special characteristics. To complete the generation of 5.19 we solved the inequality constrained BVP (5.3) (see section 5.2 for a discussion) over an interval $[z_0, z_f]$, while enforcing as boundary conditions each of the roots of (4.3) as $z \rightarrow +\infty$, $z \in \mathbb{R}$, in turn. Generation of different initial conditions for a single root w_μ^\pm was accomplished by sliding the interval $[z_0, z_f]$ along the positive real axis in very small increments.

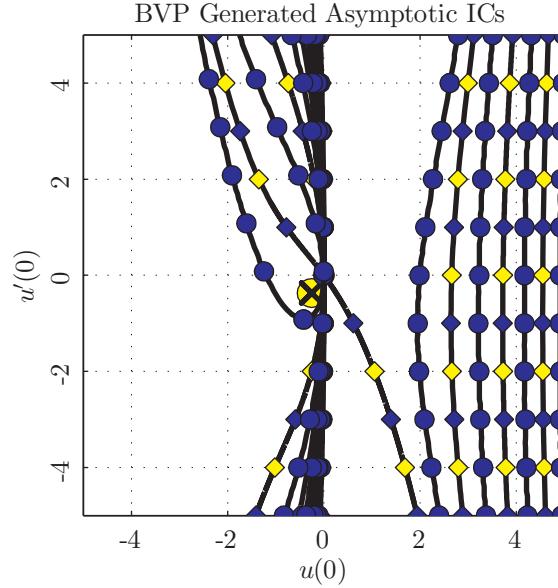


Figure 5.22: Initial conditions for solutions asymptotic to the roots of 4.3 as $z \rightarrow +\infty$, $z \in \mathbb{R}$, for $\alpha = \beta = 0$. These initial conditions are generated by solving the inequality constrained BVP 5.3 over an interval $[z_0, z_f]$. Generation of different initial conditions is accomplished by sliding the interval $[z_0, z_f]$ along the positive real axis.

With the knowledge of how figure 5.19 was made and the symmetry (2.2) we only need to consider the right frame since the left is completely analogous. As described earlier in this section, the color bar in figure 5.23 indicates the exact number of poles for a given initial condition located within a shaded region. Here darker (lighter) regions indicate an odd (even) number of poles in the solution that IC generates.

“Most of the ICs in the shaded regions generate solutions that oscillate as $z \rightarrow +\infty$ (note that an oscillation is simply a change in the sign of the derivative); however, each initial condition marked by a curve, located at the boundary of a shaded region, or designated by an isolated marker has no oscillations as $z \rightarrow +\infty$. These solutions are precisely those that are asymptotic to the roots of the quartic equation (4.3) as $z \rightarrow +\infty$. The appropriate root is indicated by the symbols shown in left frame of figure 5.23. In the case of $\alpha = \beta = 0$ (generally, when $\beta = 0$) the solutions matching the behaviors w_μ^+ , $\mu = \pm 1$, are the solutions that satisfy the decaying asymptotic condition (4.2). When two markers appear along the same curve, those ICs generate solutions matching both behaviors (in separate intervals of

As $z \rightarrow +\infty$		
◆	$u(z) \sim \frac{\sqrt{-2\beta}}{2z}$	0
◇	$u(z) \sim -\frac{\sqrt{-2\beta}}{2z}$	1
●	$u(z) \sim -2z$	2
⊗	$u(z) \sim -\frac{2}{3}z$	3
■	Closed form	4
		5
		6
		7
		8
		9

Figure 5.23: Legend and color bar for figures 5.19, 6.16, 6.17, and 6.20. The legend shows the markers indicating the ICs that generate the dominant asymptotic behaviors (4.5)-(4.8) and closed form solutions. If a marker occurs on a curve, then the dominant behavior or type of closed form solution occurs for all of the ICs along that curve. If a marker is emphasized by containing an “×”, then it indicates an isolated IC matching the dominant behavior or the IC generates an isolated rational solution. The color bar indicates the number of poles on the positive or negative real axis.

the real axis), as shown in, for example, figures 6.13, 6.14, 6.28, and 6.29 (see section 6.3.5 for further discussion).”[42]

5.5 Exploring Solutions with a Pole at the Origin

The methods of exploration have so far only considered ICs that are finite. However, beginning with a truncated series like (2.1), with $z_0 = 0$, ICs can be generated to also view solutions with a pole at the origin. Choosing $\alpha = 2$, $\beta = -2$, and $c = 0$ gives the two solutions (depending on the residue of the pole at the origin) shown in figure 5.24. In this case the solution with residue +1 is simply $u(z) = \frac{1}{z}$ and the one with residue -1 is a solution in terms of the confluent hypergeometric function.

As discussed in section 5.4, varying $u(0)$ and $u'(0)$ allows the exploration of all solutions apart from those with a pole at the origin. For instance, consider the right frame of figure 5.19 that shows the locations of initial conditions with a finite number of poles on the real axis along with the ICs for solutions asymptotic to the roots of (4.3). If $|u(0)|$ and $|u'(0)|$ were increased and remained in one of the shaded regions or along any of the lines indicating the asymptotic solutions, then this would indicate a pole moving through the origin from the negative real axis to the positive real axis. Once the transition has occurred, the initial conditions fall within a new shaded region or along

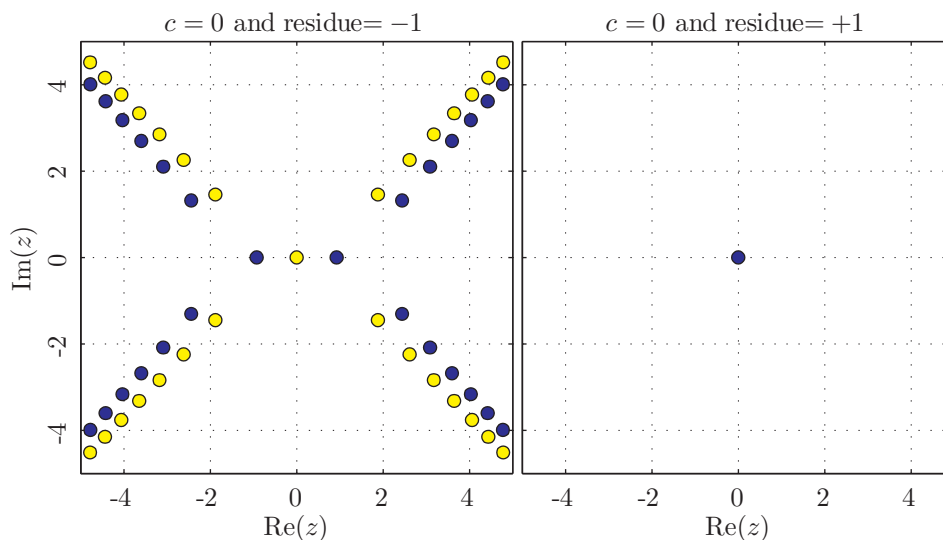


Figure 5.24: A view of solutions with a pole at the origin in the case of $\alpha = 2$, $\beta = -2$, and $c = 0$.

a different line. Figure 5.25 (adapted from one in [43]) is a caricature of the transition of the ICs from one region to another in the case $\alpha = \beta = 0$. In this case the two solutions occurring for the choice $c = 0$ are shown in figure 5.26. The labels k_j^\pm , $j = 1, 2, 3, 4$, in figure 5.25 correspond to the same labels in the right frame of figure 5.27. The choice of k here also refers to the same parameter in (4.2). That is, these indicate the values of the parameter leading to solutions satisfying the decaying asymptotic condition that also have a pole at the origin. If we followed one of the curves continued by the dashed lines as $|u(0)| \rightarrow +\infty$ and $|u'(0)| \rightarrow +\infty$, then the solution occurring at this limit could be found by evaluating (2.1) with the appropriate value of c in the right frame of figure 5.27.

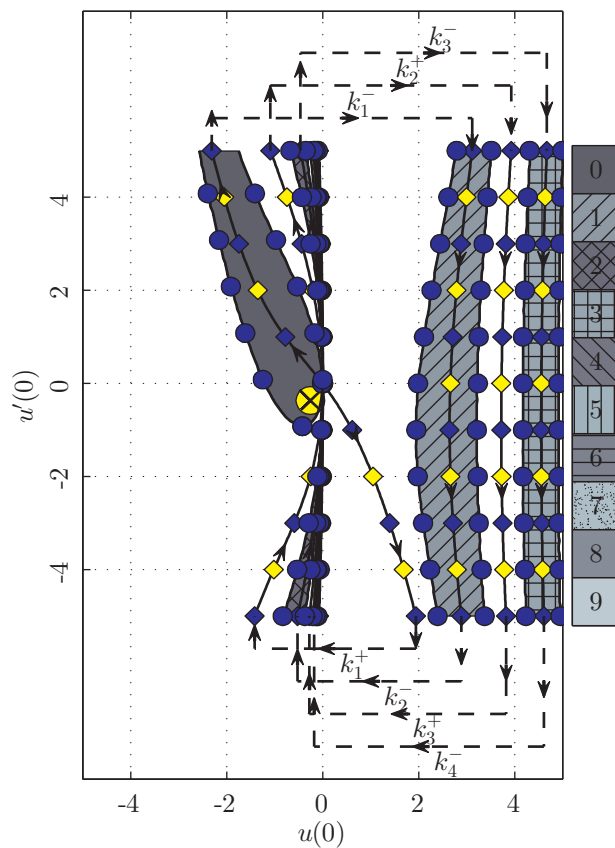


Figure 5.25: A caricature of the transition of a pole from the negative real axis to the positive real axis. Here $\alpha = \beta = 0$.

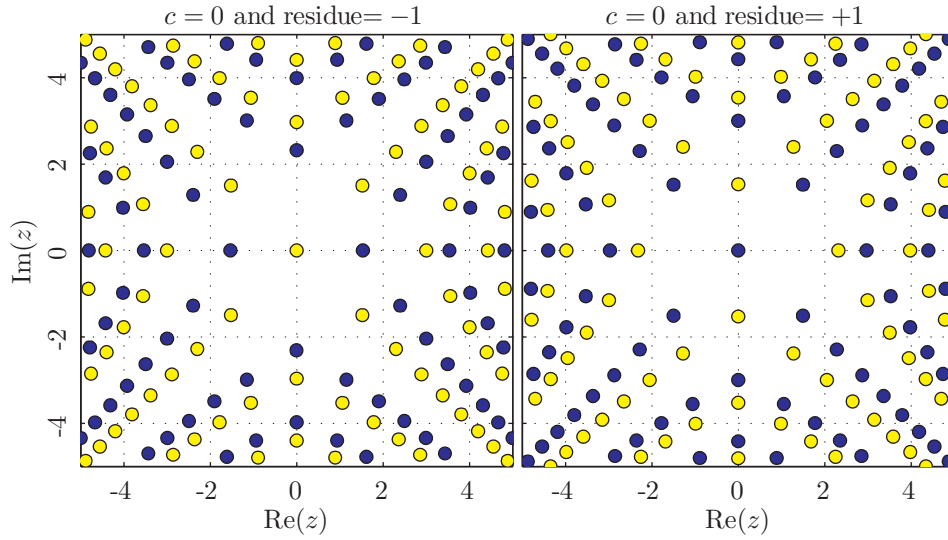


Figure 5.26: A view of solutions with a pole at the origin in the case of $\alpha = 0$, $\beta = 0$, and $c = 0$.

When exploring the cases with a pole at the origin the single parameter c can instead be varied to map out the number of poles and oscillations along the two halves of the real axis. Figure 5.27 (taken from [43]) shows in two ways that certain choices of c lead to solutions with a finite number of poles on the positive and negative real axes when the residue of the pole at the origin is $+1$. On the left the locations of the poles on the real axis are shown, while the right frame mimics figure 5.19 with lines and dots indicating values of c that generate solutions with a finite number of poles. The expansion (2.1) demonstrates that the curves in the left frame should be symmetric around the origin $\text{Re}(z) = c = 0$. Comparison of both frames with 5.19 allows us to deduce that the colored and black dots indicate the values of c that correspond to solutions generated from P_{IV} and the condition (4.2) with $k > 0$ and $k < 0$, respectively. A comparison of k and c values leading to the same solutions is given in [43]. Further, line segments correspond to shaded regions in figure 5.19. The analogous images for a pole with negative residue at the origin are given in [43].

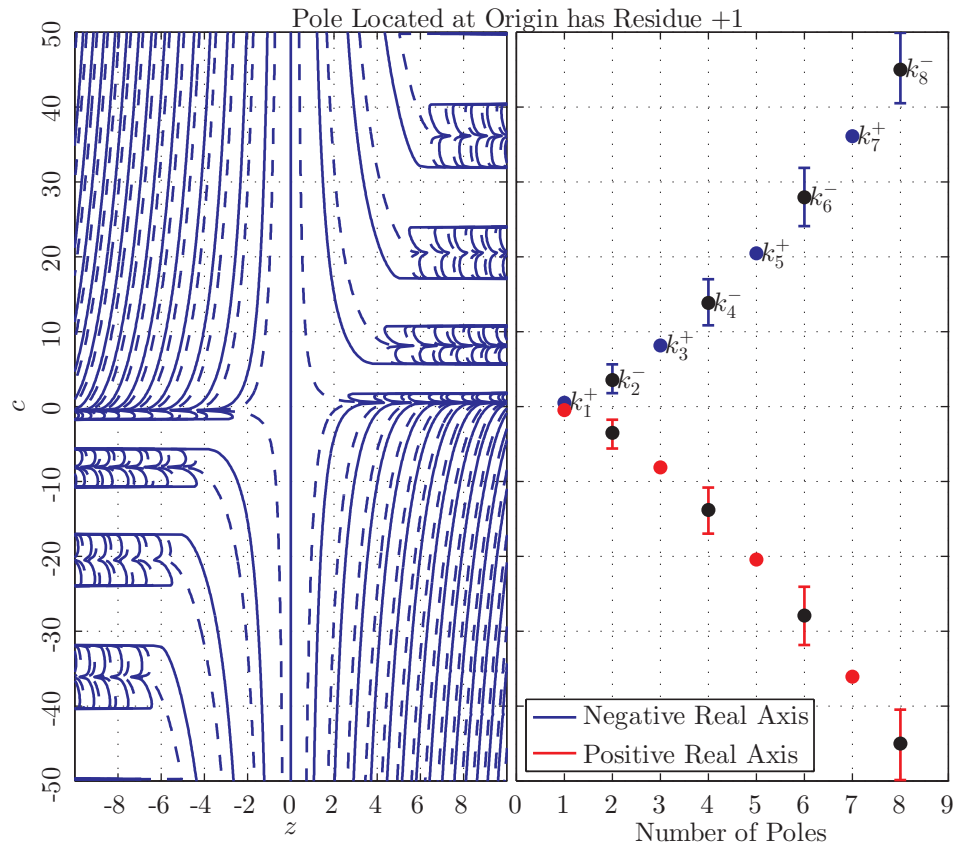


Figure 5.27: Left Frame: Locations of the poles on the real axis for various c and $\alpha = \beta = 0$. Solid lines indicate poles with residue +1 and dashed lines those with residue -1. Right Frame: Number of poles includes the pole at the origin. Values of c with no lines or dots indicate solutions with an infinity of poles on the real axis.

Similar analysis could be completed for any choice of α and β using (2.1); however, our explorations with regard to solutions with a pole at the origin did not proceed beyond $\alpha = \beta = 0$.

Chapter 6

Exploring Solutions of P_{IV} With No Closed Form

This chapter explores some of the solution types that were mostly not considered prior to the introduction of the method described in section 5.1.1. These explorations rely heavily on the tool discussed in 5.4. First, however, the high precision adaptation of the pole field solver (see section 5.1.3) is used to confirm the solution transformations (2.5) through (2.9). We then move on to a survey of general choices of α and β , where a special solution type asymptotic to (4.7) as $z \rightarrow +\infty$ and $z \in \mathbb{R}$ is discussed in detail. This solution type provides a single point of comparison among all α and β choices. These explorations include the mostly unexplored space of $\beta > 0$.

6.1 Confirming the Solution Transformations

We verify the solution transformations (2.5) through (2.9) by considering a particular choice of parameters and ICs. Consider the choice of $\alpha = 0.25$, $\beta = -0.125$, $u(0) = -1.5$ and $u'(0) = -1.5$. Figure 6.1 displays this solution over a region of the complex plane and along the real axis.

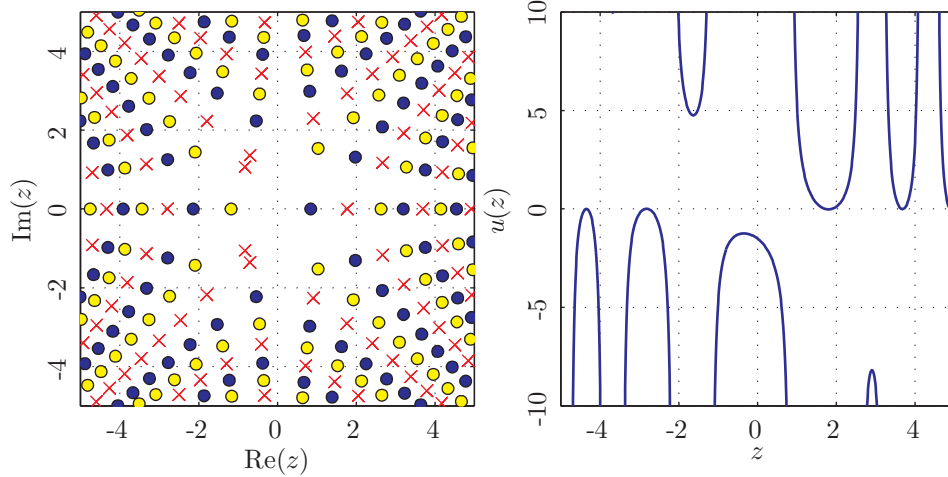


Figure 6.1: Solution to P_{IV} with $\alpha = 0.25$, $\beta = -0.125$, $u(0) = -1.5$ and $u'(0) = -1.5$. The left frame shows the zero and pole locations, while the right shows the solution along the real axis.

After applying each of the transformations $u_{k,\mu}^{\pm}(u(z), z)$, $k = 1, 2, 3$ and u_k^{\pm} , $k = 4, 5$ to each point of the solution in figure 6.1 we arrive at the solutions in figures 6.2 and 6.3. These solutions alone, however, do not provide confirmation that the solution transformations are correct. To that end, we also computed the numerical solution using the pole field solver beginning with an initial condition from a single transformed point. We then compared the numerically computed solution to the analytically transformed solution in high precision. The resulting error is shown in figure 6.4, where the solutions agree to very high accuracy.

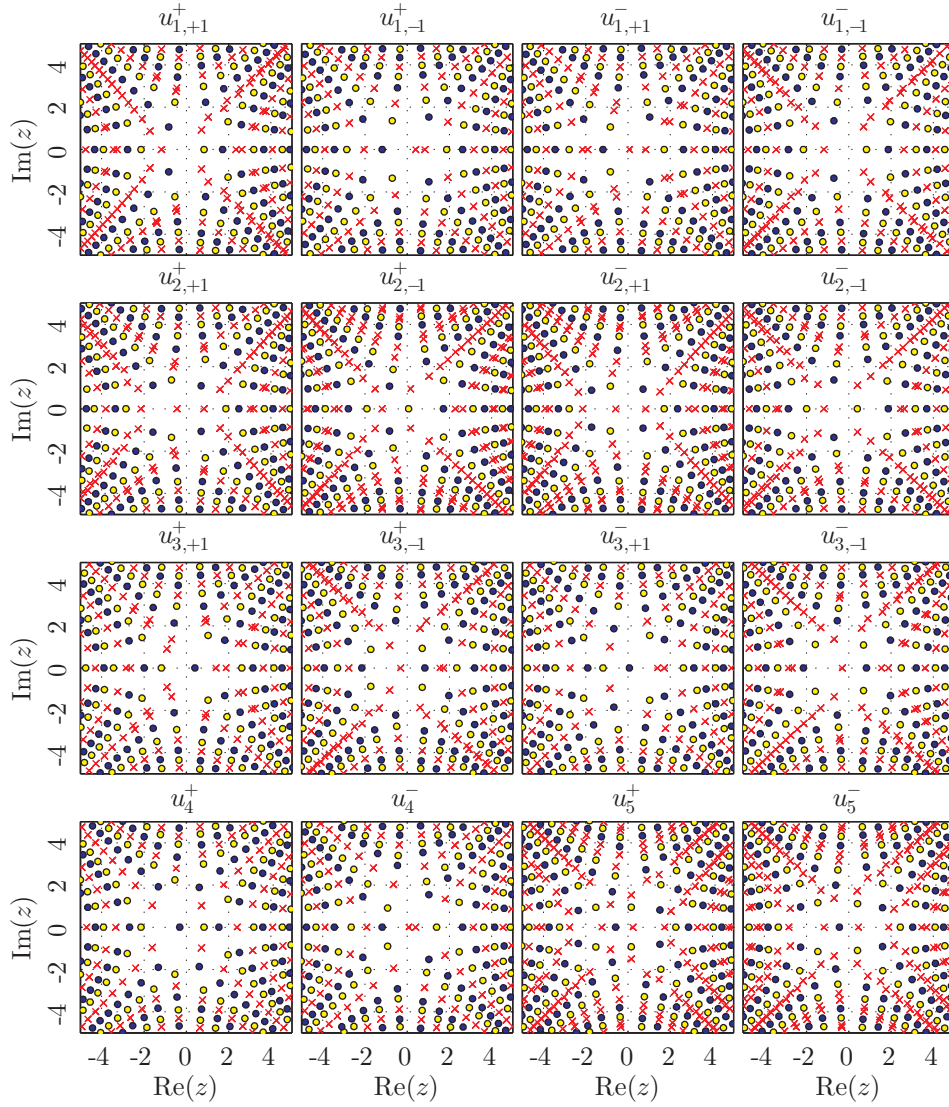


Figure 6.2: Zero and pole locations of solutions to P_{IV} resulting from the applications of (2.5) through (2.9) to the solution figure 6.1.

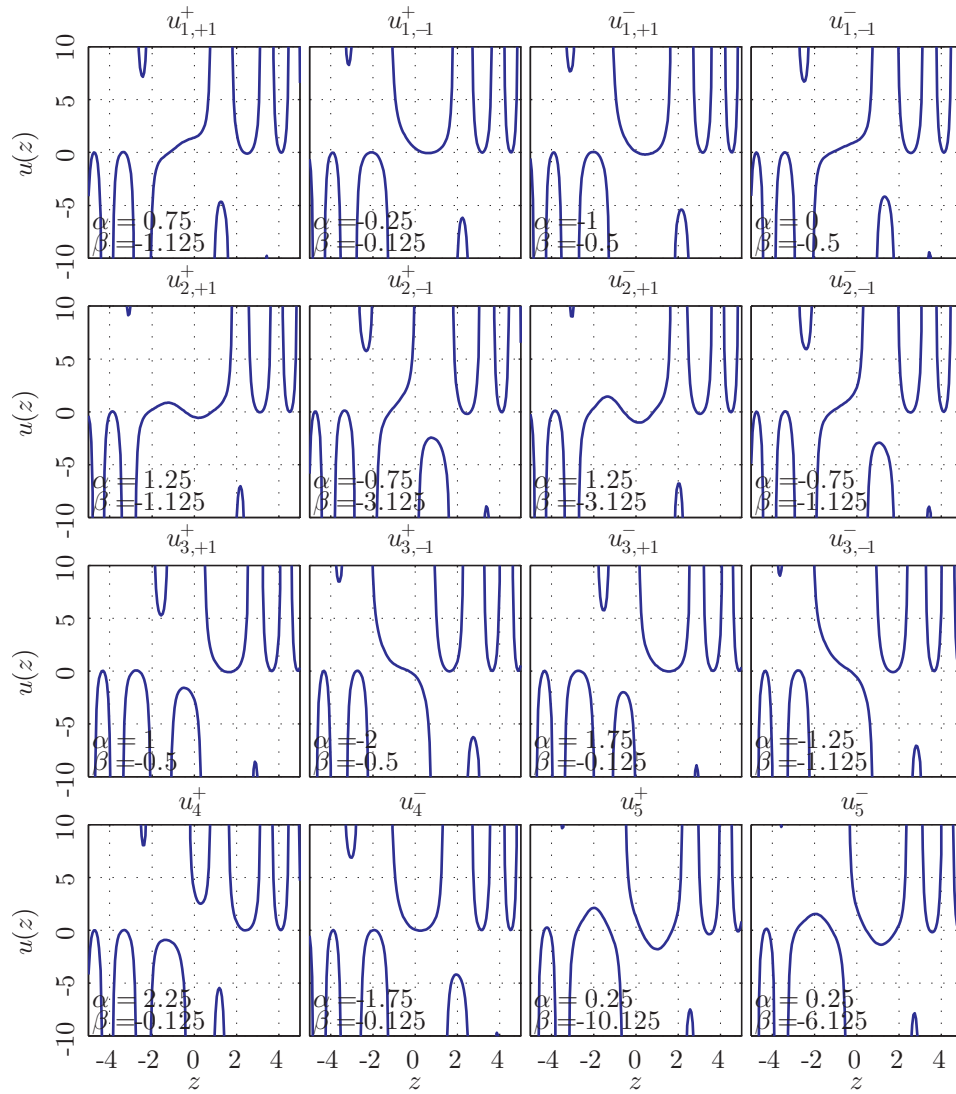


Figure 6.3: Solutions to P_{IV} along the real axis resulting from the applications of (2.5) through (2.9) to the solution figure 6.1.

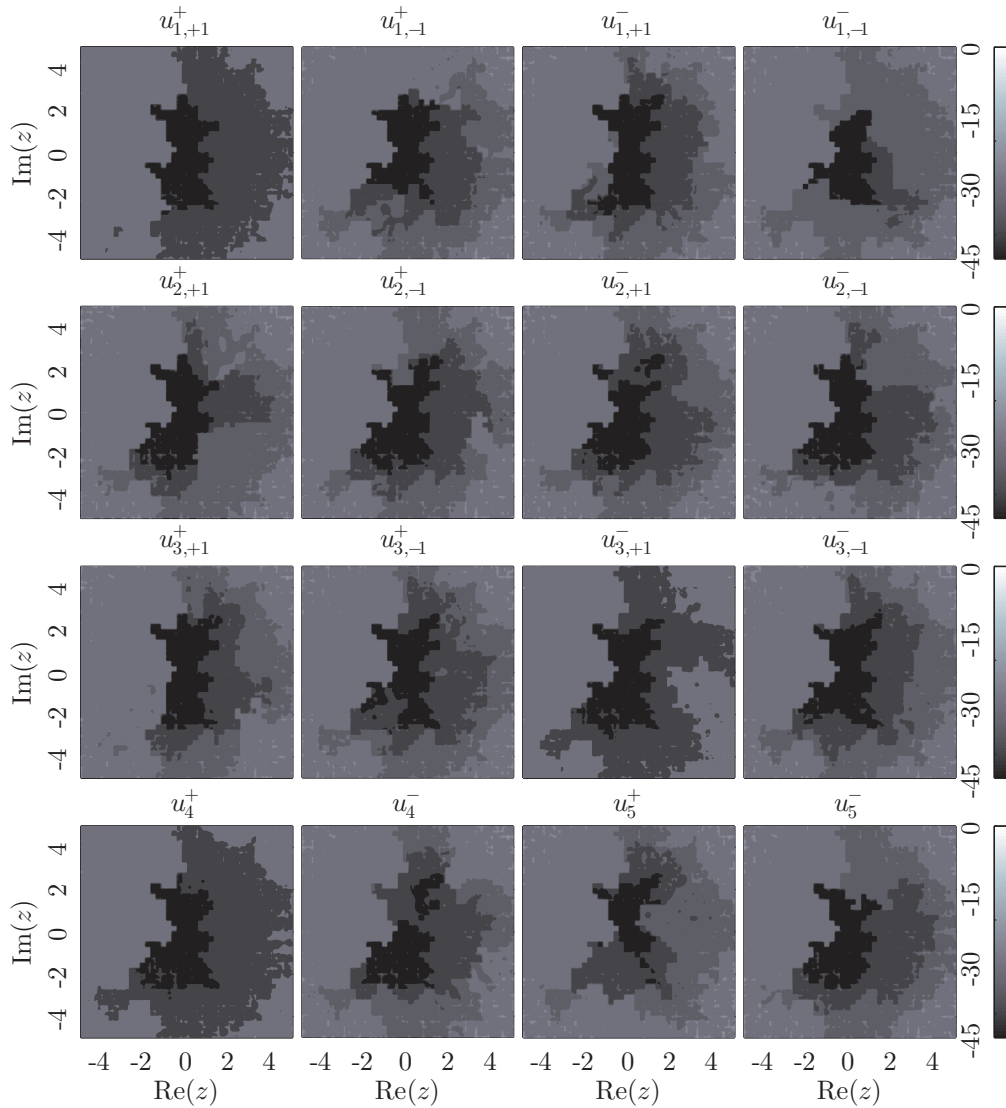


Figure 6.4: Relative error between the transformed solutions. Here each solution computed by applying (2.5) through (2.9) to each point in the high precision numerical solution in figure 6.1, call it $u(z)$, is compared to a numerical solution generated by applying (2.5) through (2.9) to $u(0)$. The color bar shows \log_{10} of the relative error.

6.2 Initial Explorations: Zero α and β

The investigations into the solutions of P_{IV} with no closed form began with a survey of the solutions resulting from changing the initial conditions when $\alpha = \beta = 0$. Aside from the knowledge of the decaying asymptotic condition (4.2) and the resulting connection formulae (see section 4.1), there was little available in the literature for this choice of parameters.

Investigations of figure 5.19 and sequences of solutions along several lines with $u'(0)$ fixed led us to believe that there were further classes of solutions with noteworthy characteristics. For instance, we witnessed that the poles in the complex plane were bound roughly by the sectors shown in figure 6.5.

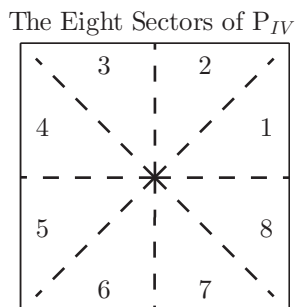


Figure 6.5: The eight sectors in the solutions of P_{IV} .

The entire survey is given in [43]. Here we only highlight the solution types that we believed had notable characteristics.

6.2.1 Sequences of Solutions Along $u'(0) = 0$, Varying $u(0)$

Initial investigations of the possible solution types when $\alpha = \beta = 0$ involved the computation of sequences of solutions over a region of the complex plane and along the real axis as we fixed $u'(0)$ and varied $u(0)$. For instance, we initially fixed $u'(0) = 0$ and produced the sequence of solutions for $u(0) \in [-5, 5]$ in increments of 0.01. We noticed that subsequences suggested solutions with adjacent sectors that were free of poles. Figures 6.6 and 6.7 provide two examples of refined subsequences hinting at the solutions with adjacent pole-free sectors.

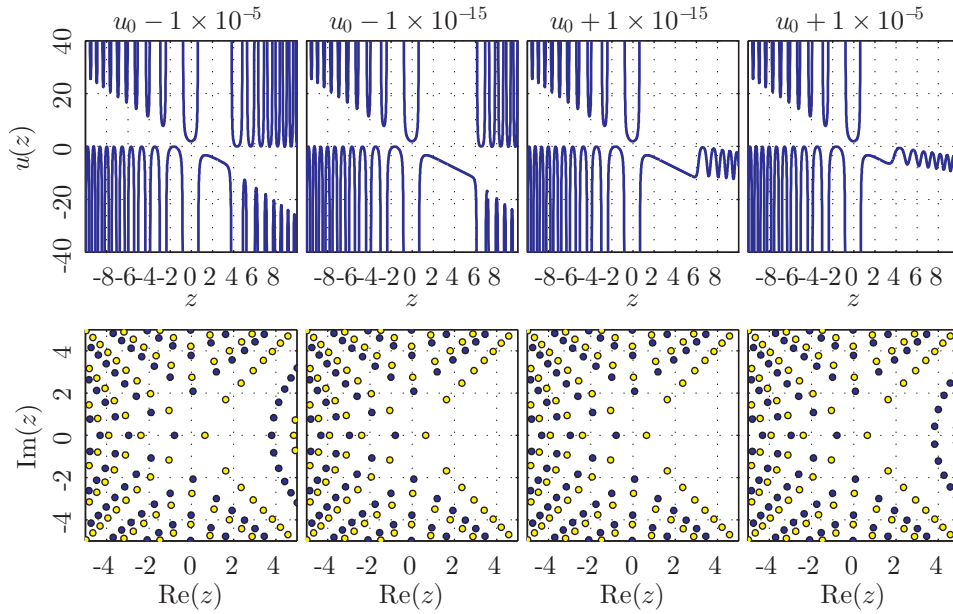


Figure 6.6: Sequence of solutions for $\alpha = \beta = 0$ near $u_0 = 1.987405112326211\dots$ along the line $u'(0) = 0$. The solution along the real axis is shown in the top row, while pole locations and residues are shown in the bottom row.

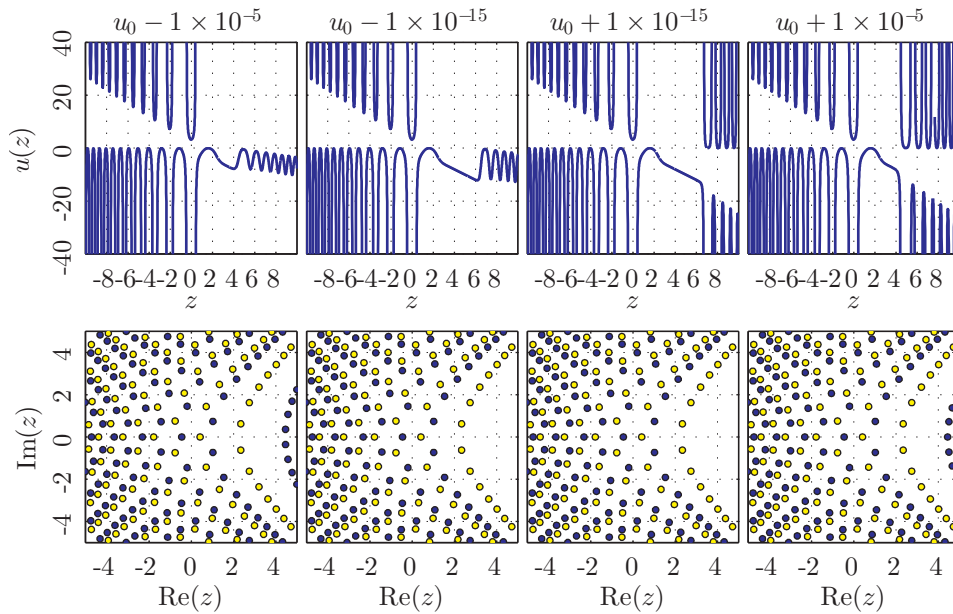


Figure 6.7: Sequence of solutions for $\alpha = \beta = 0$ near $u_0 = 3.235356086736551\dots$ along the line $u'(0) = 0$. The solution along the real axis is shown in the top row, while pole locations and residues are shown in the bottom row.

Comparing the values of $u(0) = u_0$ in these subsequences to figure 5.19, we realized that

the solutions with adjacent pole free sectors occurred certainly at the boundaries of the regions with a finite number of poles. The solutions in figures 6.6 and 6.7 occur at the left and right boundaries, respectively, of the first shaded region in the right half-plane of the right frame in figure 5.19. In figure 6.6, as $u(0)$ increases to $u_0 = 1.987405112326211\dots$ the poles within the region $\arg(z) \in [0, \frac{\pi}{4}] \cup [\frac{7\pi}{4}, 2\pi)$ move to the right with poles located directly on the real axis. After $u(0)$ passes through $u_0 = 1.987405112326211\dots$ there is a transition to poles located above and below the real axis, creating oscillations directly on the axis. This behavior, first noted in the discussions of P_I in [20], suggests that the solution occurring directly at $u(0) = u_0 = 1.987405112326211\dots$ is completely free of poles in the region $\arg(z) \in [0, \frac{\pi}{4}] \cup [\frac{7\pi}{4}, 2\pi)$. Analogous behavior can be observed in figure 6.7.

We also noticed solutions exhibiting the clearing of poles from adjacent sectors for ICs in the vicinity of the curves indicating solutions asymptotic to the roots of (4.3). Examples are given in figures 6.8 and 6.9. There is a marked difference between the solutions occurring at the boundaries of regions with a finite number of poles and those occurring along these curves. Considering figure 6.8, this sequence begins with a single pole (near $z = 0$) and oscillations on the positive real axis. The oscillations are again due to poles located just above and below the positive real axis. As $u(0)$ increases through $u_0 = 2.660688155172691\dots$ the pole fields in roughly $\arg(z) \in [0, \frac{\pi}{4}] \cup [\frac{7\pi}{4}, 2\pi)$ move to the right and return, but with no reorientation to poles on the real axis in this case. The behavior in figure 6.9 is completely analogous, only all of the solutions shown have poles on the real axis with no reorientation to poles above and below the axis. In either case, the behavior is due to the ICs of the solution with adjacent pole free sectors occurring at a point where we can find a deleted neighborhood of the ICs contained entirely in a region with a finite number of poles or with an infinity of poles in figure 5.19. Similar discussions are found throughout [43].

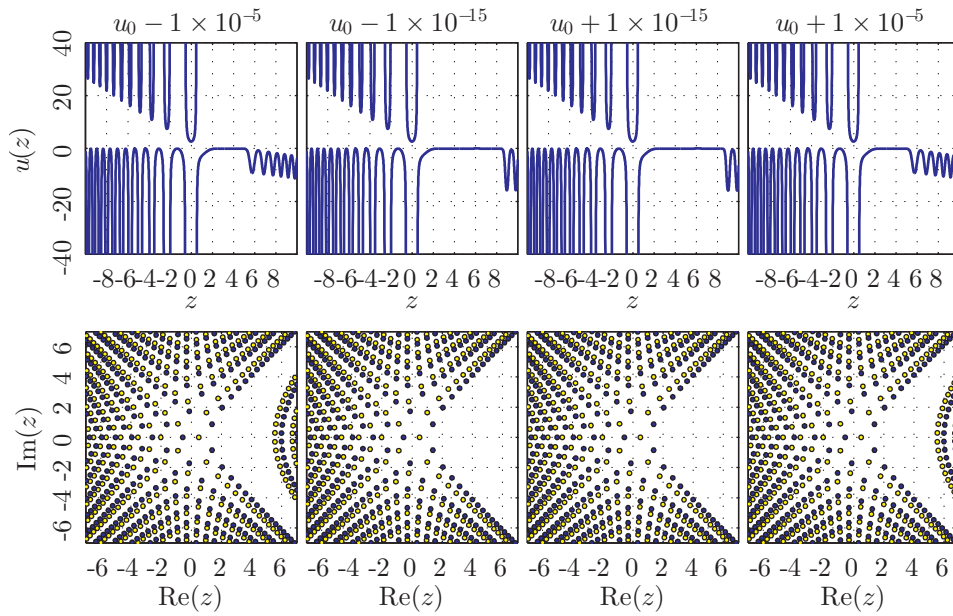


Figure 6.8: Sequence of solutions for $\alpha = \beta = 0$ near $u_0 = 2.660688155172691\dots$ along the line $u'(0) = 0$. The solution along the real axis is shown in the top row, while pole locations and residues are shown in the bottom row.

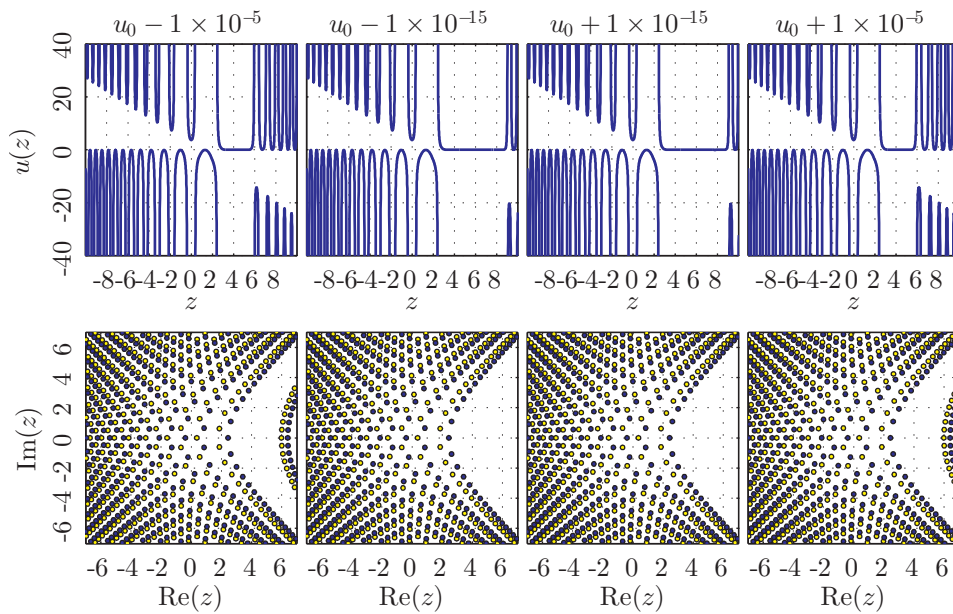


Figure 6.9: Sequence of solutions for $\alpha = \beta = 0$ near $u_0 = 3.726596884689709\dots$ along the line $u'(0) = 0$. The solution along the real axis is shown in the top row, while pole locations and residues are shown in the bottom row.

6.2.2 Sequences of Solutions Satisfying the Decaying Asymptotic Condition

Significant effort was also made to look into the solutions of P_{IV} when $\alpha = \beta = 0$ satisfying the decaying asymptotic condition (4.2). Investigations again involved the consideration of sequences of solutions and the locations of their ICs in the $u(0)$ versus $u'(0)$ plane. Recall from section 4.1 that the decaying asymptotic condition (4.2) depends on a free parameter k with a special value k^* ($k^* = \frac{1}{\pi}$ in the case $\alpha = \beta = 0$) separating solutions that are at most oscillatory on the real axis from those with poles on the real axis. This led us to generate sequences of asymptotically decaying solutions based on the parameter k .

The first example shows a sequence of solutions near k^* . Section 4.1 details connection formulae in the case of $0 < k \leq k^*$. For instance, when $0 < k < k^*$ $u(z)$ is generally oscillatory as $z \rightarrow -\infty$ when $u(z)$ satisfies (4.2) as $z \rightarrow +\infty$. Likewise, if $k = k^*$ $u(z) \rightarrow -2z$ as $z \rightarrow -\infty$. Both behaviors can be witnessed in figure 6.10.

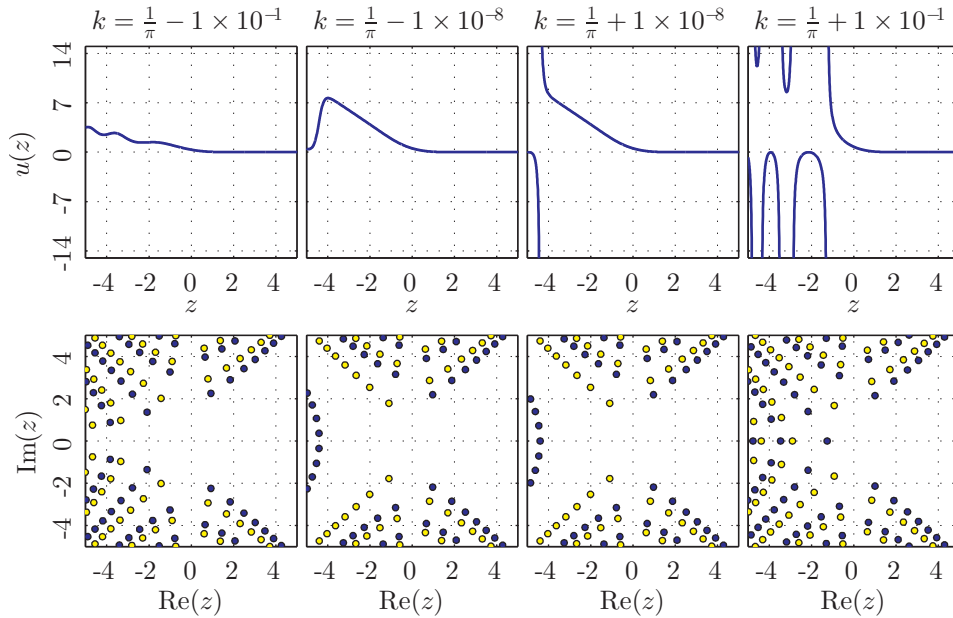


Figure 6.10: Sequence of solutions for $\alpha = \beta = 0$ near $k = \frac{1}{\pi}$ in $k(D_{\frac{1}{2}\alpha-\frac{1}{2}}(\sqrt{2}z))^2$. The solution along the real axis is shown in the top row, while pole locations and residues are shown in the bottom row.

Further explorations by varying k led to the discovery of a previously undiscussed solution

type with a half-plane entirely free of poles. If $k = \frac{1}{2}k^*$ we find that $u(z) \rightarrow -\frac{2}{3}z$ as $z \rightarrow -\infty$. In the vicinity of $k = \frac{1}{2}k^*$ the pole fields in the region $\arg(z) \in [\frac{\pi}{2}, \pi]$ (likewise, $\arg(z) \in [\pi, \frac{3\pi}{2}]$) retreat and return along the ray $r \exp(i\frac{3\pi}{4})$ (likewise, $r \exp(i\frac{5\pi}{4})$), $r > 0$, changing orientation at $k = \frac{1}{2}k^*$. This complex change in the orientation of the poles in the process of retreating and returning is indicative of a sector of the complex plane being pole free at the choice of parameter or IC exactly at the transition from retreat to return. This was first witnessed for P_I in [19], and it can be witnessed for P_{IV} in the second and third frames of figure 6.11.

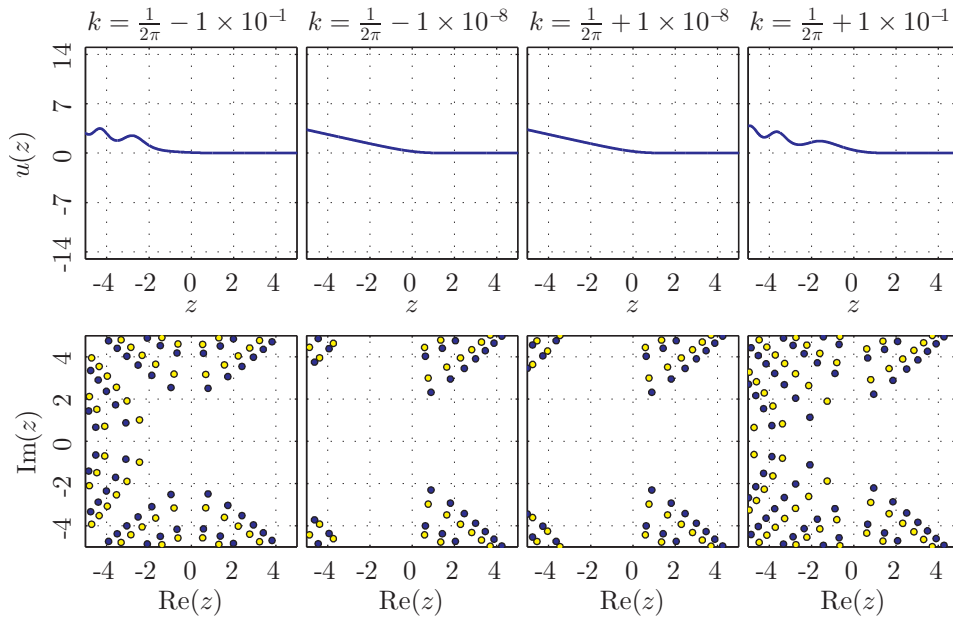


Figure 6.11: Sequence of solutions for $\alpha = \beta = 0$ near $k = \frac{1}{2\pi}$ in $k(D_{\frac{1}{2}\alpha - \frac{1}{2}}(\sqrt{2}z))^2$. The solution along the real axis is shown in the top row, while pole locations and residues are shown in the bottom row.

The solution symmetric to the one being approached in figure 6.11 through the symmetry (2.2) was later found to also match the behavior of the root (4.7). It turns out that for any (α, β) pair there is a single solution matching (4.7) as $z \rightarrow +\infty$. For each (α, β) pair the solution is characterized by much of the right half-plane being pole-free, making this a prime candidate for a single solution comparison of all (α, β) pairs.

A discussion of the decaying asymptotic solutions for $k < 0$ and $k > k^*$ (both with $\alpha = \beta = 0$)

appears in [43].

6.3 Further Explorations: α and β Not Both Zero

Armed with the knowledge of where to seek possible solutions with special characteristics in the case of $\alpha = \beta = 0$ we expanded our search to parameter choices with one or both of α and β nonzero. These explorations first considered the fundamental domain (3.7), considering multiple choices of α and β along each boundary and interior to the domain. Then the explorations moved beyond the fundamental domain, paying particular attention to the choice of $\beta > 0$. Solutions with adjacent pole free sectors and much of a half-plane pole-free were observed in all cases.

6.3.1 An Exploration of the Fundamental Domain

The literature describes solutions in the fundamental domain (3.7) only for the cases $\alpha = \beta = 0$ (numerical and asymptotic solutions), $(\alpha = 0, \beta = -\frac{2}{9})$ (a rational solution), along the line $\beta = 0$ (asymptotically decaying solutions), and along the curve $\beta = -2(\alpha - 1)^2$ (asymptotic, rational and special function solutions that occur only for highly limited choices of ICs), all of which occur on the boundary. Yet, theory states that solutions for all parameter choices in theory can be found by applying the transformations (2.5) through (2.7) to the solutions in this domain.

Figure 6.12 shows the locations of special solutions, both with and without closed forms, for the choices $(\alpha = 0, \beta = -\frac{2}{9})$, $(\alpha = 0, \beta = -2)$, and $(\alpha = 1, \beta = 0)$. The first of these frames corresponds to the parameter choice producing the rational solution $-\frac{2}{3}z$ (see table 3.1). The second frame contains the ICs for the rational solution $-2z$ (see table 3.1), while the second and third frames both show solutions in terms of the parabolic cylinder or confluent hypergeometric function. Recall from section 5.4 that the circle (blue/yellow) and diamond (blue/yellow) markers indicate solutions matching the roots of (4.3), while the square (red) markers indicate solutions that have a closed form. Figure 5.23 contains a far more detailed explanation of the markers.

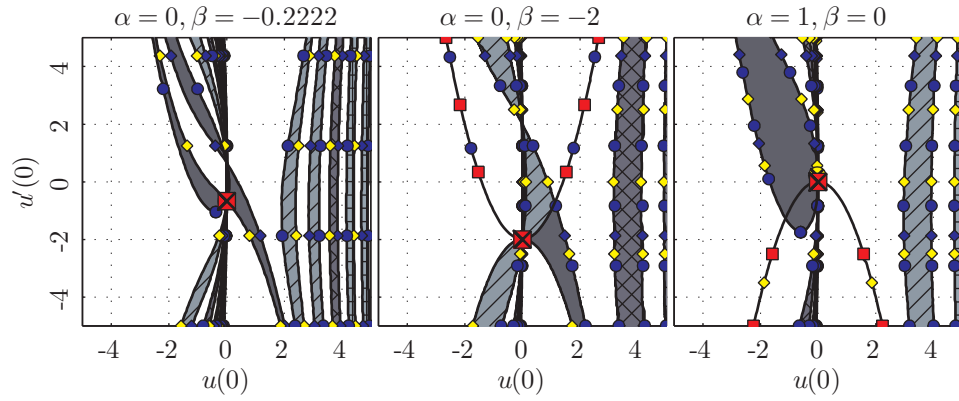


Figure 6.12: Number of poles on the positive real axis for $(\alpha = 0, \beta = -\frac{2}{9})$, $(\alpha = 0, \beta = -2)$, and $(\alpha = 1, \beta = 0)$. A detailed description of the markers and shading is given in figure 5.23.

Similar to $\alpha = \beta = 0$, the cases shown in the second two frames of figure 6.12 also have ICs that produce solutions matching two or three of the behaviors w_μ^+ , $\mu = \pm 1$, or w_{-1}^- in different segments of the real axis. These solutions feature adjacent pole free sectors and appear at the boundaries of regions in the $u(0)$ versus $u'(0)$ plane with a finite number of poles. Examples of sequences approaching these types of solutions appear in figures 6.13 and 6.14.

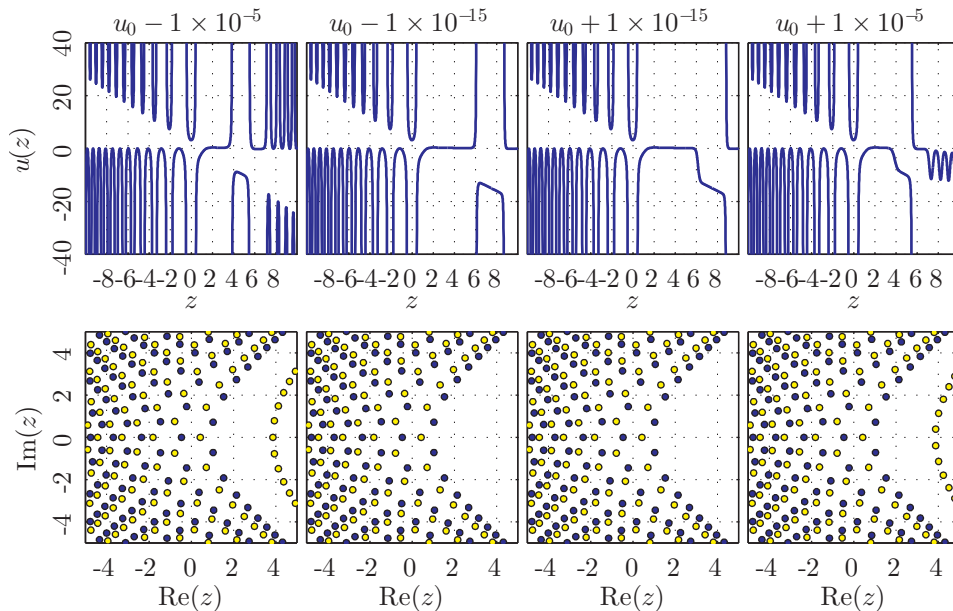


Figure 6.13: Solutions with adjacent pole free sectors for $\alpha = 0$ and $\beta = -2$. $u'(0) = 0$ and $u_0 = 3.170110354518507$. The solution along the real axis is shown in the top row, while pole locations and residues are shown in the bottom row.

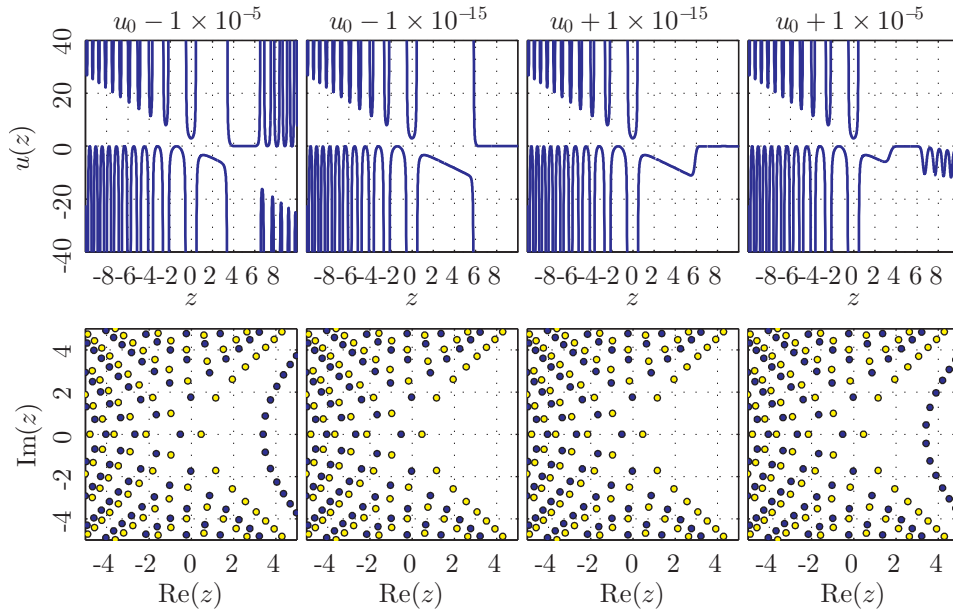


Figure 6.14: Solutions with adjacent pole free sectors for $\alpha = 1$ and $\beta = 0$. $u'(0) = 0$ and $u_0 = 2.989670219313871$. The solution along the real axis is shown in the top row, while pole locations and residues are shown in the bottom row.

Away from the vertices and along the boundary $\beta = -2(\alpha - 1)^2$ of the fundamental domain P_{IV} also has solutions in terms of the parabolic cylinder function or confluent hypergeometric function. In the case of $\alpha = 0.5$ and $\beta = -0.5$ the ICs generating these solutions are along the curve marked by squares (red) in the first frame of figure 6.15. In all three frames we find that P_{IV} exhibits solutions with adjacent pole free sectors along every boundary of the fundamental domain.

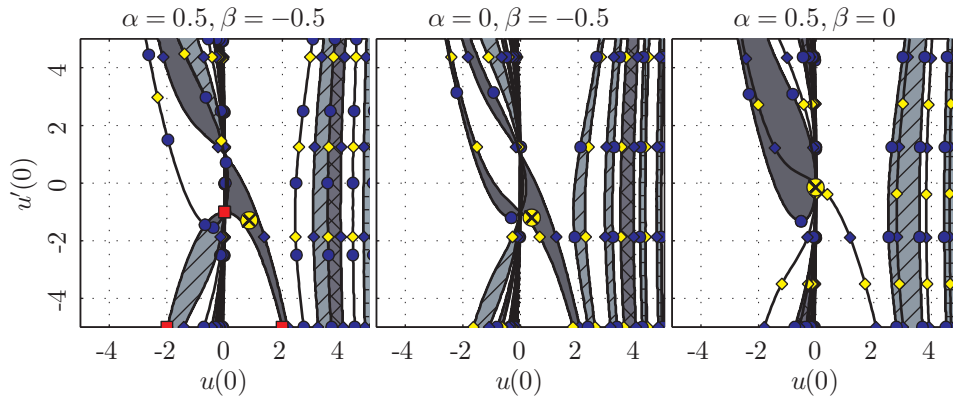


Figure 6.15: Number of poles on the positive real axis for $(\alpha = 0.5, \beta = -0.5)$, $(\alpha = 0, \beta = -0.5)$, and $(\alpha = 0.5, \beta = 0)$. A detailed description of the markers and shading is given in figure 5.23.

Likewise, choices of α and β interior to the fundamental domain feature solutions with adjacent pole free sectors as well. The ICs that generate these solutions again appear at the boundaries of regions with a finite number of poles in figure 6.16.

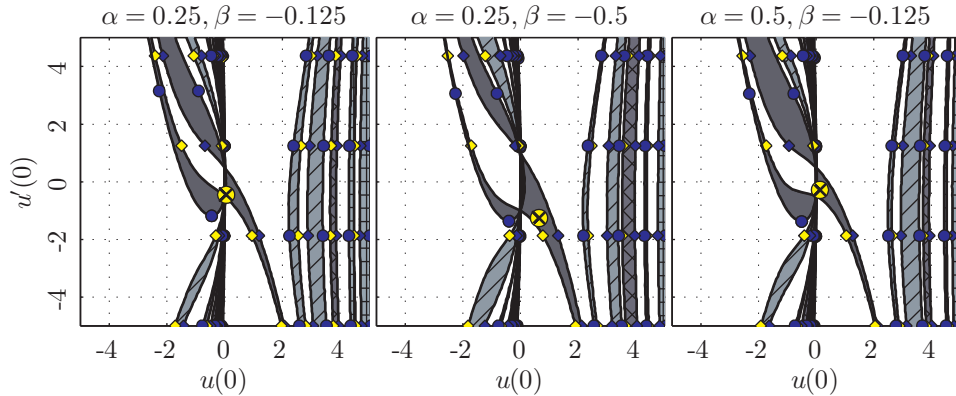


Figure 6.16: Number of poles on the positive real axis for parameter choices interior to the fundamental domain. A detailed description of the markers and shading is given in figure 5.23.

6.3.2 Parameters Exterior to the Fundamental Domain

Recall that we can in theory produce all possible solutions for parameter choices outside the fundamental domain through the application of the transformations discussed in section 2.3 to solutions with α and β within the domain. Still, the complexity of these transformations makes it difficult to understand the characteristics of the resulting solution. For instance, a first glance at (2.5) leads us expect a root of $u(z)$ to be a pole of $u_{1,\mu}^{\pm}(u(z), z)$, but comparing the first row of frames in figure 6.2 to the left frame of figure 6.1 this is not always the case. Therefore we performed some limited exploration into α and β choices outside of the fundamental domain.

First, studies of P_{IV} with $\beta > 0$ are noticeably absent from the literature. For instance, all known closed form solutions occur only when β is nonpositive and likewise for the solution transformations (assuming $u(z)$ is real when z is real). However, the knowledge of solutions with adjacent pole free sectors that appear in the cases of α and β already explored suggests that there are solutions with $\beta > 0$ featuring noteworthy characteristics.

Solutions of P_{IV} that are real along the real axis with $\beta < 0$ only match two of the roots of

(4.3) due to the term $\sqrt{-2\beta}$ in (4.5) and (4.6). This makes the figures displaying pole counts (e.g. figure 6.17) much simpler than their counterparts when $\beta \leq 0$. In these frames a there is single IC generating the asymptotic behavior of $w_{+1}^{-1} \sim -\frac{2}{3}z$ and the ICs along the boundaries of regions with finite poles match the behavior of $w_{-1}^{-1} \sim -2z$.

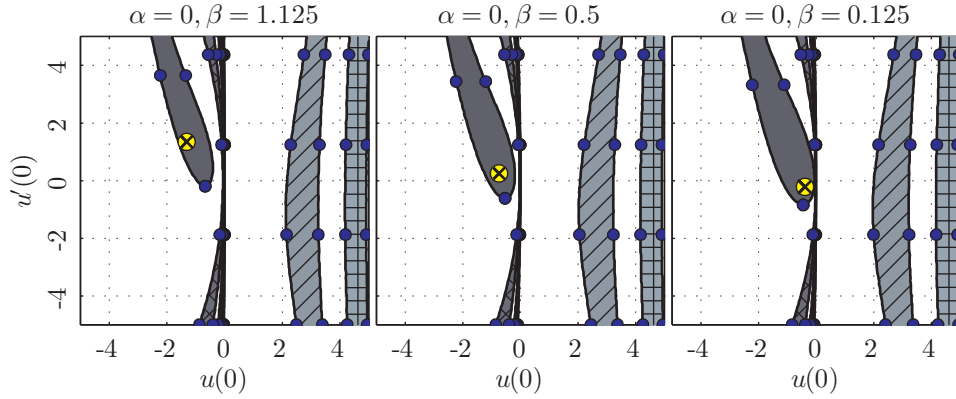


Figure 6.17: Number of poles on the positive real axis for parameter choices where $\alpha = 0$ and $\beta > 0$. A detailed description of the markers is given at the end of section 5.4.

Beyond the choices of $\beta > 0$ we also considered some parameters slightly larger in magnitude. Increasing $|\alpha|$ and/or $|\beta|$ to even three or four significantly increases the complexity of the pole counting diagrams. Still, there are solutions that match each of the roots of (4.3) when $\beta \leq 0$ and solutions that match only w_{+1}^{-1} or w_{-1}^{-1} when $\beta > 0$. See figures 6.18 and 6.19 for examples of pole counts with α and/or β equal to three or four.

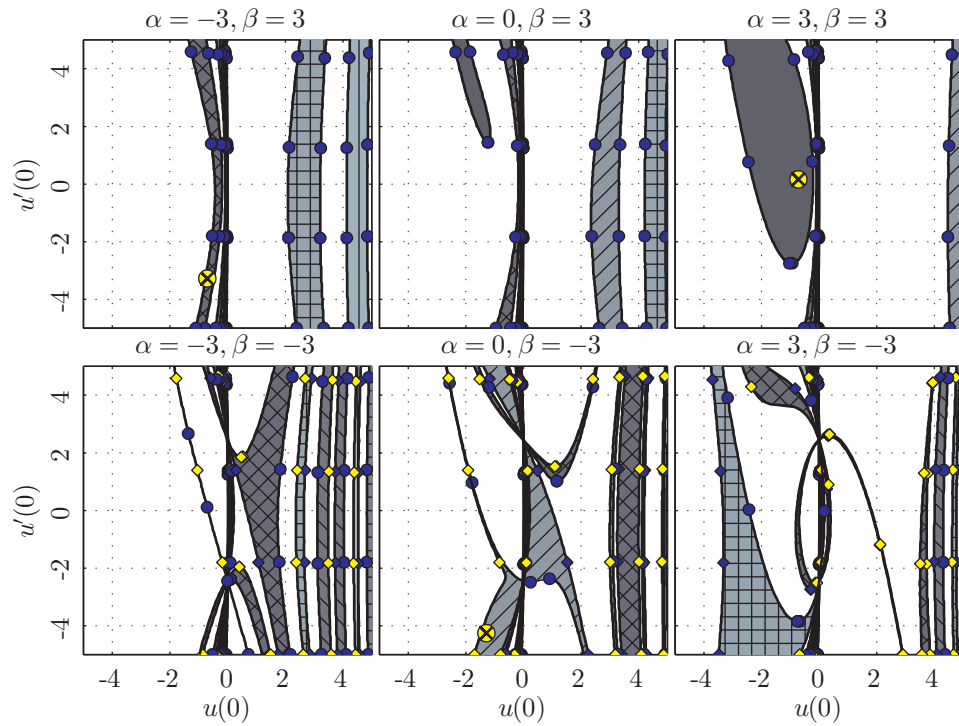


Figure 6.18: Number of poles on the positive real axis for some parameters exterior to the fundamental domain. The initial conditions for solutions asymptotic to w_{-1}^- in the top middle, bottom left, and bottom right frames occur outside of the domain shown at $(u(0) \approx -4.6822, u'(0) \approx 20.7787)$, $(u(0) \approx -10.7942, u'(0) \approx 120.3759)$, and $(u(0) \approx 49.4606, u'(0) \approx -2442.3215)$, respectively. The locations of these parameters in α vs. β space are shown later in figure 6.22. A detailed description of the markers and shading is given in figure 5.23.

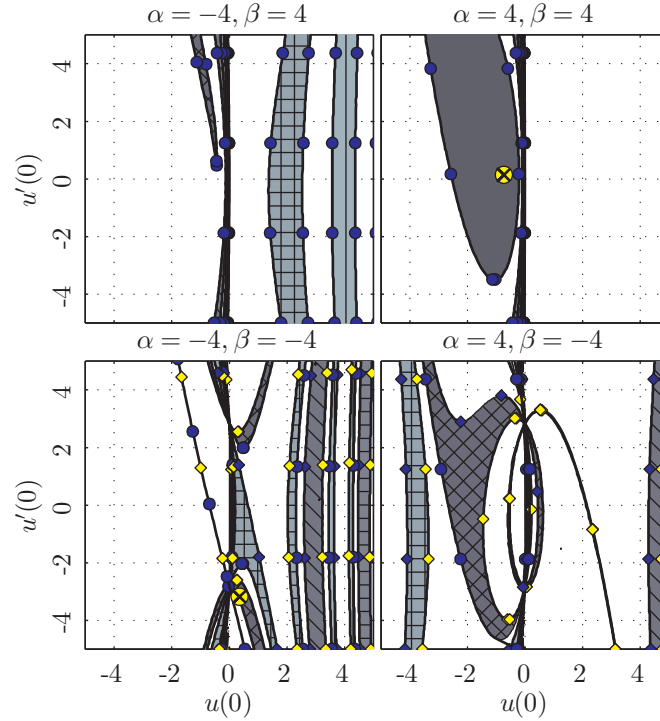


Figure 6.19: Number of poles on the positive real axis for some parameters exterior to the fundamental domain. The initial conditions for solutions asymptotic to w_{+1}^- in the top left and bottom right frames occur outside of the domain shown at $(u(0) \approx -3.2210, u'(0) \approx 15.9830)$ and $(u(0) \approx -4.3409, u'(0) \approx -8.5801)$, respectively. A detailed description of the markers and shading is given in figure 5.23.

6.3.3 A Note on Connection Formulae

In [42] there is a discussion of the possibility of solutions that are smooth (except, possibly, for a finite number of poles) along the entire real axis. This discussion arises from the comparison of the left and right frames of figure 5.19, showing the number of poles along the negative and positive real axes, respectively. This figure makes it easy to visualize that a segment of the curve extending from the origin and down to the right in the right frame cuts across the shaded region that extends from the origin up and to the right in the left frame. In this case, along this segment P_{IV} has solutions that are smooth in both directions. These, and all other choices of α when $\beta = 0$, appear to be the only examples of solutions that have connection formulae available in the literature (see, e.g. [7], [14], [38], or [31]).

Similar analysis of the number of poles on the positive and negative real axes in figures 6.12

and 6.15 (together with the symmetry (2.2)) shows that we can again identify solutions that are smooth in both directions for regions of ICs in cases of α and β on the boundary of the fundamental domain. Likewise, figure 6.16 indicates that such regions (sometimes only a curve) will exist for all parameter choices within the fundamental domain. Further, considering $\alpha = 0.25$ and $\beta = -0.125$ in figure 6.20 we can see this more concretely for an example in the fundamental domain.

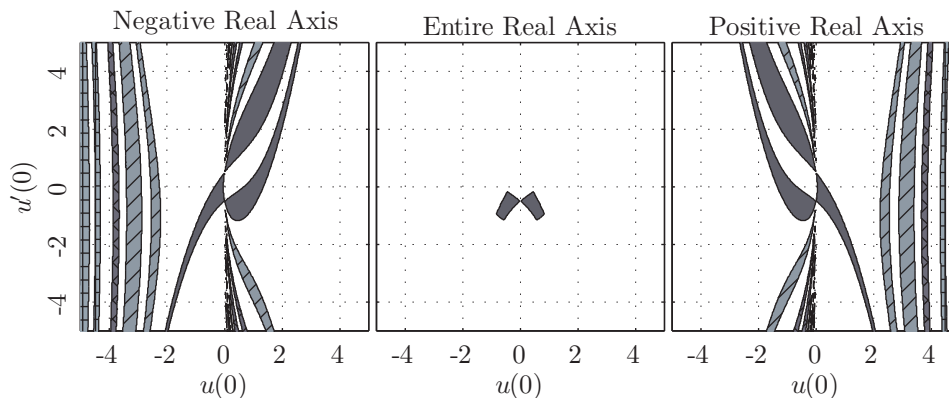


Figure 6.20: Number of poles on the negative real axis (left), entire real axis (center), and positive real axis (right) for $\alpha = 0.25$ and $\beta = -0.125$. A detailed description of the shading is given in figure 5.23.

It is easy to see that comparison of the left and right frames indicates that the shaded regions in the center will have a finite number of poles on the entire real axis.

On the other hand, figure 6.18 shows that similar regions will also occur outside the fundamental domain when $\beta < 0$, but with the difference that there now may be a finite number of poles on the real axis in either one or both directions as in the case of $\alpha = 3$ and $\beta = -3$ shown in figure 6.21 where the ICs in the regions in the center frame now generate solutions with 5 poles on the entire real axis.

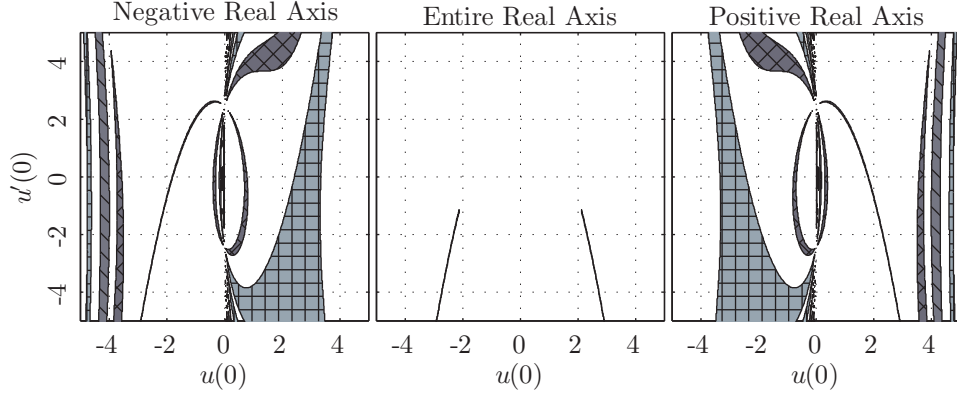


Figure 6.21: Number of poles on the negative real axis (left), entire real axis (center), and positive real axis (right) for $\alpha = 3$ and $\beta = -3$. The shaded regions in the center frame contain ICs that generate solutions with 5 poles on the real axis. A detailed description of the shading is given in figure 5.23.

In contrast, positive choices of β do not seem to produce any such regions of ICs.

6.3.4 Solutions with a Pole-Free Half-Plane

In the case of $\alpha = \beta = 0$ it was noted in [43] that P_{IV} has a solution that is pole free over an entire half-plane. Likewise, numerical observations in [42] suggest that for any choice of α and β there exists a solution and a $z_0 \in \mathbb{R}$ such that $u(z)$ is pole free for all z with $\text{Re}(z) > z_0$. In all cases these solutions are asymptotic to the root $w_{+1}^- \sim -\frac{2}{3}z$ as $z \rightarrow +\infty$ and $z \in \mathbb{R}$. Figure 6.22 (adapted from [42]) shows the number of poles on the positive and negative real axes for these solutions. Since the right half plane is pole-free after some z_0 the right frame shows only a finite number of poles for every α and β pair.

The behavior in the left half-plane can vary significantly depending on α and β . For instance, there are no cases with $\beta > 0$ where the left half-plane has a finite number of poles. On the other hand, when $\beta \leq 0$ there are both regions of ICs generating solutions with a finite number poles and subsets leading to an infinity of poles that are bounded by the parabolas $\beta = -2(\alpha - 2n)^2$, $n \in \mathbb{Z}$, and the lines $\beta = -\frac{(2m+1)^2}{2}$, $m = 0, 1, 2, \dots$. These regions can be seen in the left frame of figure 6.22 with the parabolas $\beta = -2(\alpha - 2n)^2$, $n \in \mathbb{Z}$, and the lines $\beta = -\frac{(2m+1)^2}{2}$, $m = 0, 1, 2, \dots$, shown as dashed lines. The parabolas $\beta = -2(\alpha - (2n + 1))^2$ and lines $\beta = -2(m + 1)^2$, both of

which make up the boundaries of the fundamental domain (3.7), are also included in the figure as solid lines.

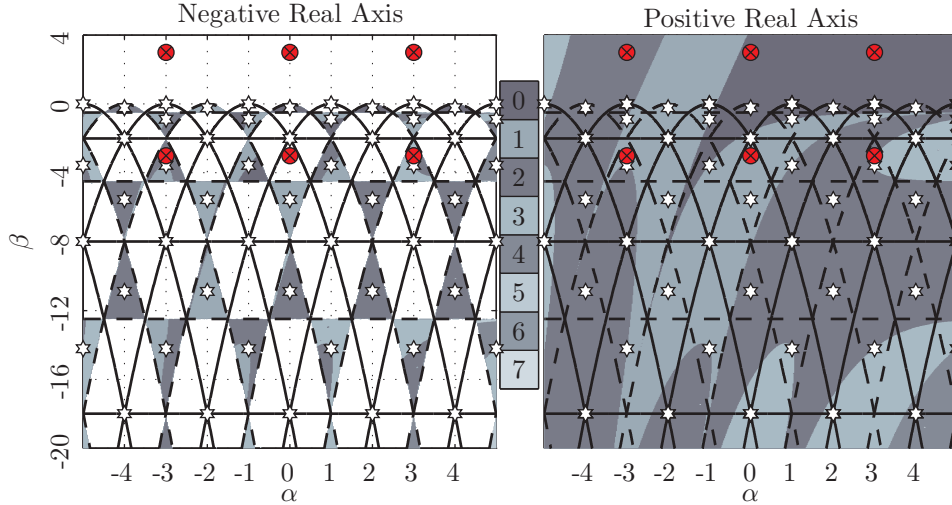


Figure 6.22: Number of poles on the positive (right) and negative (left) real axis for solutions asymptotic to $w_{+1}^- \sim -\frac{2}{3}z$ as $z \rightarrow +\infty$ and $z \in \mathbb{R}$ and each α and β . The solid curves indicate the boundaries of the Weyl chambers, while the dashed lines show the boundaries of regions of finite poles on both the positive and negative real axes. Note that in this case $\beta > 0$ implies an infinity of poles along \mathbb{R}^- . The circles (red) containing an \times indicate those parameters shown in figure 6.18.

Along each of the parabolas $\beta = -2(\alpha - 2n)^2$ the behaviors of these solutions also vary as α is changed. Likewise, if α and β are moved off of the parabolas, different behaviors in the left half of the complex plane are observed. The next few sections will discuss the different variations of these solutions. These discussions are also available in [42].

6.3.4.1 The Tops of the Parabolas

Consider the Okamoto I polynomials described in, for instance, [13]. Note that these are different than the generalized Okamoto polynomials discussed in section 3.1 and [14]. Figure 6.23 displays the roots of the Okamoto I polynomials for various orders m_l and m_d .

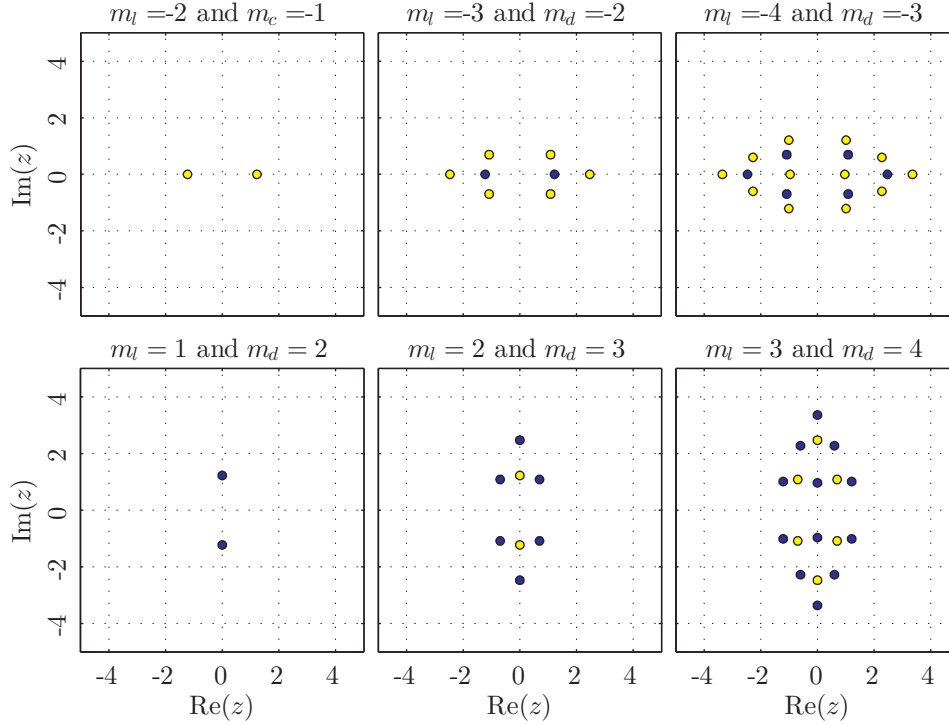


Figure 6.23: Roots of the Okamoto I polynomials for orders $m = \pm 1, \pm 2, \pm 3, \pm 4$. The subscript l or d indicates whether the polynomial of that order is shown in the frame as light (yellow) or dark (blue) circles, respectively.

At the tops of the parabolas $\beta = -2(\alpha - 2n)^2$ (that is, $\alpha = 2m$, $m \in \mathbb{Z}$, and $\beta = 0$) the poles nearest the origin align similar to the roots of the Okamoto I polynomials. Examples for several different choices of m are shown in figure 6.24. When $m < 0$ poles of residue $+1$ align in a structure similar to the roots with a positive real part of the degree m Okamoto I polynomial, while poles of residue -1 appear similar to the roots of the degree $m - 1$ polynomial. On the other hand, when $m > 0$ the poles of residue $+1$ (likewise, -1) align in a structure similar to all of the roots of the order $m + 1$ (likewise, m) polynomials.

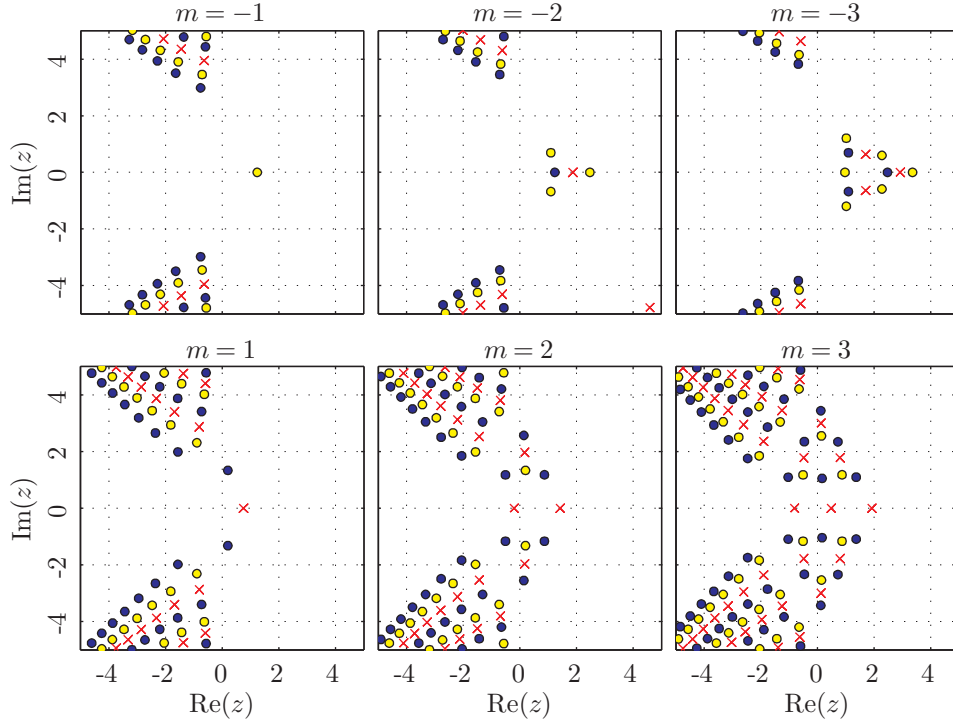


Figure 6.24: Zero and pole locations of solutions to P_{IV} with $\alpha = 2m$ and $\beta = 0$ for various values of m . These solutions match $w_{+1}^- \sim -\frac{2}{3}z$ as $z \rightarrow +\infty$ and $z \in \mathbb{R}$.

6.3.4.2 Solutions Along the Parabolas

Along the boundaries of the parabolas the solutions asymptotic to $-\frac{2}{3}z$ are nonoscillatory as $z \rightarrow -\infty$. This is due to the presence of two adjacent pole free sectors (roughly, $\arg(z) \in [\frac{3\pi}{4}, \frac{5\pi}{4}]$). Figures 6.25 and 6.26 (adapted from [42]) show solutions normal to the parabola $\beta = -2(\alpha - 2)^2$ and $\beta = -2(\alpha + 2)^2$, respectively, with the center frame showing a choice of α and β that falls directly on the parabola. The left and right frames show that if α or β are varied even slightly such that the choice of parameters no longer falls on one of the parabolas, these solutions can have either an infinity of poles or oscillate as $z \rightarrow -\infty$.

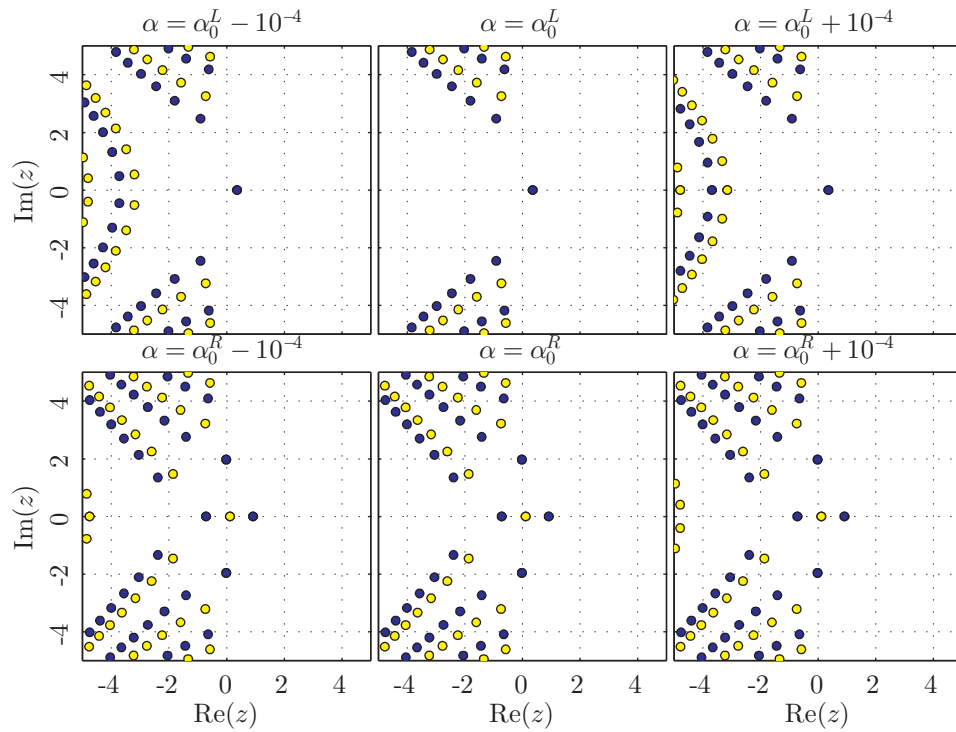


Figure 6.25: Solutions normal to the parabola $\beta = -2(\alpha - 2)^2$. All frames depict the solutions asymptotic to $-\frac{2}{3}z$ as $z \rightarrow +\infty$. The center frames occur directly along the parabolas where $\alpha = \alpha_0 = 1.25$ (top) and $\alpha = \alpha_0 = 2.75$ (bottom). The left and right frames in both the top and bottom then depict the solutions along the line normal to the parabola at $\alpha = \alpha_0$ at $\alpha_0 \pm 10^{-4}$. Pole locations and residues are shown.

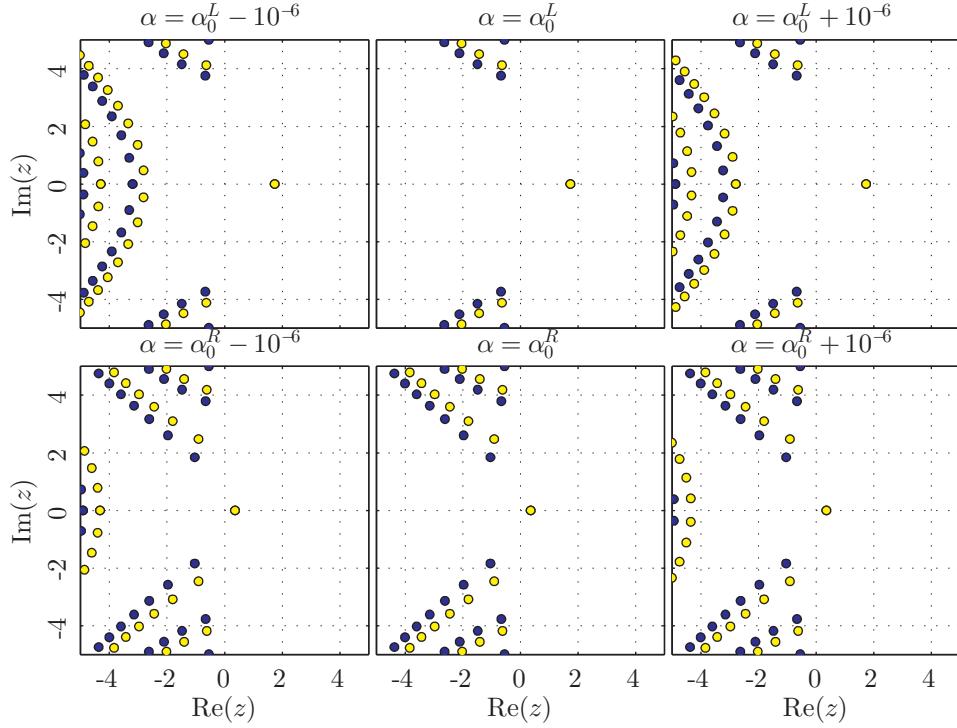


Figure 6.26: Solutions normal to the parabola $\beta = -2(\alpha + 2)^2$. All frames depict the solutions asymptotic to $-\frac{2}{3}z$ as $z \rightarrow +\infty$. The center frames occur directly along the parabolas where $\alpha = \alpha_0 = -1.25$ (top) and $\alpha = \alpha_0 = -2.75$ (bottom). The left and right frames in both the top and bottom then depict the solutions along the line normal to the parabola at $\alpha = \alpha_0$ at $\alpha_0 \pm 10^{-6}$. Pole locations and residues are shown.

6.3.4.3 When β is Positive

It is evident in figure 6.22 that all of the solutions asymptotic to $w_{+1}^- \sim -\frac{2}{3}z$ as $z \rightarrow +\infty$, $z \in \mathbb{R}$, in the case of $\beta > 0$ have an infinity of poles on the negative real axis. These solutions also do not generally have the entire right (or left) half-plane free of poles, but have a value $z_0 \in \mathbb{R}$ (possibly positive or negative) such that for all z with $\text{Re}(z) > z_0$ the solution has no poles [42].

6.3.4.4 Other Solutions With a Pole Free Half-Plane

There are also rational solutions and solutions expressible in terms of parabolic cylinder or confluent hypergeometric functions that also feature a mostly pole free half-plane. For instance, the solutions $u_{\nu, \epsilon, d_1, d_2}^{[PC; k]}$, $k = 1, 2$, when either $d_1 = 0$ or $d_2 = 0$ exhibit half-planes that are nearly pole-free as in figure 6.27 (adapted from [42]). Generally, these other solutions with a nearly pole

free half-plane match a different root of (4.3) as $z \rightarrow +\infty$ than $w_{+1}^- \sim -\frac{2}{3}z$.

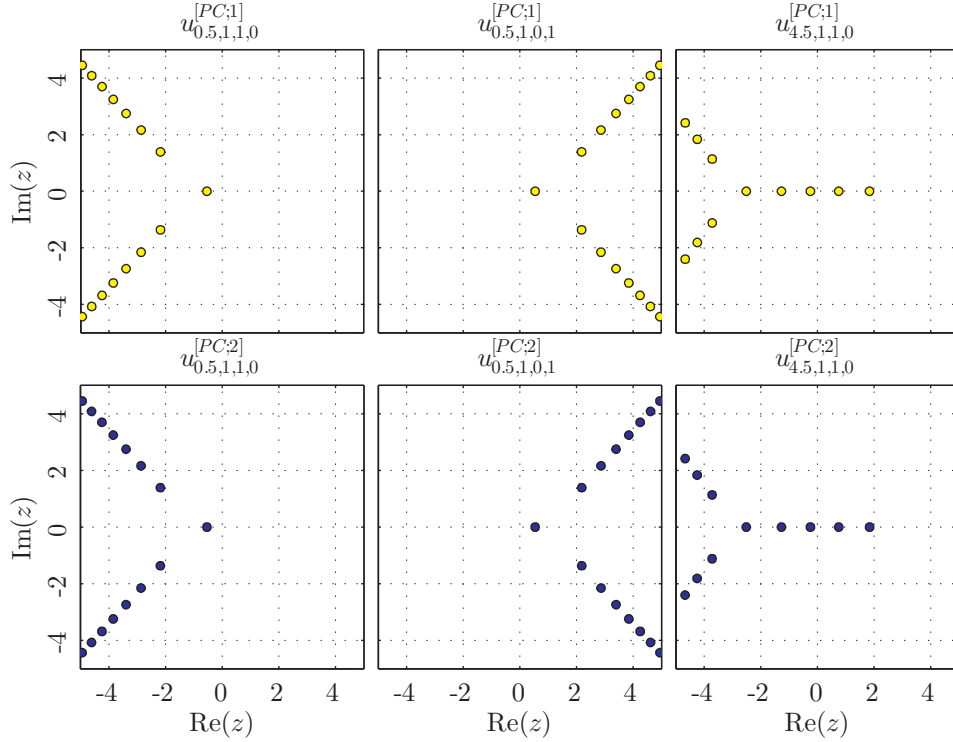


Figure 6.27: Examples of $u_{\nu, \epsilon, d_1, d_2}^{[PC;k]}$ (see section 3.2), $k = 1, 2$, for $d_1 = 0$ or $d_2 = 0$. These solutions feature a half plane that contains only a finite number of poles. Pole locations and residues are shown.

6.3.5 Solutions With Adjacent Pole-Free Sectors

It was discussed several times earlier in this chapter that aside from the rational and special function solutions P_{IV} has solutions with no closed form but feature at least two adjacent pole free sectors. In [43] these are equated to the tronquée solutions of P_I . That is, the tronquée solutions of P_I feature two adjacent pole free sectors. In [42] this analogy was dropped to avoid confusion with the very specific meaning of tronquée as related to P_I .

In the case of P_{IV} these solutions were earlier (in this thesis and in [42]) characterized as appearing at the boundaries of shaded regions or along curves within the pole counting diagrams. The solutions asymptotic to $w_{+1}^- \sim -\frac{2}{3}z$ were considered separately in the previous section 6.3.4, but they would certainly fall into this category. Likewise, the solutions that are asymptotic to w_{-1}^-

and w_μ^+ , $\mu = \pm 1$, as $z \rightarrow +\infty$ and $z \in \mathbb{R}$ feature adjacent pole free sectors. It was found in [42] that there are cases when two or three behaviors w_μ^\pm , $\mu = \pm 1$, are present simultaneously in a single solution. For instance, ICs generating solutions matching w_{+1}^+ and w_{-1}^+ over different segments of the positive real axis (but within the same solution) occur when $\beta = 0$. This is not surprising considering (4.5) and (4.6) and that these are simply the solutions asymptotic to (4.2). Several examples are available in [43].

In the following figures, multiple frames will be shown depicting the different types of solutions with adjacent pole free sectors for each (α, β) pair discussed. These are all repeated from [42]. In most cases, solutions where two or more behaviors appear at once will be given in at least one frame. In every case, the solutions shown occur at the boundary of or along the curve located in the first shaded region extending from $u'(0) = 5$ to $u'(0) = -5$ in the right half plane (i.e. $u(0) > 0$) of the appropriate pole counting figure. These solutions are all given along the line $u'(0) = 0$.

Evidence suggests that solutions that match more than one of the roots of (4.3) simultaneously (but in different segments of the real axis) will occur for parameter choices along the parabolas $\beta = -2(\alpha - (2m + 1))^2$, $m \in \mathbb{Z}$, or along the lines $\beta = 2n^2$, $n = 0, 1, 2, 3, \dots$. First, figures 6.28 and 6.29 show two types of solutions where the behaviors of w_μ^+ , $\mu = \pm 1$, and w_{-1}^- are simultaneously present in a solution generated from a single IC. These are shown for $(\alpha = 1, \beta = 0)$ and $(\alpha = 0, \beta = -2)$, which occur at two of the vertices of the fundamental domain.

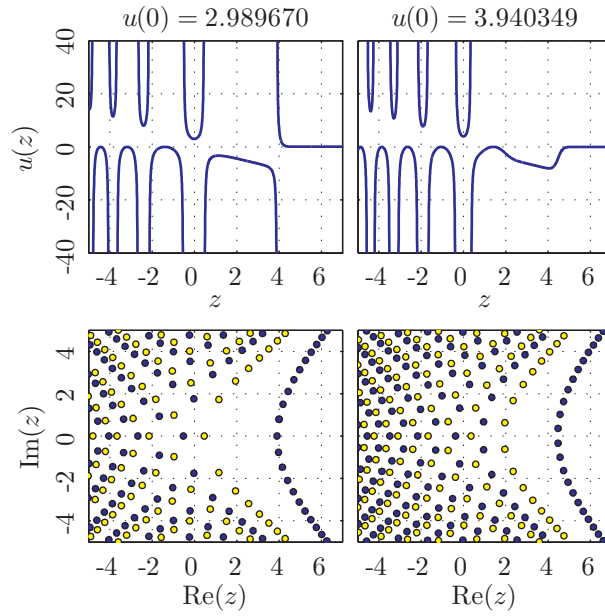


Figure 6.28: Solution types with adjacent pole free sectors for $\alpha = 1$ and $\beta = 0$. In all frames $u'(0) = 0$. The left and right frames both show that these solutions match the roots w_μ^+ , $\mu = \pm 1$, and w_{-1}^- simultaneously. The solution along the real axis is shown in the top row, while pole locations and residues are shown in the bottom row.

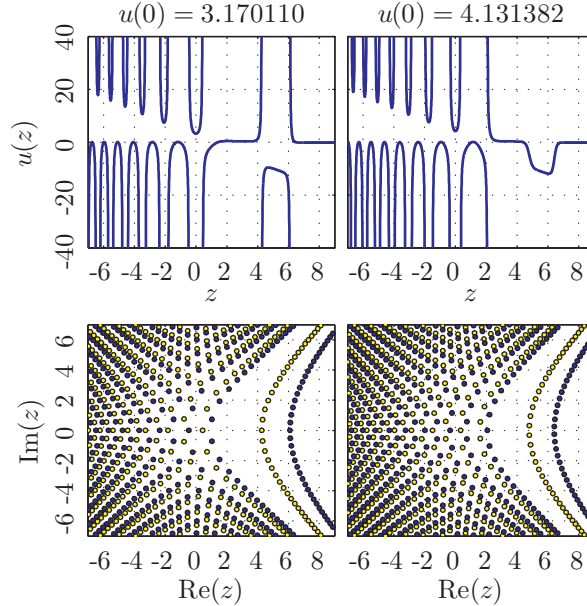


Figure 6.29: Solution types with adjacent pole free sectors for $\alpha = 0$ and $\beta = -2$. In all frames $u'(0) = 0$. The left and right frames both show that these solutions match the roots w_μ^+ , $\mu = \pm 1$, and w_{-1}^- simultaneously. The solution along the real axis is shown in the top row, while pole locations and residues are shown in the bottom row.

Similarly, solutions that match the roots w_{-1}^{\pm} concurrently (again, in different segments of the real axis) were observed along the boundary $\beta = -2(\alpha - 1)^2$ away from the vertices of the fundamental domain. An example appears in figure 6.30 for the case $\alpha = 0.5$ and $\beta = -0.5$.

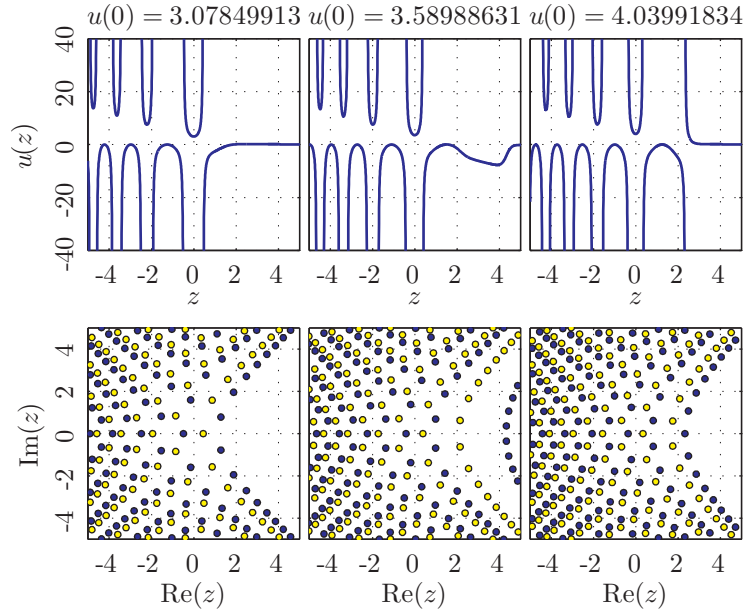


Figure 6.30: Solution types with adjacent pole free sectors for $\alpha = 0.5$ and $\beta = -0.5$. In all frames $u'(0) = 0$. The center frame shows that there are solutions that match the roots w_{-1}^{\pm} simultaneously. The solution along the real axis is shown in the top row, while pole locations and residues are shown in the bottom row.

Finally, all other parameter choices that do not occur along the parabolas $\beta = -2(\alpha - (2m + 1))^2$, $m \in \mathbb{Z}$, or along the line $\beta = 0$ have distinct ICs leading to solutions with adjacent pole free sectors and matching only one of the roots w_{μ}^{+} , $\mu = \pm 1$, or w_{-1}^{-} as in the figure 6.31.

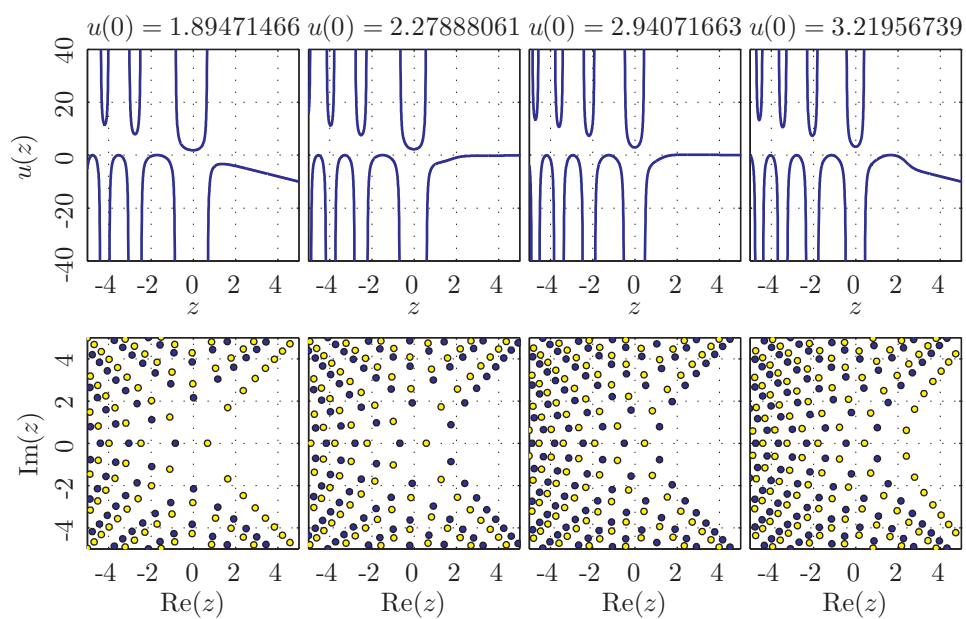


Figure 6.31: Solution types with adjacent pole free sectors for $\alpha = 0$ and $\beta = -0.5$. In all frames $u'(0) = 0$. In this case, all frames exhibit only one of the asymptotic behaviors w_{μ}^{\pm} , $\mu = \pm 1$. The solution along the real axis is shown in the top row, while pole locations and residues are shown in the bottom row.

Chapter 7

Conclusions about the Numerical Explorations of P_{IV}

Chapters 2 through 6 have focused entirely on the first research topic of this thesis. First, existing theory of P_{IV} applicable to any α and β was covered, followed by a discussion and confirmation of the rational and elementary special function solutions described in the literature. Known asymptotic approximations were presented with computational solutions that explored beyond those that have been previously presented.

The limited numerical explorations performed for this thesis already led to the identification of two types of solutions that are common to all α and β with the noteworthy property of having at least two pole-free sectors in the complex plane. This highlights the utility of the numerical method discussed in chapter 5. Prior to its introduction explorations into regions of the complex plane containing poles were inhibited and often computationally infeasible.

Since these explorations were nowhere near exhaustive there may be opportunities for the discovery of other solution types with notable characteristics. Further, these explorations were almost entirely computational leaving open the analytical consideration of, for instance, the two new solution types identified here (that is, the solutions with a nearly pole-free half-plane or with adjacent pole-free sectors). There is also the opportunity to consider solutions that are not always real on the real axis. The symmetries in section 2.2 certainly provide some information on such solutions; however, the possibilities for other explorations of this type are endless. Finally, there is opportunity to consider α and β choices that are much larger in magnitude. The numerical study here focused on the fundamental domain and a small neighborhood of it.

The contributions of this thesis include the verification of much of the theory appearing in the literature, the adaptation of the pole field solver to allow for high precision computations and also for faster computations, and the exploration of the solution space of P_{IV} to include the identification of the two new solutions types with notable characteristics.

Chapter 8

Stability Ordinates of the Adams Predictor-Corrector Methods

In this chapter I present an entirely different research topic. This research sought to characterize the stability domains of Adams predictor-corrector methods, particularly for those differential equations with purely imaginary spectra. We show that for any order p a stable predictor-corrector method can be found to integrate such a differential equation.

8.1 Introduction and Assertions

Consider the ODE $\frac{d}{dt}y(t) = f(t, y(t))$. In particular, we are considering those first-order ODE's that result from translating partial differential equations (PDEs) for wave equations to first-order systems of ODEs. If the eigenvalues of $f(t, y(t))$ were available, as in the case of a spatially discretized wave equation, we could then write $f(t, y(t)) = \lambda y(t)$, for $\lambda \in \mathbb{C}$. For instance, consider the advection equation in one dimension with zero boundary conditions

$$\begin{aligned}\frac{\partial}{\partial t}u(x, t) &= \frac{\partial}{\partial x}u(x, t), \quad x \in [a, b] \text{ and } t \in [0, T] \\ u(a, t) &= u(b, t) = 0, \quad t \in [0, T]\end{aligned}$$

Given a step size h_x the derivative on the right hand side could be approximated by a centered difference to arrive at

$$\frac{\partial}{\partial t}u(x, t) = \frac{u(x + h_x, t) - u(x - h_x, t)}{2h_x} \tag{8.1}$$

for each $x \in [a, b]$.

When finding the solution at the points $x_j = a + jh_x$, $j = 0, \dots, N$ and $h_x = \frac{b-a}{N}$ this results in

$$\frac{d}{dt}\vec{u}(t) = \frac{1}{2h_x} \begin{bmatrix} 0 & 1 & 0 & \cdots & 0 & 0 & 0 \\ -1 & 0 & 1 & \cdots & 0 & 0 & 0 \\ 0 & -1 & 0 & \cdots & 0 & 0 & 0 \\ \vdots & \vdots & \vdots & \ddots & \vdots & \vdots & \vdots \\ 0 & 0 & 0 & \cdots & 0 & 1 & 0 \\ 0 & 0 & 0 & \cdots & -1 & 0 & 1 \\ 0 & 0 & 0 & \cdots & 0 & -1 & 0 \end{bmatrix} \vec{u}(t) \quad (8.2)$$

where $\vec{u}(t) = [u(x_0, t)u(x_1, t) \cdots u(x_N, t)]^T$. The eigenvalues of this matrix are zero or purely imaginary, and when integrating this equation it suffices to consider the behavior of a numerical integrator on the linear ODE $\frac{d}{dt}y(t) = \lambda y(t)$, where λ is purely imaginary. More precisely, in our example we seek an integrator that is stable for problems with a purely imaginary spectrum.

If we are solving the linear problem $\frac{d}{dt}y(t) = f(t, y(t)) = \lambda y(t)$, with the n -step multi-step method (see, e.g. [30])

$$\sum_{j=0}^n a_j y(t - jh_t) = h_t \sum_{j=0}^n b_j f(t - jh_t, y(t - jh_t)) = \lambda h_t \sum_{j=0}^n b_j y(t - jh_t),$$

the problem is reduced to a linear homogeneous recurrence with constant coefficients. Therefore, we can apply linear stability theory to determine if this method is stable for the linear problem.

Letting $y(t - jh_t) = r^{-j}$, the characteristic equation of the linear recurrence becomes

$$\sum_{j=0}^n a_j r^{-j} - \xi \sum_{j=0}^n b_j r^{-j} = 0,$$

where $\xi = \lambda h_t$. Linear stability requires that each root r have magnitude less than 1 or be of magnitude 1 and single multiplicity [5]. Thus, letting $r = \exp(i\theta)$, $\theta \in [0, 2\pi)$ (i.e. r travels around the unit circle), we can define the boundary of the region in \mathbb{C} that contains all values of ξ for which the method is stable. This region is known as the stability region or stability domain. A far more detailed discussion of the stability of general multi-step methods can be found in, for example, [30].

There is a distinct difference between the applicability of a stability domain to a scalar ODE or system of a finite number of ODEs and the relevance of the stability domain for spatially discretized PDEs. Considering that the exact solution to $\frac{d}{dt}y(t) = \lambda y(t)$ is $y(t) = c \exp(\lambda t)$ (c a constant), the stability domain addresses whether a solution grows or decays depending on the value of λ . This is true for a scalar ODE or a system of a finite number of ODEs. On the other hand, considering a spatially discretized PDE, where the number of equations increases as the discretization is refined, the stability domain supplies information similar to von Neumann analysis. That is, the stability domain now indicates whether a numerical integrator converges to the actual solution of the PDE or diverge.

In order for such a method to be valid for our example, and for wave equations posed as first order systems, the stability domain must contain a portion of the imaginary axis. The largest value S_I such that the interval $[-iS_I, iS_I]$ is contained in the stability domain is known as the imaginary stability boundary (ISB) or stability ordinate. Clearly, integrators with $S_I = 0$ are of no use in our example, and larger ISB's allow for greater flexibility in the choice of h_t when solving the ODE.

Some of the more popular multistep methods are known as the Adams methods, of which we discuss two types. Adams-Bashforth (AB) methods are explicit multi-step methods that take the form

$$y(t) = y(t - h_t) + h_t \sum_{j=1}^n \tilde{b}_j f(t - jh_t, y(t - jh_t)) \quad (8.3)$$

Likewise, Adams-Moulton (AM) methods are implicit methods (the indexing now starts at $j = 0$ so that $f(t, y(t))$ is needed) where

$$y(t) = y(t - h_t) + h_t \sum_{j=0}^n b_j f(t - jh_t, y(t - jh_t)). \quad (8.4)$$

The methods are well known and reasonably stable, but have lower computational cost per iteration than equivalent-order Runge-Kutta methods (see, e.g. [30], [4, Ch. 6]). AB methods have order $p = n$ while AM methods have order $p = n + 1$. The stability domains for both the AB and AM methods for orders 1, 2, and 3 are shown in figure 8.1. We will denote an Adams-Bashforth (Adams-Moulton) method of order p by AB p (AM p).

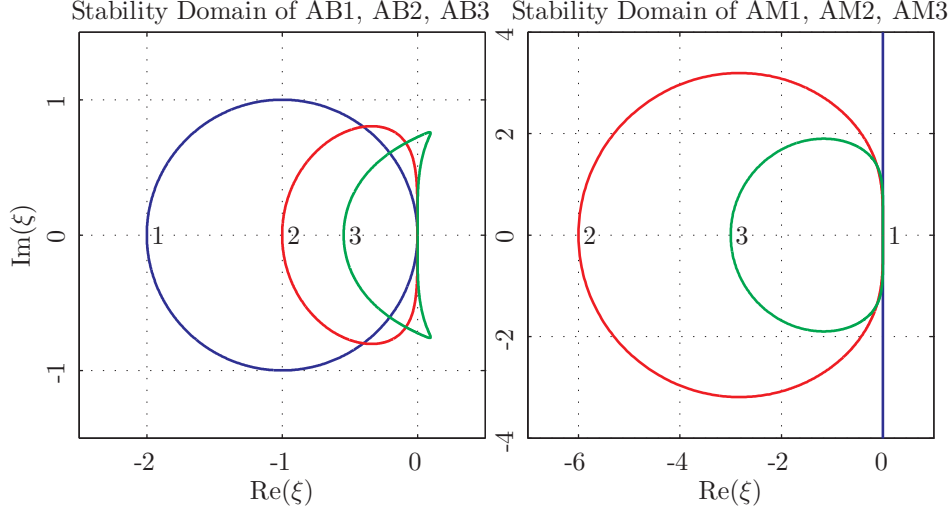


Figure 8.1: The stability domains for the AB (left) and AM (right) methods of orders 1, 2, and 3. The domains are numbered appropriately in the frames. Stable choices of ξ for AM1 occur for any choice in the left half of the complex plane. The other methods are stable for any choice interior to the boundary of the domain.

Since AM methods are implicit, we use an AB method to determine (predict) $y(t)$. In this way, we can avoid the use of costly linear solvers to achieve some of the benefits of an implicit method. We then substitute our predicted value within the AM method to correct some of the error, producing an Adams predictor-corrector method. We consider the predictor corrector methods ABp - AMp and $AB(p-1)$ - AMp , both of which have order p . When considering the linear ODE $\frac{d}{dt}y(t) = \lambda y(t)$, these methods take the form

$$y(t) = (1 + \lambda h_t b_0)y(t - h_t) + \sum_{j=1}^{p-1} \left[(\lambda h_t)^2 b_0 \tilde{b}_j + \lambda h_t b_j \right] y(t - j h_t) \quad (8.5)$$

for $AB(p-1)$ - AMp and

$$y(t) = (1 + \lambda h_t b_0)y(t - h_t) + \sum_{j=1}^{p-1} \left[(\lambda h_t)^2 b_0 \tilde{b}_j + \lambda h_t b_j \right] y(t - j h_t) + \lambda^2 h_t^2 b_0 \tilde{b}_p y(t - p h_t) \quad (8.6)$$

in the case of ABp - AMp .

To provide some examples, we consider $AB1$ - $AM2$ and $AB2$ - $AM2$. For the predictor $AB1$, we have

$$y(t) = y(t - h_t) + h_t f(t - h_t, y(t - h_t)), \quad (8.7)$$

and for the predictor AB2, we have

$$y(t) = y(t - h_t) + \frac{h_t}{2} (3f(t - h_t, y(t - h_t)) - f(t - 2h_t, y(t - 2h_t))). \quad (8.8)$$

In both cases, the corrector AM2 is given by

$$y(t) = y(t - h_t) + \frac{h_t}{2} (f(t, y(t)) + f(t - h_t, y(t - h_t))). \quad (8.9)$$

For the linear ODE $\frac{d}{dt}y(t) = \lambda y(t)$, substitution of (8.7) and (8.8) for $y(t)$ in the right hand side of (8.9) leads to

$$y(t) = (1 + \lambda h_t + \frac{1}{2}(\lambda h_t)^2)y(t - h_t) \quad (\text{AB1-AM2}) \quad (8.10)$$

$$y(t) = (1 + \lambda h_t + \frac{3}{4}(\lambda h_t)^2)y(t - h_t) - \frac{1}{4}(\lambda h_t)^2 y(t - 2h_t) \quad (\text{AB2-AM2}). \quad (8.11)$$

We first consider AB1-AM2. Using the expression for AB1-AM2 and letting $y(t - jh_t) = r^{-j}$, we find that the characteristic equation becomes

$$r = (1 + \xi + \frac{1}{2}\xi^2), \quad (8.12)$$

where $\xi = \lambda h_t$. To find the boundary of the stability domain, we can follow the root ξ in (8.12) where $|r| = 1$. The stability domain of this method is shown in top left frame of figure 8.2.

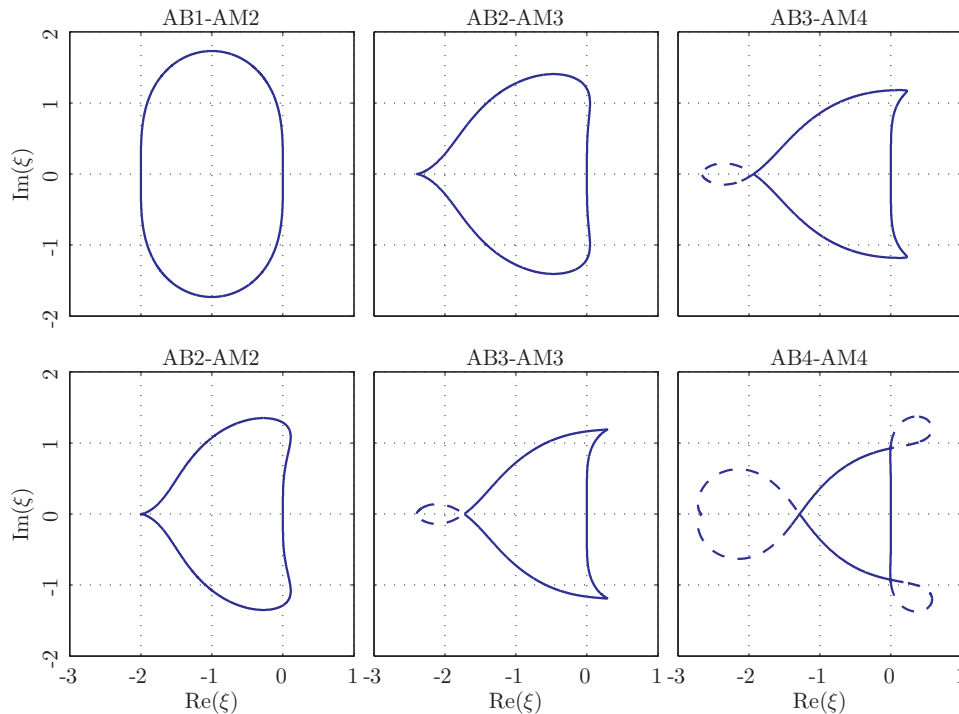


Figure 8.2: The stability domains for the predictor corrector methods of various orders. The interiors of the dashed loops do not indicate stable values of ξ and should be ignored. This can be confirmed by substituting a ξ value on the interior of a loop into (8.5) or (8.6) and determining that the roots r of the corresponding characteristic equations do not all have magnitude less than 1.

Zooming in near the origin we find that the stability boundary swings to the left of the imaginary axis, resulting in a zero ISB. This can be seen in figure 8.3.

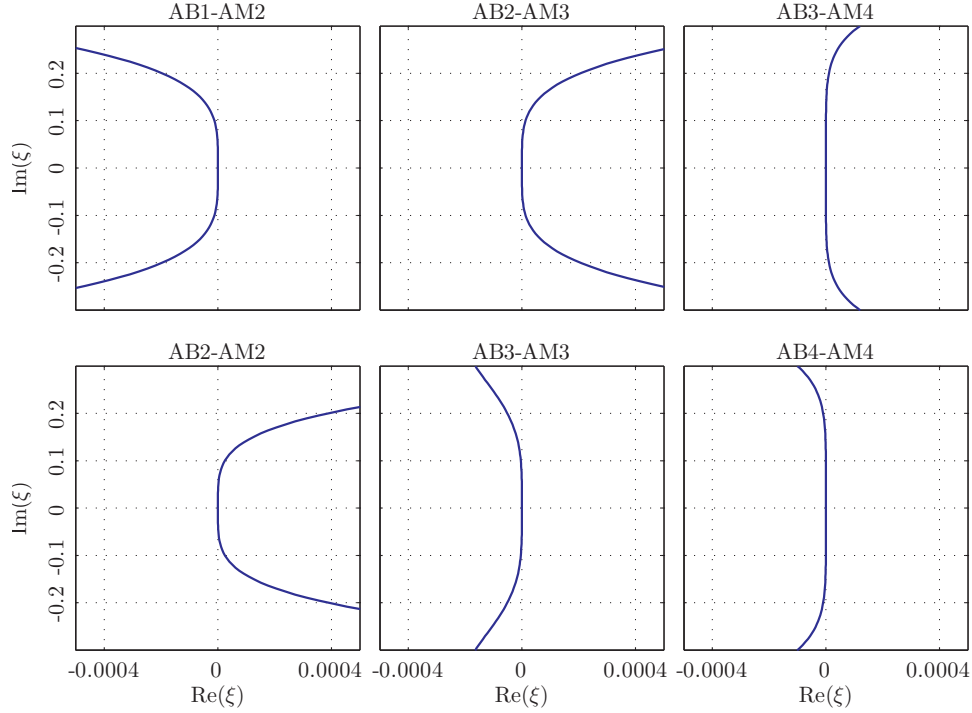


Figure 8.3: Magnified views of the stability domains for the predictor corrector methods of various orders near the origin.

Alternatively, we could let $r = e^{i\theta}$ and perform a Taylor expansion for $\xi(\theta)$ to find that

$$\xi = i\theta + \frac{1}{6}(i\theta)^3 - \frac{1}{8}(i\theta)^4 + \dots \quad (8.13)$$

Because the first real term in this expansion is negative, AB1-AM2 has a zero ISB.

We next consider AB2-AM2. The analogous equation to (8.12) is

$$r^2 = \left(1 + \xi + \frac{3}{4}\xi^2\right)r - \frac{1}{4}\xi^2. \quad (8.14)$$

The stability domain of this method is shown in the bottom left frame of figure 8.2. We find that the expansion $\xi(\theta)$ for AB2-AM2 is $\xi = i\theta - \frac{1}{12}(i\theta)^3 + \frac{1}{4}(i\theta)^4 + \dots$. Since the first real term in this expansion is positive, AB2-AM2 has a nonzero ISB which is approximately 1.29. This can also be seen in figure 8.3 where the stability boundary now swings to the right of the imaginary axis.

To determine whether the stability domains lie on the interior or exterior of the boundaries, we could easily pick a value of ξ on the interior and solve for the root(s) r (recall, $y(t - jh_t) = r^{-j}$)

in (8.5) or (8.6). For instance, if $\xi = -1$ is substituted into (8.14) and the equation is solved for r , then both roots have magnitude $0.5 < 1$, and we know that the interior of the boundary is stable. On the other hand, for $\xi = -3$ one of the roots has a magnitude of approximately $4.21 > 1$ and the exterior of the boundary is unstable.

Similar details and discussion on the ISB's of AB and AM methods of order p as well as AB and AM methods on a staggered grid are available in, for example, [22], [23], or [24]; however, this study examines only the predictor-corrector methods ABp - AMp and $AB(p-1)$ - AMp , both of which have order p , and is discussed further in [25]. Analysis of images like those in figure 8.3 easily led us to the following two assertions, which will be proven in the following sections.

- ABp - AMp methods have nonzero ISBs only for orders $p = 1, 2, 5, 6, 9, 10, \dots$
- $AB(p-1)$ - AMp methods have nonzero ISBs only for orders $p = 3, 4, 7, 8, \dots$

8.2 Proof Methodology

The behavior of the stability domain boundary near the origin (that is, $\xi = 0$) explains much about the method as shown in discussions in the previous section for $AB1$ - $AM2$ and $AB2$ - $AM2$. For instance, knowledge of whether the boundary swings initially to the right or the left of the origin characterizes whether the ISB is nonzero or not, respectively. Considering $r \leq 1$ and an exact method (here this means $p \rightarrow \infty$) we have from Theorem 2.1 of [30] that

$$\sum_{j=0}^n a_j r^j - \ln(r) \sum_{j=0}^n b_j r^j = 0,$$

and $\xi(\theta) = i\theta$ because

$$\xi = \frac{\sum_{j=0}^n a_j r^j}{\sum_{j=0}^n b_j r^j} = \ln r = \ln(e^{i\theta}) = i\theta. \quad (8.15)$$

On the other hand, a numerical scheme of finite order p instead leads to the expansion

$$\xi(\theta) = i\theta + c_p(i\theta)^{p+1} + d_p(i\theta)^{p+2} + \dots \quad (8.16)$$

The sign of the first real term in this expansion will dictate whether the stability domain boundary near the origin swings to the right or to the left of the imaginary axis. In [24] and [25] it was shown

that AB methods of orders $p = 3, 4, 7, 8, 11, 12, \dots$ and AM methods of orders $p = 1, 2, 5, 6, 9, 10, \dots$ have nonzero ISBs.

For the rest of this thesis, we will consider a form equivalent to (8.3) and (8.4) when discussing a standard n -step Adams method. This expression is

$$y(t) = y(t - h_t) + \int_{t-h_t}^t q(\tau) d\tau, \quad (8.17)$$

where $q(t)$ is the polynomial interpolating f at the points $t - jh_t$ for $1 \leq j \leq n$ (AB methods) or $0 \leq j \leq n$ (AM methods). Without loss of generality we could just as easily consider the interval $[0, h_t]$ instead of $[t - h_t, t]$ (i.e replace t with $t + h_t$, then set $t = 0$), which leads to the much simpler

$$y(h_t) = y(0) + \int_0^{h_t} p(\tau) d\tau, \quad (8.18)$$

with $p(t)$ now interpolating f at

$$0, -h_t, -2h_t, \dots, -(n-1)h_t \quad (8.19)$$

for n -step AB methods and at

$$h_t, 0, -h_t, -2h_t, \dots, -(n-1)h_t \quad (8.20)$$

in the case of n -step AM methods. This will be the form considered throughout the rest of the chapter.

In order to prove that AB($p-1$)-AM p methods have nonzero ISBs for orders $p = 3, 4, 7, 8, 11, 12, \dots$ and AB p -AM p methods have nonzero ISB's for orders $p = 1, 2, 5, 6, 9, 10, \dots$, we rely on several lemmas to determine the coefficients c_p and d_p . The first lemma, extended by Ghrist from Lemma H.4 in [22], gives a particular form of an expansion of the error in the interpolating polynomial through a specific set of equally spaced points. The first two terms were proved by Fornberg.

Lemma 8.2.1 Given $f(t)$, let $p_n(t)$ be the polynomial of degree n that interpolates $f(t)$ at $t = 0, -h_t, -2h_t, \dots, -nh_t$. Then,

$$f(t) - p_n(t) = t(t + h_t)(t + 2h_t) \dots (t + nh_t)g(t) \quad (8.21)$$

where

$$g(t) = \frac{f^{(n+1)}(0)}{(n+1)!} + \frac{f^{(n+2)}(0)}{(n+2)!} \left(t - \frac{n(n+1)}{2} h_t \right) + \frac{f^{(n+3)}(0)}{(n+3)!} \left(t^2 - \frac{n(n+1)}{2} h_t t + \frac{n(n+1)(n+2)(3n+1)}{24} h_t^2 \right) + \dots \quad (8.22)$$

Proof. Pick $g(t)$ such that

$$f(t) - p_n(t) = [t(t+h_t) \dots (t+nh_t)] g(t). \quad (8.23)$$

By Lagrange's interpolation formula, $p_n(t)$ depends linearly on $f(t)$, so $(f(t) - p_n(t))$ must also depend linearly on $f(t)$. Thus by equation (8.23), $g(t)$ must also depend linearly on $f(t)$. We now consider various cases for $f(t)$ to obtain the expansion of $g(t)$.

For proof of the first two terms of $g(t)$ see Theorem H.1 of Appendix H in [22].

If $f(t) = t^{n+3}$, then $g(t) = t^2 - \frac{n(n+1)}{2} h_t t + \frac{n(n+1)(n+2)(3n+1)}{24} h_t^2$. To prove this, consider $g(t) = \frac{t^{n+3} - p_n(t)}{t(t+h_t) \dots (t+nh_t)}$. In this case, $g(t)$ is a quadratic polynomial with leading coefficient 1. The leading coefficient must be a constant since the numerator and denominator have the same degree and the same roots. The leading coefficients of the numerator and denominator are both 1, so this constant must be 1. Let $g(t) = t^2 + \alpha t + \beta$; note that the sum of the roots t_1, t_2 of $g(t)$ is $-\alpha$. Multiplying, we find

$$t^{n+3} - p_n(t) = (t^2 + \alpha t + \beta) [t(t+h_t) \dots (t+nh_t)]. \quad (8.24)$$

Since the left-hand side of (8.24) is missing the t^{n+2} term, the sum of its roots must equal 0. Using this on the right-hand side of (8.24) gives the result

$$-\alpha - 0 - h_t - 2h_t - \dots - nh_t = 0. \quad (8.25)$$

Thus $\alpha = -\frac{n(n+1)}{2} h_t$.

The left-hand side of (8.24) is missing the t^{n+1} term, so the sum of the pairwise products of its roots must equal 0, where the roots are $0, -h_t, -2h_t, \dots, -nh_t$, and the two roots t_1, t_2 of

$t^2 + \alpha t + \beta$ with $t_1 + t_2 = -\alpha$ and $t_1 t_2 = \beta$. Then

$$\begin{aligned} & -h_t(-2h_t - 3h_t - \dots - nh_t - \alpha) - 2h_t(-3h_t - \dots - nh_t - \alpha) \\ & - \dots - mh_t(-(m+1)h_t - \dots - nh_t - \alpha) - \dots - nh_t(-\alpha) + \beta = 0. \end{aligned} \quad (8.26)$$

Thus

$$\begin{aligned} \beta &= -h_t \alpha (1 + 2 + \dots + n) - h_t^2 \sum_{i=1}^{n-1} \left(\sum_{j=i+1}^n ij \right) \\ &= -h_t \left(-\frac{n(n+1)}{2} \right) h_t \frac{n(n+1)}{2} - h_t^2 \frac{n(n+1)(n-1)(3n+2)}{24} \\ &= \frac{n(n+1)(n+2)(3n+1)}{24} h_t^2. \end{aligned} \quad (8.27)$$

We now combine all of the previous results from Theorem H.1 of Appendix H in [22] and this proof. Let $f(t) = \sum_{j=0}^{\infty} a_j x^j$, where $a_j = \frac{f^{(j)}(0)}{j!}$ by Taylor expansion. Then we have

$$f(t) - p_n(t) = \sum_{j=0}^{\infty} a_j t^j - p_n(t) = [(t)(t+h_t) \dots (t+nh_t)] g(t). \quad (8.28)$$

Thus we find that

$$\begin{aligned} g(t) &= \frac{f^{(n+1)}(0)}{(n+1)!} + \frac{f^{(n+2)}(0)}{(n+2)!} \left(t - \frac{n(n+1)}{2} h_t \right) \\ &+ \frac{f^{(n+3)}(0)}{(n+3)!} \left(t^2 - \frac{n(n+1)}{2} h_t t + \frac{n(n+1)(n+2)(3n+1)}{24} h_t^2 \right) + \dots, \end{aligned} \quad (8.29)$$

concluding the proof of Lemma 8.2.1. \square

The second Lemma provides an expansion of a term common to both of the AB($p-1$)-AMP and AB p -AMP methods with a proof due to Ghrist. The remaining lemmas will be specific to either of these methods.

Lemma 8.2.2 The beginning of the series expansion of $\sum_{m=-1}^n (-1)^{m+1} \binom{n+1}{m+1} e^{-im\theta}$ is given by

$$(i\theta)^{n+1} + \frac{1-n}{2} (i\theta)^{n+2} + \frac{1}{24} (3n^2 - 5n + 4) (i\theta)^{n+3} + \dots \quad (8.30)$$

Proof. We apply the Binomial Theorem twice.

$$\begin{aligned}
& \sum_{m=-1}^n (-1)^{m+1} \binom{n+1}{m+1} e^{-im\theta} \\
&= e^{i\theta} \sum_{k=0}^n (-1)^k \binom{n+1}{k} e^{-ik\theta} \\
&= e^{i\theta} \left(1 - e^{-i\theta}\right)^{n+1} \\
&= \left(e^{i\theta} - 1\right) \left(1 - e^{-i\theta}\right)^n \\
&= \left(i\theta + \frac{(i\theta)^2}{2!} + \frac{(i\theta)^3}{3!} + \mathcal{O}(\theta^4)\right) \left(i\theta - \frac{(i\theta)^2}{2!} + \frac{(i\theta)^3}{3!} + \mathcal{O}(\theta^4)\right)^n \\
&= (i\theta)^{n+1} \left(1 + \frac{i\theta}{2} - \frac{\theta^2}{6} + \mathcal{O}(\theta^3)\right) \left(1 - \left(\frac{i\theta}{2} + \frac{\theta^2}{6}\right) + \mathcal{O}(\theta^3)\right)^n \\
&= (i\theta)^{n+1} \left(1 + \frac{i\theta}{2} - \frac{\theta^2}{6} + \mathcal{O}(\theta^3)\right) \left(1 - n\frac{i\theta}{2} - (n+3n^2)\frac{\theta^2}{24} + \mathcal{O}(\theta^3)\right).
\end{aligned} \tag{8.31}$$

By series multiplication, we find that the right-hand side is equal to (8.30). \square

8.3 Proof of the Assertions

The proofs in this chapter are alternatives to those in [25]. The proof of Lemma 8.3.4 is adapted from Lemma 2.1 in [25]. Proofs of the remaining Lemmas 8.3.1 and 8.3.3 are due to me, while the proofs of the Theorems 8.3.2 and 8.3.5 are due to Ghrist. The alternative proofs in [25] are more concise through the use of a backward difference representation of the Adams methods given by Henrici [28] and were motivated by comments by Ernst Hairer.

8.3.1 AB p -AM p methods

We now consider general AB p -AM p methods, which have order p . A general n -step AB predictor integrates $p_n(t)$, which interpolates the data points $(-jh_t, y(jh_t))$ for $-n \leq j \leq 0$; it will then approximate $y(h_t)$ via $\tilde{y}(h_t) = y(0) + \int_0^{h_t} p_n(\tau) d\tau$.

The AM corrector then integrates $q_n(t)$, which interpolates the data points $(h_t, \tilde{y}(h_t))$ and $(jh_t, y(jh_t))$ for $-(n-1) \leq j \leq 0$; the final approximation for $y(h_t)$ is given by $y(h_t) = y(0) +$

$\int_0^{ht} q_n(\tau) d\tau$. This combined method has order $p = n$.

We first prove a lemma that gives an exact form for the general difference between the interpolating polynomials of the AB predictor and the AM corrector. To simplify notation, let $t_j = jh_t$ and $y_j = y(t_j)$ and drop the subscript t so that $h = h_t$.

Lemma 8.3.1

$$q_n(t) - p_n(t) = \frac{1}{h^n n!} \left(\tilde{y}_1 + \sum_{m=0}^n (-1)^{m+1} \binom{n+1}{m+1} y_{-m} \right) \prod_{j=0}^{n-1} (t + jh) \quad (8.32)$$

Proof. We create the Lagrange interpolating polynomials for $p_n(t)$ and $q_n(t)$ and then examine their difference.

$$\begin{aligned} & q_n(t) - p_n(t) \\ &= \tilde{y}_1 \prod_{j=0}^{n-1} \left(\frac{t + jh}{h(j+1)} \right) - y_{-n} \prod_{j=0}^{n-1} \left(\frac{t + jh}{h(j-n)} \right) \\ &\quad + \sum_{m=0}^{n-1} y_{-m} \left(\prod_{j=-1, j \neq m}^{n-1} \frac{t + jh}{h(j-m)} - \prod_{j=0, j \neq m}^n \frac{t + jh}{h(j-m)} \right) \\ &= \frac{\tilde{y}_1 + (-1)^{n+1} y_{-n}}{h^n n!} \prod_{j=0}^{n-1} (t + jh) + \sum_{m=0}^{n-1} \frac{y_{-m}}{h^n} \frac{-(n+1)(t+mh)}{(1+m)(n-m)} \prod_{j=0, j \neq m}^{n-1} \left(\frac{t + jh}{j-m} \right) \\ &= \frac{1}{h^n} \left(\frac{\tilde{y}_1 + (-1)^{n+1} y_{-n}}{n!} + \sum_{m=0}^{n-1} (-1)^{m+1} y_{-m} \frac{n+1}{(m+1)!(n-m)!} \right) \prod_{j=0}^{n-1} (t + jh) \\ &= \frac{1}{h^n n!} \left(\tilde{y}_1 + \sum_{m=0}^n (-1)^{m+1} \binom{n+1}{m+1} y_{-m} \right) \prod_{j=0}^{n-1} (t + jh). \end{aligned}$$

□

Theorem 8.3.2 Predictor-corrector AB p -AM p methods have nonzero ISBs only for orders $p = 1, 2, 5, 6, 9, 10, \dots$

Proof. Analogous to (8.18), a general AB p -AM p scheme, when applied to $\frac{dy}{dt} = \lambda y$ (with

$\lambda = \xi/h$, takes the form

$$\begin{aligned} y(h) &= y(0) + \frac{\xi}{h} \int_0^h (q_n(t)) dt \\ &= y(0) + \frac{\xi}{h} \left[\int_0^h y(t) dt + \int_0^h (p_n(t) - y(t)) dt + \int_0^h (q_n(t) - p_n(t)) dt \right]. \end{aligned} \quad (8.33)$$

This method will have an order of $p = n + 1$. Our general proof will require $n \geq 1$; one can separately check that AB1-AM1 has the expansion $\xi = i\theta - \frac{1}{2}(i\theta)^2 + \dots$. Because the first real term in this expansion is positive, AB1-AM1 does have a nonzero ISB.

We seek an expansion of $\xi(\theta)$. We first apply Lemmas 8.2.1 and 8.3.1 to the second and third terms of (8.33), respectively. This gives

$$\begin{aligned} y(h) &= y(0) + \frac{\xi}{h} \int_0^h y(t) dt \\ &\quad - \frac{\xi}{h} \int_0^h \left[\frac{y^{(n+1)}(0)}{(n+1)!} + \frac{y^{(n+2)}(0)}{(n+2)!} \left(t - \frac{n(n+1)}{2}h + \dots \right) \right] \prod_{j=0}^n (t+jh) dt \\ &\quad + \frac{\xi}{h^{n+1}n!} \int_0^h \left[\tilde{y}_1 - y_1 + \sum_{m=-1}^n (-1)^{m+1} \binom{n+1}{m+1} y_{-m} \right] \prod_{j=0}^{n-1} (t+jh) dt. \end{aligned} \quad (8.34)$$

We apply the exact solution $y(t) = e^{\lambda t} = e^{i\theta t/h}$ from (8.39) and define

$$a_n = \frac{1}{h^{n+2}} \int_0^h t(t+h) \dots (t+nh) dt = \int_0^1 s(s+1) \dots (s+n) ds \quad (8.35)$$

and

$$\begin{aligned} b_n &= \frac{1}{h^{n+3}} \int_0^h t(t+h) \dots (t+nh) \left(t - \frac{n(n+1)}{2}h \right) dt \\ &= \int_0^1 s(s+1) \dots (s+n) \left(s - \frac{n(n+1)}{2} \right) ds \end{aligned} \quad (8.36)$$

to express (8.34) in terms of θ :

$$\begin{aligned} e^{i\theta} &= 1 + \frac{\xi}{i\theta} (e^{i\theta} - 1) - \xi \left(\frac{a_n}{(n+1)!} (i\theta)^{n+1} + \frac{b_n}{(n+2)!} (i\theta)^{n+2} + \dots \right) \\ &\quad + \frac{a_{n-1}}{n!} \xi \left(\tilde{y}_1 - e^{i\theta} + \sum_{m=-1}^n (-1)^{m+1} \binom{n+1}{m+1} e^{-im\theta} \right). \end{aligned} \quad (8.37)$$

We note that \tilde{y}_1 is given by the right-hand side of

$$\begin{aligned}
y(h) &= \frac{\xi}{h} \left[\int_0^h (p_n(t) - y(t)) dt + \int_0^h y(t) dt \right] + y(0) \\
&= -\frac{\xi}{h} \int_0^h \prod_{j=0}^n (t + jh) \left[\frac{y^{(n+1)}(0)}{(n+1)!} + \frac{y^{(n+2)}(0)}{(n+2)!} \left(t - \frac{n(n+1)}{2}h \right) + \dots \right] dt \\
&\quad + \frac{\xi}{h} \int_0^h y(t) dt + y(0).
\end{aligned} \tag{8.38}$$

Substituting the exact solution

$$y(t) = e^{\lambda t} = e^{i\theta t/h}, \tag{8.39}$$

and the expressions for a_n and b_n gives

$$\tilde{y}_1 = 1 + \frac{\xi}{i\theta} (e^{i\theta} - 1) - \xi \left(\frac{a_n}{(n+1)!} (i\theta)^{n+1} + \frac{b_n}{(n+2)!} (i\theta)^{n+2} + \dots \right) \tag{8.40}$$

When we substitute this expression into (8.37) the result will contain a term with ξ^2 which distinguishes it from the AB and AM cases. After substituting for \tilde{y}_1 , applying Lemma 8.2.2, and factoring, (8.37) becomes

$$\begin{aligned}
0 &= (e^{i\theta} - 1) \left(\frac{\xi}{i\theta} - 1 \right) - \xi \left(\frac{a_n}{(n+1)!} (i\theta)^{n+1} + \frac{b_n}{(n+2)!} (i\theta)^{n+2} + \dots \right) \\
&\quad + \frac{a_{n-1}}{n!} \xi \left[(e^{i\theta} - 1) \left(\frac{\xi}{i\theta} - 1 \right) - \xi \left(\frac{a_n}{(n+1)!} (i\theta)^{n+1} + \frac{b_n}{(n+2)!} (i\theta)^{n+2} + \dots \right) \right. \\
&\quad \left. + (i\theta)^{n+1} + \frac{1-n}{2} (i\theta)^{n+2} + \dots \right].
\end{aligned} \tag{8.41}$$

We can now find the expansion of ξ about $i\theta = 0$ from (8.41):

$$\xi(\theta) \approx i\theta + c_n (i\theta)^{n+2} + d_n (i\theta)^{n+3} + \dots \tag{8.42}$$

where

$$c_n = \frac{a_n}{(n+1)!} - \frac{a_{n-1}}{n!} = \frac{1}{(n+1)!} \int_0^1 \prod_{j=-1}^{n-1} (s+j) ds < 0 \tag{8.43}$$

and

$$\begin{aligned}
d_n &= \frac{b_n}{(n+2)!} - c_n \left(\frac{1}{2} + \frac{a_{n-1}}{n!} \right) + (n-1) \frac{a_{n-1}}{2n!} + \frac{a_{n-1}}{n!} \frac{a_n}{(n+1)!} \\
&= \left(\frac{a_{n-1}}{n!} \right)^2 + \frac{b_n}{(n+2)!} + n \frac{a_{n-1}}{2n!} - \frac{a_n}{2(n+1)!} \\
&= \left(\frac{a_{n-1}}{n!} \right)^2 + \frac{1}{2(n+2)!} \int_0^1 (1-s)(n^2 - 2s) \prod_{j=0}^{n-1} (s+j) ds.
\end{aligned} \tag{8.44}$$

The last integrand is nonnegative for $n \geq 2$, so $d_n > 0$ for $n \geq 2$. We can separately check that $d_1 = \frac{1}{4}$. Substituting $p = n + 1$ in (8.43) and (8.44) gives the coefficients c_p and d_p in (8.15) in terms of the order p . After examining the sign of the first real term in (8.42), we conclude that ABp - AMp methods have nonzero ISBs only for orders $p = 1, 2, 5, 6, 9, 10, \dots$, similar to AMp methods. \square

8.3.2 $AB(p-1)$ - AMp methods

We now examine general $AB(p-1)$ - AMp methods, which also have order p . A general AB predictor integrates $p_n(t)$, which interpolates the data points (t_k, y_k) for $-n \leq k \leq 0$; it approximates $y(h)$ via $\tilde{y}_1 = y_0 + \int_0^h p_n(t) dt$.

The AM corrector then integrates $q_{n+1}(t)$, which interpolates the data points (t_1, \tilde{y}_1) and (t_k, y_k) for $-n \leq k \leq 0$; the final approximation for $y(h)$ is given by $y_1 = y_0 + \int_0^h q_{n+1}(t) dt$. This combined method has order $p = n + 2$.

The following lemma is analogous to Lemma 8.3.1. It can be proved similarly, again using Lagrange basis polynomials.

Lemma 8.3.3

$$\begin{aligned} & q_{n+1}(t) - p_n(t) \\ &= \frac{1}{h^{n+1}(n+1)!} \left(\tilde{y}_1 + \sum_{m=0}^n (-1)^{m+1} \binom{n+1}{m+1} y_{-m} \right) \prod_{j=0}^n (t + jh) \end{aligned} \quad (8.45)$$

Proof. We create the Lagrange interpolating polynomials for $p_n(t)$ and $q_{n+1}(t)$ and then

examine their difference.

$$\begin{aligned}
q_{n+1}(t) - p_n(t) &= \tilde{y}_1 \prod_{m=0}^n \frac{t+mh}{(m+1)h} + \sum_{k=0}^n y_{-k} \prod_{m=-1, m \neq k}^n \frac{t+mh}{(m-k)h} - \sum_{k=0}^n y_{-k} \prod_{m=0, m \neq k}^n \frac{t+mh}{(m-k)h} \\
&= \tilde{y}_1 \prod_{m=0}^n \frac{t+mh}{(m+1)h} + \sum_{k=0}^n y_{-k} \left[\prod_{m=-1, m \neq k}^n \frac{t+mh}{(m-k)h} - \prod_{m=0, m \neq k}^n \frac{t+mh}{(m-k)h} \right] \\
&= \tilde{y}_1 \prod_{m=0}^n \frac{t+mh}{(m+1)h} + \sum_{k=0}^n y_{-k} \left[\frac{t-h}{(-1-k)h} - 1 \right] \prod_{m=0, m \neq k}^n \frac{t+mh}{(m-k)h} \\
&= \tilde{y}_1 \prod_{m=0}^n \frac{t+mh}{(m+1)h} + \sum_{k=0}^n y_{-k} \left[\frac{-(t+kh)}{(k+1)h} \right] \prod_{m=0, m \neq k}^n \frac{t+mh}{(m-k)h} \\
&= \prod_{m=0}^n (t+mh) \left[\tilde{y}_1 \prod_{m=0}^n \frac{1}{(m+1)h} + \sum_{k=0}^n y_{-k} \frac{-1}{(k+1)h} \prod_{m=0, m \neq k}^n \frac{1}{(m-k)h} \right] \\
&= \prod_{m=0}^n (t+mh) \frac{1}{h^{n+1}} \left[\tilde{y}_1 \frac{1}{(n+1)!} + \sum_{k=0}^n y_{-k} \frac{-1}{(k+1)} \frac{(n+1)!}{(n+1)! k!(n-k)!} \right] \\
&= \prod_{m=0}^n (t+mh) \frac{1}{h^{n+1} (n+1)!} \left[\tilde{y}_1 + \sum_{k=0}^n y_{-k} (-1)^{k+1} \frac{(n+1)!}{(k+1)!(n-k)!} \right] \\
&= \prod_{m=0}^n (t+mh) \frac{1}{h^{n+1} (n+1)!} \left[\tilde{y}_1 + \sum_{k=0}^n y_{-k} (-1)^{k+1} \binom{n+1}{k+1} \right]
\end{aligned}$$

□

Lemma 8.3.4 For all $n \geq 2$, $a_n > n!$.

Proof. We prove this lemma via induction. For $n = 2$ we can easily compute $a_2 = \int_0^1 s(s+1)(s+2)ds = \frac{9}{4} > 2 = 2!$. For the inductive step, we assume $a_n > n!$ for some $n \geq 2$.

$$\begin{aligned}
\frac{a_{n+1}}{(n+1)!} &= \frac{1}{n!} \int_0^1 s(s+1)(s+2) \cdots (s+n) \frac{(s+(n+1))}{(n+1)} ds \\
&> \frac{a_n (n+1)}{n! (n+1)} \\
&> \frac{n!}{n!} = 1
\end{aligned} \tag{8.46}$$

Therefore, $a_{n+1} > (n+1)!$ by induction for all $n \geq 2$. □

Theorem 8.3.5 Predictor-corrector AB($p-1$)-AMP methods have nonzero ISBs only for orders $p = 3, 4, 7, 8, \dots$

Proof. A general AB($p-1$)-AM p scheme, when applied to $\frac{dy}{dt} = \lambda y$ (with $\lambda = \xi/h$), takes the form

$$\begin{aligned} y(h) &= y(0) + \frac{\xi}{h} \int_0^h (q_{n+1}(t)) dt \\ &= y(0) + \frac{\xi}{h} \left[\int_0^h y(t) dt + \int_0^h (p_n(t) - y(t)) dt + \int_0^h (q_{n+1}(t) - p_n(t)) dt \right]. \end{aligned} \quad (8.47)$$

Our general proof will require $n \geq 1$; we have already established that AB1-AM2 has a zero ISB.

We now proceed with the general case for $p \geq 3$. As before, we seek an expansion of $\xi(\theta)$.

Because we will need one more term in the expansion given by Lemma 8.2.1, we define

$$\begin{aligned} B_n &= \frac{1}{h^{n+4}} \int_0^h \left(t^2 - \frac{n(n+1)}{2} ht + \frac{n(n+1)(n+2)(3n+1)}{24} h^2 \right) \prod_{j=0}^n (t + jh) dt \\ &= \int_0^1 \left(s^2 - \frac{n(n+1)}{2} s + \frac{n(n+1)(n+2)(3n+1)}{24} \right) \prod_{j=0}^n (s + j) ds. \end{aligned} \quad (8.48)$$

We apply Lemmas 8.2.1 and 8.3.3 to the second and third terms of (8.47), respectively, apply the exact solution $y(t) = e^{\lambda t} = e^{i\theta t/h}$ from (8.39), and substitute our expressions for a_n , b_n , and B_n from (8.35), (8.36), and (8.48) to find the analogous equation to (8.37):

$$\begin{aligned} e^{i\theta} &= -\xi \left(\frac{a_n}{(n+1)!} (i\theta)^{n+1} + \frac{b_n}{(n+2)!} (i\theta)^{n+2} + \frac{B_n}{(n+3)!} (i\theta)^{n+3} + \dots \right) \\ &\quad + \frac{a_n}{(n+1)!} \xi \left(\tilde{y}_1 - e^{i\theta} + \sum_{m=-1}^n (-1)^{m+1} \binom{n+1}{m+1} e^{-im\theta} \right) + 1 + \frac{\xi}{i\theta} (e^{i\theta} - 1). \end{aligned} \quad (8.49)$$

We again note that \tilde{y}_1 is given by the right-hand side of (8.38), where we need to keep one more term in the expansion given by Lemma 8.2.1; substituting the exact solution (8.39) and the expressions for a_n , b_n , and B_n from (8.35), (8.36), and (8.48) gives

$$\begin{aligned} \tilde{y}_1 &= 1 + \frac{\xi}{i\theta} (e^{i\theta} - 1) \\ &\quad - \xi \left(\frac{a_n}{(n+1)!} (i\theta)^{n+1} + \frac{b_n}{(n+2)!} (i\theta)^{n+2} + \frac{B_n}{(n+3)!} (i\theta)^{n+3} + \dots \right) \end{aligned} \quad (8.50)$$

After substituting this for \tilde{y}_1 , applying Lemma 8.2.2 (again keeping one more term in the expansion),

and factoring, (8.49) becomes

$$\begin{aligned}
0 &= (e^{i\theta} - 1) \left(\frac{\xi}{i\theta} - 1 \right) + \frac{a_n}{(n+1)!} \xi \left[(e^{i\theta} - 1) \left(\frac{\xi}{i\theta} - 1 \right) \right. \\
&\quad \left. - \xi \left(\frac{a_n}{(n+1)!} (i\theta)^{n+1} + \frac{b_n}{(n+2)!} (i\theta)^{n+2} + \frac{B_n}{(n+3)!} (i\theta)^{n+3} + \dots \right) \right. \\
&\quad \left. + (i\theta)^{n+1} + \frac{1-n}{2} (i\theta)^{n+2} + \frac{3n^2-5n+4}{24} (i\theta)^{n+3} + \dots \right] \quad (8.51) \\
&\quad - \xi \left(\frac{a_n}{(n+1)!} (i\theta)^{n+1} + \frac{b_n}{(n+2)!} (i\theta)^{n+2} + \frac{B_n}{(n+3)!} (i\theta)^{n+3} + \dots \right).
\end{aligned}$$

We can now find the expansion of ξ about $i\theta = 0$ from (8.51):

$$\xi(\theta) \approx i\theta + c_n (i\theta)^{n+3} + d_n (i\theta)^{n+4} + \dots \quad (8.52)$$

where

$$c_n = \frac{b_n}{(n+2)!} + \frac{a_n}{(n+1)!} \left(\frac{n-1}{2} + \frac{a_n}{(n+1)!} \right) \quad (8.53)$$

and

$$\begin{aligned}
d_n &= \frac{B_n}{(n+3)!} - c_n \left(\frac{1}{2} + \frac{a_n}{(n+1)!} \right) - \frac{3n^2-5n+4}{24} \frac{a_n}{(n+1)!} + \frac{a_n}{(n+1)!} \frac{b_n}{(n+2)!} \\
&= \frac{B_n}{(n+3)!} - \frac{b_n}{2(n+2)!} - \frac{a_n(3n^2+n-2)}{24(n+1)!} - \frac{n}{2} \left(\frac{a_n}{(n+1)!} \right)^2 - \left(\frac{a_n}{(n+1)!} \right)^3. \quad (8.54)
\end{aligned}$$

We claim that $c_n > 0$ and $d_n < 0$ for $n \geq 1$. We first check that $c_1 = \frac{19}{144}$ and $d_1 = -\frac{1243}{8640}$.

We note that $a_n = \int_0^1 s(s+1)\dots(s+n)ds > n!$ for $n \geq 2$ by Lemma 8.3.4. We first use this to show that $c_n > 0$.

$$\begin{aligned}
c_n &= \frac{b_n}{(n+2)!} + \frac{a_n}{(n+1)!} \left(\frac{n-1}{2} + \frac{a_n}{(n+1)!} \right) \quad (8.55) \\
&> \frac{b_n}{(n+2)!} + \frac{a_n}{(n+1)!} \left(\frac{n-1}{2} + \frac{1}{n+1} \right) \\
&= \frac{1}{(n+2)!(n+1)} \int_0^1 (ns+s+1) \prod_{j=0}^n (s+n) ds > 0.
\end{aligned}$$

We next show that $d_n < 0$. We first note that the last term in (8.54) is negative. Using

(8.35), (8.36), and (8.48) in (8.54), we have

$$\begin{aligned}
 d_n &< \frac{1}{24(n+3)!(n+1)} [24(n+1)B_n - 12(n+3)(n+1)b_n \\
 &\quad - (n+3)(n+2) ((n+1)(3n^2+n-2) + 12n) a_n] \quad (8.56) \\
 &= \frac{1}{24(n+3)!(n+1)} \int_0^1 \prod_{j=0}^n (s+j) F(n, s) ds
 \end{aligned}$$

where

$$\begin{aligned}
 F(n, s) &= 24(n+1)s^2 - 12(2n^2+3n-1) - 12(n^3+3n^2+5n+3)s \quad (8.57) \\
 &< -12(n-1)(2n+3) - 12(n^3+3n^2+5n+3)s,
 \end{aligned}$$

where in the last step we have evaluated the first term at $s = 1$ to maximize it. Since this last expression is negative for $n \geq 2$, the integrand in (8.56) is also negative, so $d_n < 0$ for AB($p-1$)-AM p methods for $n \geq 2$, where $p = n + 2$.

Since $c_n > 0$ and $d_n < 0$ for $n \geq 1$, after examining the sign of the first real term in (8.52), we conclude that AB($p-1$)-AM p methods have nonzero ISBs only for orders $p = 3, 4, 7, 8, \dots$, similar to AB p methods. \square

8.4 Conclusions

This chapter considered a separate research topic to answer the question of when Adams predictor-corrector methods of general order p have nonzero stability ordinates, which corresponds to being stable when applied to discretized wave equations (for small enough stepsize). With regards to predictor-corrector methods, we have proven that AB p -AM p methods have nonzero stability ordinate only for $p = 1, 2, 5, 6, 9, 10, \dots$, which matches AM p methods. We have also shown that AB($p-1$)-AM p methods have nonzero stability ordinates only for $p = 3, 4, 7, 8, 11, 12, \dots$, which matches AB p methods. Therefore, regardless of the desired order, an appropriate predictor-corrector can be found to successfully integrate a spatially discretized wave equation.

Bibliography

- [1] M. J. Ablowitz and H. Segur. Exact linearization of a Painlevé transcendent. Phys. Rev. Lett., 38:1103–1106, 1977.
- [2] ADVANPIX: Multiprecision Computing Toolbox, version 3.4.2.3222. Advanpix.com, Yokohama, Japan, 2013.
- [3] E. Anderson, Z. Bai, C. Bischof, S. Blackford, J. Demmel, J. Dongarra, J. Du Croz, A. Greenbaum, S. Hammarling, A. McKenney, and D. Sorensen. LAPACK Users' Guide. Society for Industrial and Applied Mathematics, Philadelphia, PA, third edition, 1999.
- [4] K. E. Atkinson. An Introduction to Numerical Analysis. Wiley, New York, 1989.
- [5] V. K. Balakrishnan. Introductory Discrete Mathematics. Dover, New York, 1991.
- [6] A. P. Bassom, P. A. Clarkson, and A. C. Hicks. Numerical studies of the fourth Painlevé equation. IMA Journal of Applied Mathematics, 50:167–193, 1993.
- [7] A. P. Bassom, P. A. Clarkson, A. C. Hicks, and J. B. McLeod. Integral equations and exact solutions of the fourth Painlevé equation. In Proceedings of the Royal Socited of London A, April 1992.
- [8] C. M. Bender and S. A. Orszag. Advanced Methods for Scientists and Engineers. McGraw-Hill, New York, 1978.
- [9] D. Bermúdez and D. J. Fernández. Non-hermitiaon Hamiltonians and the Painlevé IV equation with real parameters. Phys. Lett. A, 375(33):2974–2978, 2011.
- [10] D. Bermúdez and D. J. Fernández. Supersymmetric quantum mechanics and Painlevé IV equation. SIGMA, 7(25), 2011.
- [11] D. Bermúdez and D. J. Fernández. Solution hierarchies for the Painlevé IV equation. In Proceedings of the XXXI Workshop on Geometric Methods in Physics, Bialowieza, Poland, June 2012.
- [12] P. Boutroux. Recherches sur les transcendantes de M. Painlevé et l'étude asymptotique des équations différentielles du second ordre. Ann. École Norm., 30:265–375, 1913.
- [13] P. A. Clarkson. The fourth Painlevé equation and associated special polynomials. Journal of Mathematical Physics, 44(11), November 2003.

- [14] P. A. Clarkson. The fourth Painlevé transcendent. Technical Report UNK, Institute of Mathematics, Statistics and Actuarial Science, University of Kent, November 2008.
- [15] P. A. Clarkson and K. Jordaan. The relationship between semi-classical Laguerre polynomials and the fourth Painlevé equation. preprint arXiv:1301.4134[nlin.SI].
- [16] G. F. Corliss. Integrating ODE's in the complex plane-pole vaulting. Mathematics of Computation, 35(152):1181–1189, 1980.
- [17] F. Fahroo and I. M. Ross. Costate estimation by a Legendre pseudospectral method. Journal of Guidance, Control and Dynamics, 24:270–271, 2001.
- [18] A. S. Fokas, U. Mugan, and M. J. Ablowitz. A method of linearization for Painlevé equations: Painlevé IV, V. Physica D., 30:247–283, 1988.
- [19] B. Fornberg and J. A. C. Weideman. A numerical methodology for the Painlevé equations. Journal of Computational Physics, 230:23–32, 2011.
- [20] B. Fornberg and J. A. C. Weideman. A computational exploration of the second Painlevé equation. 2013. Accepted by Found. Comp. Math.
- [21] P. J. Forrester and N. S. Witte. Application of τ -function theory of Painlevé equations to random matrices: PIV, PII, and the GUE. Commun. Math. Phys., 219:357–398, 2001.
- [22] M. Ghrist. High-order Finite Difference Methods for Wave Equations. PhD thesis, Department of Applied Mathematics, Boulder, CO, 2000.
- [23] M. Ghrist and B. Fornberg. Two results concerning the stability of staggered multistep methods. SIAM J. Num. Anal., 50(4):1849–1860.
- [24] M. Ghrist, B. Fornberg, and T. Driscoll. Staggered time integrators for wave equations. SIAM J. Num. Anal., 38:718–741, 2000.
- [25] M. Ghrist, J. A. Reeger, and B. Fornberg. Stability ordinates of Adams predictor-corrector methods. Submitted to BIT.
- [26] V. I. Gromak, I. Laine, and S. Shimomura. Painlevé Differential Equations in the Complex Plane. Walter de Gruyter, Berlin, 2002.
- [27] S. P. Hastings and J. B. McLeod. A boundary value problem associated with the second Painlevé transcendent and the Korteweg-de Vries equation. Arch. Rational Mech. Anal., 73:31–51, 1980.
- [28] P. Henrici. Discrete Variable Methods in Ordinary Differential Equations. John Wiley & Sons, New York, 1962.
- [29] J. S. Hesthaven, S. Gottlieb, and D. Gottlieb. Spectral Methods for Time-Dependent Problems. Cambridge Monographs on Applied and Computational Mathematics (No. 21). Cambridge University Press, Cambridge, 2007.
- [30] A. Iserles. Numerical Analysis of Differential Equations. Cambridge University Press, Cambridge, 2004.

- [31] A. R. Its and A. A. Kapaev. Connection formulae for the fourth Painlevé transcendent: Clarkson-McLeod solution. J. Phys. A: Math. Gen., 31:4073–4113, 1998.
- [32] N. A. Lukashevich. Theory of the fourth Painlevé equation. Diff. Eq., 3:395–399, 1967.
- [33] MATLAB[®], version 8.0.0.783 (R2012b). The MathWorks Inc., Natick, Massachusetts, 2012.
- [34] Y. Murata. Rational solutions of the second and fourth Painlevé equations. Funkcial. Ekvac., 28:1–32, 1985.
- [35] M. Noumi and Y. Yamada. Symmetries in the fourth Painlevé equation and Okamoto polynomials. Nagoya Math J., 153:53–86, 1999.
- [36] V. Y. Novokshenov. Padé approximations for Painlevé I and II transcendents. Theoretical and Mathematical Physics, 159(3):853–862, 2009.
- [37] K. Okamoto. Studies on the Painlevé equations III. Second and fourth Painlevé equations, P_{II} and P_{IV} . Math. Ann., 275:221–255, 1986.
- [38] F. W. J. Olver, D. W. Lozier, R. F. Boisvert, and C. W. Clark. NIST Handbook of Mathematical Functions. Cambridge Univ. Press, 2010. <http://dlmf.nist.gov/>.
- [39] S. Olver. A general framework for solving Riemann-Hilbert problems numerically. Numer. Math., 122(2):305–340, 2012.
- [40] L. Peltonen. Numerical solution of ODEs with poles. Master’s thesis, Worcester College, Walton Street, Oxford, Oxfordshire, OX1 2HB, 01865 278300, University of Oxford, 2011.
- [41] J. A. Pietz. Pseudospectral collocation methods for the direct transcription of optimal control problems. Master’s thesis, Department of Computational and Applied Mathematics, MS 134, Rice University, Houston, Texas, 77005-1892, 2003. Available as CAAM Technical Report TR03–10 http://www.caam.rice.edu/tech_reports/2003/TR03-10.pdf.
- [42] J. A. Reeger and B. Fornberg. Painlevé IV: A numerical study of the fundamental domain and beyond. 2013. In preparation.
- [43] J. A. Reeger and B. Fornberg. Painlevé IV with both parameters zero: A numerical study. Stud. Appl. Math., 130(2):108–133, 2013.
- [44] I. M. Willers. A new integration algorithm for ordinary differential equations based on continued fraction approximations. Comm. ACM, 17:504, 1974.

Appendix A

Paper 1-“Painlevé IV with Both Parameters Zero: A Numerical Study”

Painlevé IV with both Parameters Zero: A Numerical Study

By *Jonah A. Reeger*¹ and *Bengt Fornberg*²

The six Painlevé equations were introduced over a century ago, motivated by rather theoretical considerations. Over the last several decades, these equations and their solutions, known as the Painlevé transcendents, have been found to play an increasingly central role in numerous areas of mathematical physics. Due to extensive dense pole fields in the complex plane, their numerical evaluation remained challenging until the recent introduction of a fast “pole field solver” [1]. The fourth Painlevé equation has two free parameters in its coefficients, as well as two free initial conditions. The present study applies this new computational tool to the special case when both of its parameters are zero. We confirm existing analytic and asymptotic knowledge about the equation, and also explore solution regimes which have not been described in the previous literature.

1. Introduction

The six Painlevé equations (P_I – P_{VI}) are second-order ordinary differential equations (ODEs) with solutions that are free from movable branch points, but with the possibility of movable poles or movable isolated essential singularities [2, Section 32.2]. The term movable refers to the dependence of their location on the ODE’s initial data. The second through sixth Painlevé equations also exhibit dependence on one to four arbitrary parameters. The fourth Painlevé

Address for correspondence: Jonah A. Reeger, University of Colorado, Department of Applied Mathematics, 526 UCB, Boulder, CO 80309, USA; e-mail: jonah.reeger@gmail.com

¹Captain, United States Air Force, supported by the Department of Defense. The views expressed in this article are those of the authors and do not reflect the official policy or position of the United States Air Force, Department of Defense, or U.S. Government.

²Supported by NSF grant DMS-0914647.

equation (P_{IV}),

$$\begin{aligned} \frac{d^2}{dz^2}u(z) &= \frac{1}{2u(z)} \left(\frac{d}{dz}u(z) \right)^2 + \frac{3}{2}u(z)^3 + 4zu(z)^2 \\ &+ 2(z^2 - \alpha)u(z) + \frac{\beta}{u(z)}, \end{aligned} \quad (1)$$

has two such parameters, α and β . Together with two initial conditions (ICs) a vast array of solutions can arise.

The solutions to the Painlevé equations are often dubbed the Painlevé transcendents because, except for a very small subset of the possible parameter choices and ICs, they are not expressible in terms of elementary or traditional special functions. With regard to P_{IV} , a particularly small portion of the two-dimensional parameter space leads to solutions expressible as rational functions or in terms of special functions such as the parabolic cylinder function. These solutions are well documented; however, nearly all of the parameter and IC choices are unexplored. For the case $\alpha = \beta = 0$, which this study focuses on, no closed form solution is known (apart from the trivial $u(z) = 0$).

The growing importance of the Painlevé transcendents in mathematical physics is reflected in that they, although absent in the classical “Handbook of Mathematical Functions” [3], have received a full chapter in the NIST handbook [2]. Numerous applications for the Painlevé equations are given in [2, Sections 32.13–32.16], along with extensive references. These include reductions of partial differential equations, combinatorics, and many physical applications including statistical and quantum physics. Some applications specific to the P_{IV} equation include random matrix theory (see, e.g., [4–7]) and supersymmetric quantum mechanics (e.g., [8]). Further applications are noted in [9].

The explorations we describe in this paper are mostly computational. Some early computational work on P_{IV} in [10] focused on the real line with little or no exploration into the complex plane. The numerical approach introduced in [1]—combining a Padé based ODE solver [11] with a partly randomized integration path strategy—allowed for the first time rapid numerical solutions of the Painlevé equations over extended regions in the complex plane. It was first used for P_I in [1] and later for P_{II} in [12]. This paper describes similar computations for P_{IV} .

1.1. Organization of the paper

This paper will first cover some background information about P_{IV} , such as the series expansion around a pole and a notable symmetry in the differential equation. The known asymptotic approximations are followed up with a discussion on computing corresponding ICs. Verifications of these asymptotic approximations and further numerical explorations are then considered, including solutions with a pole located at the origin.

2. Background observations

2.1. Series expansion

In a neighborhood of a pole z_0 the coefficients of the Laurent expansion of P_{IV} can be determined by substituting a truncated expansion

$$u(z) = \sum_{k=-1}^n a_k(z - z_0)^k + O((z - z_0)^{n+1}) \quad (2)$$

into (1) (starting with $k = -1$ since otherwise $a_k = 0$ for $k < -1$). For example, choosing $n = 4$ and equating coefficients gives

$$\begin{aligned} a_{-1} &= \pm 1, \\ a_0 &= -z_0, \\ a_1 &= \frac{1}{3}(-4 \pm z_0^2 \pm 2\alpha), \\ a_2 &= c, \\ a_3 &= \frac{1}{45}(\pm 26 \mp 36cz_0 + 20z_0^2 \mp z_0^4 - 32\alpha \mp 4z_0^2\alpha \pm 14\alpha^2 \pm 9\beta), \\ a_4 &= \frac{1}{9}(\mp 9c + 5z_0 + 3cz_0^2 \mp 2z_0^3 + 6c\alpha \mp 4z_0\alpha). \end{aligned}$$

Hence, all poles in the solutions to P_{IV} are simple and have residue of either $+1$ or -1 . The only further free parameter is c , first appearing in a_2 .

2.2. Symmetry in the P_{IV} equation

Let $P_{IV}(\alpha, \beta)$ be the set of all solutions of (1) for the particular α and β . Direct inspection of (1) shows that if $u(z) \in P_{IV}(\alpha, \beta)$, then

$$-u(-z) \in P_{IV}(\alpha, \beta), \quad (3)$$

$$-iu(iz) \in P_{IV}(-\alpha, \beta), \text{ and} \quad (4)$$

$$iu(-iz) \in P_{IV}(-\alpha, \beta) \text{ [13]}. \quad (5)$$

Incidentally, the first of these symmetries also holds for P_{III} (for all parameter choices), but never for any of the other Painlevé equations. With our current focus on $\alpha = \beta = 0$, we note in particular that if $u(z) \in P_{IV}(0, 0)$, then $-u(-z)$, $-iu(iz)$, and $iu(-iz) \in P_{IV}(0, 0)$. This first symmetry simplifies the analysis of the various computations considered in this paper. For instance, the number of poles and oscillations over a given interval of the real line is monitored to determine ICs that give pole- and/or oscillation-free solutions over the entire real line. When given initial data to the ODE at $z = 0$ it then suffices to

consider the solution for an interval along the positive real axis. It is important to keep this symmetry in mind because any solution presented in this paper has a counterpart that is the odd reflection about the origin among others.

3. Asymptotic approximations

Much of the previous computational work on P_{IV} was designed to verify its asymptotic approximations. A contributing factor to this was likely the difficulty experienced by typical ODE solvers when encountering a pole. For instance, solutions with very special parameter choices were explored in [10] using a classical fourth-order Runge–Kutta scheme, a sixth-order scheme, and an Adams Moulton predictor–corrector method, each of which are rendered ineffective when encountering a pole. Alternate approaches that are applicable also when poles are encountered have been proposed in [14] and [15]. A wider selection of parameter choices will be discussed in the following subsections.

3.1. Parameter choices, an approximation, and connection formulae

Before limiting to the case of $\alpha = \beta = 0$, let $\alpha = 2\nu + 1 \in \mathbb{R}$ and $\beta = 0$ (with $\nu = -\frac{1}{2}$ giving $\alpha = 0$). Equation (1) then becomes

$$\begin{aligned} \frac{d^2}{dz^2}u(z) &= \frac{1}{2u(z)} \left(\frac{d}{dz}u(z) \right)^2 + \frac{3}{2}u(z)^3 \\ &\quad + 4zu(z)^2 + 2(z^2 - 2\nu - 1)u(z). \end{aligned} \quad (6)$$

This particular form of P_{IV} is presented in [2, Section 32.11] and is in contrast to those presented in [10] and [16], where the change of variables

$$u(z) = 2\sqrt{2}w(x)^2 \quad \text{and} \quad z = \frac{1}{2}\sqrt{2}x \quad (7)$$

is applied. For some of the following examples, the boundary condition

$$u(z) \rightarrow 0, \quad \text{as} \quad z \rightarrow +\infty \quad \text{and} \quad z \in \mathbb{R} \quad (8)$$

is also imposed. Based on the symmetry (3) discussed previously, the condition $u(z) \rightarrow 0$, as $z \rightarrow -\infty$ could likewise be considered, to achieve analogous results.

It is noted in the NIST handbook [2, Section 32.11(v)] that any nontrivial solution of (6) satisfying (8) is asymptotic to

$$k(D_\nu(\sqrt{2z}))^2 \quad \text{as} \quad z \rightarrow +\infty \quad \text{and} \quad k \neq 0, \quad (9)$$

where $k \in \mathbb{R}$ and $D_\nu(\zeta)$ is the parabolic cylinder function, satisfying

$$\frac{d^2}{d\zeta^2} D_\nu(\zeta) = \left(\frac{1}{4} \zeta^2 - \nu - \frac{1}{2} \right) D_\nu(\zeta)$$

with boundary conditions

$$D_\nu(\zeta) \sim \zeta^\nu e^{-\frac{1}{4}\zeta^2}, \quad \zeta \rightarrow +\infty.$$

Previous studies of P_{IV} present only cases where $k > 0$; however, this study will also consider $k < 0$.

There is a critical value of k given by

$$k^* = \frac{1}{\sqrt{\pi} \Gamma(\nu + 1)} \tag{10}$$

such that when $0 \leq k < k^*$ there are no poles on the real axis. In the case of $\nu = -\frac{1}{2}$, $k^* = \frac{1}{\pi}$.

One can further distinguish between two cases for ν when $0 \leq k < k^*$. First, if $\nu \in \mathbb{Z}^+$, then $u(z)$ is asymptotic to

$$k 2^\nu z^{2\nu} e^{-z^2}, \quad z \rightarrow -\infty. \tag{11}$$

Likewise, if $0 \neq \nu \notin \mathbb{Z}^+$, which includes the present case of $\nu = -\frac{1}{2}$, then $u(z)$ is asymptotic to

$$-\frac{2}{3}z + \frac{4}{3}d\sqrt{3} \sin(\phi(z) - \theta_0) + O(z^{-1}), \quad z \rightarrow -\infty, \tag{12}$$

where

$$\phi(z) = \frac{1}{3}\sqrt{3}z^2 - \frac{4}{3}d^2\sqrt{3} \ln(\sqrt{2}|z|). \tag{13}$$

Here d and θ_0 are given by the connection formulas, derived in [17], as

$$d^2 = -\frac{1}{4}\sqrt{3}\pi^{-1} \ln(1 - |\mu|^2) \tag{14}$$

and

$$\theta_0 = \frac{1}{3}d^2\sqrt{3} \ln(3) + \frac{2}{3}\pi\nu + \frac{7}{12}\pi + \arg(\mu) + \arg\left(\Gamma\left(-\frac{2}{3}i\sqrt{3}d^2\right)\right), \tag{15}$$

with

$$\mu = 1 + \frac{2ik\pi^{3/2}e^{-i\pi\nu}}{\Gamma(-\nu)}. \tag{16}$$

Note that the connection formulas for d and θ_0 were presented incorrectly in [18] and [19], but corrected in, for example, [10] and [16].

Next, for $k = k^*$, $u(z)$ again has no poles on the real axis and is asymptotic to $-2z$ for $z \rightarrow -\infty$. Finally, if $k > k^*$ or $k < 0$, then $u(z)$ has poles on the

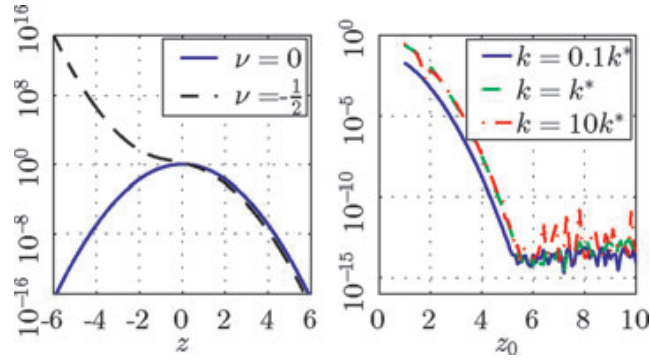


Figure 1. Left: A plot of $(D_\nu(\sqrt{2}z))^2$ with $k = 1$. Right: A plot of $|\frac{u^{(0)}-\hat{u}^{(0)}}{u^{(0)}}|$ for various values of k and $\nu = 0$. Roundoff begins to dominate the error in $\hat{u}^{(0)}$ when z_0 is slightly more than 5.

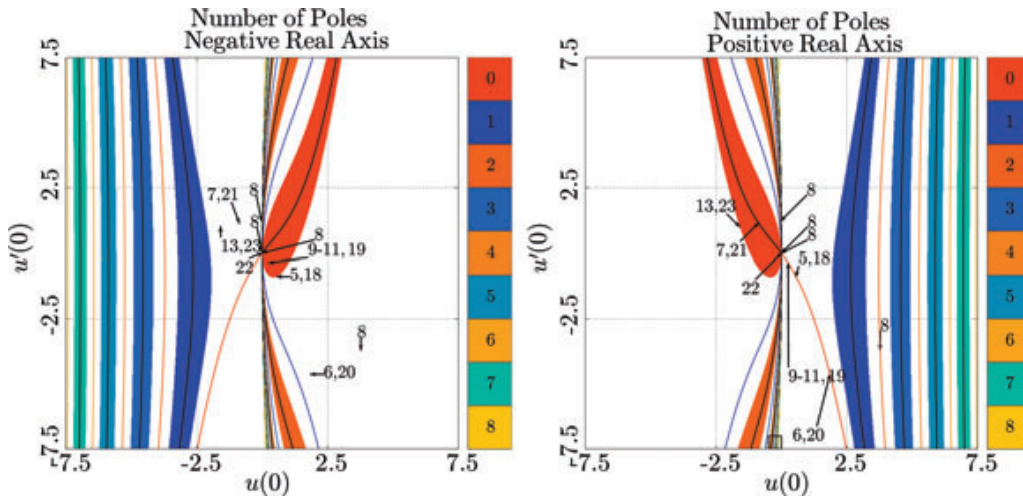


Figure 2. Number of poles on the negative (left) and positive (right) real axes. The colored regions correspond to solutions with a fixed number of poles on the appropriate half of the real axis; however, these solutions may have oscillations over that half. The black and colored curves indicate ICs with a fixed number of poles and no oscillations on the corresponding half of the real axis. White regions correspond to an infinity of poles. The area in the small box at the bottom of the right figure is enlarged in Figure 3.

real axis whose locations are dependent on k . Previous studies of P_{IV} do not explicitly describe the behavior of (6) with $k < 0$. Infinitely, many poles are found along the negative real axis in these cases.

Applying the method of dominant balance (see, e.g., [20, Section 3.4]) to (6) leads to the asymptotic relation

$$u_{\pm}(z) \sim \frac{-4z \pm 2\sqrt{z^2 + 6\nu + 3}}{3} \quad \text{as } |z| \rightarrow \infty.$$

Taking $\nu = -\frac{1}{2}$ leads to $u_+(z) \sim -\frac{2}{3}z$ and $u_-(z) \sim -2z$, respectively, with the upper and lower sign choice. The dominance of this relation is apparent

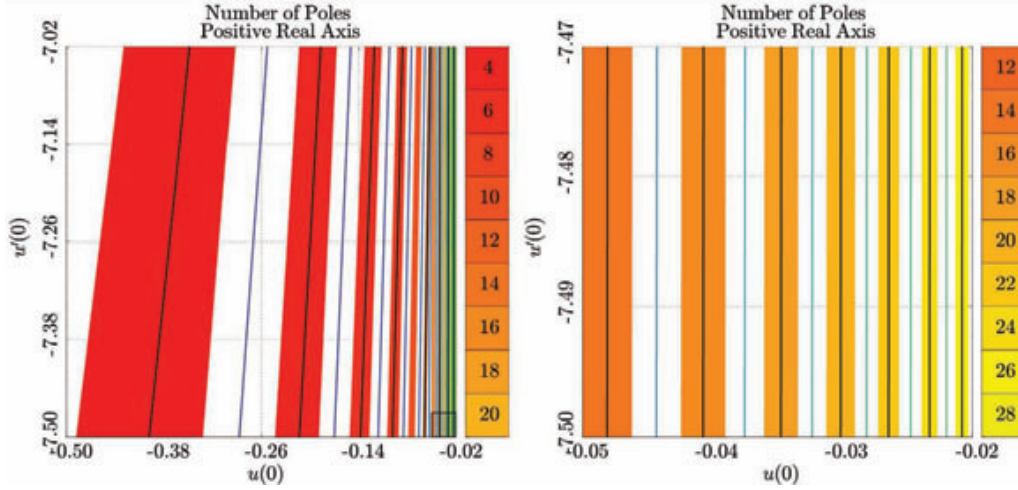


Figure 3. Zoomed views of the number of poles on the positive real line. The left frame corresponds to the box outlined in the right frame of Figure 2 and the right frame corresponds to the box highlighted in the left frame of this figure. Note that the right edge corresponds to $u(0) = -0.02$, rather than $u(0) = 0$, to avoid displaying an infinity of shaded regions.

for $0 < k \leq k^*$; however, this approximation is not meaningful for $k > k^*$ or $k < 0$. It is particularly important in the cases of $k = k^*$ and $k = \frac{1}{2}k^*$, as we will show later.

3.2. Computing the ICs for asymptotic approximations

Consider the asymptotic condition (9), shown in the left of Figure 1. The values of $(D_\nu(\sqrt{2}z))^2$ are less than machine precision for even relatively small values of z . As it will transpire, z can nevertheless be selected such that it is large enough to make the approximation useful and small enough so that a solution of (6) is computable to machine precision.

It is stated in [10] that, for $\nu = 0, 1, 2, \dots$, a closed form solution to (6) for arbitrary values of k and $z \in \mathbb{R}$ exists. For instance, for $\nu = 0$ the solution becomes

$$u(z) = \frac{2\sqrt{2}k \exp(-z^2)}{2^{3/2} - k\sqrt{2\pi} \operatorname{erfc}(z)},$$

where

$$\operatorname{erfc}(\zeta) = \frac{2}{\sqrt{\pi}} \int_{\zeta}^{\infty} \exp(-s^2) ds$$

is the complementary error function discussed in [2, Section 7.2]. Knowing this closed form solution, the exact value of $u(0)$ can be compared to the value obtained numerically beginning with ICs

$$k(D_\nu(\sqrt{2}z_0))^2, \tag{17}$$

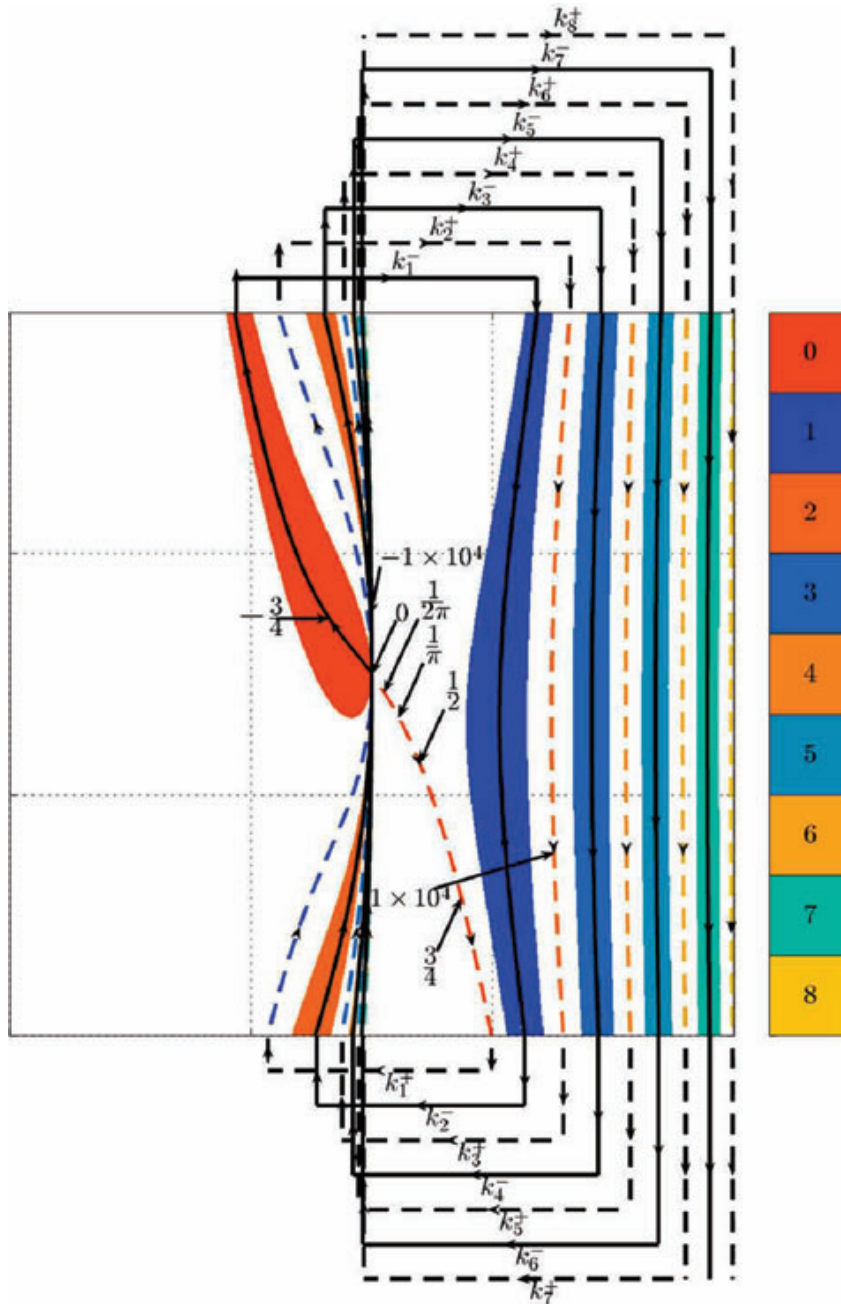


Figure 4. A view of how $u(0)$ and $u'(0)$ change as k is varied. The locations of several values of k are marked. The dashed and solid curves represent values when $k > 0$ and $k < 0$, respectively. The labels k_j^\pm , $j = 1, 2, \dots, 8$, correspond to different values of c in Figures 15 and 16, which represent the movement of a pole through the origin. Approximate values of k and c are also shown in table 1. Note that this image is a detailed version of the right frame of Figure 2, where the horizontal axis indicates the value of $u(0)$ from -7.5 to 7.5 and the vertical axis indicates the values of $u'(0)$, again from -7.5 to 7.5 .

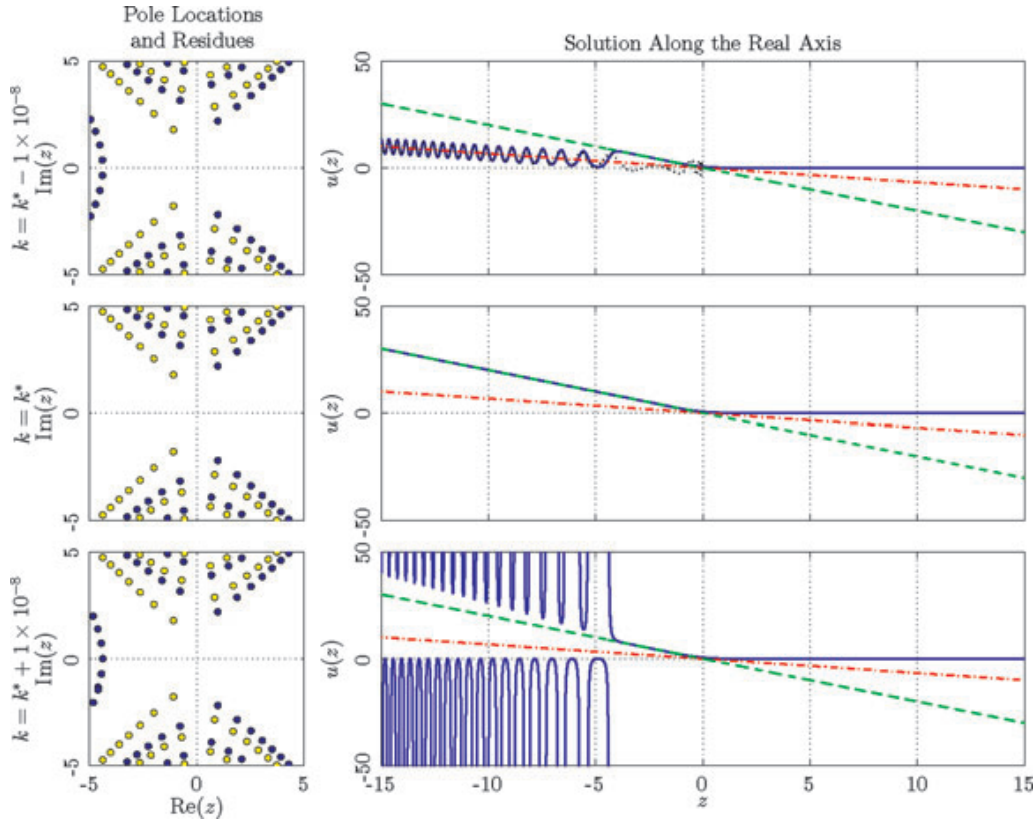


Figure 5. Solutions to (6) with $\nu = -\frac{1}{2}$. The solid (blue) lines indicate the numerical solutions. The dashed-dotted (red) and dashed (green) lines show $-\frac{2}{3}z$ and $-2z$, respectively. The dotted (black) lines in the first and second rows show (12).

$z_0 \in [1, 10]$. Call this numerical solution $\widehat{u}(0)$. Comparing the left and right images in Figure 1 shows that for various k $z_0 \approx 5$ can be chosen to achieve an accurate solution with $(D_\nu(\sqrt{2}z_0))^2$ large enough. To be in agreement with the choice of z_0 to generate initial data in [10] $z_0 = 4\sqrt{2} \approx 5.65$ is used throughout this article, which has been shown to be sufficient.

In the case of the P_{II} equation,

$$\frac{d^2}{dz^2}u(z) = 2u(z)^3 + zu(z) + \alpha,$$

it was found in [12] that its leading asymptotic term alone was numerically sufficient when $\alpha = 0$, but otherwise needed to be supplemented by asymptotic expansions. We encounter the same situation with P_{IV} in its $\alpha = \beta = 0$ case. The leading term in

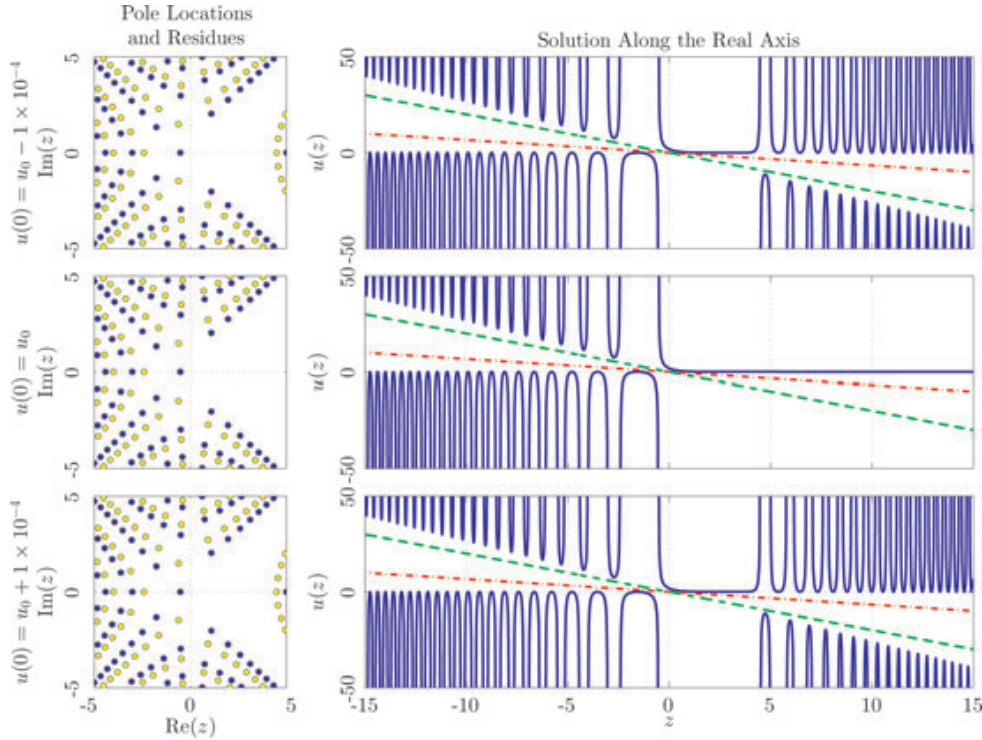


Figure 6. A view of the solutions that have poles that move to $+\infty$ leaving a near zero segment behind and then return. In all cases $u_0 = 1.84810583$ and $u'(0) = -4.61669536$, which result from integrating (6) ($v = -\frac{1}{2}$) starting with (9) ($k = 0.75$) from $z = 4\sqrt{2}$ to $z = 0$. There is no noticeable difference between the top and bottom figure sets, highlighting that there is no change in pole field orientation as we pass through these special ICs.

$$\begin{aligned}
 u(z) &\sim k(D_{-\frac{1}{2}}(\sqrt{2}z))^2 \\
 &+ k^2 \frac{e^{-2z^2}}{z^3} \left[\frac{1}{4} - \frac{9}{16} \frac{1}{z^2} + \frac{205}{128} \frac{1}{z^4} - + \dots \right] \\
 &+ k^3 \frac{e^{-3z^2}}{\sqrt{2}z^5} \left[\frac{1}{8} - \frac{31}{64} \frac{1}{z^2} + \frac{1853}{1024} \frac{1}{z^4} - + \dots \right] \\
 &+ O\left(\frac{e^{-4z^2}}{z^7}\right)
 \end{aligned}$$

suffices for any choice of $z > 4$. Further terms are here unnecessary for the identification of critical k -values.

4. An exploration of the $u(0)$, $u'(0)$ -plane

4.1. Pole and oscillation counting

A particularly useful tool in determining the various types of solutions that exist for fixed α and β is to count the number of poles and oscillations that

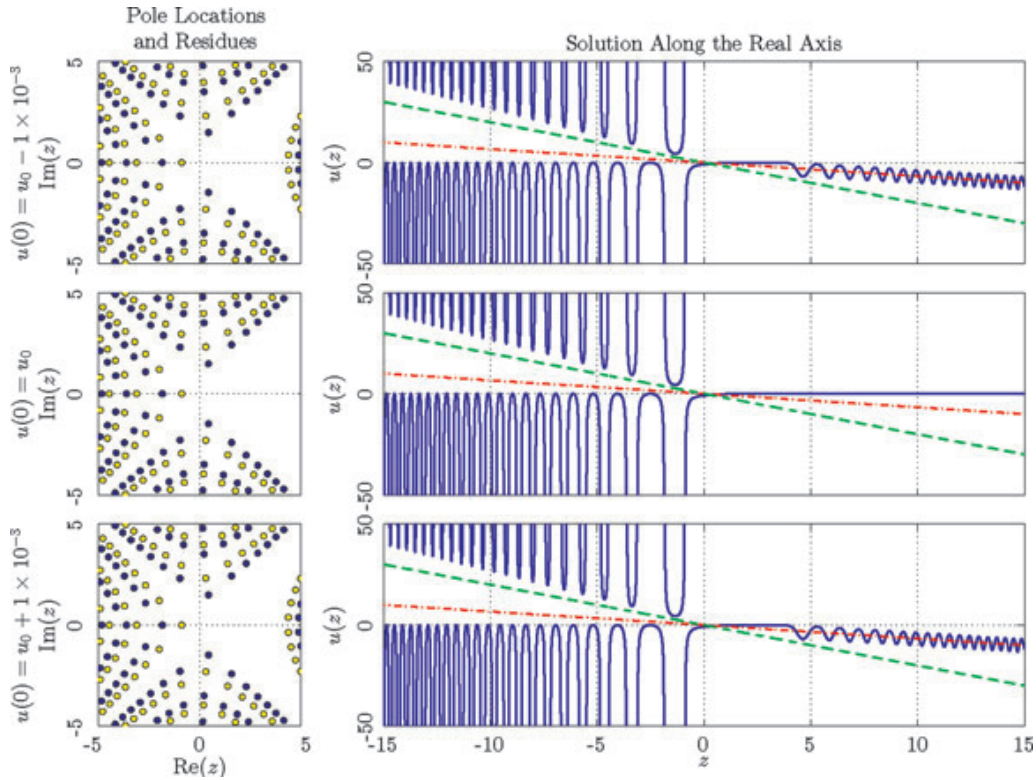


Figure 7. A view of the solutions that have oscillations that move to $+\infty$ leaving a near zero segment behind and then return. In all cases $u_0 = -0.87721765$ and $u'(0) = 1.14146647$, which result from integrating (6) ($\nu = -\frac{1}{2}$) starting with (9) ($k = -0.75$) from $z = 4\sqrt{2}$ to $z = 0$. There is no noticeable difference between the top and bottom figure sets, highlighting that there is no change in pole field orientation as we pass through these special ICs.

occur in a given interval on either the positive or negative real axis. Displays can then be created that indicate the number of poles appearing on the positive or negative real axis for different regions of the $u(0), u'(0)$ plane. This is shown in Figure 2 for the case $\alpha = \beta = 0$ (that is, $\nu = -\frac{1}{2}$). The left and right images were produced by counting the number of poles to the left and right of the origin, respectively. The symmetry (3) is apparent in these figures.

Consider, for now, only the right frame in Figure 2, since the left is completely analogous. Each of the ICs marked by a curve or contained within a shaded region generates a solution with a finite number of poles on the positive real axis. The color bar indicates the exact number of poles for a given IC with darker (blues/greens) and lighter (reds/yellows) indicating odd and even numbers of poles, respectively.

Each of the shaded regions in the right half-plane contains ICs that generate solutions with an odd number of poles on the positive real axis, while the $u(0), u'(0)$ values along the colored curves lead to solutions with an even number. The left half-plane is the opposite.

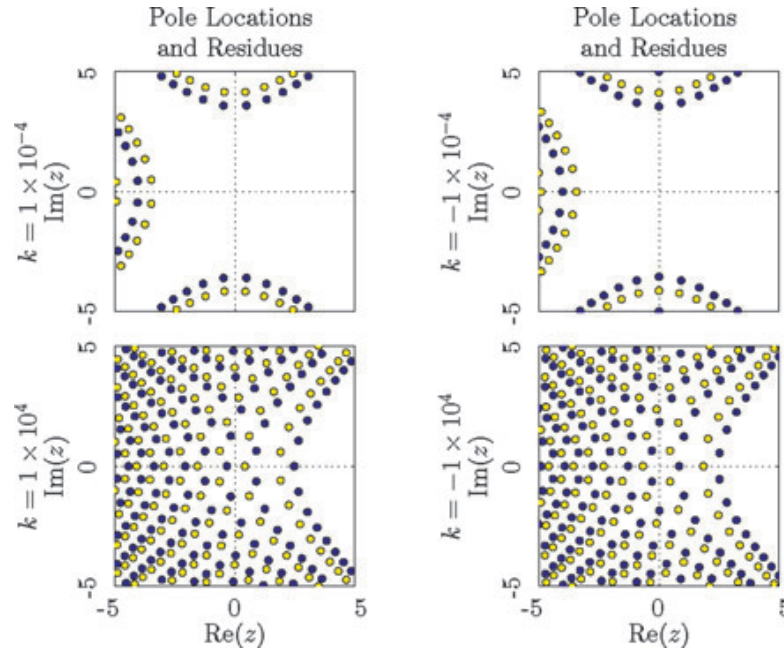


Figure 8. A view of the solutions which result from (6) starting with (9), where $\nu = -\frac{1}{2}$ and four different values for k .

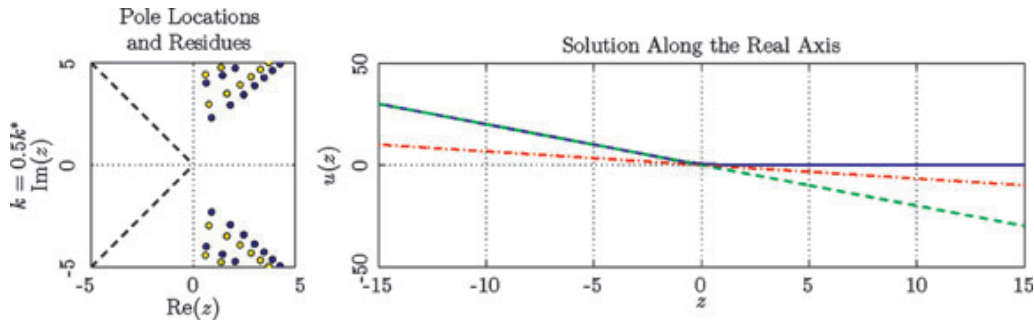


Figure 9. Solution to (6) with $\nu = -\frac{1}{2}$ and $k = 0.5k^*$. The dashed (black) lines on the left indicate the rays $re^{\pm i \frac{3\pi}{4}}$, $r \geq 0$. The dashed-dotted (red) and dashed (green) lines on the right show $-\frac{2}{3}z$ and $-2z$, respectively.

Most of the ICs in the shaded regions generate solutions that oscillate as $z \rightarrow +\infty$; however, each IC marked by a curve or located at the boundary of a shaded region has no oscillations as $z \rightarrow +\infty$.

Figure 2 also identifies the ICs of many of the solutions shown in this paper by marking them with an arrow and the corresponding figure number(s).

Still focusing on the right frame, notice that as $u(0) \rightarrow 0$ from the left the shaded regions become finer. Figure 3 shows two zoomed windows to further highlight this behavior. In these images it is shown that these regions become

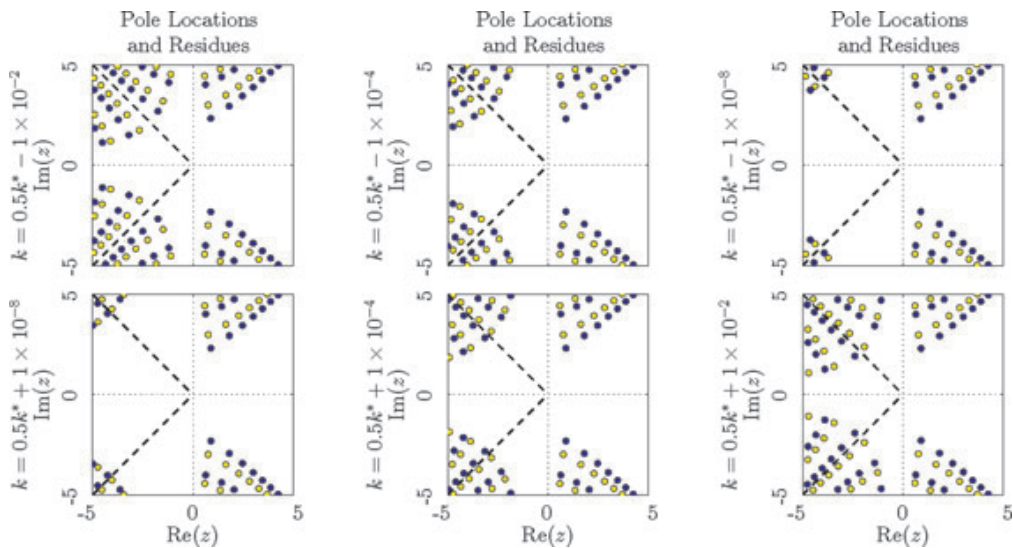


Figure 10. Solutions in the complex plane to (6) with $\nu = -\frac{1}{2}$ for six k -values near $k = \frac{1}{2}k^*$. The dashed (black) lines indicate the rays $re^{\pm i\frac{3\pi}{4}}$, $r \geq 0$.

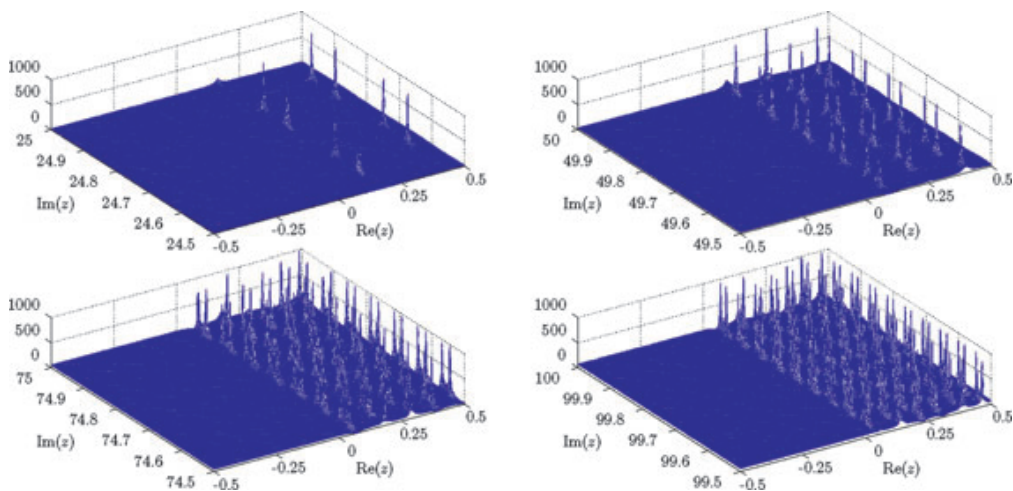


Figure 11. Solutions in the complex plane to (6) with $\nu = -\frac{1}{2}$ and $k = \frac{1}{2}k^*$. Here, we show $|u(z)|$. That is we show pole locations only, without the alternating pattern of residues.

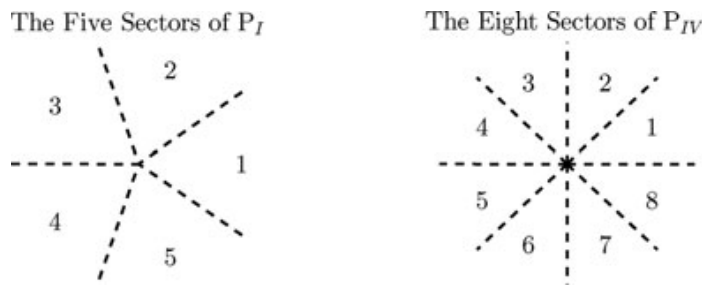


Figure 12. The asymptotic far field sector structures for the P_I and P_{IV} equations.

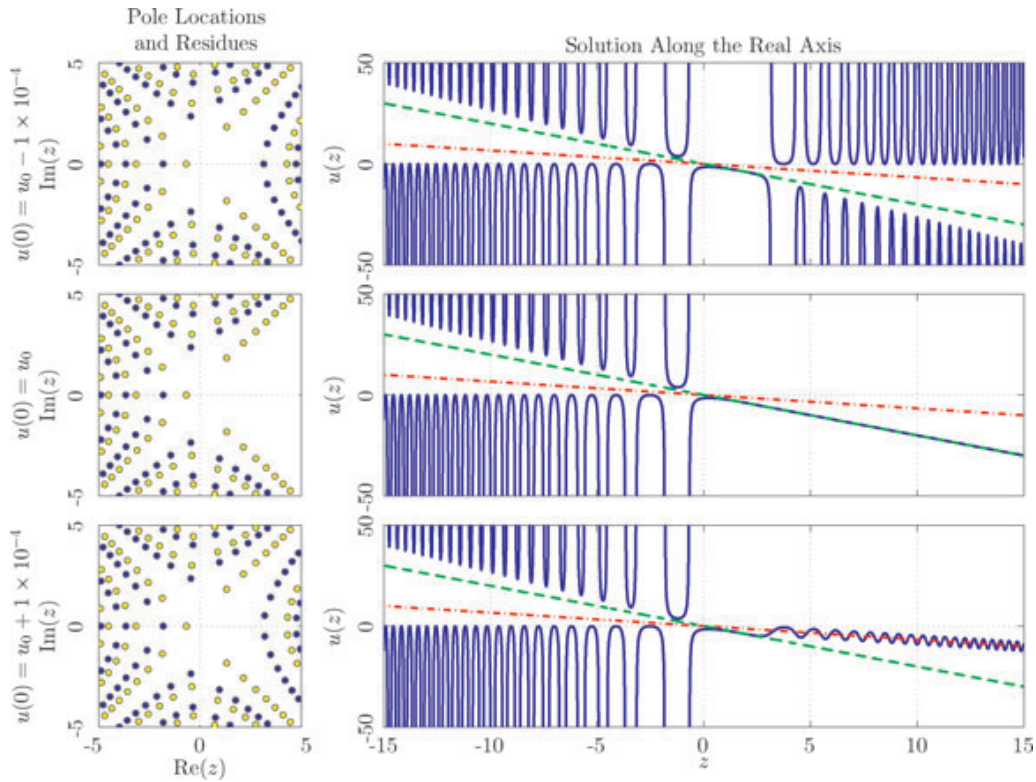


Figure 13. Solutions to (1) with $\alpha = \beta = 0$ and ICs $u_0 = -1.59610846592044$ and $u'(0) = 1$.

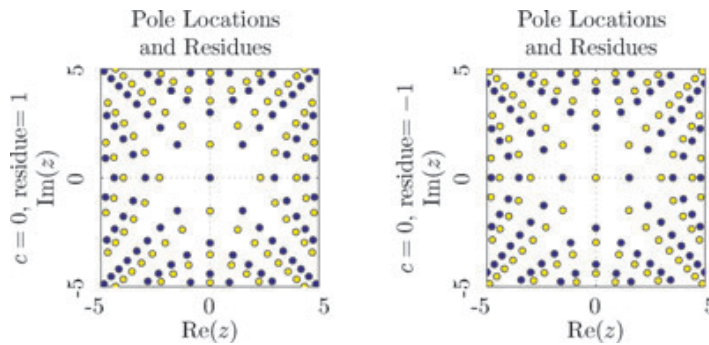


Figure 14. A view of solutions with a pole at the origin in the case of $c = 0$.

infinitely narrower as $u(z)$ approaches zero and in each consecutive region the number of poles increases by two.

4.2. Exploring the known asymptotic solutions

Armed with the pole- and oscillation-counting images, two natural questions become: "Which initial conditions correspond to varying k ?" and "What do

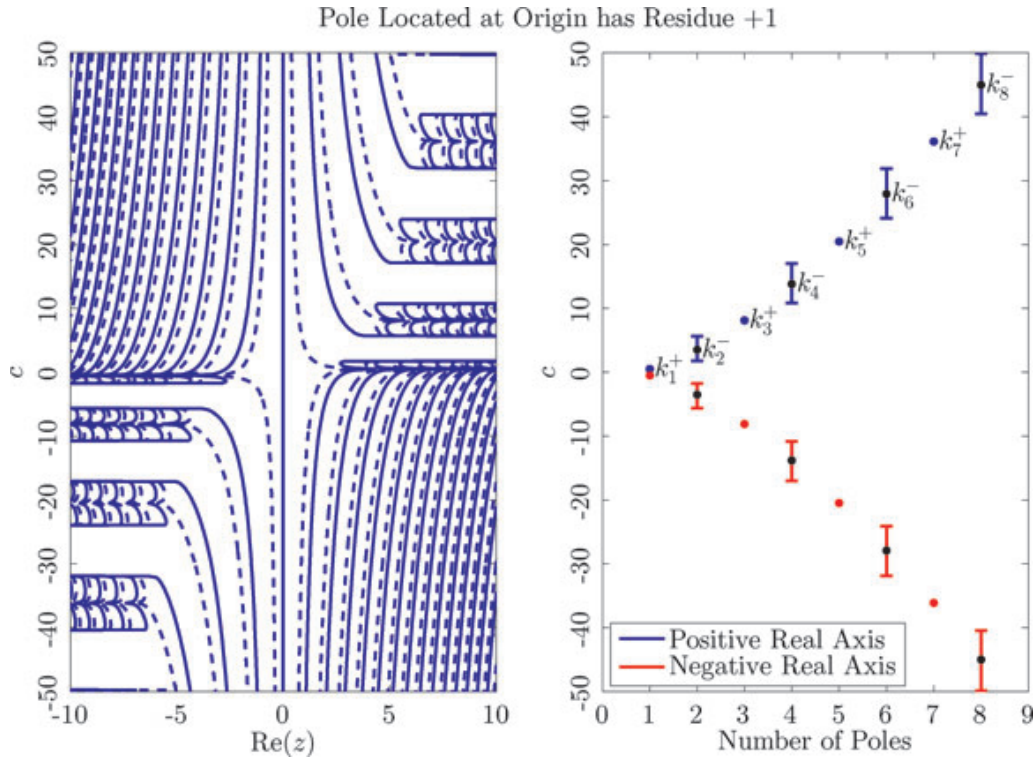


Figure 15. Left Frame: Locations of the poles on the real axis for various c . Solid lines indicate poles with residue +1 and dashed lines those with residue -1. Right Frame: Number of poles includes the pole at the origin. Values of c with no lines or dots indicate solutions with an infinity of poles on the real axis.

the solutions to these asymptotic approximations look like across the complex plane?”

To answer the first question k is varied from near zero to $|k| \gg 0$. The dashed and solid curves in Figure 4 indicate the location of $u(0)$ and $u'(0)$ found by varying k and computing the numerical solution beginning with (17) at $z_0 = 4\sqrt{2}$. The continuation of the curves outside the axes illustrates the transitions of $u(0)$ and $u'(0)$ to $+\infty$ or $-\infty$ and back as we increase or decrease k . This is due to the movement of a pole through the origin $z = 0$. A following section will show that the continuation of the dashed and solid curves corresponds to a pole at the origin with positive and negative residue, respectively.

Next, the second question is answered with examples of the solutions similar to those presented (along the real axis) for the transformed case of P_{IV} in [2], [10], and [16]. To this end, a number of solutions are presented in a two frame format. The left frames display the pole locations and corresponding residues, dark (blue) for +1 and light (yellow) for -1. The right frames display the

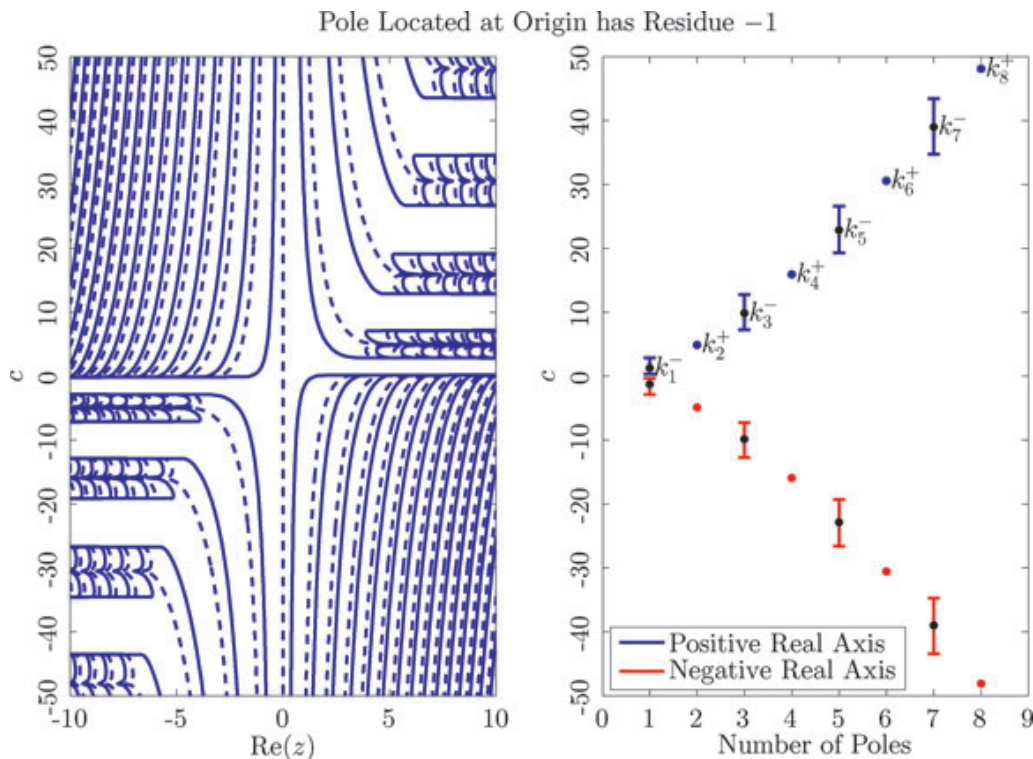


Figure 16. Left Frame: Locations of the poles on the real axis for various c . Solid lines indicate poles with residue $+1$ and dashed lines those with residue -1 . Right Frame: Number of poles includes the pole at the origin. Values of c with no lines or dots indicate solutions with an infinity of poles on the real axis.

solution along the real axis, in a style similar to Figure 32.3.6 in [2] (but without stopping when a pole is encountered); i.e., solutions are displayed for $k = k^* - 1 \times 10^{-8}$, $k = k^*$ and $k = k^* + 1 \times 10^{-8}$. Notice that for $0 < k \leq k^*$ there are no poles on the real axis and that the asymptotic approximations of $-2z$ and (12) match well even for z close to the origin.

Generally, the solutions of (6) satisfying (9) with $k > 0$ occur at critical initial data where a region of poles has moved out to infinity leaving a pole free region of the complex plane behind. For simplicity, refer to this type of solution as a k -positive solution. An example of this appears in Figure 6, where the ICs for the middle row of frames are generated from (6) and (9) by choosing $k = +0.75$. The top and bottom rows show the solutions in a neighborhood of the generated initial data.

On the other hand, choosing $k < 0$ leads to another type of solution. As $u(0)$ and $u'(0)$ generated from (6) and (9) for $k < 0$ are approached the solutions have an infinity of oscillations that move toward $+\infty$ while leaving a near zero solution behind. These solutions will be referred to as k -negative solutions.

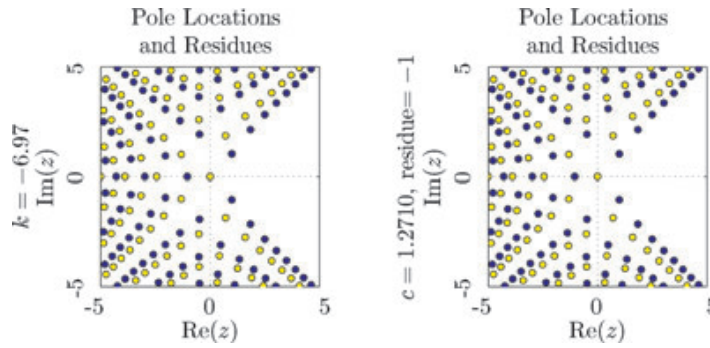


Figure 17. Solutions corresponding to the values in the $-\infty$ and c columns of k_1^- in Table 1. Notice that even these low precision values lead to solutions that are very similar. The pole locations shared by both frames differ by at most $O(10^{-3})$.

Picking $k = -0.75$ the solution in the middle row of Figure 7 is found. The top and bottom rows again highlight the movement of the oscillations for $u(0)$ and $u'(0)$ in a neighborhood of the generated initial data.

Figures 6 and 7 show another, yet peculiar, behavior of the solutions of the P_{IV} equation. As $u(0)$ and $u'(0)$ pass through critical ICs for both P_I and P_{II} there is a distinct change in the location of the poles closest to the real axis. For instance, let u_0 and u'_0 be critical ICs for P_I and $u(0) = u_0 - \epsilon$ and $u'(0) = u'_0$ generate a solution with no poles on the negative real axis. Then the solution for $u(0) = u_0 + \epsilon$ and $u'(0) = u'_0$ will have an infinity of the poles on the negative real axis. An example of this is shown for P_I in Figure 4.3 of [1], which is also shown only on the real axis in Figure 32.3.3 of [2]. This same behavior has been witnessed for all possible choices of critical ICs shown in the available literature for P_{II} .

On the other hand, if $u(0)$ or $u'(0)$ generated from (6) and (9) are fixed and a small neighborhood of $u'(0)$ or $u(0)$, respectively, is considered, then there is no change in pole field orientation or residue when passing through the critical ICs. The action of passing through the critical ICs is the same as passing through either a solid or dashed line in Figure 4. This is the behavior for nearly all of the k -positive and k -negative solutions, except those which occur at the boundary of a shaded region in Figure 4. An example of this appears in Figure 5.

To complete this section consider extreme values of k . That is, consider values of k with very large and very small magnitudes. Figure 8 shows some such solutions.

Notice that values of k that are equal in magnitude but opposite in sign lead to solutions that are similar, but with the sign of the residue of the pole located furthest to the right on the real axis equalling the sign of k .

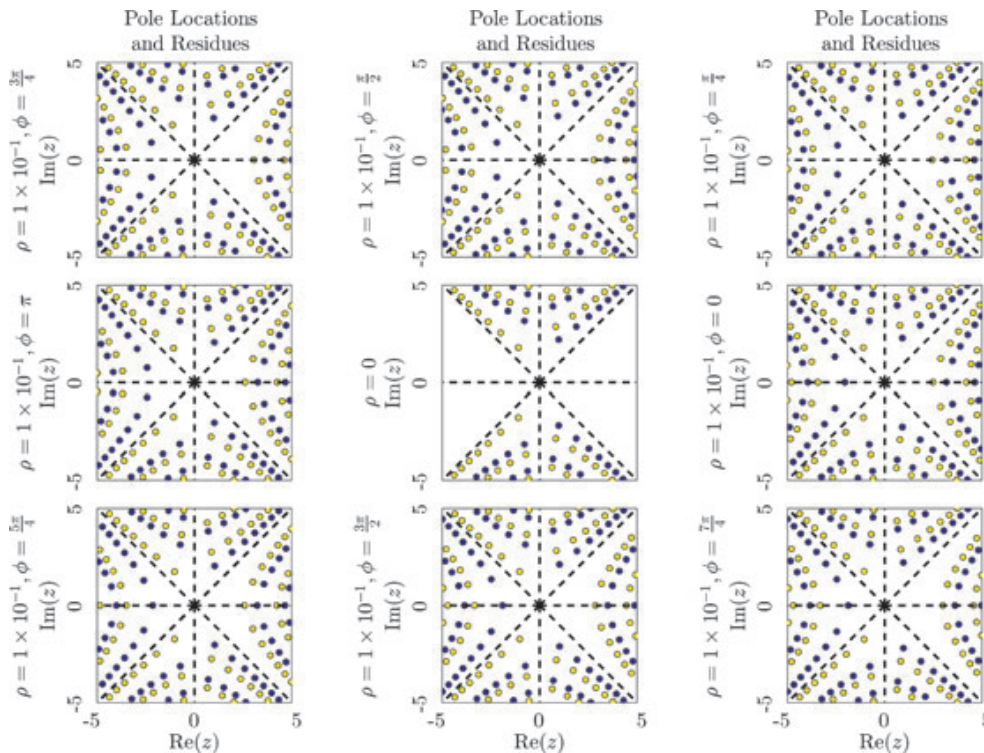


Figure 18. A view of the solutions with $u(0)$ and $u'(0)$ in a neighborhood of the values generated by (6) with ICs given by (9) where $\nu = -\frac{1}{2}$ and $k = k^*$ shown in Figure 5. Here $u(0) = 0.555491078710868 + \rho \cos(\phi)$ and $u'(0) = -0.886725480333295 + \rho \sin(\phi)$ to generate the solutions.

4.3. Solution with a pole free half-plane

One of the more interesting cases appears in Figure 9, when $k = 0.5k^*$. In this case, the solution follows $-\frac{2}{3}z$, as $z \rightarrow -\infty$ and $z \in \mathbb{R}$, and appears pole and oscillation free across the entire real axis. In fact, (12) becomes $-\frac{2}{3}z$, and substitution of $u(z) = -\frac{2}{3}z$ into (6) with $\nu = -\frac{1}{2}$ leads to a residual of $\frac{1}{3z}$. Figure 10 shows a sequence of solutions where k increases to $\frac{1}{2}k^*$ and beyond. Notice that two regions of poles, nearly symmetric about the rays $re^{\pm i\frac{3\pi}{4}}$, $r \geq 0$, move away from the origin and, after the critical $k = 0.5k^*$, return with changed orientation.

Figure 11 displays a sequence of frames of size 1×0.5 in the real and imaginary directions, respectively, depicting $|u(z)|$ adjacent to the imaginary axis. This frame size was chosen so that the magnitude of $u(z)$ could be clearly displayed when the density of the poles is so great near $\text{Im}(z) = 100$. The distance of the nearest row of poles from the imaginary axis appears to be $O(\frac{1}{\text{Im}(z)})$, with the left half-plane pole free.

The pole-free nature of the left half-plane and a large portion of the right half-plane is reminiscent of a special solution to P_I known as the tritronquée

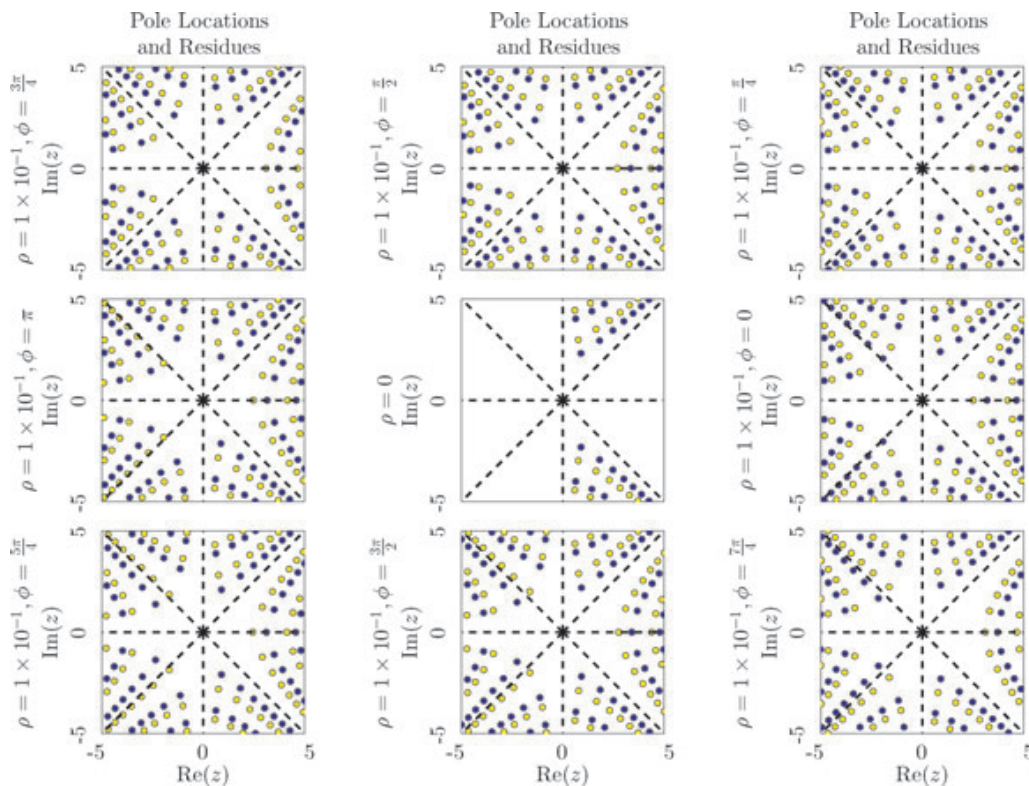


Figure 19. A view of the solutions with $u(0)$ and $u'(0)$ in a neighborhood of the values generated by (6) with ICs given by (9) where $\nu = -\frac{1}{2}$ and $k = \frac{1}{2}k^*$ shown in Figure 9. Here $u(0) = 0.253975473568026 + \rho \cos(\phi)$ and $u'(0) = -0.367698229229807 + \rho \sin(\phi)$ to generate the solutions.

solution (see, e.g., [21], [1], or [14]). It is well known that the P_I equation,

$$\frac{d^2}{dz^2}u(z) = 6u(z)^2 + z, \tag{18}$$

is invariant under the changes $u \rightarrow \omega^3 u, z \rightarrow \omega z$ when $\omega^5 = 1$ (see, e.g., [1]). This results in solutions with poles aligned in the five distinct sectors shown the left in Figure 12. The tritronquée solution for P_I is pole free except for the region 1 in the figure, leaving the entire left half-plane pole free. Similarly, many of the P_{IV} solutions considered here indicate that the poles line up in the eight sectors shown to the right in Figure 12. This will become even more apparent in Section 4.6.

4.4. Tronquée-like solutions

In both the k -positive and k -negative cases, behavior different from the tronquée solutions for P_I discussed in, for example, [1] and [14] is encountered. Concerning P_I , transitioning through tronquée initial data leads to a fundamental

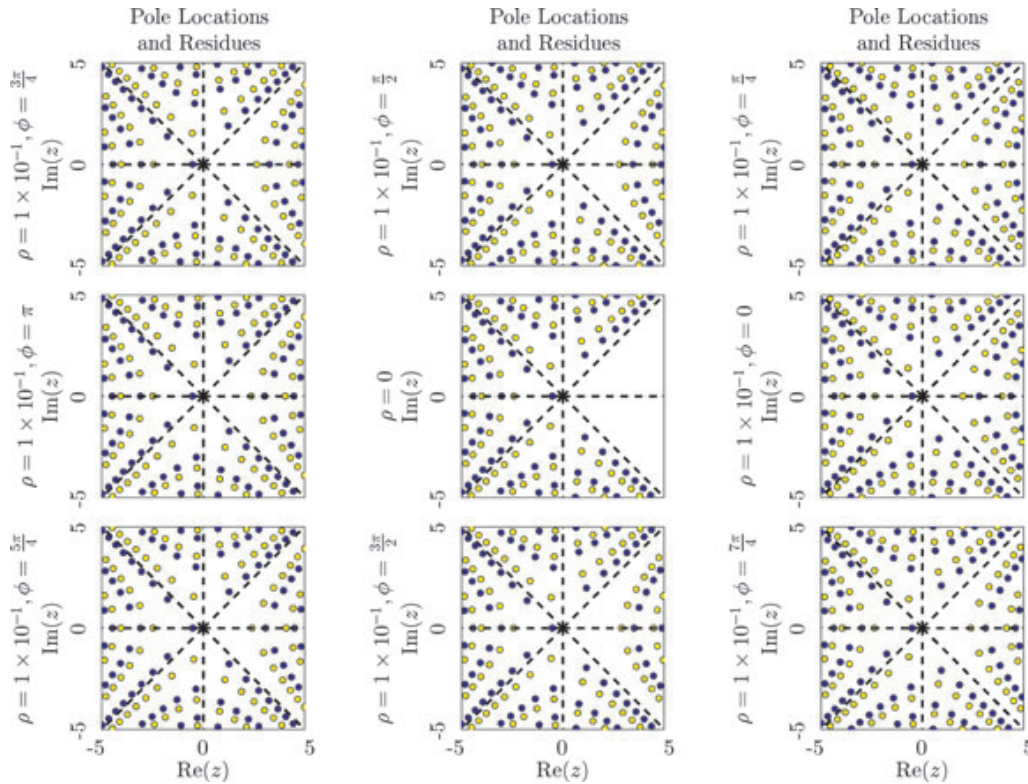


Figure 20. A view of the solutions with $u(0)$ and $u'(0)$ in a neighborhood of the values generated by (6) with ICs given by (9) where $\nu = -\frac{1}{2}$ and $k = 0.75$ shown in Figure 6. Here $u(0) = 1.852476801971173 + \rho \cos(\phi)$ and $u'(0) = -4.634118664573674 + \rho \sin(\phi)$ to generate the solutions.

change in the location of the poles in the solutions. That is, beginning with a solution to P_I with no poles on the real axis, the ICs on the other side of the tronquée initial data will have poles on the real axis. The opposite occurs when beginning with poles on the real axis. Tronquée-like behavior for P_{IV} occurs at the transition from a shaded region in Figure 2 to a blank region.

One of the tronquée-like solutions occurs when $u(0) \approx -1.59610846592044$ and $u'(0) = 1$. Figure 13 displays the behavior just described. Notice, also, that as $z \rightarrow \infty$ the solution at the critical initial data is asymptotic to $-2z$. This is found to be the case for nearly all tronquée-like solutions. The exception is the trivial solution when $u(0) = u'(0) = 0$.

4.5. Solutions with a pole at the origin

Until now solutions have only been considered for which $u(0)$ and $u'(0)$ are finite. However, beginning with a truncated series like (2), with $z_0 = 0$, ICs can be generated to also view solutions with a pole at the origin. In the case of

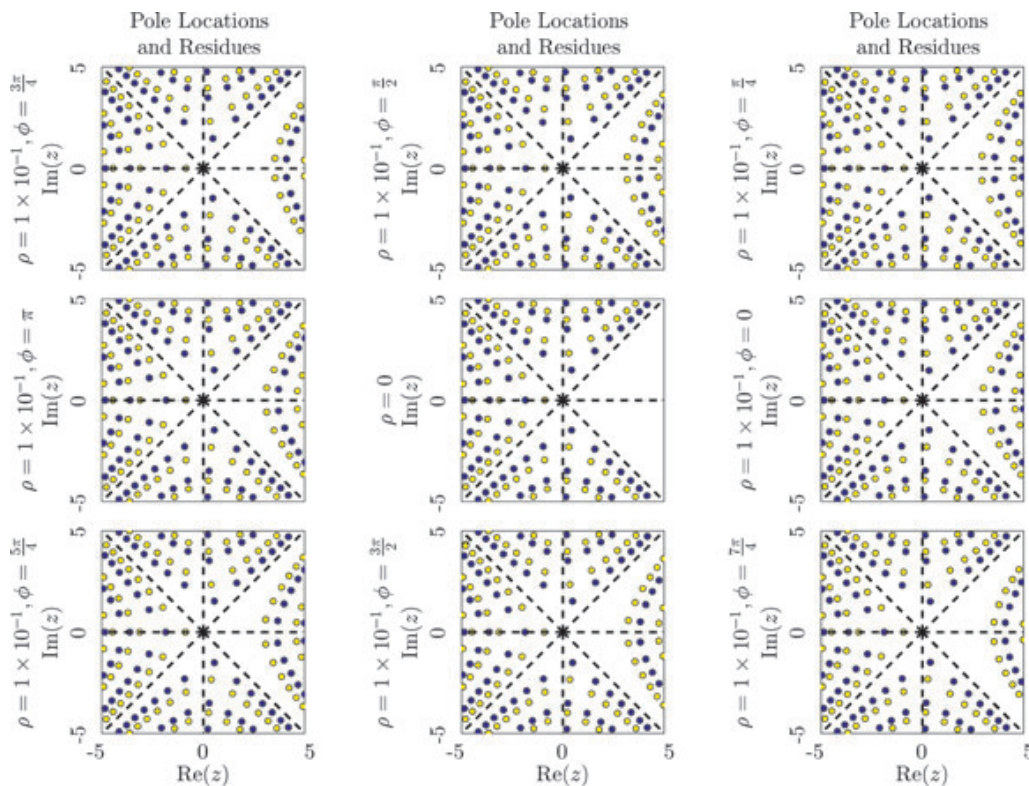


Figure 21. A view of the solutions with $u(0)$ and $u'(0)$ in a neighborhood of the values generated by (6) with ICs given by (9) where $v = -\frac{1}{2}$ and $k = -0.75$ shown in Figure 7. Here $u(0) = -0.878189808443538 + \rho \cos(\phi)$ and $u'(0) = 1.142924661194064 + \rho \sin(\phi)$ to generate the solutions.

$\alpha = \beta = 0$ the expansion becomes

$$\begin{aligned}
 u(z) \approx & \pm \frac{1}{z} - \frac{4}{3}z + cz^2 \pm \frac{26}{45}z^3 \mp cz^4 + \frac{1}{945}(-128 \pm 405c^2)z^5 + \frac{41}{90}cz^6 \\
 & + \frac{(\pm 1604 - 12960c^2)}{28350}z^7 + \frac{(\mp 3092 + 1800c^2)}{12600}cz^8 \\
 & + \frac{(-10240 \pm 136512c^2)}{374220}z^9 + \frac{(45555 \mp 77760c^2)}{340200}cz^{10} \\
 & + \frac{(\pm 15846104 - 324788400c^2 \pm 66156750c^4)}{1277025750}z^{11} \\
 & + \frac{(\mp 27096717 + 92409660c^2)}{392931000}cz^{12} + O(z^{13}).
 \end{aligned} \tag{19}$$

Reiterating, the residue at the origin can be either +1 or -1, and the only remaining free parameter is c . Choosing $c = 0$ gives the two solutions shown in Figure 14.

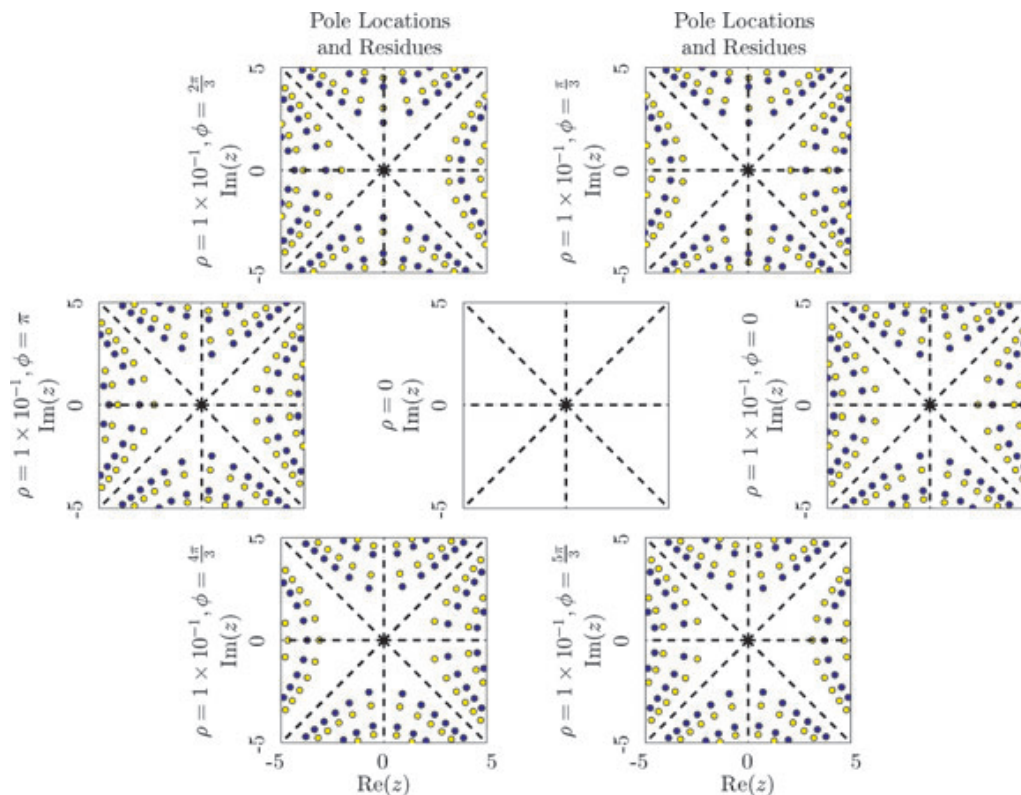


Figure 22. A view of the solutions in a neighborhood of the origin. Here, $u(0) = \rho \cos(\phi)$ and $u'(0) = \rho \sin(\phi)$ to generate the solutions. Because we cannot compute numerically the solution when $u(0) = 0$, except when $u'(0) = 0$ also, we show only six neighboring solutions in a neighborhood of the origin to preserve symmetry.

Varying $u(0)$ and $u'(0)$ allows the exploration of all solutions apart from those with a pole at the origin. In that case, the single parameter c can instead be varied to explore the number of poles and oscillations along the two halves of the real axis. Figures 15 and 16 show that certain choices of c lead to solutions with a finite number of poles on the positive and negative real axes. This is shown in two ways for both possible choices of the residue for the pole located at the origin. On the left the locations of the poles on the real axis are shown, with solid lines indicating $+1$ residue and dashed lines indicating -1 residue. Due to (2) and (19) the curves are symmetric around the origin $\text{Re}(z) = c = 0$. The right images mimic Figure 2. In these images, lines and dots correspond to values of c that generate solutions with a finite number of poles. The horizontal axis indicates the exact number of poles on either the positive or negative real axis. The corresponding half of the real axis is indicated by the color of the line or dot. Consequently, we can deduce that the colored and black dots indicate the values of c that correspond to solutions generated from (6) and (9) with $k > 0$ and $k < 0$,

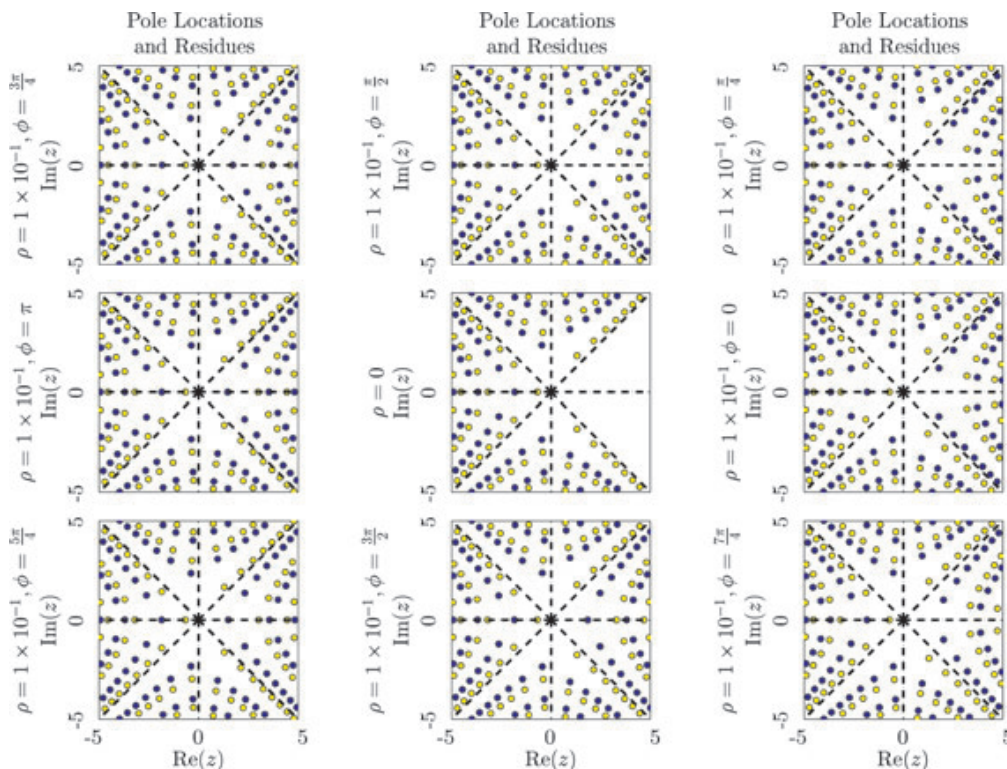


Figure 23. A view of the solutions in a neighborhood of the tronquée-like solution shown in 13. Here $u(0) = -1.59610846592044 + \rho \cos(\phi)$ and $u'(0) = 1 + \rho \sin(\phi)$ to generate the solutions.

respectively. Colored line segments, then, correspond to colored regions in Figure 2.

Table 1 shows the approximate values of k and c corresponding to the k_j^+ and k_j^- , $j = 1, 2, \dots, 8$, solutions, respectively, in Figures 4, 15, and 16. The columns ± 7.5 (out) and ± 7.5 (in) show the values of k where the dashed and solid line segments leave and enter the window in Figure 4. The column labeled $\pm\infty$ gives the value of k corresponding to the transition of a pole through the origin. The c column and $\pm\infty$ column lead to the same solution when substituted into (19) and (9), respectively, to generate ICs.

To see how close the solutions corresponding to the $\pm\infty$ and c columns are, consider those for k_1^- in table 1. If the corresponding solutions are computed, the pole locations and residues are shown in Figure 17. Notice that even these low precision values for k and c already lead to solutions that are very similar. The pole locations shared by both frames differ by at most $O(10^{-3})$.

4.6. Neighborhoods of solutions

Throughout this paper several special solutions to P_{IV} with $\alpha = \beta = 0$ have been considered along with many of their neighboring solutions. However,

Table 1
The Approximate Values of k and c Corresponding to the k^+ and k^- Solutions, Respectively, in Figures 4, 15, and 16

Pole Located at Origin Has Residue +1				
k Corresponding to $u'(0)$ equal to				
	7.5 (out)	∞	7.5 (in)	c
k_1^+	0.87×10^0	1.54×10^0	3.49×10^0	0.5100
k_2^-	-6.82×10^1	-2.47×10^2	-1.42×10^3	3.5240
k_3^+	1.23×10^4	5.48×10^4	7.13×10^5	8.1000
k_4^-	-2.52×10^6	-1.25×10^7	-2.12×10^8	13.8100
k_5^+	5.50×10^8	2.85×10^9	5.75×10^{10}	20.4520
k_6^-	-1.22×10^{11}	-6.55×10^{11}	-1.45×10^{13}	27.9203
k_7^+	2.74×10^{13}	1.50×10^{14}	3.63×10^{15}	36.1202
k_8^-	-6.22×10^{15}	-3.45×10^{16}	-8.85×10^{17}	44.9203
Pole Located at Origin Has Residue -1				
k Corresponding to $u'(0)$ equal to				
	-7.5 (out)	$-\infty$	-7.5 (in)	c
k_1^-	-2.72×10^0	-6.97×10^0	-1.75×10^1	1.2710
k_2^+	2.69×10^2	1.49×10^3	5.34×10^3	4.9020
k_3^-	-2.97×10^4	-3.35×10^5	-1.42×10^6	9.8903
k_4^+	4.67×10^6	7.61×10^7	3.49×10^8	15.9233
k_5^-	-8.75×10^8	-1.75×10^{10}	-8.45×10^{10}	22.8524
k_6^+	1.77×10^{11}	4.00×10^{12}	2.02×10^{13}	30.5710
k_7^-	-3.75×10^{13}	-9.20×10^{14}	-4.77×10^{15}	38.3697
k_8^+	8.12×10^{15}	2.12×10^{17}	1.12×10^{18}	48.1000

Note: The columns ± 7.5 (out) and ± 7.5 (in) show the values of k where the dashed and solid line segments leave and enter the window in Figure 4. The column labeled $\pm \infty$ gives the value of k corresponding to the transition of a pole through the origin. The c column and $\pm \infty$ column lead to the same solution when substituted into (19) and (9), respectively, to generate ICs.

the neighboring solutions that have been considered only resulted from a perturbation in the asymptotic parameter k or the single IC $u(0)$. To complete this study, consider six of the same special solutions, with the difference that now neighboring solutions that result from varying both $u(0)$ and $u'(0)$ are shown.

Figures 18, 19, 20, and 21 show solutions in the neighborhood of the middle row of each of the Figures 5, 9, 6, and 7, respectively. The rays $re^{i\frac{j\pi}{4}}$, $r \geq 0$ and $j = 1, 2, \dots, 8$, are included to highlight the behavior of the poles when the ICs are near or equal to those of a special solution. We find that near these particular ICs the poles fall within the eight distinct sectors discussed previously and shown in Figure 12.

Solutions with ICs given in a neighborhood of the origin (Figure 22) and near the tronquée-like solution (Figure 23) shown in Figure 13 are also displayed. Notice Figures 2–4 show that when $u(0) = 0$ and $u'(0) \neq 0$ the solutions have pole fields of infinite density. Therefore, only six neighboring solutions around $u(0) = u'(0) = 0$ are given.

5. Conclusions

In this study of the fourth Painlevé equation for the case $\alpha = \beta = 0$ (i.e., $\nu = -\frac{1}{2}$), existing analytic and asymptotic knowledge about the equation has been confirmed, and solution regimes which have not been described in the previous literature were explored. The fast numerical approach introduced in [1] allowed the location ICs with unique characteristics. Notably, a solution that has no poles located in the entire left half-plane was discovered. Likewise, symmetry leads to a solution that is pole free in the entire right half-plane.

This study has highlighted some peculiar behavior in the neighborhood of some of the known asymptotic solutions. Further, the existence of an entire family of solutions, like the one in Figure 13, was confirmed that is similar to the tronquée solutions of P_I. Connections were also made between the free parameter, c , in the Laurent expansion of a pole located at the origin and the asymptotic parameter k .

The flexibility of the numerical algorithm has left ample opportunities for further explorations of the solutions of P_{IV}, particularly for nonzero α and β . A few of these include:

- Confirmation of known rational and special function solutions, and exploration of solutions with neighboring ICs.
- Finding connections between parameter choices with known asymptotic and analytic solutions and neighboring parameter choices with no such information available.
- Locating yet unknown solutions with large pole-free sectors in the complex plane.

Acknowledgment

Discussions with André Weideman and Peter Clarkson are gratefully acknowledged.

References

1. B. FORNBERG and J. A. C. WEIDEMAN, A numerical methodology for the Painlevé equations, *Journal of Computational Physics* 230:5957–5973 (2011).
2. F. W. J. OLVER, D. W. LOZIER, C. W. CLARK, and R. F. BOISVERT, *NIST Handbook of Mathematical Functions*, Cambridge University Press, Cambridge, 2010. <http://dlmf.nist.gov/>.
3. M. ABROMOWITZ and I. A. STEGUN, *Handbook of Mathematical Functions*, Dover, New York, 1964.
4. P. J. FORRESTER and N. S. WITTE, Application of τ -function theory of Painlevé equations to random matrices: PIV, PII, and the GUE, *Commun. Math. Phys.* 219:357–398 (2001).
5. E. KANZIEPER, Replica field theories, Painlevé transcendents, and exact correlation functions, *Phys. Rev. Lett.* 89(25):250201–250204 (2002).
6. V. A. OSIPOV and E. KANZIEPER, Correlations of RMT characteristic polynomials and integrability: Hermitian matrices, *Ann. Phys.* 325:2251–2306 (2010).
7. C. TRACY and H. WIDOM, Fredholm determinants, differential equations and matrix models, *Commun. Math. Phys.* 163:33–72 (1994).
8. D. BERMÚDEZ and D. FERNÁNDEZ, Solution hierarchies for the Painlevé iv equation, in *Proceedings of the XXXI Workshop on Geometric Methods in Physics*, Bialowieza, Poland, June 2012.
9. P. A. CLARKSON, The fourth Painlevé equation and associated special polynomials, *J. Math. Phys.* 44:5350–5374 (2003).
10. A. P. BASSOM, P. A. CLARKSON, and A. C. HICKS, Numerical studies of the fourth Painlevé equation, *IMA J. Appl. Math.* 50:167–193 (1993).
11. I. M. WILLERS, A new integration algorithm for ordinary differential equations based on continued fraction approximations, *Commun. ACM* 17:504–508 (1974).
12. B. FORNBERG and J. A. C. WEIDEMAN, A computational exploration of the second Painlevé equation, *in preparation*, 2012.
13. V. I. GROMAK, I. LAINE, and S. SHIMOMURA, *Painlevé Differential Equations in the Complex Plane*, Walter de Gruyter, Berlin, 2002.
14. V. Y. NOVOKSHENOV, Padé approximations for Painlevé I and II transcendents, *Theor. Math. Phys.* 159:853–862 (2009).
15. S. OLVER, A general framework for solving Riemann–Hilbert problems numerically, *Numer. Math.* (2012). DOI 10.1007/s00211-012-0459-7.
16. P. A. CLARKSON, The fourth Painlevé transcendent, Technical Report UNK, Institute of Mathematics, Statistics and Actuarial Science, University of Kent, November 2008.
17. A. R. ITS and A. A. KAPAEV, Connection formulae for the fourth Painlevé transcendent: Clarkson–McLeod solution, *J. Phys. A: Math. Gen.* 31:4073–4113 (1998).
18. A. P. BASSOM, P. A. CLARKSON, A. C. HICKS, and J. B. MCLEOD, Integral equations and exact solutions of the fourth Painlevé equation, *Proc. R. Soc. Lond. A* 437:1–24 (1992).
19. P. A. CLARKSON and J. B. MCLEOD, *Painlevé Transcendents, their Asymptotics and Physical Applications*, Plenum, New York, 1992.
20. C. M. BENDER and S. A. ORSZAG, *Advanced Methods for Scientists and Engineers*, McGraw-Hill, New York, 1978.
21. P. BOUTROUX, Recherches sur les transcendents de M. Painlevé et l'étude asymptotique des équations différentielles du second ordre, *Ann. École Norm. Sup.* 30:255–375 (1913).

UNIVERSITY OF COLORADO

(Received June 7, 2012)

Appendix B

Paper 2-“Painlevé IV: A Numerical Study of the Fundamental Domain and Beyond”

Painlevé IV: A Numerical Study of the Fundamental Domain and Beyond

Jonah A. Reeger^{1, a)} and Bengt Fornberg^{1, b)}

¹*University of Colorado, Department of Applied Mathematics, 526 UCB, Boulder, CO 80309 USA*

(Dated: 19 April 2013)

The six Painlevé equations were introduced over a century ago, motivated by rather theoretical considerations. Over the last several decades, these equations and their solutions, known as the Painlevé transcendents, have been found to play an increasingly central role in numerous areas of mathematical physics. Due to extensive dense pole fields in the complex plane, their numerical evaluation remained challenging until the recent introduction of a fast ‘pole field solver’ (Fornberg and Weideman, *J. Comp. Phys.* 230 (2011), 5957-5973). The fourth Painlevé equation has two free parameters in its coefficients, as well as two free initial conditions. After summarizing key analytical results for P_{IV} , the present study applies this new computational tool to the the fundamental domain and a surrounding region of the parameter space. We confirm existing analytic and asymptotic knowledge about the equation, and also explore solution regimes which have not been described in the previous literature.

^{a)}jonah.reeger@colorado.edu; Captain, United States Air Force

^{b)}fornberg@colorado.edu

I. INTRODUCTION

The solutions of the six Painlevé equations (P_I - P_{VI}) are free from movable branch points, but with the possibility of movable poles or movable isolated essential singularities (Ref. 1, Section 32.2). This Painlevé property inspired the introduction of a novel numerical approach²—combining a Padé based ODE solver³ with a partly randomized integration path strategy—and allowed for the first time rapid numerical solutions of the Painlevé equations over extended regions in the complex plane. It was first used for P_I ² and later for P_{II} ⁴. It was then applied to the fourth Painlevé equation

$$\frac{d^2}{dz^2}u(z) = \frac{1}{2u(z)} \left(\frac{d}{dz}u(z) \right)^2 + \frac{3}{2}u(z)^3 + 4zu(z)^2 + 2(z^2 - \alpha)u(z) + \frac{\beta}{u(z)}, \quad (1)$$

in the special case of $\alpha = \beta = 0$ ⁵. As in these three previous numerical studies, computational explorations in this paper are limited to solutions $u(z)$ that are real when z is real, although some of the presented theory includes solutions that are not always real on the real axis.

For a small portion of the two-dimensional (α, β) -parameter space there exist examples of solutions expressible as rational functions or in terms of special functions, such as the parabolic cylinder function. These well documented solutions appear, however, as only isolated points or one-parameter families in the four-dimensional space of parameters and initial conditions (ICs). Much of the present study is focused on the distribution of singularities for solutions to (1). These are all first order poles with residue +1 or -1.

A. Organization of the paper

Section 2 recalls some available theory, including symmetries in P_{IV} and different solution transformations. Section 3 discusses closed form solutions of P_{IV} , in particular solutions in terms of rational and elementary special functions and also the asymptotic behaviors presented in the literature. This is followed in section 4 by the numerical approach used here to explore the much larger space of solutions for which no closed form solutions are available. Sections 5 and 6 describe such explorations of the parameter and solution spaces, first highlighting the “fundamental domain” and then extending into inspections of the previously unexplored region of $\beta > 0$, for which no instances of closed form solutions or

transformations have been reported.

II. SYMMETRIES AND SOLUTION HIERARCHIES

This section describes the known symmetries in the P_{IV} equation and transformations that relate solutions for different parameter choices.

A. Symmetries in the Equation

Let $P_{IV}(\alpha, \beta)$ be the set of all solutions of (1) for the particular α and β . Direct inspection of (1) shows that if $u(z) \in P_{IV}(\alpha, \beta)$, then⁶

$$-u(-z) \in P_{IV}(\alpha, \beta), \tag{2}$$

$$-iu(-iz) \in P_{IV}(-\alpha, \beta), \text{ and} \tag{3}$$

$$iu(iz) \in P_{IV}(-\alpha, \beta). \tag{4}$$

Incidentally the first of these symmetries also holds for P_{III} (for all parameter choices), but never for any of the other Painlevé equations. It is important to keep these symmetries in mind since any solution presented in this paper has at least one other counterpart for the same choice of α and β .

B. The Bäcklund and Schlesinger Transformations

It is known that P_{II} through P_{VI} have collections of transformations relating solutions for given parameters to those of different choices. For instance, Refs. 7, 8, and others relate solutions $u(z) \in P_{IV}(\alpha, \beta)$ to $u_{k,\mu}^\pm(z) \in P_{IV}(\alpha_{k,\mu}^\pm, \beta_{k,\mu}^\pm)$, $k = 1, 2, 3$ through the relationships (5) through (7). Confining this study to solutions that are real on the real axis limits these

transformations to nonpositive β . These transformations are

$$u_{1,\mu}^{\pm}(u(z), z) = \frac{1}{2\mu u(z)} \left(\frac{d}{dz} u(z) \mp \mu(u(z)^2 + 2zu(z)) - \mu\sqrt{-2\beta} \right) \quad (5)$$

$$u_{2,\mu}^{\pm}(u(z), z) = \frac{\left(\frac{d}{dz} u(z) \pm \mu\sqrt{-2\beta}\right)^2 + (4\alpha + 4\mu \mp 2\sqrt{-2\beta})u(z)^2}{2u(z) \left(u(z)^2 + 2zu(z) - \mu\frac{d}{dz} u(z) \mp \sqrt{-2\beta}\right)} - \frac{u(z)^2(u(z) + 2z)^2}{2u(z) \left(u(z)^2 + 2zu(z) - \mu\frac{d}{dz} u(z) \mp \sqrt{-2\beta}\right)} \quad (6)$$

$$u_{3,\mu}^{\pm}(u(z), z) = u(z) + \frac{2 \left(1 - \mu\alpha \mp \frac{1}{2}\mu\sqrt{-2\beta}\right) u(z)}{\frac{d}{dz} u(z) \pm \mu\sqrt{-2\beta} + \mu(2zu(z) + u(z)^2)} \quad (7)$$

where $\mu = \pm 1$. The transformed solutions $u_{k,\mu}^{\pm}$, $k = 1, 2, 3$ occur for the parameter choices

$$\alpha_{1,\mu}^{\pm} = \frac{1}{4}(\pm 2\mu - 2\alpha \pm 3\sqrt{-2\beta}) \text{ and } \beta_{1,\mu}^{\pm} = -\frac{1}{2} \left(1 \pm \alpha\mu + \frac{1}{2}\mu\sqrt{-2\beta}\right)^2 \quad (8)$$

$$\alpha_{2,\mu}^{\pm} = \alpha + \mu \text{ and } \beta_{2,\mu}^{\pm} = -\frac{1}{2}(2 \mp \mu\sqrt{-2\beta})^2 \quad (9)$$

$$\alpha_{3,\mu}^{\pm} = \frac{3}{2}\mu - \frac{1}{2}\alpha \mp \frac{3}{4}\sqrt{-2\beta} \text{ and } \beta_{3,\mu}^{\pm} = -\frac{1}{2} \left(\mu - \alpha \pm \frac{1}{2}\sqrt{-2\beta}\right)^2. \quad (10)$$

There are also composite transformations $u_4^{\pm} = u_{2,\pm}^+(u_{2,\pm}^-(u(z), z), z)$ and $u_5^{\pm} = u_{2,\mp}^+(u_{2,\pm}^-(u(z), z), z)$ discussed in Refs. 7, 9, 10. As noted in Ref. 11, $u_{2,+1}^-$ was not always presented correctly in previous literature.

III. CLOSED FORM SOLUTIONS AND ASYMPTOTIC APPROXIMATIONS

Before discussing the closed form solutions and asymptotic behaviors presented in the literature, note again that, even for choices of α and β admitting these solutions, little is known aside from at an isolated location or along one-parameter family of points in the two-dimensional plane of ICs.

A. Rational Solutions

The fourth Painlevé equation has six different sequences of parameter choices leading to rational solutions expressible in terms of either Generalized Hermite or Generalized Okamoto

polynomials (see, e.g., Ref. 7), with two particular choices leading to the nontrivial entire solutions $-2z$ and $-2/3z$. Tables I and II state the choices leading to such solutions when $m, n \in \mathbb{Z}^+$. These locations in the (α, β) -plane will later be shown in figure 1 as dark (blue) and light (yellow) hexagrams for Generalized Hermite and Generalized Okamoto polynomials, respectively.

Generalized Hermite Polynomial Type Solutions, $u_{m,n}^{[GH;k]7}$				
k	α	β	Special Choice	Special Solution
1	$2m + n + 1$	$-2n^2$	$m = 0, n = 1$	$\frac{1}{z}$
2	$-(m + 2n + 1)$	$-2m^2$	$m = 1, n = 0$	$-\frac{1}{z}$
3	$n - m$	$-2(m + n + 1)^2$	$m = 0, n = 0$	$-2z$

TABLE I. Parameter choices leading to solutions of P_{IV} expressible in terms of Generalized Hermite polynomials.

Generalized Okamoto Polynomial Type Solutions, $u_{m,n}^{[OK;k]7}$				
k	α	β	Special Choice	Special Solution
1	$2m + n$	$-2(n - \frac{1}{3})^2$	$m = 0, n = 0$	$-\frac{2}{3}z$
2	$-m - 2n$	$-2(m - \frac{1}{3})^2$	$m = 0, n = 0$	$-\frac{2}{3}z$
3	$n - m$	$-2(m + n + \frac{1}{3})^2$	$m = 0, n = 0$	$-\frac{2}{3}z$

TABLE II. Parameter choices leading to solutions of P_{IV} expressible in terms of generalized Okamoto polynomials.

B. Special Function Solutions

In addition to the rational solutions, P_{IV} admits solutions that are described by combinations of special functions. In particular, P_{IV} has solutions expressible in terms of combinations of parabolic cylinder functions, $D_\nu(\zeta)$ (Ref. 1, Chapter 12), or confluent hypergeometric functions, ${}_1F_1(a, b; \zeta)$ (Ref. 1, Chapter 13).

There are three distinct determinantal representations of solutions in terms of the parabolic cylinder functions available¹²⁻¹⁴; however, only one of these expressions has been confirmed numerically.¹¹ There are still other, simpler expressions involving parabolic cylinder functions that have been validated with the appropriate parameter choices for these

appearing in table III. Also, figure 1 displays the locations of all of these parameter choices that have been discussed in the literature as black curves.

Parabolic Cylinder Function Type Solutions, $u_{\nu,\epsilon,d_1,d_2}^{[PC;k]}$ 7,12-14				
k	α	β	Special Choice	Special Solution
1	$-\epsilon(\nu + 1)$	$-2\nu^2$	$\nu \in \mathbb{Z}^+$ $\nu = 0$	Standard Hermite Complementary Error
2	$-\epsilon\nu$	$-2(\nu + 1)^2$	$\nu \in \mathbb{Z}^+$	Standard Hermite
3	$-\epsilon(2n - \nu)$	$-2(\nu + 1)^2$	See Ref. 12	

TABLE III. Parameter choices leading to solutions of P_{IV} expressible in terms of parabolic cylinder functions. Notice that there are two parameters d_1 and d_2 that can one can vary to generate a family of special function solutions for a given choice of α and β .

It should be noted that when $\epsilon = -1$ the solutions $u_{\nu,-1,d_1,d_2}^{[PC;k]}$, $k = 1, 2, 3$, are no longer always real along the real axis. Otherwise in this paper, only solutions of P_{IV} that are real along the real axis will be considered.

Further, in the case of these parabolic cylinder function solutions the parameters d_1 and d_2 can be combined into a single parameter d . This combination leads to a one parameter family of solutions for each fixed α and β satisfying the expressions in table III.

Particular choices of $\nu \in \mathbb{R}$ allow the solutions $u_{\nu,\epsilon,d_1,d_2}^{[PC;1]}$ and $u_{\nu,\epsilon,d_1,d_2}^{[PC;2]}$ to be expressed in special forms. For instance, if $\nu \in \mathbb{Z}^+$ it is discussed in Ref. 7 that the special function solutions reduce to standard Hermite polynomials, while if $\nu = 0$ then the solutions of P_{IV} can be expressed as complementary error functions. A similar extensive explanation of the determinantal solutions is available¹².

More recently, it was discovered in the context of supersymmetric quantum mechanics that P_{IV} has solutions that can be described by confluent hypergeometric functions¹⁵⁻¹⁷. The parameter choices corresponding to these solutions are actually a subset of the larger set of parameter choices that lead to solutions expressed in terms of parabolic cylinder functions. Let

$$v_0(z) = e^{-\frac{1}{2}z^2} \left({}_1F_1 \left(-\frac{1}{2}\nu, \frac{1}{2}; z^2 \right) + 2z \frac{\Gamma(-\frac{1}{2}\nu + \frac{1}{2})}{\Gamma(-\frac{1}{2}\nu)} (c_1 + ic_2) {}_1F_1 \left(-\frac{1}{2}\nu + \frac{1}{2}, \frac{3}{2}; z^2 \right) \right),$$

where $n \in \mathbb{Z}^+$, $\nu, c_1, c_2 \in \mathbb{R}$ and ${}_1F_1$ is the confluent hypergeometric function¹. Further,

define for $j = 1, 2, \dots$,

$$v_j(z) = \frac{1}{\sqrt{2}} \left(\frac{d}{dz} v_{j-1}(z) + z v_{j-1}(z) \right).$$

P_{IV} has solutions

$$u_{\nu, n, c_1, c_2}^{[CH;1]} = u(z; 2n - \nu, -2(\nu + 1)^2) = -z - \frac{d}{dz} \ln \left(\frac{\mathcal{W}(v_0(z), v_1(z), \dots, v_{n-1}(z))}{\mathcal{W}(v_0(z), v_1(z), \dots, v_n(z))} \right),$$

$n > 0$ with \mathcal{W} the usual Wronskian¹⁵. When $n = 0$ this solution reduces to

$$u_{\nu, 0, c_1, c_2}^{[CH;1]} = u(z; -\nu, -2(\nu + 1)^2) = -z + \frac{d}{dz} \ln(v_0(z)),$$

Notice that the choice of nonzero c_2 leads to solutions that are not real along the real axis. Therefore, $P_{IV}(2n - \nu, -2(\nu + 1)^2)$ has a one parameter family of solutions when $c_2 = 0$ for each fixed value of ν and n .

If d_1 and d_2 are chosen to correspond to the choice of c_1 and c_2 , and vice versa, then the resulting solutions $u_{\nu, 1, d_1, d_2}^{[PC;2]}$ and $u_{\nu, 0, c_1, c_2}^{[CH;1]}$ are identical. In fact, the relationships are given by

$$\begin{aligned} d_1 &= 2\sqrt{2} - 2\sqrt{2}(c_1 + ic_2) \\ d_2 &= 2\sqrt{2} + 2\sqrt{2}(c_1 + ic_2). \end{aligned}$$

C. Asymptotic Approximation

Beyond the known closed form solutions, it is noted in Ref. 1, Section 32.11, that when $\alpha \in \mathbb{R}$ and $\beta = 0$, nontrivial solutions satisfying

$$u(z) \rightarrow 0, \text{ as } z \rightarrow +\infty \tag{11}$$

are asymptotic to

$$k \left(D_{\frac{1}{2}\alpha - \frac{1}{2}}(\sqrt{2}z) \right)^2 \text{ as } z \rightarrow +\infty \text{ and } k \neq 0, \tag{12}$$

where $D_\nu(\zeta)$ is, again, the parabolic cylinder function. A more detailed explanation of these asymptotics can be found in Ref. 1, Section 32.11, including connection formulae and behaviors as $z \rightarrow -\infty$.

When assuming the derivative terms in (1) are negligible, the method of dominant balance (see, e.g., Ref. 18, Section 3.4) leads to the quartic equation

$$\frac{3}{2}w(z)^4 + 4zw(z)^3 + 2(z^2 - \alpha)w(z)^2 + \beta = 0. \quad (13)$$

The roots of (13) supply asymptotic approximations as $z \rightarrow \pm\infty$, $z \in \mathbb{R}$, and any choice of α and β . Asymptotic expansion as $z \rightarrow +\infty$ reveals that for all α and β

$$w_{+1}^+(z; \alpha, \beta) = \frac{\sqrt{-2\beta}}{2z} + \frac{\alpha\sqrt{-2\beta} + 2\beta}{4z^3} + O\left(\frac{1}{z^5}\right) \quad (14)$$

$$w_{-1}^+(z; \alpha, \beta) = -\frac{\sqrt{-2\beta}}{2z} + \frac{-\alpha\sqrt{-2\beta} + 2\beta}{4z^3} + O\left(\frac{1}{z^5}\right) \quad (15)$$

$$w_{+1}^-(z; \alpha, \beta) = -\frac{2}{3}z + \frac{\alpha}{z} - \frac{2(2\alpha^2 + 3\beta)}{8z^3} + O\left(\frac{1}{z^5}\right) \quad (16)$$

$$w_{-1}^-(z; \alpha, \beta) = -2z - \frac{\alpha}{z} + \frac{6\alpha^2 + \beta}{8z^3} + O\left(\frac{1}{z^5}\right). \quad (17)$$

No other smooth asymptotic behaviors were observed in the numerical explorations. With the assumption $u(z) \in \mathbb{R}$ for $z \in \mathbb{R}$, only the latter two roots are available as asymptotic approximations when $\beta > 0$. Later in this paper, ICs leading to solutions asymptotic to (14)-(17) will be marked in several figures, described as pole counting diagrams, as shown in figure 3.

As with the information presented in this section, the rest of this paper will discuss only the asymptotic behaviors as $z \rightarrow +\infty$, $z \in \mathbb{R}$, since the symmetry (2) makes it clear that there are analogous solutions with similar asymptotic behaviors as $z \rightarrow -\infty$. This is seen by comparing the left and right frames in figure 2.

D. The Parameter Space and the Weyl Chambers

Based on the various symmetries, solution hierarchies and known closed form solutions, the parameter space of P_{IV} with $\beta \leq 0$ can be described in terms of the so-called Weyl chambers (see e.g., Refs. 15, 19, Section II-A, 6, Section 26). These chambers feature a complete regularity in the $(\alpha, \sqrt{-2\beta})$ -plane, where α and β are the two free parameters in the P_{IV} equation (1).

All of the (α, β) pairs described in the literature leading to rational and special func-

tion solutions are shown in figure 1. First, the dark (blue)/light (yellow) hexagrams indicate the parameter values that admit instances of solutions described by Generalized Hermite/Okamoto polynomials. Next, the parameter choices along the black lines admit special function solutions that are described by combinations of either parabolic cylinder functions or confluent hypergeometric and gamma functions. Finally, for parameter choices along the line $\sqrt{-2\beta} = 0$ (i.e. $\beta = 0$) the literature contains asymptotic approximations along the real axis. Each of these cases is considered in one of the following sections.

The significance of the Weyl Chambers, when extended to complex α and β , is that a single chamber in theory provides all of the information to construct solutions for every arbitrary (α, β) pair. Gromak, et al, state in Ref. 6, Section 25, “To construct the solutions of (1) for arbitrary values of parameters (α, β) it is sufficient to construct solutions for every (α, β) in the domain

$$\mathcal{F} := \left\{ (\alpha, \beta) \mid 0 \leq \operatorname{Re}(\alpha) \leq 1, \operatorname{Re}(\sqrt{-2\beta}) \geq 0, \operatorname{Re}(\sqrt{-2\beta} + 2\alpha) \leq 2 \right\}. \quad (18)$$

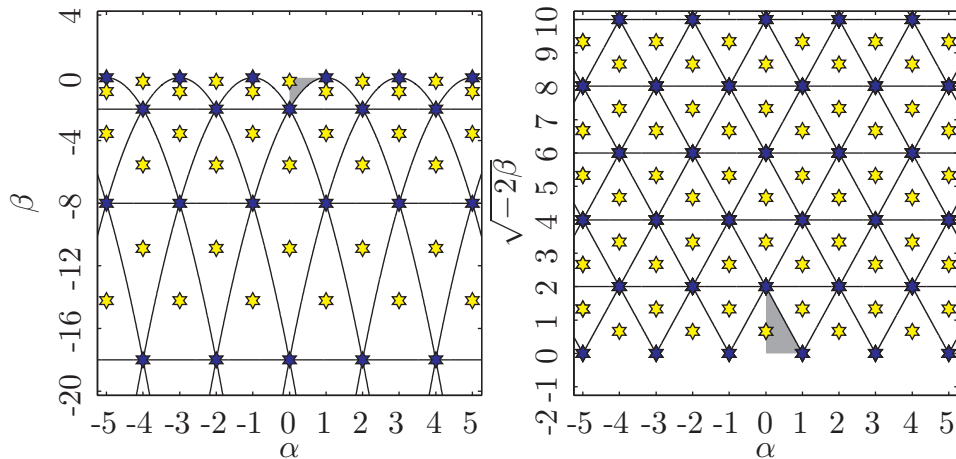


FIG. 1. Two views of the Weyl Chambers. The shaded region indicates the real part of the fundamental domain given in (18). Both figures show several of the chambers and locations of the rational and special function solutions to P_{IV} (dark hexagrams (blue) represent generalized Hermite type, light hexagrams (yellow) show generalized Okamoto type, and lines (black) show parabolic cylinder and confluent hypergeometric types).

Returning to $\alpha, \beta \in \mathbb{R}$ the region \mathcal{F} is indicated by the shaded region in each subplot of figure 1. Notice that every parameter choice leading to a rational or special function solution of P_{IV} has $\beta \leq 0$. This is also true for the asymptotic approximation (12). For this reason,

part of this study will be devoted to the mostly unexplored region of $\beta > 0$.

IV. THE NUMERICAL METHOD AND EXPLORATION APPROACH

Explorations of the vast space of parameters and ICs require a fast numerical method and a systematic approach for comparing solutions of different parameter choices. These techniques are discussed here.

The extensive pole fields appearing in these solutions have motivated the development of various solution techniques over the years since their discovery. However, many of the previous methods were limited in the choice of the parameters in the coefficients by considering special forms of the equation (e.g. Riemann Hilbert problems²⁰), constrained to the real axis^{21,22}, or restricted to a small domain around the origin²³. The presently used method extends the ‘pole vaulting’ idea²¹ in three fundamental ways: (i) use of a ‘pole friendly’ ODE integrator³, (ii) not using any rigid choices of diversion paths around a pole, but instead utilizing a freely branching network of paths in the complex plane, and (iii) targeting paths toward whole regions in the complex plane (rather than only toward other real axis locations). A survey of many of these existing numerical methods appears in Ref. 24.

A. A Brief Description of the Numerical Method

The numerical scheme introduced in Ref. 2 features very high orders of accuracy (typically 30 to 50), minimal loss of accuracy in the vicinity of poles, and a flexible path selection strategy that can efficiently cover large areas of the complex plane, while allowing arbitrary values of α and β . When integrating from one start location to a single end location this scheme uses the following strategy, which will be called pole avoidance:

1. Choose the location of the initial condition as the first expansion point.
2. Compute the Padé approximation about the expansion point.
3. Evaluate the Padé approximation a distance h away in each of five directions in a swath directed toward the target point and choose as the next expansion point the one with the smallest solution magnitude.
4. Unless the target point has been reached, return to step 2.

This pole avoidance strategy is effective when finding the solution to an IVP at a single point. However, if the solution is desired at many different points (for instance, for the visualization of the solution over a region in the complex plane) the method is extended to the pole field solver.

1. Set up a coarse grid of target points in the complex plane.
2. Select the target points in random order.
3. Apply the pole avoidance strategy to reach a predetermined neighborhood of the current target point, starting from the closest point that has already been evaluated. In the first step this is the location of the IC.
4. Once all of the coarse grid target points have been accounted for, set up a fine grid of the desired evaluation points.
5. Compute a single last step from the end of each of the previous paths to several nearby fine grid evaluation points.

B. Pole Counting

The pole field solver makes it possible to rapidly view solutions for a variety of initial conditions. Therefore, to explore the differences in solution characteristics for each fixed choice of α and β , but for varying $(u(0), u'(0)) \in \mathbb{R}^2$, the number of poles on either the positive or negative real axis is examined. This, paired with the asymptotic behavior discussed in section III C, allows the characterization of the numerous solution possibilities for each fixed α and β . Figure 2 (adapted from Ref. 5) provides a prototypical example in the case of $\alpha = \beta = 0$. This figure displays the number of poles on the positive and negative real axes for each choice of initial conditions shown, and each of the frames is dubbed a pole counting diagram.

Consider, for now, only the right frame in figure 2, since the left is completely analogous due to the symmetries discussed in section II A. Each of the ICs marked by a curve or contained within a shaded region generates a solution with a finite number of poles on the positive real axis. The color bar indicates the exact number of poles for a given initial condition with darker and lighter indicating odd and even numbers of poles, respectively.

On the other hand, ICs neither contained in a shaded region nor marked by a curve should generate solutions with an infinity of poles on the corresponding half (positive/negative) of the real axis.

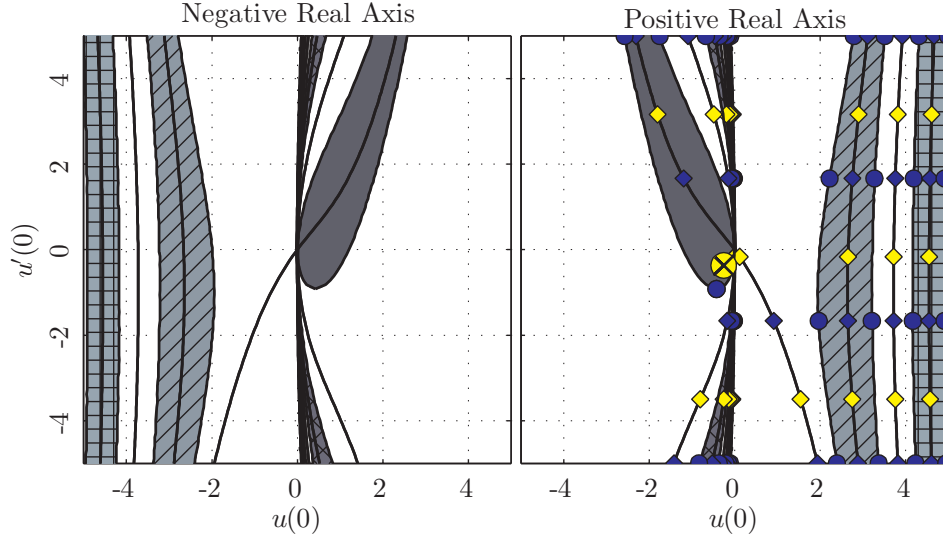


FIG. 2. Number of poles on the positive and negative real axes for $\alpha = 0$ and $\beta = 0$. For a description of the markers and shading see figure 3. When $\beta = 0$ the ICs marked with light and dark diamonds are precisely those satisfying the decaying asymptotic condition (12).

In this case of $\alpha = \beta = 0$, each of the shaded regions in the right half-plane contains ICs that generate solutions with an odd number of poles on the positive real axis, while the $u(0)$, $u'(0)$ values along the isolated curves lead to solutions with an even number, with the opposite holding in the left half-plane.

Most of the ICs in the shaded regions generate solutions that oscillate as $z \rightarrow +\infty$ (note that an oscillation is simply a change in the sign of the derivative); however, each initial condition marked by a curve, located at the boundary of a shaded region, or designated by an isolated marker has no oscillations as $z \rightarrow +\infty$. These solutions are precisely those that are asymptotic to the roots of the quartic equation (13) as $z \rightarrow +\infty$. The appropriate root is indicated by the symbols shown in left frame of figure 3. In the case of $\alpha = \beta = 0$ (generally, when $\beta = 0$) the solutions matching the behaviors w_μ^+ , $\mu = \pm 1$, are the solutions that satisfy the decaying asymptotic condition (12). When two markers appear along the same curve, those ICs generate solutions matching both behaviors (in separate intervals of the real axis), as shown in, for example, figures 11, 12, 26, and 27 (see section VID for

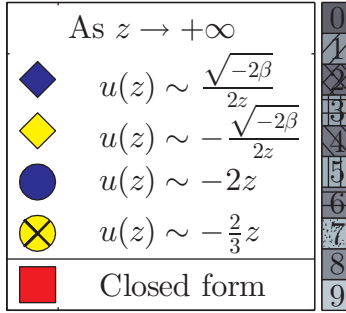


FIG. 3. Legend and color bar for figures 2, 10, 13, 14, 15, 16, 17, 18, 19, and 20. The legend shows the markers indicating the ICs that generate the dominant asymptotic behaviors (14)-(17) and closed form solutions. If a marker occurs on a curve, then the dominant behavior or type of closed form solution occurs for all of the ICs along that curve. If a marker is emphasized by containing an “×”, then it indicates an isolated IC matching the dominant behavior or the IC generates an isolated rational solution. The gray-scale/pattern bar on the right indicates the number of poles on the positive or negative real axis.

further discussion).

C. Confirmation of Solution Transformations Using the Numerical Method

The numerical explorations in this study begin with confirmation of the transformations (5)-(7). This confirmation was completed by first computing the exact transformations of a (numerically obtained) solution using (5)-(7) at each point in the solution. Then, the transformed results were compared to numerical solutions generated using a single transformed initial condition.

It was noted⁵ that $P_{IV}(0,0)$ has a solution with a pole-free half-plane. Figure 4 shows a counterpart to this solution with $\alpha = 0.5$ and $\beta = -0.5$. The transformations $u_{k,\mu}^{\pm}$ lead to the solutions of P_{IV} in figures 6 and 7. In the left frame of figure 4 and all of the frames in figure 6, the zeros are marked with “×” (red) while the poles are marked with circles (blue and yellow for residues of +1 and -1, respectively). This same convention will be used for pole locations throughout the rest of the paper, but zeros will not always be shown since they appear very regularly with the poles. The left frame of figure 4 shows a pole field in each of the upper- and lower-left quadrants of the complex plane, while the right frame indicates that this solution approaches roughly $-2/3z$ as $z \rightarrow +\infty$ and $-2z$ as $z \rightarrow -\infty$ for $z \in \mathbb{R}$ with a zero of order 1 at $z \approx 0.75$.

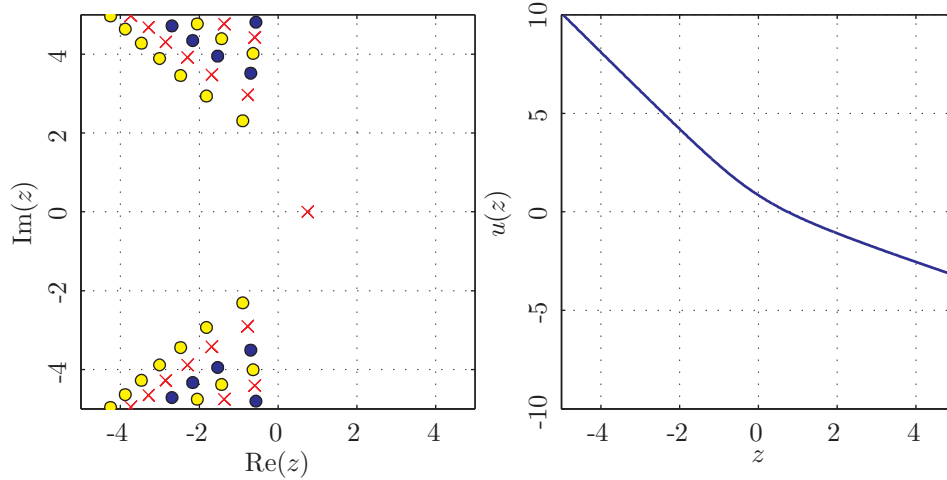


FIG. 4. Solution with a pole free half-plane for $\alpha = 0.5$ and $\beta = -0.5$. The left frame shows the zero and pole locations, while the right shows the solution along the real axis.

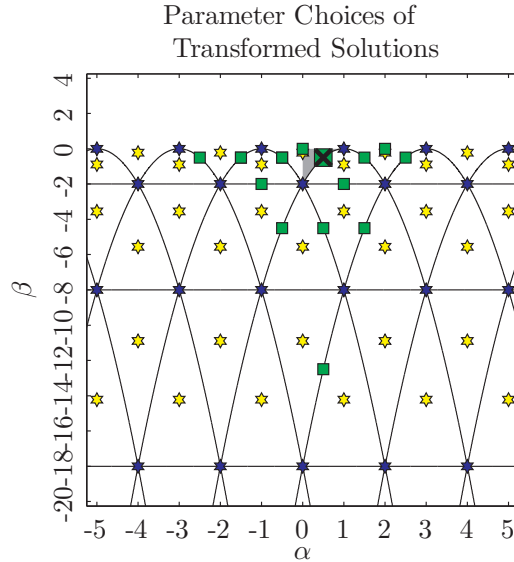


FIG. 5. Another view of the Weyl chamber. The larger square with an \times marks the original choice of $\alpha = 0.5$ and $\beta = -0.5$. The other squares mark the parameter space locations of the transformed solutions.

Notice that in figure 6 the general locations of the pole fields in the upper- and lower-right quadrants are maintained; however, aside from this similarity, it is cumbersome to characterize how the transformations (5) through (7) alter the locations of these poles and zeros. Even for a fixed k , the transformations $u_{k,\mu}^{\pm}$ can vary drastically for the choice of μ and the upper and lower sign. Further, the transformations (5) and (6) suggest at first glance

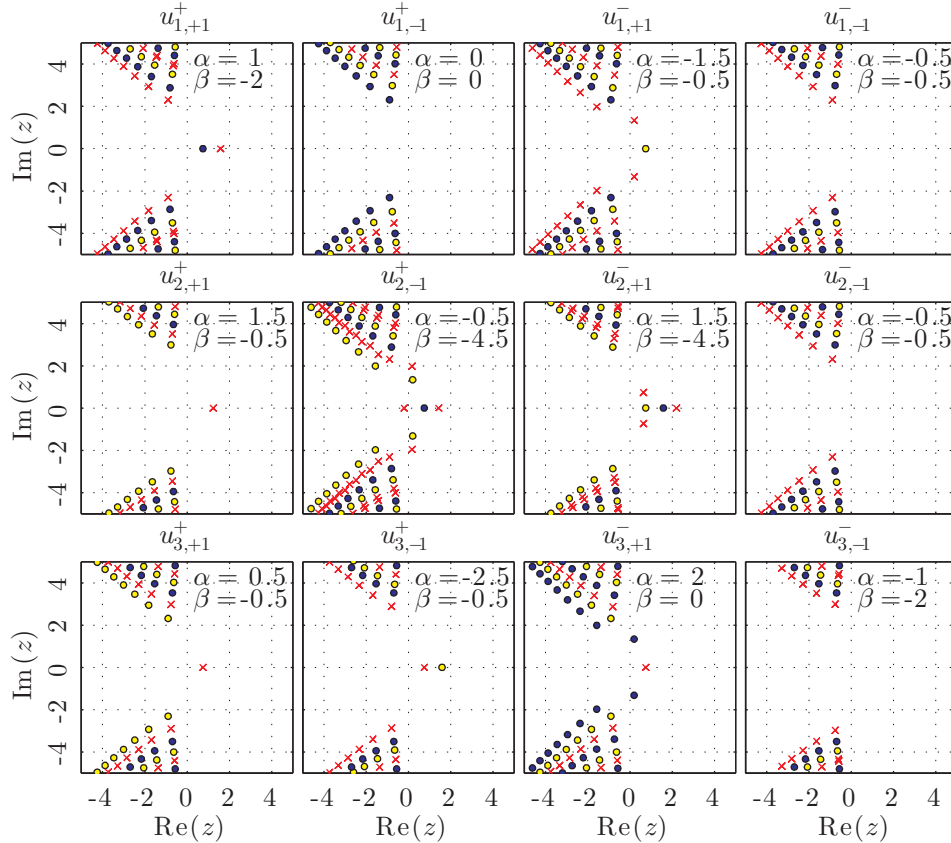


FIG. 6. Zero and pole locations of solutions to P_{IV} resulting from the applications of (5) through (7) to the solution figure 4.

that any zeros of $u(z)$ should be poles of $u_{k,\mu}^{\pm}(u(z), z)$, $k = 1, 2$, an $u_4^{\pm}(u(z), z)$; however, this simple analysis does not tell the whole story, and is certainly not always the case.

Consider the solutions to P_{IV} asymptotic to the roots of the quartic equation (13) as $z \rightarrow +\infty$. Table IV contains the resulting asymptotic behaviors. Specifically, if $u(z)$ possesses the asymptotic behavior in the row marked $u(z)$ as $z \rightarrow +\infty$ and $z \in \mathbb{R}$, then the transformed solutions possess the asymptotic behavior in the following rows as $z \rightarrow +\infty$ and $z \in \mathbb{R}$. A further discussion of the asymptotic behaviors w_{μ}^{\pm} , with $\mu = \pm 1$, appears in section III C.

V. NUMERICAL ILLUSTRATIONS OF THE FUNDAMENTAL DOMAIN

Solution types occurring for parameter choices in the fundamental domain are discussed in the following sections. These (and subsequent) sections describe some solutions as having adjacent pole free sectors. This terminology arises from evidence in the numerical expo-

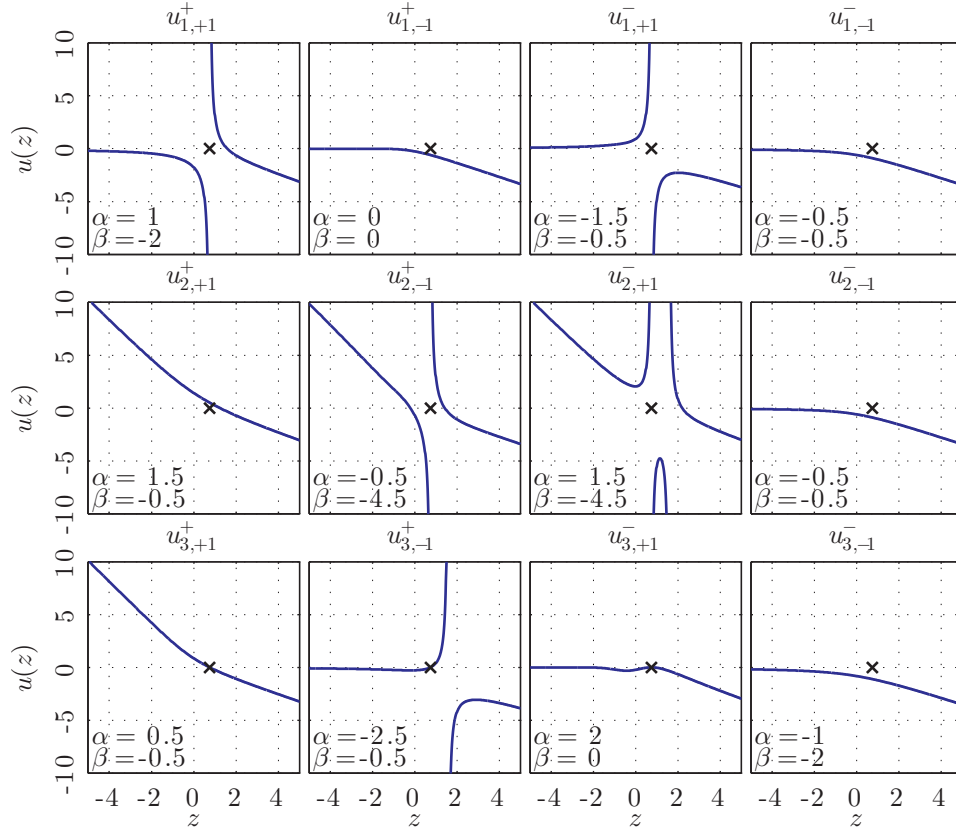


FIG. 7. Solutions along the real axis to P_{IV} resulting from the applications of (5) through (7) to the solution figure 4.

rations that the poles in the solutions of P_{IV} align in the eight sectors shown in figure 8. Further discussions of these sectors are available⁵.

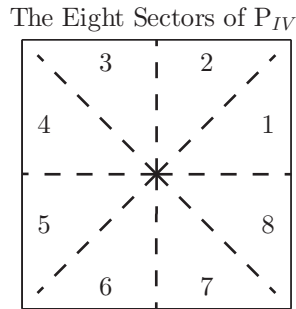


FIG. 8. The eight sectors of poles in the solutions of P_{IV} .

Leading Order Asymptotic Behavior of $u(z)$ as $z \rightarrow +\infty$				
$u(z)$	$w_{+1}^+ \sim \frac{\sqrt{-2\beta}}{2z}$	$w_{-1}^+ \sim -\frac{\sqrt{-2\beta}}{2z}$	$w_{+1}^- \sim -\frac{2}{3}z$	$w_{-1}^- \sim -2z$
Leading Order Asymptotic Behavior of Transformed Solutions as $z \rightarrow +\infty$				
$u_{1,\mu}^+(u(z), z)$	$-2z$	$\frac{-2\mu-2\alpha-\sqrt{-2\beta}}{4z}$	$-\frac{2}{3}z$	$\frac{2\mu+2\alpha+\sqrt{-2\beta}}{4z}$
$u_{1,\mu}^-(u(z), z)$	$\frac{2\mu-2\alpha+\sqrt{-2\beta}}{4z}$	$-2z$	$-\frac{2}{3}z$	$\frac{-2\mu+2\alpha+\sqrt{-2\beta}}{4z}$
$u_{2,\mu}^+(u(z), z)$	$\frac{\mu-2\alpha-(2-\alpha)\sqrt{-2\beta}+\beta\mu}{(2+2\alpha\mu-\mu\sqrt{-2\beta})z}$	$\frac{2\mu-\sqrt{-2\beta}}{2z}$	$-\frac{2}{3}z$	$-2z$
$u_{2,\mu}^-(u(z), z)$	$\frac{2\mu+\sqrt{-2\beta}}{2z}$	$\frac{1-2\alpha\mu-\mu(2+\mu\alpha)\sqrt{-2\beta}+\beta}{(2\mu+2\alpha+\sqrt{-2\beta})z}$	$-\frac{2}{3}z$	$-2z$
$u_{3,\mu}^+(u(z), z)$	$\frac{2\mu-2\alpha+\sqrt{-2\beta}}{4z}$	$-2z$	$-\frac{2}{3}z$	$\frac{-4\mu\alpha+2\alpha^2+\beta}{(-4\mu+4\alpha+2\sqrt{-2\beta})z}$
$u_{3,\mu}^-(u(z), z)$	$-2z$	$\frac{2\mu-2\alpha-\sqrt{-2\beta}}{4z}$	$-\frac{2}{3}z$	$\frac{4\alpha-2\mu\alpha^2-\mu\beta}{(4-4\mu\alpha+2\mu\sqrt{-2\beta})z}$

TABLE IV. Asymptotic behaviors of transformed solutions. If $u(z)$ possesses the asymptotic behavior in the row marked $u(z)$ as $z \rightarrow +\infty$ and $z \in \mathbb{R}$, then the transformed solutions possess the asymptotic behavior in the following rows as $z \rightarrow +\infty$ and $z \in \mathbb{R}$. With restriction to the solutions that are real on the real axis, all options in the table are feasible when $\beta \leq 0$. When $\beta > 0$ those that contain the term $\sqrt{-2\beta}$ are not.

A. An Exploration of the Fundamental Domain

In section IIID the fundamental domain (18) was introduced, and it was noted that solutions for all parameter choices in theory can be found by applying the transformations (5) through (7) to the solutions in this domain. However, the literature describes solutions in this domain only for the cases $\alpha = \beta = 0$ (numerical and asymptotic solutions), ($\alpha = 0, \beta = -2/9$) (a rational solution), along the line $\beta = 0$ (asymptotically decaying solutions), and along the curve $\beta = -2(\alpha - 1)^2$ (asymptotic, rational and special function solutions). All of these occur on the boundaries of the fundamental domain. In particular, the special solutions described for each of these parameter choices are indicated in figure 9.

1. Parameter Choices with Rational or Special Function Solutions

It should again be noted that, for each of the parameter choices ($\alpha = 0, \beta = -\frac{2}{9}$) and along the curve $\beta = -2(\alpha - 1)^2$, the closed form or asymptotic solutions only lead to a single solution or a one parameter family of solutions in the $u(0)$ versus $u'(0)$ plane. To gain some insight into arbitrary ICs (in the same manner as figure 2) the frames in figure 10 show the number of poles appearing on the positive real axis for each of the two remaining vertices of the fundamental domain, as well as the case ($\alpha = 0, \beta = -2/9$). A detailed description

Closed Form and Asymptotic Solution
Types of the Fundamental Domain

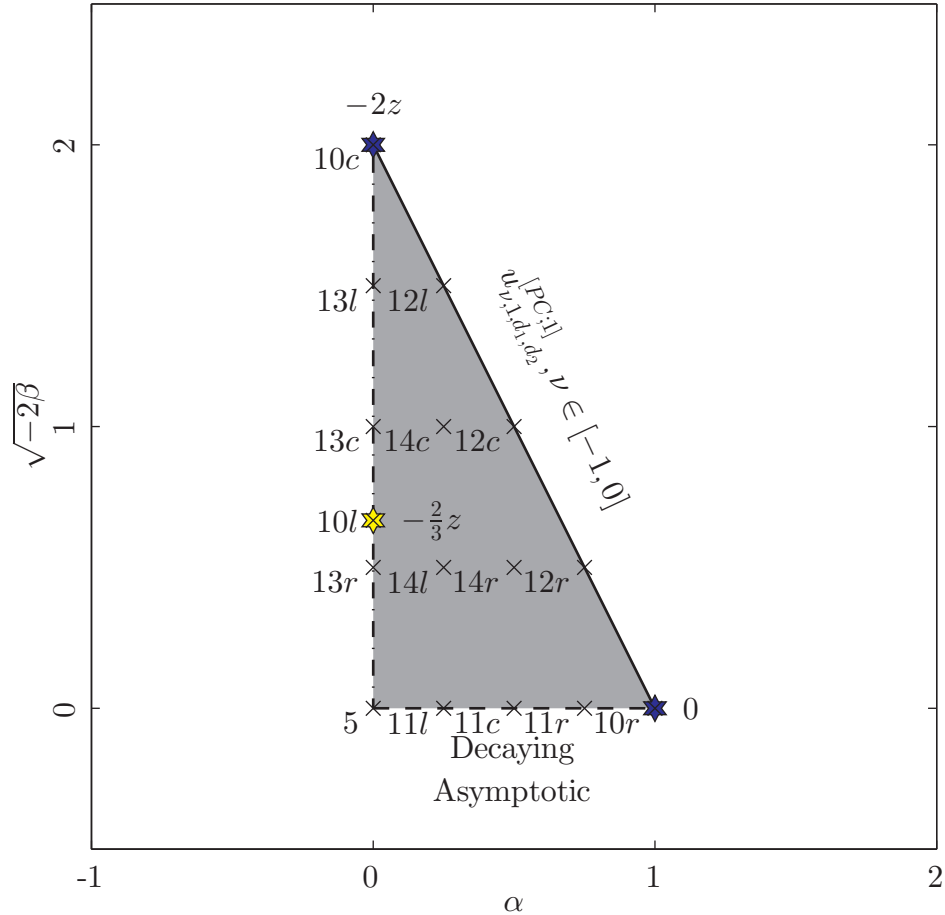


FIG. 9. Locations of the closed form and asymptotic solution types appearing in the fundamental domain. The \times 's mark the parameter choices in the fundamental domain where pole counts will be shown along with the appropriate figure number (l , c , and r refer to the left, center, and right frames, respectively).

of the markers and shading is given in figure 3.

Within the frames of figures 2 and 10 it is easy to see that the ICs of solutions asymptotic to the roots of (13) appear regularly as the boundaries of shaded regions or along curves generated by the ICs of solutions asymptotic to (12) or those of special function solutions. To this point, the last two frames show a peculiar behavior of these asymptotic solutions when the α and β choices occur at the vertex of a Weyl chamber. For these solutions, the behaviors of w_μ^+ , $\mu = \pm 1$, and w_{-1}^- are present in the same solution, but in different segments of the positive real axis. Take, for instance, the ICs for $(\alpha = 0, \beta = -2)$ and $(\alpha = 1, \beta = 0)$

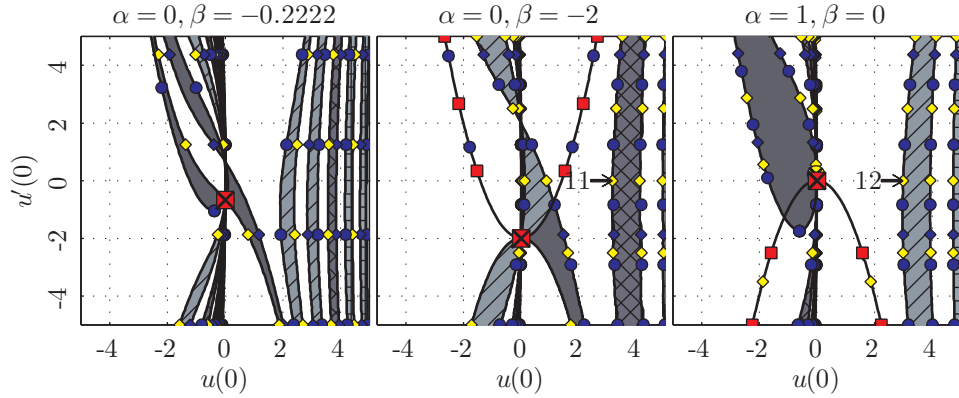


FIG. 10. Number of poles on the positive real axis for $\alpha = 0$ and $\beta = -2/9$, $\alpha = 0$ and $\beta = -2$, and $\alpha = 1$ and $\beta = 0$. A detailed description of the markers and shading is given in figure 3.

indicated by the arrows in the second two frames of figure 10. Along the curves containing these ICs there are two or three separate markers. The solutions in a neighborhood of these particular ICs are shown in figures 11 and 12, illustrating that different dominant asymptotic behaviors can occur in the same solution (but, in different segments of the real axis).

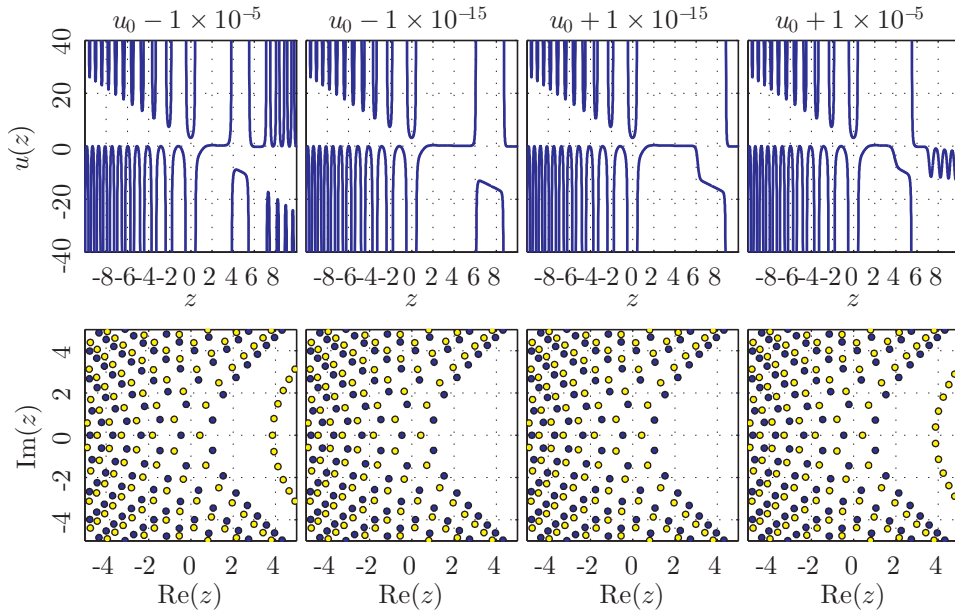


FIG. 11. Solutions (along the real axis (top) and pole locations and residues (bottom)) with adjacent pole free sectors for $\alpha = 0$ and $\beta = -2$. $u'(0) = 0$ and $u_0 = 3.170110354518507$. This initial condition is marked with an arrow in the center frame of figure 10.

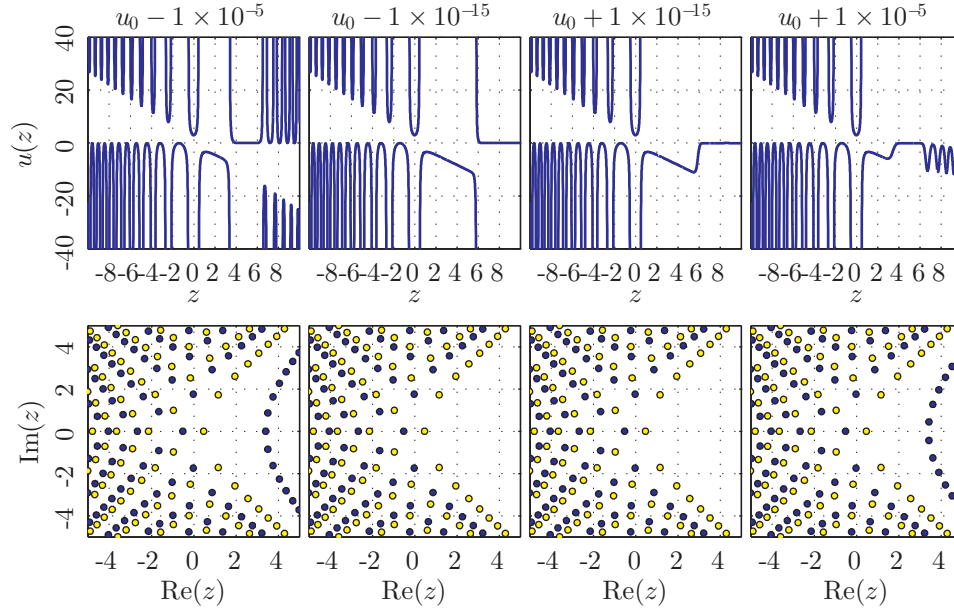


FIG. 12. Solutions (along the real axis (top) and pole locations and residues (bottom)) with adjacent pole free sectors for $\alpha = 1$ and $\beta = 0$. $u'(0) = 0$ and $u_0 = 2.989670219313871$. This initial condition is marked with an arrow in the right frame of figure 10.

2. Parameter Choices Along the Boundary $\beta = 0$

When the boundary $\beta = 0$ is considered the literature generally only describes solutions to P_{IV} that decay asymptotically as $z \rightarrow +\infty$. Considering the frame in the right of figure 2, all of the frames of figure 13, and the rightmost frame of figure 10, the ICs generating these solutions appear as curves with the appropriate markers (i.e. those shown in figure 3). These ICs are precisely the ones that correspond to solutions matching both the roots w_μ^+ , $\mu = \pm 1$. That is, these trends are both present when $\beta = 0$.

3. Parameter Choices Along the Boundary $\beta = -2(\alpha - 1)^2$

Next, P_{IV} has a one-parameter family of solutions expressible in terms of the parabolic cylinder function or confluent hypergeometric function for each choice of α and β along the boundary described by $\beta = -2(\alpha - 1)^2$. Table III gives two choices of the parameters leading to these types of solutions. It was noted previously that the choice of $\epsilon = -1$ leads to solutions that are not always real along the real axis. Further, the parameter choices $\beta = -2(\alpha - 1)^2$ only satisfy the relationships for α and β (excluding $\epsilon = -1$) leading to

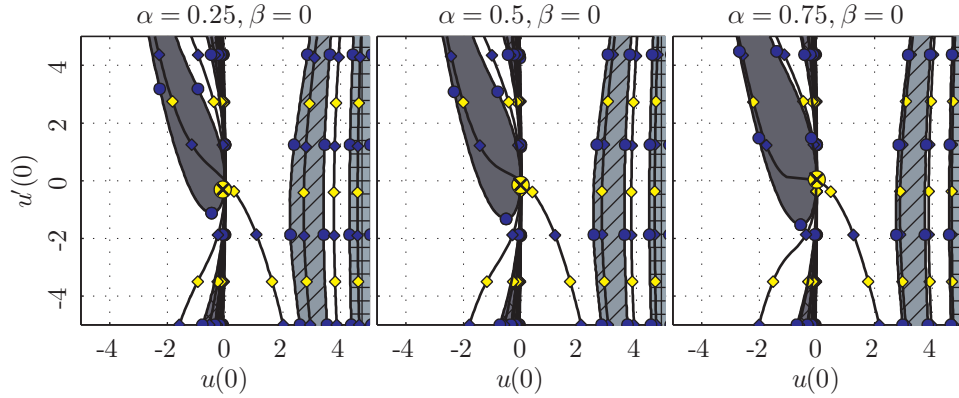


FIG. 13. Number of poles on the positive real axis for parameter choices on the boundary of the fundamental domain where $\beta = 0$. A detailed description of the markers and shading is given in figure 3. Here the light and dark diamonds refer to the solutions that match the behaviors w_{μ}^{+} , $\mu = \pm 1$. These ICs are precisely those satisfying the decaying asymptotic condition (12).

the solutions $u_{\nu,1,d_1,d_2}^{[PC;k]}$ if $k = 2$. Therefore, only the initial conditions leading to solutions $u_{\nu,1,d_1,d_2}^{[PC;2]}$ are explicitly shown in figure 14. For these parameter choices the trends of w_{-1}^{\pm} are present, and these are again $u(z) \rightarrow O\left(\frac{1}{z}\right)$ and $u(z) \rightarrow -2z$ as $z \rightarrow \infty$ and $z \in \mathbb{R}$.

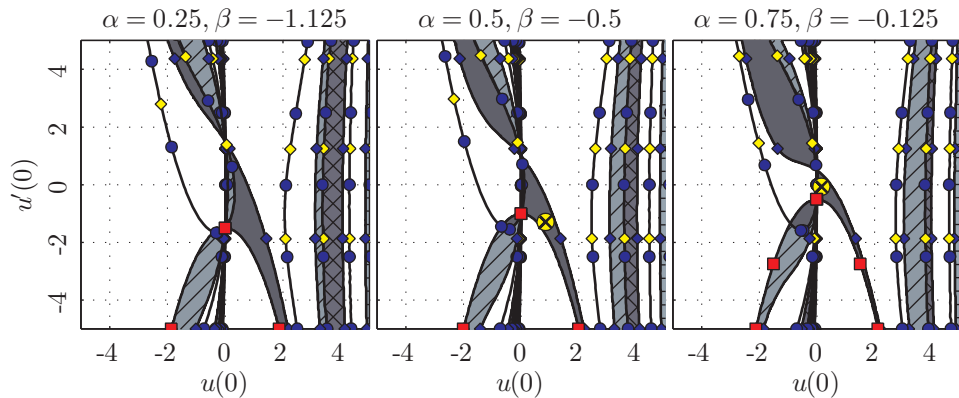


FIG. 14. Number of poles on the positive real axis for parameter choices on the boundary of the fundamental domain where $\beta = -2(\alpha - 1)^2$. A detailed description of the markers and shading is given in figure 3.

4. Parameter Choices Along the Boundary $\alpha = 0$

Finally, along the boundary $\alpha = 0$ the locations of ICs generating solutions asymptotic to the roots w_{+1}^{+} and w_{-1}^{+} become distinct, separating or expanding into regions with a finite

number of poles. This is easily seen in the sequence of frames in figure 15.

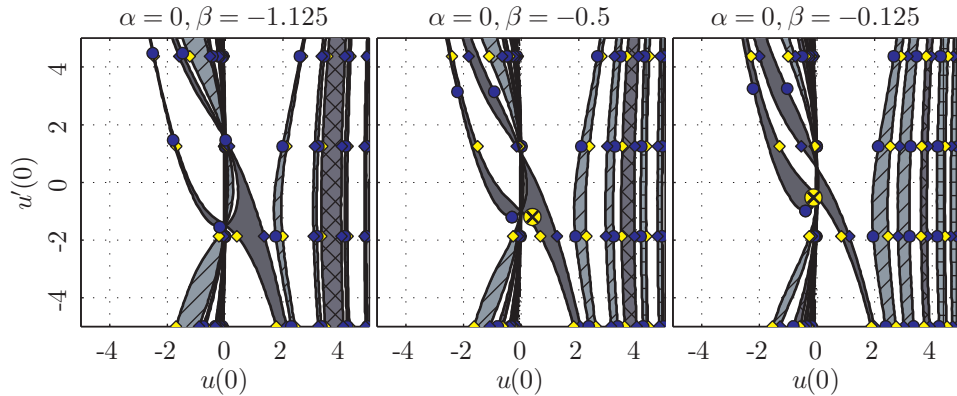


FIG. 15. Number of poles on the positive real axis for parameter choices on the boundary of the fundamental domain where $\alpha = 0$. Note that the initial conditions for the solution asymptotic to the root w_{-1}^- occur just outside the window shown here at $u(0) \approx 2.429702$ and $u'(0) \approx -7.568548$ (still within the same shaded region as the other two cases) in the case of $\beta = -1.125$. A detailed description of the markers and shading is given in figure 3.

5. The Interior to the Fundamental Domain

Parameter choices interior to the fundamental domain behave much like those along the boundary $\alpha = 0$. In these cases, solutions asymptotic to each of the roots of (13) are generated from distinct ICs. This can be witnessed in figure 16.

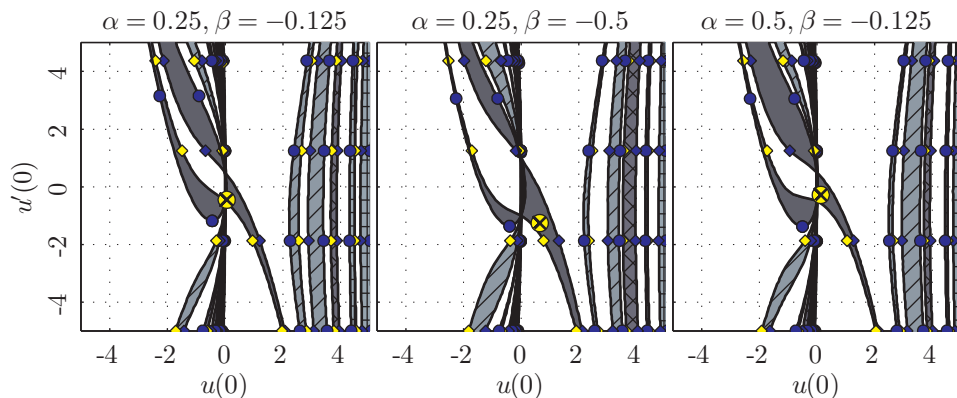


FIG. 16. Number of poles on the positive real axis for parameter choices interior to the fundamental domain. A detailed description of the markers and shading is given in figure 3.

6. A Note on Connection Formulae

Consider the left and right frames of figure 2, showing the number of poles along the negative and positive real axes, respectively. One finds that a segment of the curve extending from the origin and down to the right in the right frame cuts across the shaded region that extends from the origin up and to the right in the left frame. Along this segment P_{IV} therefore has solutions that are smooth in both directions. A similar analysis of the pole counting diagrams for any choice of α when $\beta = 0$ would result in an analogous family of solutions that are smooth in both directions. These appear to be the only examples of solutions that have connection formulae available in the literature (see, e.g. Refs. 1, 7, 25, or 26).

Examination of figures 10 through 15 (together with the symmetry (2)) shows that similar comparisons of the number of poles on the positive and negative real axes will again identify solutions that are smooth in both directions for regions of ICs near $u(0) = u'(0) = 0$ in cases where β is negative. For instance, figures 15 and 16 indicate that such regions (sometimes only a curve) will exist for all parameter choices within the fundamental domain. Figure 17 illustrates this for a choice interior to the fundamental domain ($\alpha = 0.25$, $\beta = -0.125$).

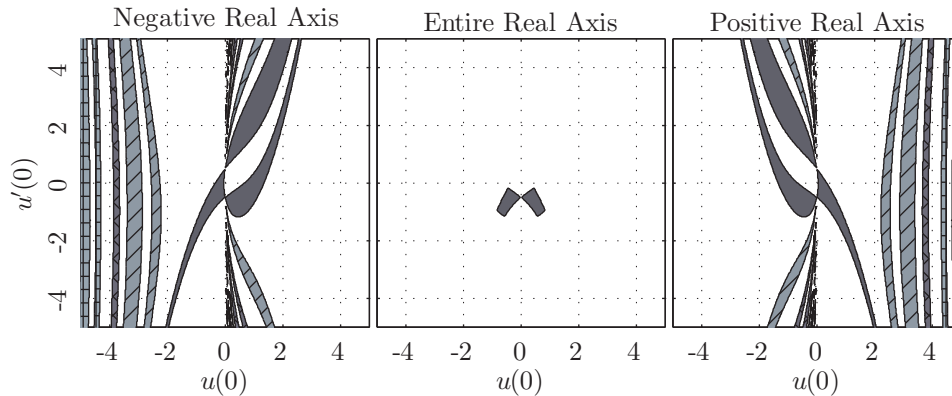


FIG. 17. Number of poles on the negative real axis (left), entire real axis (center), and positive real axis (right) for $\alpha = 0.25$ and $\beta = -0.125$.

In a following section, figure 20 will show that similar regions will also occur outside the fundamental domain when $\beta < 0$, however, with the difference that there now may be a finite number of poles on the real axis in either one or both directions. In contrast, positive choices of β do not seem to produce any such regions of ICs.

VI. SOLUTION PATTERNS OUTSIDE THE FUNDAMENTAL DOMAIN

The (α, β) space is far too wide to complete an exhaustive survey here. Therefore, the rest of this paper focuses on the unexplored space of $\beta > 0$ and highlights some solution types that seem to appear for all α and β .

A. The Unexplored Space of Positive Beta

Studies of P_{IV} with $\beta > 0$ are noticeably absent from the literature. For instance, all known closed form solutions occur only when β is nonpositive. Even the Bäcklund and Schlesinger transformations are only applicable to β -values that are nonpositive (assuming $u(z)$ is real when z is real). Exploration of such cases and knowledge of the tronquéé like solutions that appear in the $\alpha = \beta = 0$ case suggests that solutions with $\beta > 0$ also feature noteworthy characteristics. For instance, there are further analogues to the solution that is pole free for a half-plane.

The asymptotic behaviors (14) and (15) no longer occur as solutions that are real along the real axis, due to the term $\sqrt{-2\beta}$. Therefore, the figures 18 and 19 are much simpler than their counterparts with a single IC generating the asymptotic behavior of $w_{+1}^{-1} \sim -2/3z$ and ICs along the boundaries of regions with finite poles leading to that of $w_{-1}^{-1} \sim -2z$.

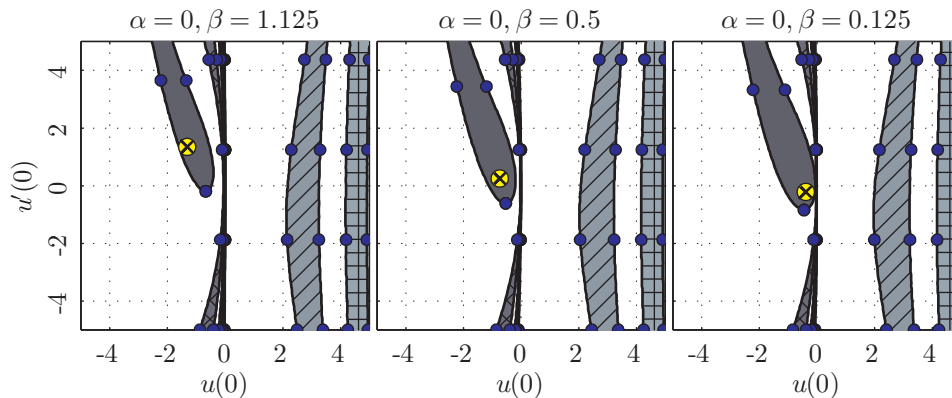


FIG. 18. Number of poles on the positive real axis for parameter choices where $\alpha = 0$ and $\beta > 0$. A detailed description of the markers and shading is given in figure 3.

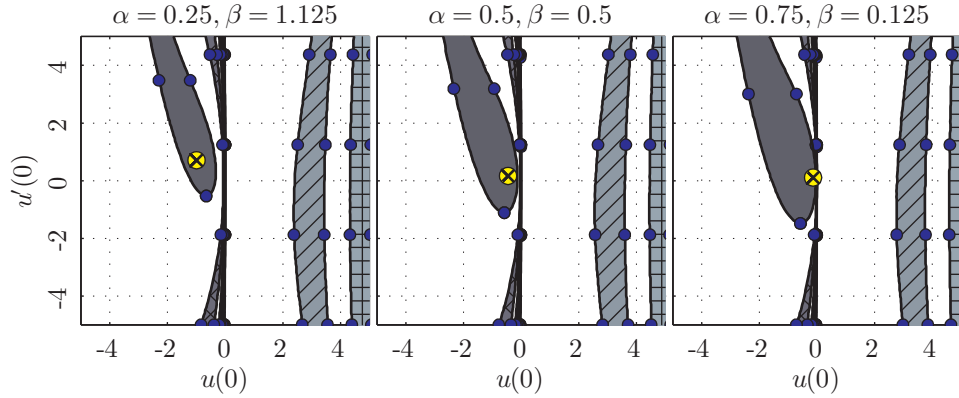


FIG. 19. Number of poles on the positive real axis for parameter choices where $\beta = 2(\alpha - 1)^2$ and $\beta > 0$. A detailed description of the markers and shading is given in figure 3.

B. Parameters Larger in Magnitude

This section illustrates some α, β choices slightly larger in magnitude. When $\beta > 0$ there is little difference from the choices presented in the earlier figures. However, nonpositive choices of β become far more complicated without indicating the existence of further types of solutions with special characteristics. Even parameter choices in adjacent Weyl chambers generate significantly different behaviors near $u(0) = u'(0) = 0$.

C. Solutions With a Nearly Pole Free Half Plane

It was noted⁵ that when $u(z)$ satisfies the decaying asymptotic condition (12) and $\alpha = \beta = 0$ a particular choice of k leads to a solution that is pole free across the entire left half-plane. A similar solution is shown for $\alpha = 0.5$ and $\beta = -0.5$ in figure 4. Solutions with a nearly pole free half plane are not confined to only these special choices of α and β .

In fact, evidence suggests that for each α and β there exists at least one such solution, and very likely only one. The likelihood that there is only one such solution for each α and β pair makes this solution a prime candidate for comparing and making connections between all parameter choices.

For each α and β this special solution type is asymptotic to the root $w_{+1}^- \sim -2/3z$ as $z \rightarrow +\infty$ and $z \in \mathbb{R}$. Knowing this, computing the initial conditions leading to such a solution is a simple matter of solving a boundary value problem (BVP). Applying the familiar

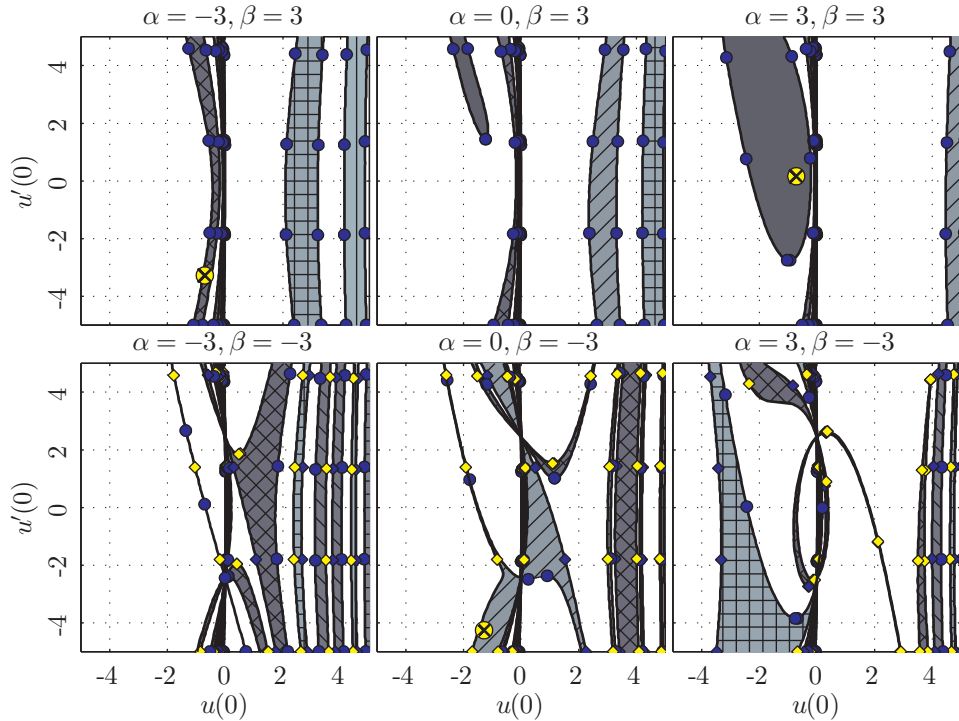


FIG. 20. Number of poles on the positive real axis along the edge of a grid exterior to the fundamental domain. The initial conditions for solutions asymptotic to w_{+1}^- in the top middle, bottom left, and bottom right frames occur outside of the domain shown at $(u(0) = -4.6822, u'(0) = 20.7787)$, $(u(0) = -10.7942, u'(0) = 120.3759)$, and $(u(0) = 49.4606, u'(0) = -2442.3215)$, respectively. The locations of these parameters in α vs. β space are shown later in figure 21. A detailed description of the markers and shading is given in figure 3.

methodology of counting poles along the positive, and now negative, real axes allows the identification of further special characteristics of these solutions.

In figure 21 the pole counts are shown along the negative and positive real axes (left and right frames, respectively) overlaid with the Weyl chambers marked by solid curves. Also in these frames, dashed lines mark the boundaries of regions in the α versus β plane where these solutions have only a finite number of poles on the negative real axis. Notice that these dashed curves form a regular structure similar to that of the Weyl chambers, with the parabolas offset by one unit on the α axis and the horizontal lines occurring at β values where these new parabolas and those from the Weyl chambers intersect.

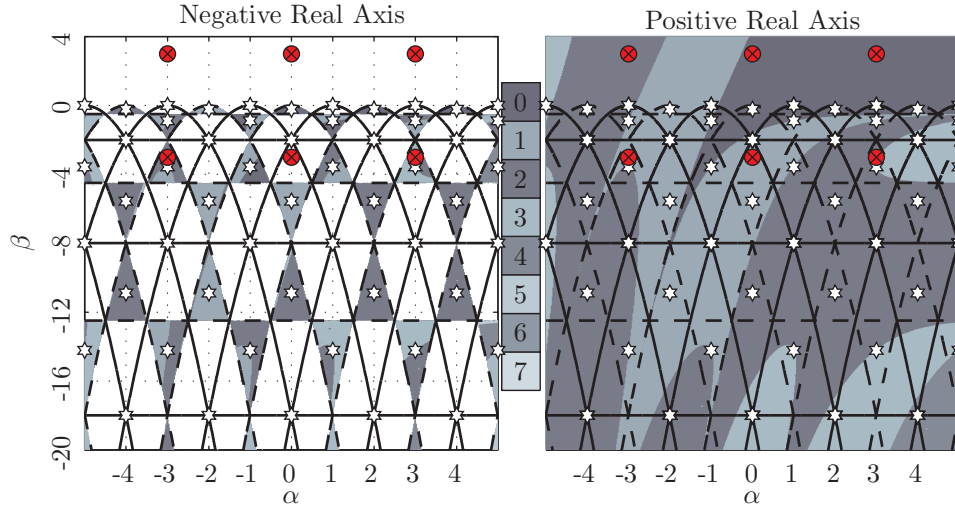


FIG. 21. Number of poles on the positive (right) and negative (left) real axis for solutions asymptotic to $w_{+1}^- \sim -2/3z$ as $z \rightarrow +\infty$ and $z \in \mathbb{R}$ and each α and β . The solid curves indicate the boundaries of the Weyl chambers, while the dashed lines show the boundaries of regions of finite poles on both the positive and negative real axes. Note that in this case $\beta > 0$ implies an infinity of poles along \mathbb{R}^- . The circles (red) containing an \times indicate those parameters shown in figure 20. The changes in shading occur simultaneously in the left and right frames corresponding to a pole moving from one half of the real axis (positive/negative) to the other.

1. The Tops of the Parabolas

To begin, consider the parameter choices at the tops of these new parabolas. These occur at $\alpha = 2m$ and $\beta = 0$, $m \in \mathbb{Z}$. In these cases the poles nearest the origin form very regular patterns. Examples for several different choices of m are shown in figure 22. Notice the pole structure near the center of these figures. When $m < 0$ poles of residue $+1$ align in a structure similar to the roots with a positive real part of the degree m Okamoto I polynomial, while poles of residue -1 appear similar to the roots of the degree $m - 1$ polynomial. On the other hand, when $m > 0$ the poles of residue $+1$ (likewise, -1) align in a structure similar to all of the roots of the order $m + 1$ (likewise, m) polynomials. Note that the Okamoto I polynomials in this context are singly indexed as in Ref. 19 while those in the rational solutions of P_{IV} are doubly indexed generalized Okamoto polynomials as in Ref. 7.

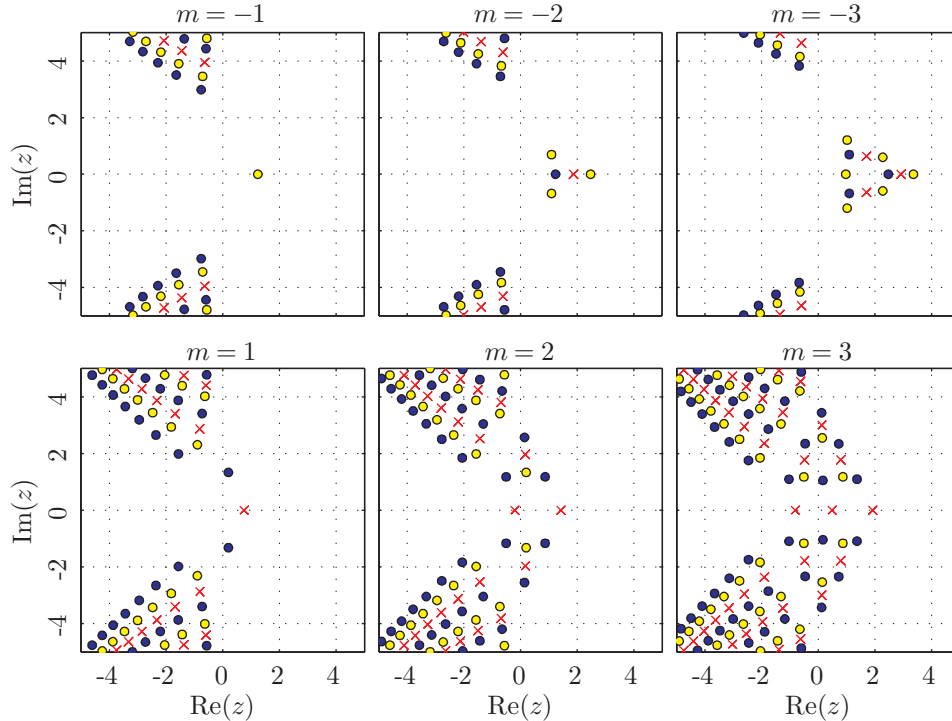


FIG. 22. Zero and pole locations of solutions to (1) with various values of m . Note that $\alpha = 2m$ and $\beta = 0$. The case $\alpha = m = 0$ is shown in one of the subplots of figure 5.

2. Solutions Along the Boundaries of the New Weyl-Like Chambers

When α and β are taken along the boundaries of the new chambers the solutions asymptotic to $-2/3z$ are nonoscillatory as $z \rightarrow -\infty$. Examples of this are shown in the center frames of figures 23 and 24. Now, if α or β are varied slightly such that the choice of parameters no longer falls on one of the boundaries, these solutions can have either an infinity of poles or oscillate as $z \rightarrow -\infty$. Examples of this are also shown in the left and right frames of figures 23 and 24.

3. When β is Positive

If $\beta > 0$, then figure 21 shows that all of the solutions asymptotic to $w_{+1}^- \sim -2/3z$ as $z \rightarrow +\infty$, $z \in \mathbb{R}$, have an infinity of poles on the negative real axis. These solutions also do not generally have an entire half-plane free of poles. Instead, numerical evidence points to a value $z_0 \in \mathbb{R}$ (possibly positive or negative) such that for all z with $\text{Re}(z) > z_0$ the solution

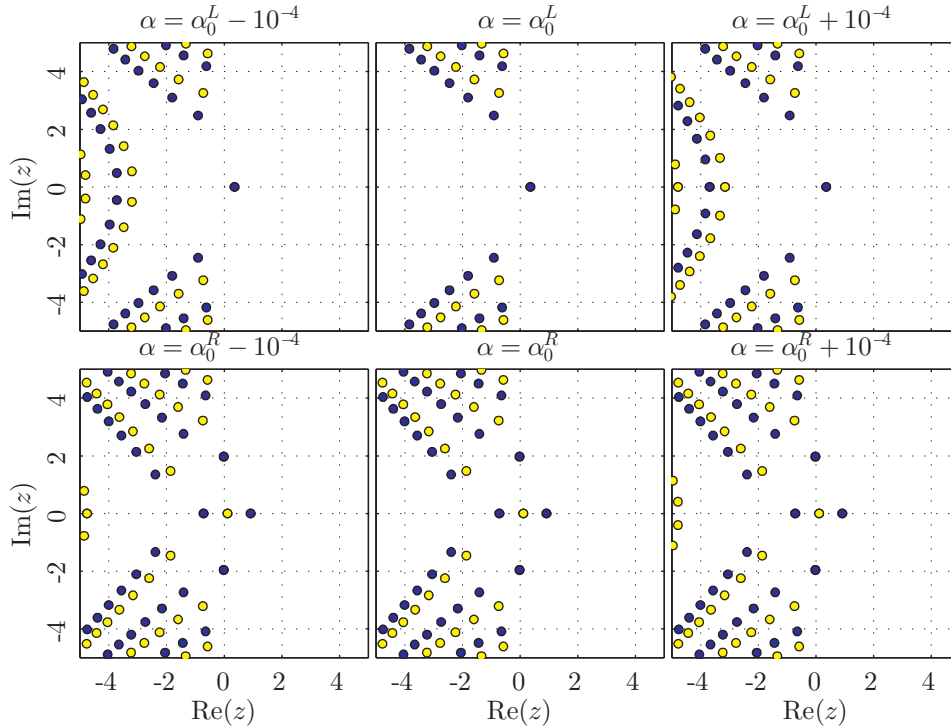


FIG. 23. Solutions (pole locations and residues) normal to the parabola $\beta = -2(\alpha - 2)^2$. All frames depict the solutions asymptotic to $-2/3z$ as $z \rightarrow +\infty$. The center frames occur directly along the parabolas where $\alpha = \alpha_0 = 1.25$ (top) and $\alpha = \alpha_0 = 2.75$ (bottom). The left and right frames in both the top and bottom then depict the solutions along the line normal to the parabola at $\alpha = \alpha_0$ at $\alpha_0 \pm 10^{-4}$.

has no poles.

4. Other Solutions With a Pole Free Half-Plane

These solutions asymptotic to $-2/3z$ as $z \rightarrow +\infty$ are not the only solutions that have a half-plane pole free. There are, of course, the rational solutions. Likewise, there are solutions expressible in terms of parabolic cylinder or confluent hypergeometric functions that also feature a pole free half-plane. These solutions arise for $u_{\nu, \epsilon, d_1, d_2}^{[PC; k]}$, $k = 1, 2$, when either $d_1 = 0$ or $d_2 = 0$ with examples shown in figure 25. Generally, these other solutions with a pole free half-plane feature different asymptotics as $z \rightarrow +\infty$ than $-\frac{2}{3}z$.

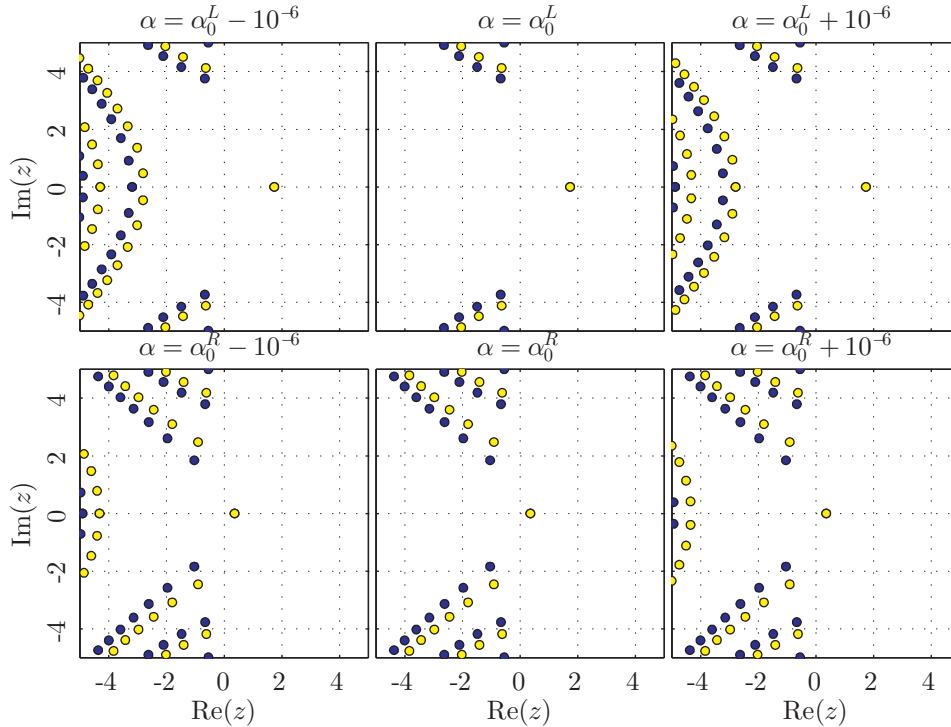


FIG. 24. Solutions (pole locations and residues) normal to the parabola $\beta = -2(\alpha + 2)^2$. All frames depict the solutions asymptotic to $-2/3z$ as $z \rightarrow +\infty$. The center frames occur directly along the parabolas where $\alpha = \alpha_0 = -1.25$ (top) and $\alpha = \alpha_0 = -2.75$ (bottom). The left and right frames in both the top and bottom then depict the solutions along the line normal to the parabola at $\alpha = \alpha_0$ at $\alpha_0 \pm 10^{-6}$.

D. Solutions With Adjacent Pole Free Sectors

In Ref. 5 it is pointed out that there are solutions for P_{IV} when $\alpha = \beta = 0$ that are similar to the tronquée solutions of P_I . For both P_I and P_{IV} (with $\alpha = \beta = 0$) these solutions are characterized by at least two adjacent pole free sectors. In the case of P_{IV} these sectors are shown in figure 8. Also, when $\alpha = \beta = 0$, these solutions are characterized as appearing at the boundaries of shaded regions or along curves within the pole counting diagrams. From here on, the analogy with the tronquée solutions of P_I will be dropped and these solutions will be referred to only as having adjacent pole free sectors. The solutions asymptotic to $w_{+1}^- \sim -2/3z$ were considered separately in section VIC, but they would certainly fall into this category. Other solutions with adjacent pole free sectors are asymptotic to w_{-1}^- and w_{μ}^+ , $\mu = \pm 1$, as $z \rightarrow +\infty$ and $z \in \mathbb{R}$. In certain cases there are two or three such trends present simultaneously in a single solution, but the trends occur along different segments of

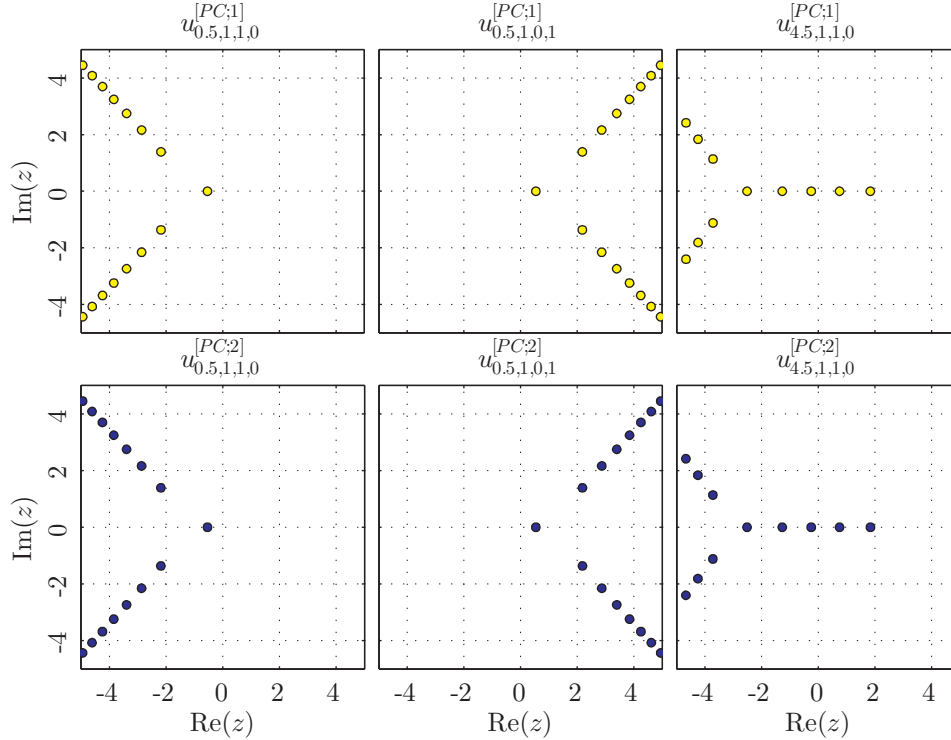


FIG. 25. Examples (pole locations and residues) of $u_{\nu,\epsilon,d_1,d_2}^{[PC;k]}$, $k = 1, 2$, for $d_1 = 0$ or $d_2 = 0$. These solutions feature a half plane that contains only a finite number of poles.

the positive real axis. For instance, ICs generating solutions matching both w_{+1}^+ and w_{-1}^+ occur when $\beta = 0$. This is not surprising considering (14) and (15) and that these are simply the solutions asymptotic to (12). Several examples are available in⁵.

In the following figures multiple frames will be shown depicting the different types of solutions with adjacent pole free sectors for each (α, β) pair discussed. In most cases, solutions where two or more behaviors appear in the same solution will be given in at least one frame. In every case, the solutions shown occur at the boundary of or along the curve located in the first shaded region extending from $u'(0) = 5$ to $u'(0) = -5$ in the right half plane (i.e. $u(0) > 0$) of the appropriate pole counting figure. These solutions are all given along the line $u'(0) = 0$.

First, figures 26 and 27 show two types of solutions where the asymptotic behaviors of w_μ^+ , $\mu = \pm 1$, and w_{-1}^- are simultaneously present (along different segments of the real axis) in a solution generated from a single IC. These are shown for $(\alpha = 1, \beta = 0)$ and $(\alpha = 0, \beta = -2)$.

On the other hand, solutions that match both the roots w_{-1}^\pm (again, in different segments

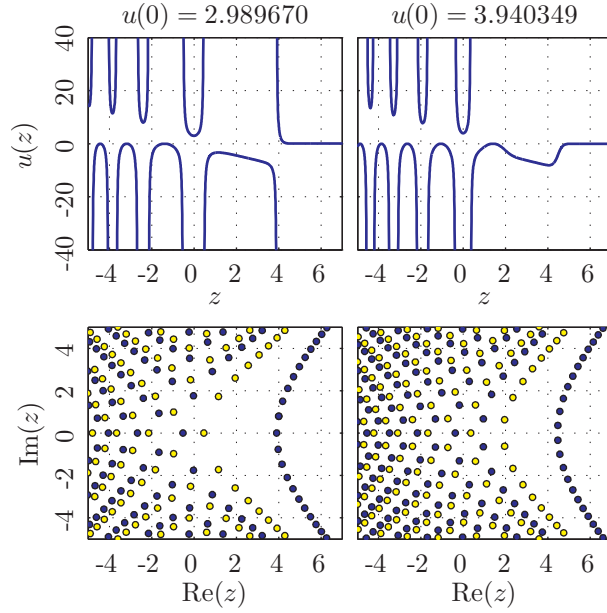


FIG. 26. Solution types (along the real axis (top) and pole locations and residues (bottom)) with adjacent pole free sectors for $\alpha = 1$ and $\beta = 0$. In all frames $u'(0) = 0$. The left and right frames both show that these solutions simultaneously match the roots (in different segments of the real axis) w_μ^+ , $\mu = \pm 1$, and w_{-1}^- .

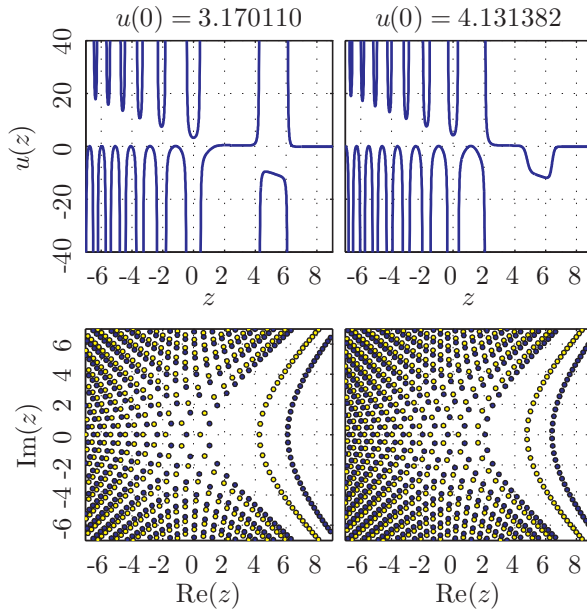


FIG. 27. Solution types (along the real axis (top) and pole locations and residues (bottom)) with adjacent pole free sectors for $\alpha = 0$ and $\beta = -2$. In all frames $u'(0) = 0$. The left and right frames both show that these solutions simultaneously match the roots w_μ^+ , $\mu = \pm 1$, and w_{-1}^- .

of the real axis) were observed along the boundary $\beta = -2(\alpha - 1)^2$. An example appears in figure 28 for the case $\alpha = 0.5$ and $\beta = -0.5$.

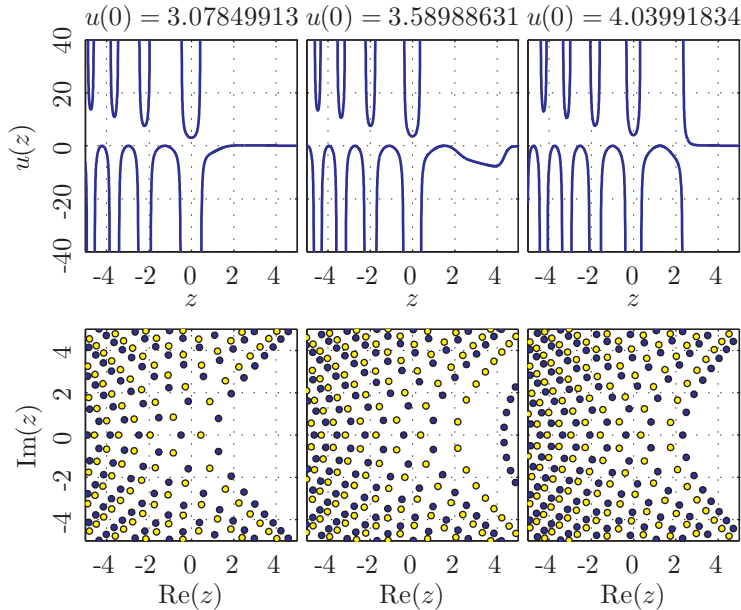


FIG. 28. Solution types (along the real axis (top) and pole locations and residues (bottom)) with adjacent pole free sectors for $\alpha = 0.5$ and $\beta = -0.5$. In all frames $u'(0) = 0$. The center frame shows that there are solutions simultaneously matching both the roots w_{-1}^{\pm} .

Finally, all other parameter choices with adjacent pole free sectors have distinct ICs that generate solutions asymptotic to each of the roots w_{μ}^{\pm} , $\mu = \pm 1$, and w_{-1}^{-} as in the figure 29.

VII. CONCLUSIONS

This study of the fourth Painlevé equation started by numerically confirming various previous analytic and asymptotic results. A further exploration of the fundamental domain then identified solutions for general (α, β) -values with noteworthy characteristics, such as numerous families of solutions with adjacent pole-free sectors. Also, solutions with a nearly pole-free half plane were found.

Most of the observations in this study were obtained numerically, leaving analytical considerations of some of the illustrated solution types an open topic. Although the explorations extended outside of the fundamental domain in the (α, β) -plane, they considered only (α, β) -values with relatively small magnitude. Further studies could be performed to look at pairs

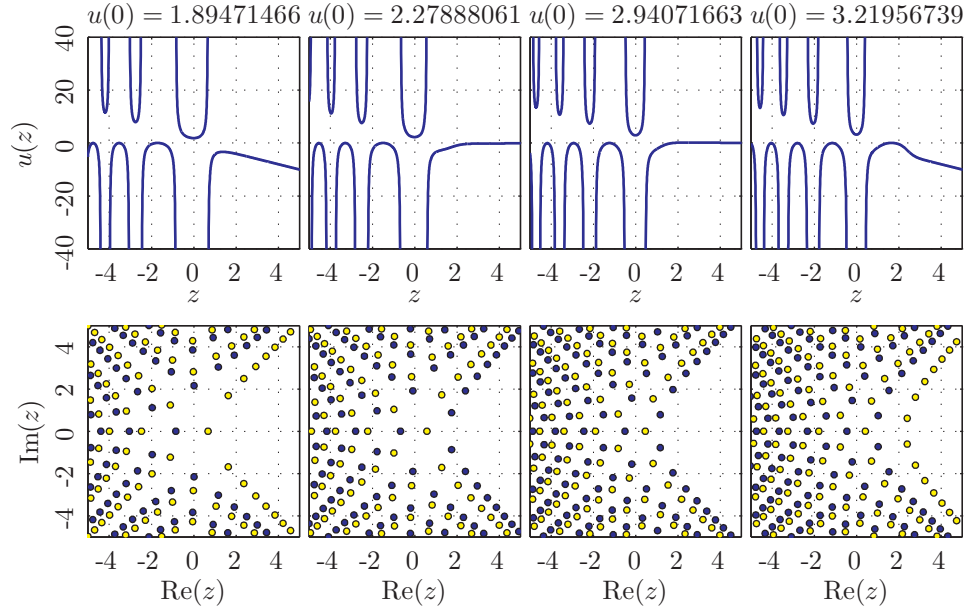


FIG. 29. Solution types (along the real axis (top) and pole locations and residues (bottom)) with adjacent pole free sectors for $\alpha = 0$ and $\beta = -0.5$. In all frames $u'(0) = 0$. In this case, all frames exhibit only one of the asymptotic behaviors w_{μ}^{\pm} , $\mu = \pm 1$.

with much larger magnitude. Another extension would be to also consider solutions that are complex-valued along the real axis.

ACKNOWLEDGMENTS

Discussions with Peter Clarkson, Harvey Segur, and André Weideman are gratefully acknowledged. J. A. R. was supported by the Department of Defense. The views expressed in this article are those of the authors and do not reflect the official policy or position of the United States Air Force, Department of Defense, or U.S. Government. B. F. wishes to thank the National Science Foundation (NSF) for support under NSF grant DMS-0914647.

REFERENCES

- ¹F. W. J. Olver, D. W. Lozier, R. F. Boisvert, and C. W. Clark, *NIST Handbook of Mathematical Functions* (Cambridge Univ. Press, 2010) <http://dlmf.nist.gov/>.
- ²B. Fornberg and J. A. C. Weideman, “A numerical methodology for the Painlevé equations,” *Journal of Computational Physics* **230**, 23–32 (2011).

- ³I. M. Willers, “A new integration algorithm for ordinary differential equations based on continued fraction approximations,” *Comm. ACM* **17**, 504 (1974).
- ⁴B. Fornberg and J. A. C. Weideman, “A computational exploration of the second Painlevé equation,” (2013), accepted by *Found. Comp. Math.*
- ⁵J. A. Reeger and B. Fornberg, “Painlevé IV with both parameters zero: A numerical study,” *Stud. Appl. Math.* **130**, 108–133 (2013).
- ⁶V. I. Gromak, I. Laine, and S. Shimomura, *Painlevé Differential Equations in the Complex Plane* (Walter de Gruyter, Berlin, 2002).
- ⁷P. A. Clarkson, “The fourth Painlevé transcendent,” Tech. Rep. UNK (Institute of Mathematics, Statistics and Actuarial Science, University of Kent, 2008).
- ⁸N. A. Lukashevich, “Theory of the fourth Painlevé equation,” *Diff. Eq.* **3**, 395–399 (1967).
- ⁹A. S. Fokas, U. Mugan, and M. J. Ablowitz, “A method of linearization for Painlevé equations: Painlevé IV, V,” *Physica D.* **30**, 247–283 (1988).
- ¹⁰Y. Murata, “Rational solutions of the second and fourth Painlevé equations,” *Funkcial. Ekvac.* **28**, 1–32 (1985).
- ¹¹J. A. Reeger, *A Computational Study of the Fourth Painlevé Equation and a Discussion of Adams Predictor-Corrector Methods*, Ph.D. thesis, University of Colorado, Boulder, Colorado (2013).
- ¹²P. A. Clarkson and K. Jordaan, “The relationship between semi-classical Laguerre polynomials and the fourth Painlevé equation,” Preprint arXiv:1301.4134[nlin.SI].
- ¹³P. J. Forrester and N. S. Witte, “Application of τ -function theory of Painlevé equations to random matrices: PIV, PII, and the GUE,” *Commun. Math. Phys.* **219**, 357–398 (2001).
- ¹⁴K. Okamoto, “Studies on the Painlevé equations III. Second and fourth Painlevé equations, P_{II} and P_{IV} ,” *Math. Ann.* **275**, 221–255 (1986).
- ¹⁵D. Bermúdez and D. J. Fernández, “Solution hierarchies for the Painlevé IV equation,” in *Proceedings of the XXXI Workshop on Geometric Methods in Physics* (Białowieża, Poland, 2012).
- ¹⁶D. Bermúdez and D. J. Fernández, “Supersymmetric quantum mechanics and Painlevé IV equation,” *SIGMA* **7** (2011), 10.3842/SIGMA.2011.025.
- ¹⁷D. Bermúdez and D. J. Fernández, “Non-hermitian Hamiltonians and the Painlevé IV equation with real parameters,” *Phys. Lett. A* **375**, 2974–2978 (2011).
- ¹⁸C. M. Bender and S. A. Orszag, *Advanced Methods for Scientists and Engineers* (McGraw-

- Hill, New York, 1978).
- ¹⁹P. A. Clarkson, “The fourth Painlevé equation and associated special polynomials,” *Journal of Mathematical Physics* **44** (2003).
- ²⁰S. Olver, “A general framework for solving Riemann-Hilbert problems numerically,” *Numer. Math* **122**, 305–340 (2012).
- ²¹G. F. Corliss, “Integrating ODE’s in the complex plane-pole vaulting,” *Mathematics of Computation* **35**, 1181–1189 (1980).
- ²²A. P. Bassom, P. A. Clarkson, and A. C. Hicks, “Numerical studies of the fourth Painlevé equation,” *IMA Journal of Applied Mathematics* **50**, 167–193 (1993).
- ²³V. Y. Novokshenov, “Padé approximations for Painlevé I and II transcendents,” *Theoretical and Mathematical Physics* **159**, 853–862 (2009).
- ²⁴L. Peltonen, *Numerical Solution of ODEs with poles*, Master’s thesis, Worcester College, Walton Street, Oxford, Oxfordshire, OX1 2HB, 01865 278300, University of Oxford (2011).
- ²⁵A. R. Its and A. A. Kapaev, “Connection formulae for the fourth Painlevé transcendent: Clarkson-McLeod solution,” *J. Phys. A: Math. Gen.* **31**, 4073–4113 (1998).
- ²⁶A. P. Bassom, P. A. Clarkson, A. C. Hicks, and J. B. McLeod, “Integral equations and exact solutions of the fourth Painlevé equation,” in *Proceedings of the Royal Socited of London A* (1992).

Appendix C

Paper 3-“Stability Ordinates of Adams Predictor-Corrector Methods”

Stability Ordinates of Adams Predictor-Corrector Methods

M. L. Ghrist · J. A. Reeger · B. Fornberg

Received: date / Accepted: date

Abstract How far the stability domain of a numerical method for approximating solutions to differential equations extends along the imaginary axis indicates how useful the method is for approximating solutions to wave equations; this maximum extent is termed the imaginary stability boundary, also known as the stability ordinate. It has previously been shown that exactly half of Adams-Bashforth, Adams-Moulton, and staggered Adams-Bashforth methods have nonzero stability ordinates. In this paper, we consider two categories of Adams predictor-corrector methods and prove that they follow a similar pattern. In particular, if p is the order of the method, ABp - AMP methods have nonzero stability ordinate only for $p = 1, 2, 5, 6, 9, 10, \dots$, and $AB(p-1)$ - AMP methods have nonzero stability ordinates only for $p = 3, 4, 7, 8, 11, 12, \dots$

Keywords Adams methods · Linear multistep methods · Stability ordinate · Predictor-corrector · Imaginary stability boundary · Finite difference methods · Stability region

Mathematics Subject Classification (2000) 65L06 · 65L12 · 65L20 · 65M06 · 65M12

1 Introduction

When wave equations are posed as first-order systems and discretized in space to yield a system of ordinary differential equations (ODEs), a purely imaginary spectrum will correspond to the fact that only propagation takes place. Many classical numerical methods for

Support for M. Ghrist and J. Reeger provided by the United States Air Force. Support for B. Fornberg provided by NSF DMS-0914647.

M. Ghrist

Department of Mathematical Sciences, United States Air Force Academy, USAF Academy, CO 80840, USA
E-mail: michelle.ghrist@usafa.edu

J. Reeger · B. Fornberg

Department of Applied Mathematics, Campus Box 526, University of Colorado, Boulder, CO 80309, USA

J. Reeger

E-mail: jonah.reeger@colorado.edu

B. Fornberg

E-mail: fornberg@colorado.edu

ODEs have stability regions that include an interval of the form $[-iS_I, iS_I]$ on the imaginary axis. We call the largest such value of S_I the *imaginary stability boundary (ISB)* of the ODE integrator, which is also known as the stability ordinate. In the context of solving semidiscrete wave equations, one desires to use a method with a large ISB, which allows larger stable time steps; methods with zero ISB's (i.e., no imaginary axis coverage in the stability domain) will be unconditionally unstable. In this paper, we explore the question of which Adams methods have nonzero ISB's.

Adams-Bashforth (AB), Adams-Moulton (AM), and Adams predictor-corrector methods are widely used multistep methods for approximating solutions to first-order differential equations. These methods generally have lower computational cost per iteration than equivalent-order Runge-Kutta methods (due to requiring only one new function evaluation per time step) while maintaining reasonably good accuracy and stability properties [1], [6]. A standard m -step Adams method for approximating solutions to $\frac{dy}{dt} = f(t, y)$ has the form

$$y_{j+1} = y_j + \int_{t_j}^{t_{j+1}} p(t) dt, \quad (1)$$

where $t_j = t_0 + jh$, h is the stepsize, and $y_0 = y(t_0)$. Here, $p(t)$ is the polynomial interpolating the points (t_k, y_k) for $j - m + 1 \leq k \leq j$ (AB methods) or $j - m + 1 \leq k \leq j + 1$ (AM methods). We will henceforth use $j = 0$ to simplify the notation. AB methods have order $p = m$ while AM methods have order $p = m + 1$.

In [2, Table G.3-1], it was observed (without proof) that AB methods of order p (AB p) have nonzero ISB's only for orders $p = 3, 4, 7, 8, 11, 12, \dots$ and AM p methods have nonzero ISB's only for orders $p = 1, 2, 5, 6, 9, 10, \dots$. These results can be deduced from [7] and were independently shown in [4] and [3]. While [7] is not applicable to staggered methods, [4] and [3] proved that staggered AB methods of order p have nonzero ISB's only for $p = 2, 3, 4, 7, 8, 11, 12, \dots$; none of these articles addressed Adams predictor-corrector methods. Henceforth, we will only consider nonstaggered methods.

This study revisits our previous results from [4] with a new formulation and then extends our results to Adams predictor-corrector methods. In particular, we examine the methods AB p -AM p and AB($p-1$)-AM p , both of which have order p . We are unaware of any other studies addressing the ISB's of such methods for general order p . In [2, Table G.3-1], it was claimed that for such methods, 'most' had nonzero ISB's while 'some' had zero ISB's. We now proceed with proving that such methods follow very similar patterns to those of AB and AM methods, with AB p -AM p methods following the same pattern as AM p methods and AB($p-1$)-AM p methods following the same pattern as AB p methods.

2 Preliminaries

When solving the linear problem $\frac{dy}{dt} = \lambda y$, the edge of a stability domain is described by the root $\xi = \lambda h$ of $\rho(r) - \xi \sigma(r) = 0$ when r travels around the unit circle $r = e^{i\theta}$. Here, $\rho(r)$ and $\sigma(r)$ are the generating polynomials of the method (see, e.g., p. 27 of [6]).

To consider whether or not a stability domain has imaginary axis coverage, we wish to describe the behavior of the stability domain boundary near $\xi = 0$. For an exact method, we have $\xi(\theta) = \ln r$ (see, e.g. Theorem 2.1 of [6], using $\xi = \frac{\rho(r)}{\sigma(r)}$.) Thus an exact method satisfies

$$\xi = \ln r = \ln(e^{i\theta}) = i\theta. \quad (2)$$

A numerical scheme of order p will instead lead to

$$\xi(\theta) = i\theta + c_p(i\theta)^{p+1} + d_p(i\theta)^{p+2} + O((i\theta)^{p+3}) \tag{3}$$

for some constants c_p and d_p . The sign of the first *real* term in this expansion will dictate whether the stability domain near the origin swings to the right or to the left of the imaginary axis. See Figure 1 for an illustration comparing the stability domains of AB2 and AB3.

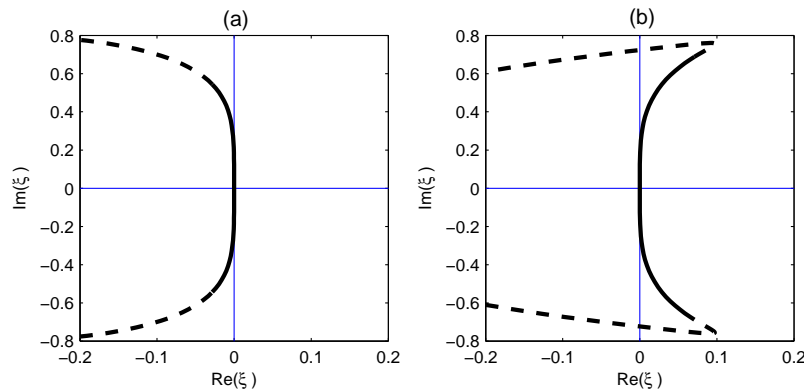


Fig. 1 Shown are portions of the boundaries of the stability regions for (a) AB2 and (b) AB3, with the solid line marking the presently relevant section of the stability domain boundary near the origin. In both graphs, we see that $\xi \approx i\theta$ near $\theta = 0$. (a) If the first real term in the expansion of $\xi(\theta)$ is negative, then the ISB is 0. (b) If the first real term in the expansion of $\xi(\theta)$ is positive, then the ISB is nonzero. For AB3, the ISB is $\frac{12}{5\sqrt{11}} \approx 0.724$. The intercepts of AB2 and AB3 on the real axis are -1 and $-\frac{6}{11}$, respectively.

2.1 Backwards difference forms of AB and AM methods

In [5][pp. 191-195], Henrici gave a backwards difference representation of (1) for AB and AM methods. When applied to $\frac{dy}{dt} = \lambda y$, an m -step AB method can be represented by

$$y_1 = y_0 + h\lambda \sum_{k=0}^{m-1} \gamma_k \nabla^k y_0, \tag{4}$$

where

$$\gamma_k = (-1)^k \int_0^1 \binom{-s}{k} ds. \tag{5}$$

Similarly, an m -step AM method can be represented by

$$y_1 = y_0 + h\lambda \sum_{k=0}^m \gamma_k^* \nabla^k y_1, \tag{6}$$

where

$$\gamma_k^* = (-1)^k \int_0^1 \binom{-s+1}{k} ds. \tag{7}$$

Henrici [5][p. 195] also established that

$$\sum_{j=0}^k \gamma_j^* = \gamma_k \quad (8)$$

from which $\gamma_k^* = \gamma_k - \gamma_{k-1}$.

Lemma 2.1 For all integers $k \geq 3$, $\gamma_k > \frac{1}{k}$.

Proof We first note an alternate way to express γ_k . From (5),

$$\gamma_k = (-1)^k \int_0^1 \binom{-s}{k} ds = \frac{1}{k!} \int_0^1 s(s+1)(s+2)\dots(s+k-1) ds. \quad (9)$$

We now prove this lemma via induction. Evaluating (9) directly gives $\gamma_3 = \frac{3}{8} > \frac{1}{3}$, establishing a base case. For the inductive step, we assume that $\gamma_j > \frac{1}{j}$ for some $j \geq 3$ and seek to establish that $\gamma_{j+1} > \frac{1}{j+1}$. From (9),

$$\gamma_{j+1} = \int_0^1 \frac{s(s+1)(s+2)\dots(s+j-1)}{j!} \binom{s+j}{j+1} ds > \left(\frac{j}{j+1}\right) \gamma_j > \left(\frac{j}{j+1}\right) \frac{1}{j} = \frac{1}{j+1}.$$

Thus $\gamma_k > \frac{1}{k}$ by induction. \square

Direct evaluation of (9) gives $\gamma_0 = 1$, $\gamma_1 = \frac{1}{2}$, and $\gamma_2 = \frac{5}{12}$. Thus as a corollary, we also have that $\gamma_k > 0$ for all integers $k \geq 0$.

Lemma 2.2 For all integers $k \geq 1$, $\gamma_k^* < 0$.

Proof Evaluating (7) directly gives $\gamma_0^* = 1$ and $\gamma_1^* = -\frac{1}{2}$. For the general case, we rewrite (7) to find

$$\gamma_k^* = \frac{1}{k!} \int_0^1 (s-1)s(s+1)(s+2)\dots(s+k-2) ds. \quad (10)$$

The integrand is negative for $0 < s < 1$, so $\gamma_k^* < 0$ for $k \geq 1$. \square

2.2 Exploring the exact solution

Using $\xi = \lambda h$, the exact solution to $\frac{dy}{dt} = \lambda y$ is $y(t) = e^{\lambda t} = e^{\xi t/h}$ where, without loss of generality, we have chosen $t_0 = 0$ and $y(t_0) = 1$. For an exact method, $\xi = i\theta$ from (2), so

$$y_n = y(nh) = e^{in\theta}. \quad (11)$$

An alternate way to view this equation is that we are seeking the exact solution to the relevant difference equation when following the root r that has $r = e^{i\theta}$, which gives $y_n = r^n = (e^{i\theta})^n = e^{in\theta}$.

Lemma 2.3 When $y_n = e^{in\theta}$,

$$\nabla^k y_0 = (i\theta)^k \left[1 - \frac{k}{2}(i\theta) + O((i\theta)^2) \right].$$

Proof For $y_n = e^{in\theta}$, $\nabla y_0 = (1 - e^{-i\theta})$ and $\nabla^k y_0 = (1 - e^{-i\theta})^k$ so that

$$\begin{aligned}\nabla^k y_0 &= \left[1 - \left(1 + (-i\theta) + \frac{1}{2!} (-i\theta)^2 + O((i\theta)^3) \right) \right]^k \\ &= (i\theta)^k \left[1 - \frac{1}{2} (-i\theta) + O((i\theta)^2) \right]^k \\ &= (i\theta)^k \left[1 - \frac{k}{2} (i\theta) + O((i\theta)^2) \right].\end{aligned}$$

□

Corollary 2.1 When $y_n = e^{in\theta}$,

$$\nabla^k y_1 = (i\theta)^k \left[1 + \frac{2-k}{2} (i\theta) + O((i\theta)^2) \right].$$

Proof For $y_n = e^{in\theta}$, $\nabla^k y_1 = e^{i\theta} \nabla^k y_0$, so by Lemma 2.3,

$$\begin{aligned}\nabla^k y_1 &= e^{i\theta} (i\theta)^k \left[1 - \frac{k}{2} (i\theta) + O((i\theta)^2) \right] \\ &= (i\theta)^k \left[1 + (i\theta) + O((i\theta)^2) \right] \left[1 - \frac{k}{2} (i\theta) + O((i\theta)^2) \right] \\ &= (i\theta)^k \left[1 + \frac{2-k}{2} (i\theta) + O((i\theta)^2) \right].\end{aligned}$$

□

Lemma 2.4 When $y_n = e^{in\theta}$,

$$\sum_{k=0}^m \gamma_k \nabla^k y_0 = 1 + \frac{1}{2} (i\theta) + O((i\theta)^2).$$

Proof From (9), $\gamma_0 = 1$ and $\gamma_1 = \frac{1}{2}$. Using Lemma 2.3, we find

$$\begin{aligned}\sum_{k=0}^m \gamma_k \nabla^k y_0 &= \sum_{k=0}^m \gamma_k (i\theta)^k \left[1 - \frac{k}{2} (i\theta) + O((i\theta)^2) \right] \\ &= \gamma_0 \left[1 + O((i\theta)^2) \right] + \gamma_1 (i\theta) \left[1 + O(i\theta) \right] + O((i\theta)^2) \\ &= 1 + \frac{1}{2} i\theta + O((i\theta)^2).\end{aligned}$$

□

Lemma 2.5 When $y_n = e^{in\theta}$,

$$\sum_{k=0}^m \gamma_k^* \nabla^k y_1 = 1 + \frac{1}{2} (i\theta) + O((i\theta)^2).$$

Proof From (10), $\gamma_0^* = 1$ and $\gamma_1^* = -\frac{1}{2}$. Using Corollary 2.1, we find

$$\begin{aligned} \sum_{k=0}^m \gamma_k^* \nabla^k y_1 &= \sum_{k=0}^m \gamma_k^* (i\theta)^k \left[1 + \frac{2-k}{2} (i\theta) + O((i\theta)^2) \right] \\ &= \gamma_0^* \left[1 + i\theta + O((i\theta)^2) \right] + \gamma_1^* (i\theta) [1 + O(i\theta)] + O((i\theta)^2) \\ &= 1 + \frac{1}{2} i\theta + O((i\theta)^2). \end{aligned}$$

□

3 Revisiting stability ordinates for AB and AM methods

To obtain the background for deriving the present predictor-corrector results and demonstrate a simpler proof than [4], we now apply the backwards difference forms of the Adams methods to rederive the results for ISB's of general AB and AM methods.

Theorem 3.1 *AB methods have nonzero ISB's only for orders $p = 3, 4, 7, 8, \dots$*

Proof We first note that it is well known that the ISB for AB1 (Euler's method) is zero (see, for example [2]). One can also check the expansion; AB1 has an expansion of $\xi = e^{i\theta} - 1 = i\theta + \frac{1}{2}(i\theta)^2 + \dots$, which has a negative first real term, offering further evidence that the ISB for AB1 is zero. We now proceed with the general case for $p \geq 2$.

For AB methods, we will show that $c_p > 0$ and $d_p < 0$ for all orders p , where c_p and d_p are defined by (3). The pattern for which methods have nonzero ISB's then follows from the powers of the imaginary unit in (3). For example, for $p = 3$, the first real term in the expansion (3) is $c_3(i\theta)^4 = c_3\theta^4 > 0$. Thus the boundary of the stability domain of AB3 swings to the right of the imaginary axis, and we have a nonzero ISB for this method, as seen in Figure 1b. For $p = 6$, the first real term in the expansion (3) is $d_6(i\theta)^8 = d_6(\theta)^8 < 0$; thus the stability domain boundary of AB6 swings to the left of the imaginary axis, and the ISB of this method is zero.

We seek to find the values of c_p and d_p in the case of a general AB p method. We apply (11) to (4), using $\xi = \lambda h$ to find

$$e^{i\theta} = 1 + \xi \sum_{k=0}^{m-1} \gamma_k \nabla^k y_0. \quad (12)$$

As $m \rightarrow \infty$, the AB method (4) reproduces the exact solution. Thus, using (2), we find

$$e^{i\theta} = 1 + i\theta \sum_{k=0}^{\infty} \gamma_k \nabla^k y_0. \quad (13)$$

Combining (13) and (12) gives

$$(\xi - i\theta) \sum_{k=0}^{m-1} \gamma_k \nabla^k y_0 = i\theta \sum_{k \geq m} \gamma_k \nabla^k y_0.$$

We now substitute for ξ using (3), where the order $p = m$ for AB. Using Lemma 2.3 and Lemma 2.4, we find

$$\begin{aligned} & \left[c_m (i\theta)^{m+1} + d_m (i\theta)^{m+2} + O((i\theta)^{m+3}) \right] \left[1 + \frac{1}{2} (i\theta) + O((i\theta)^2) \right] \\ &= \gamma_m (i\theta)^{m+1} \left[1 - \frac{m}{2} (i\theta) + O((i\theta)^2) \right] + \gamma_{m+1} (i\theta)^{m+2} [1 + O(i\theta)] + O((i\theta)^{m+3}). \end{aligned}$$

Collecting like powers of $i\theta$, we find that $c_m = \gamma_m$ and

$$\frac{1}{2}c_m + d_m = \gamma_m \left(-\frac{m}{2} \right) + \gamma_{m+1}$$

so that

$$d_m = \gamma_{m+1} - \frac{m}{2}\gamma_m - \frac{1}{2}c_m = \gamma_{m+1} - \left(\frac{m+1}{2} \right) \gamma_m. \quad (14)$$

From Lemma 2.1, we have $c_m = \gamma_m > 0$. Using this result and (9) in (14) gives

$$\begin{aligned} d_m &= \gamma_{m+1} - \left(\frac{m+1}{2} \right) \gamma_m \\ &= \frac{1}{2(m+1)!} \int_0^1 s(s+1)(s+2) \cdots (s+m-1) [2(s+m) - (m+1)^2] ds \\ &= -\frac{1}{2(m+1)!} \int_0^1 s(s+1)(s+2) \cdots (s+m-1) [m^2 + 1 - 2s] ds. \end{aligned}$$

Because $m^2 + 1 - 2s > 0$ for $m \geq 2$ and $0 \leq s \leq 1$, we find that $d_m < 0$ for $m \geq 2$. Noting that $p = m$ for AB methods, examining the sign of the first real term in (3) establishes our result that AB methods have nonzero ISB's only for orders $p = 3, 4, 7, 8, 11, 12, \dots$ \square

Theorem 3.2 *AM methods have nonzero ISB's only for orders $p = 1, 2, 5, 6, 9, 10, \dots$*

Proof We first note that $p = 1$ (Backwards Euler) and $p = 2$ (AM2) are well-known A-stable methods and thus have nonzero ISB's; one can also check their expansions. AM1 has an expansion of $\xi = 1 - e^{-i\theta} = i\theta - \frac{1}{2}(i\theta)^2 + \dots$, which has a positive first real term, indicating that AM1 has a nonzero ISB. The expansion for AM2 contains only purely imaginary terms; this is to be expected since the stability domain boundary for AM2 consists of the entire imaginary axis.

We now prove the general result for $p \geq 3$. We seek to find the values of c_p and d_p in (3) for a general AM p method. We apply (11) to (6), using $\xi = \lambda h$ to find

$$e^{i\theta} = 1 + \xi \sum_{k=0}^m \gamma_k^* \nabla^k y_1. \quad (15)$$

As $m \rightarrow \infty$, the AM method (6) reproduces the exact solution. Thus, using (2), we find

$$e^{i\theta} = 1 + i\theta \sum_{k=0}^{\infty} \gamma_k^* \nabla^k y_1. \quad (16)$$

Combining (16) and (15) gives

$$(\xi - i\theta) \sum_{k=0}^m \gamma_k^* \nabla^k y_1 = i\theta \sum_{k \geq m+1} \gamma_k^* \nabla^k y_1.$$

We now substitute for ξ using (3), where the order $p = m + 1$ for AM. Using Corollary 2.1 and Lemma 2.5, we find

$$\begin{aligned} & \left[c_m (i\theta)^{m+2} + d_m (i\theta)^{m+3} + O\left((i\theta)^{m+4}\right) \right] \left[1 + \frac{1}{2} (i\theta) + O\left((i\theta)^2\right) \right] \\ &= \gamma_{m+1}^* (i\theta)^{m+2} \left[1 + \frac{1-m}{2} (i\theta) + O\left((i\theta)^2\right) \right] + \gamma_{m+2}^* (i\theta)^{m+3} [1 + O(i\theta)] + O\left((i\theta)^{m+4}\right). \end{aligned}$$

Collecting like powers of $i\theta$, we find that $c_m = \gamma_{m+1}^*$ and

$$\frac{1}{2}c_m + d_m = \gamma_{m+2}^* - \gamma_{m+1}^* \left(\frac{m-1}{2} \right). \quad (17)$$

From Lemma 2.2, we have $c_m = \gamma_{m+1}^* < 0$ for $m \geq 1$. Using this result and (10) in (17) and simplifying gives

$$\begin{aligned} d_m &= \gamma_{m+2}^* - \left(\frac{m}{2} \right) \gamma_{m+1}^* \\ &= \frac{1}{2(m+2)!} \int_0^1 (s-1)s(s+1)(s+2)\cdots(s+m-1)(2s-m^2) ds. \end{aligned} \quad (18)$$

Because $(s-1)$ and $(2s-m^2)$ are both negative for $0 < s < 1$ and $m \geq 2$, we have $d_m > 0$ and $c_m < 0$ for AM methods, exactly opposite the result for AB methods. After examining the sign of the first real term in (3) and noting that $p = m + 1$ for AM methods, we conclude that Adams-Moulton methods have nonzero ISB's only for orders $p = 1, 2, 5, 6, 9, 10, \dots$ \square

4 Stability ordinates of Adams predictor-corrector methods

We now consider two different categories of Adams predictor-corrector methods: AB p -AM p methods and AB $(p-1)$ -AM p methods.

4.1 Two examples

We first give two examples, AB1-AM2 and AB2-AM2. The predictor AB1 is given by

$$y_1^p = y_0 + hf(t_0, y_0), \quad (19)$$

and the predictor AB2 is given by

$$y_1^p = y_0 + \frac{h}{2} (3f(t_0, y_0) - f(t_{-1}, y_{-1})). \quad (20)$$

In both cases, the corrector AM2 is given by

$$y_1 = y_0 + \frac{h}{2} (f(t_1, y_1^p) + f(t_0, y_0)). \quad (21)$$

We first consider AB1-AM2. Using (19), substituting $f(t, y) = \lambda y = \frac{\xi}{h}y$, and letting $y_k = r^k$ to solve the resulting difference equation, we find that (21) becomes

$$r = 1 + \frac{1}{2}\xi(1 + \xi) + \frac{1}{2}\xi. \quad (22)$$

To find the boundary of the stability domain, we follow the root ξ in (22) where $|r| = 1$. The stability domain of this method is shown in Figure 2(a). We can also let $r = e^{i\theta}$ and do a Taylor expansion for $\xi(\theta)$ in (22) to find that

$$\xi = i\theta + \frac{1}{6}(i\theta)^3 - \frac{1}{8}(i\theta)^4 + \dots \tag{23}$$

Because the first real term in this expansion is negative, AB1-AM2 has a zero ISB.

We next consider AB2-AM2. Using (20) and (21), we find that the analogous equation to (22) is

$$r^2 = r + \frac{1}{2}\xi \left(r + \frac{\xi}{2}(3r-1) \right) + \frac{1}{2}\xi r,$$

which leads to the expansion

$$\xi = i\theta - \frac{1}{12}(i\theta)^3 + \frac{1}{4}(i\theta)^4 + \dots \tag{24}$$

Since the first real term in this expansion is positive, AB2-AM2 has a nonzero ISB (approximately 1.29). The stability domain of this method is shown in Figure 2(b).

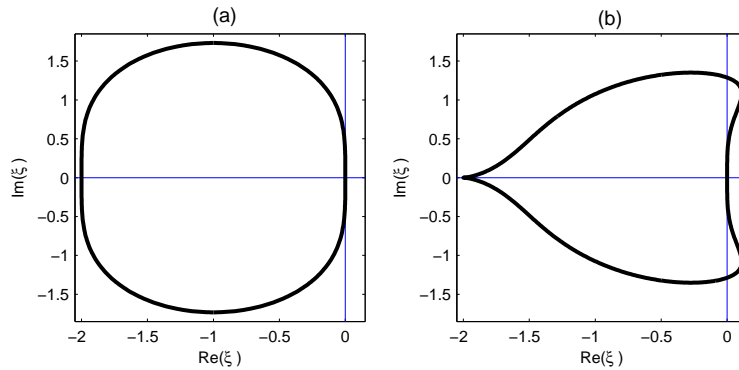


Fig. 2 Shown are the boundaries of the stability regions for (a) AB1-AM2 and (b) AB2-AM2. The stability regions consist of the inside of these curves. For (b), the ISB is approximately 1.29. The intercept on the real axis is -2 for both methods.

4.2 The general case

In general, from (4), our AB predictor will take the form

$$y_1^p = y_0 + \xi \sum_{k=0}^M \gamma_k \nabla^k y_0 \tag{25}$$

where $M = m - 1$ for $AB(p-1)$ - AM_p methods and $M = m$ for AB_p - AM_p methods; both methods have order $p = m + 1$. The general form of the AM corrector method is given by

(6), where we replace all instances of y_1 on the right-hand side by y_1^P after the backwards difference operations are done. This leads to

$$\begin{aligned} y_1 &= y_0 + \xi \sum_{j=0}^m \gamma_k^* \nabla^k y_1 + \xi (\gamma_0^* + \gamma_1^* + \cdots + \gamma_m^*) (y_1^P - y_1) \\ &= y_0 + \xi \sum_{j=0}^m \gamma_k^* \nabla^k y_1 + \xi \gamma_m (y_1^P - y_1), \end{aligned} \quad (26)$$

where we have used (8).

We use (25) to substitute for y_1^P in (26) and then use the exact solution (11) to find

$$e^{i\theta} = 1 + \xi \sum_{j=0}^m \gamma_k^* \nabla^k y_1 + \xi \gamma_m \left(1 - e^{i\theta} + \xi \sum_{k=0}^M \gamma_k \nabla^k y_0 \right). \quad (27)$$

We now use the exact AM and AB expressions (16) and (13) to substitute for the two instances of $e^{i\theta}$ in (27) respectively. Simplifying gives

$$\begin{aligned} 0 &= (\xi - i\theta) \left(\sum_{k=0}^m \gamma_k^* \nabla^k y_1 \right) - i\theta \sum_{k \geq m+1} \gamma_k^* \nabla^k y_1 \\ &\quad + \xi \gamma_m \left[(\xi - i\theta) \left(\sum_{k=0}^M \gamma_k \nabla^k y_0 \right) - i\theta \sum_{k \geq M+1} \gamma_k \nabla^k y_0 \right], \end{aligned}$$

where $M = m - 1$ for AB($p-1$)-AMP methods and $M = m$ for AB p -AMP methods.

Applying Lemmas 2.3, 2.4, and 2.5 and Corollary 2.1 gives

$$\begin{aligned} 0 &= (\xi - i\theta) \left(1 + \frac{i\theta}{2} + O((i\theta)^2) \right) - i\theta \sum_{k \geq m+1} \gamma_k^* \left[(i\theta)^k \left(1 + \frac{2-k}{2} (i\theta) + \cdots \right) \right] \\ &\quad + \xi \gamma_m \left[(\xi - i\theta) (1 + O(i\theta)) - i\theta \sum_{k \geq M+1} \gamma_k (i\theta)^k \left(1 - \frac{k}{2} (i\theta) + O((i\theta)^2) \right) \right]. \end{aligned} \quad (28)$$

This formula permits us to compute the expansion of the boundary of the stability region $\xi(\theta)$ near the origin for Adams predictor-corrector methods.

We first consider general AB p -AMP methods, which have order p .

Theorem 4.1 *Predictor-corrector AB p -AMP methods have nonzero ISB's only for orders $p = 1, 2, 5, 6, 9, 10, \dots$*

Proof Our general proof will require $p \geq 3$; we have already established that AB2-AM2 has a nonzero ISB in (24); also see Figure 2(b). For $p = 1$, we can find that the series expansion for the combination of forward Euler predictor and backward Euler correction is $\xi = i\theta - \frac{1}{2}(i\theta)^2 + \cdots$. Because this has a positive first real term, AB1-AM1 also has a nonzero ISB.

We let $M = m$ in (28) and substitute (3), using $p = m + 1$ to find

$$\begin{aligned} 0 &= \left(c_m (i\theta)^{m+2} + d_m (i\theta)^{m+3} + \cdots \right) \left(1 + \frac{i\theta}{2} + \gamma_m (i\theta) + \cdots \right) \\ &\quad - i\theta \sum_{k \geq m+1} \gamma_k^* (i\theta)^k \left(1 - \frac{k-2}{2} (i\theta) + \cdots \right) \\ &\quad - (i\theta)^2 \gamma_m \sum_{k \geq m+1} \gamma_k (i\theta)^k \left(1 - \frac{k}{2} (i\theta) + \cdots \right) + \cdots, \end{aligned} \quad (29)$$

where we have kept only the terms that are needed to find the dominant terms in this expression. Examining the coefficients of the $(i\theta)^{m+2}$ and $(i\theta)^{m+3}$ terms in (29) gives:

$$c_m = \gamma_{m+1}^* \quad (30)$$

$$d_m = \gamma_{m+2}^* - \gamma_{m+1}^* \frac{m-1}{2} + \gamma_m \gamma_{m+1} - c_m \left(\frac{1}{2} + \gamma_m \right). \quad (31)$$

From Corollary 2.1, we know that $c_m < 0$. Simplifying (30) gives

$$d_m = \gamma_{m+2}^* - \frac{m}{2} \gamma_{m+1}^* + \gamma_m^2.$$

From (18), we know that $\gamma_{m+2}^* - \frac{m}{2} \gamma_{m+1}^* > 0$ for $m \geq 2$, so we have $d_m > 0$ for $m \geq 2$. Thus $c_m < 0$ and $d_m > 0$ for $m \geq 2$ where $p = m + 1$. After examining the sign of the first real term in (3) for this case, we conclude that AB p -AM p methods have nonzero ISB's only for orders $p = 1, 2, 5, 6, 9, 10, \dots$, a result identical to AM p methods. \square

We now examine general AB($p-1$)-AM p methods, which also have order $p = m + 1$.

Theorem 4.2 *Predictor-corrector AB($p-1$)-AM p methods have nonzero ISB's only for orders $p = 3, 4, 7, 8, \dots$*

Proof Our general proof will require $p \geq 3$; we have already established that AB1-AM2 has a zero ISB in (23); also see Figure 2(a).

We now proceed with the general case for $p \geq 3$. We let $M = m - 1$ in (28) and substitute (3), using $p = m + 1$ to find

$$\begin{aligned} 0 = & \left(c_m (i\theta)^{m+2} + d_m (i\theta)^{m+3} + \dots \right) \left(1 + \frac{i\theta}{2} + \gamma_m (i\theta + \dots) \right) \\ & - i\theta \sum_{k \geq m+1} \gamma_k^* (i\theta)^k \left(1 - \frac{k-2}{2} (i\theta) + \dots \right) \\ & - (i\theta)^2 \gamma_m \sum_{k \geq m} \gamma_k (i\theta)^k \left(1 - \frac{k}{2} (i\theta) + \dots \right) + \dots, \end{aligned} \quad (32)$$

where we have kept only the terms that are needed to find the first dominant terms in this expression. Examining the coefficients of the $(i\theta)^{m+2}$ and $(i\theta)^{m+3}$ terms in (32) gives

$$c_m = \gamma_{m+1}^* + \gamma_m^2 \quad (33)$$

and

$$d_m = \gamma_{m+2}^* - \left(\frac{m-1}{2} \right) \gamma_{m+1}^* + \gamma_m \left(\gamma_{m+1} - \frac{m}{2} \gamma_m \right) - c_m \left(\frac{1}{2} + \gamma_m \right). \quad (34)$$

We claim that $c_m < 0$ and $d_m > 0$ for $m \geq 2$. We first separately compute from (33) and (34) that $c_2 = \frac{329}{2880}$ and $d_2 = -\frac{265}{1536}$. From Lemma 2.1, we have $\gamma_m > \frac{1}{m}$ for $m \geq 3$. Applying this, substituting (9) and (10) in (33), and simplifying gives

$$c_m > \gamma_{m+1}^* + \frac{1}{m} \gamma_m = \frac{1}{m(m+1)!} \int_0^1 (ms+1)s(s+1)(s+2)\dots(s+m-1)ds > 0$$

for $m \geq 3$.

We now consider the expression for d_m in (34). We substitute for c_m from (33), note that $\gamma_m > 0$, and apply Lemma 2.1.

$$\begin{aligned} d_m &= \gamma_{m+2}^* - \frac{m}{2} \gamma_{m+1}^* + \left(\frac{1-m}{2}\right) \gamma_m^2 - \gamma_m^3 \\ &< \gamma_{m+2}^* - \frac{m}{2} \gamma_{m+1}^* + \left(\frac{1-m}{2}\right) \frac{\gamma_m}{m} \\ &= \frac{1}{2m(m+2)!} \int_0^1 s(s+1) \dots (s+m-1) [(2+m-2m^2) + ms(2s-m^2-2)] ds \end{aligned}$$

for $m \geq 3$, where we have used (9) and (10) and simplified. Note that $(2+m-2m^2)$ and $(2s-m^2-2)$ are both negative for $0 < s < 1$ and $m \geq 3$, so $d_m < 0$ for this case. Thus $c_m > 0$ and $d_m < 0$ for $m \geq 3$ where $p = m+1$. After examining the sign of the first real term in (3), we conclude that AB($p-1$)-AMP methods have nonzero ISB's only for orders $p = 3, 4, 7, 8, \dots$, a result identical to AB p methods. \square

5 Conclusions

We have considered the question of when Adams methods of general order p have nonzero stability ordinates (ISB's), which corresponds to being stable when applied to discretized wave equations (for small enough stepsize). By applying the backwards difference formulation of the AB and AM methods [5], we have proven that AB p -AMP methods have nonzero stability ordinates only for $p = 1, 2, 5, 6, 9, 10, \dots$, which matches AMP methods. We have also shown that AB($p-1$)-AMP methods have nonzero stability ordinates only for $p = 3, 4, 7, 8, 11, 12, \dots$, which matches AB p methods.

Acknowledgements The authors are extremely grateful to Ernst Hairer for suggesting major simplifications in a previous form of this manuscript, in particular with regard to using the backwards difference forms of AB and AM methods.

References

1. Atkinson, K.: An Introduction to Numerical Analysis. Wiley, New York (1989)
2. Fornberg, B.: A Practical Guide to Pseudospectral Methods. Cambridge University Press, Cambridge (1996)
3. Ghrist, M.: High-order Finite Difference Methods for Wave Equations. Ph.D. thesis, Department of Applied Mathematics, University of Colorado-Boulder, Boulder, CO (2000)
4. Ghrist, M., Fornberg, B., Driscoll, T.A.: Staggered time integrators for wave equations, SIAM J. Num. Anal., 38, 718–741 (2000)
5. Henrici, P.: Discrete Variable Methods in Ordinary Differential Equations. John Wiley & Sons, New York (1962)
6. Iserles, A.: Numerical Analysis of Differential Equations. Cambridge University Press, Cambridge (1996)
7. Jeltsch, R.: A necessary condition for A-Stability of multistep multiderivative methods, Math. Comp., 30, 739–746 (1976)